HZDR-013

Wissenschaftlich-Technische Berichte
HZDR-013 2012 · ISSN 2191-8708

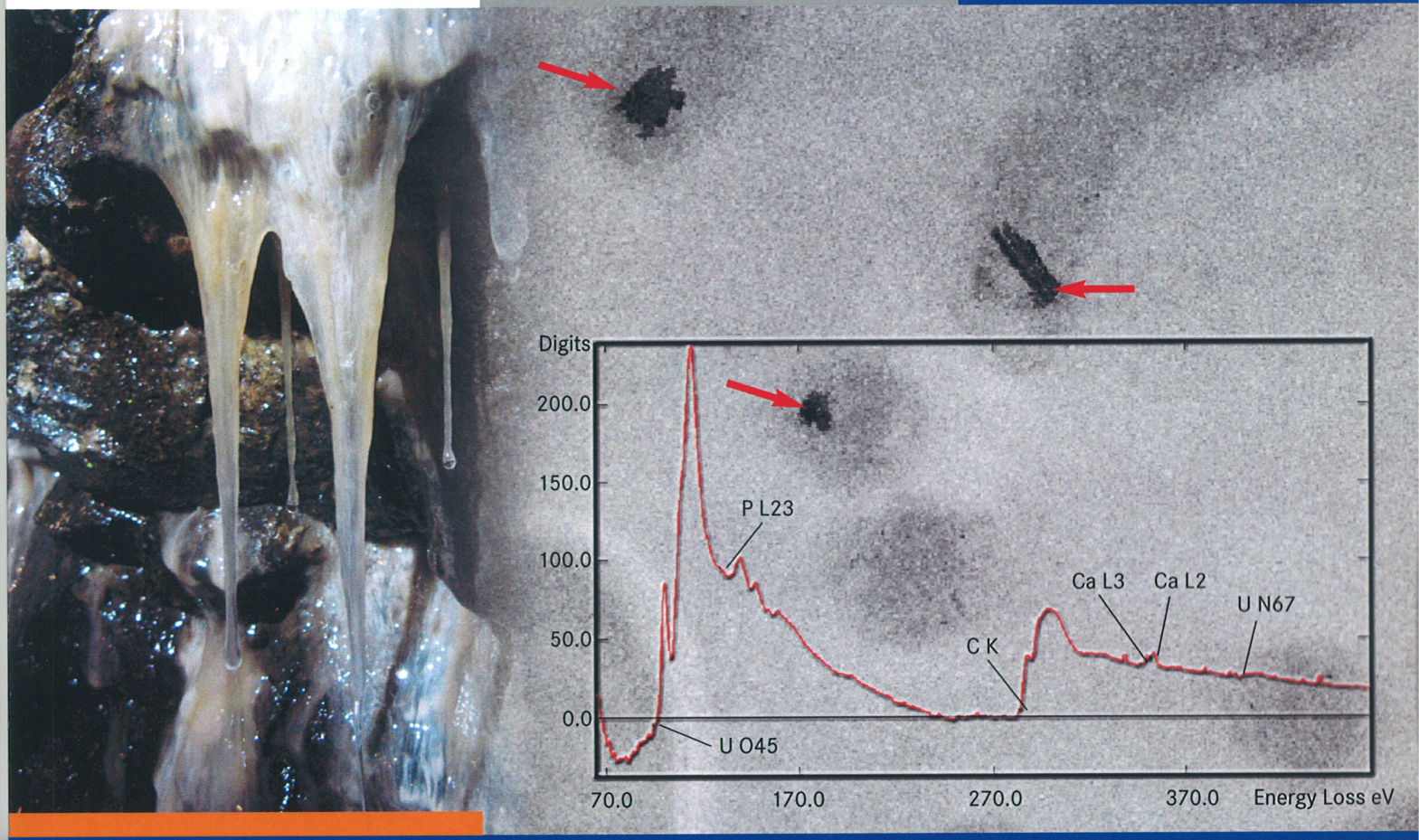

ANNUAL REPORT 2011

INSTITUTE OF RADIOCHEMISTRY

HZDR

HELMHOLTZ
ZENTRUM DRESDEN
ROSSENDORF

Wissenschaftlich-Technische Berichte
HZDR-013

Annual Report 2011

Institute of Radiochemistry

Editor:
Prof. Dr. G. Bernhard

Executive editors:
Dr. H. Foerstendorf
Dr. A. Richter

HZDR
HELMHOLTZ ZENTRUM DRESDEN ROSSENDORF

Print edition: ISSN 2191-8708

Electronic edition: ISSN 2191-8716

Qucosa: http://fzd.qucosa.de/startseite/

Published by Helmholtz-Zentrum Dresden-Rossendorf e.V.

Contact

Helmholtz-Zentrum Dresden-Rossendorf e.V.
Institute of Resource Ecology

Postal Address	*Address for visitors*
P.O. Box 51 01 19	Bautzner Landstraße 400
D-01314 Dresden	D-01328 Dresden
Germany	Germany

Phone: ++49 (0) 351 260 3210
Fax: ++49 (0) 351 260 3553
e-mail: contact.resourceecology@hzdr.de
http://www.hzdr.de/FWO

This report is also available at http://www.hzdr.de/FWO

Editorial note

With the beginning of 2012, the ***Institute of Resource Ecology*** (IRE) was newly founded at the ***Helmholtz-Zentrum Dresden-Rossendorf e.V.*** (HZDR). All divisions of the former ***Institute of Radiochemistry*** (IRC) were merged into the IRE. The content of this *Annual Report* exclusively provides a representative cross section of the scientific activities of the former IRC during 2011.

Cover picture

Slimy, massive biofilms, attached to the granitic bedrock of the underground rock characterization facility tunnel ONKALO (Finland). The TEM picture shows autunite mineral (arrows) formed in the cytoplasm of some rod shaped gram negative bacteria after the addition of uranium to the groundwater, which is percolating the biofilm. The uranium-phosphate mineral was identified by EELS analysis showing intensity peaks of O- and N-edges of uranium, L-edges of Ca and L-edges of P (see p. 16).
Reference:
E. Krawczyk-Bärsch, H. Lünsdorf, K. Pedersen, T. Arnold, F. Bok, R. Steudtner, A. Lehtinen, V. Brendler (2012) Immobilization of uranium in biofilm microorganisms exposed to groundwater seeps over granitic rock tunnel walls in Olkiluoto, Finland, *Geochimica et Cosmochimica Acta* (under review).

Preface

THE INSTITUTE OF RADIOCHEMISTRY (IRC) IS one of the seven institutes of the Helmholtz-Zentrum Dresden-Rossendorf (HZDR). The research activities are fully integrated into the "Nuclear Safety Research Program" of the Helmholtz Association and focused on the topic "Safety of Nuclear Waste Disposal".

The research objectives are to generate better process understanding and data for the long-term safety analysis of a nuclear waste disposal in the deep geological underground. A better knowledge about the dominating processes essential for radionuclide (actinide) mobilization and immobilization on the molecular level is needed for the assessment of the macroscopic processes which determine the transport and distribution of radioactivity in the environment.

Special emphasis is put on the biological mediated transport of long-lived radionuclides in the geosphere and their interaction with different biosystems like biota and human organism for a better calculation of environmental and health risks.

Advanced knowledge is needed for description of the processes dominating at the interfaces between geo- and bio-systems related to the distribution of long-lived radionuclides in various bio-systems along the food chain.

More than 120 scientists, technicians, and students, working on their Ph.D., diploma, master, or bachelor thesis, were employed at the Institute of Radiochemistry in 2011. About 20 Ph.D. students are working at the institute. Promotion of young scientists is an important requirement to ensure the competence and further excellent scientific results in the discipline of radiochemistry in future times. We accomplished many new scientific results in the past year, which are presented in this Annual Report, and about 50 original papers were published in peer-reviewed international scientific journals.

In 2011, the future research profile of the HZDR was under discussion with the aim to focus the research fields and programs. One result of this process was the foundation of the Institute of Resource Ecology (IRE) with the beginning of 2012. All divisions of the former Institute of Radiochemistry were integrated into the new Institute. Commonly, the research is concentrated on the ecology of radioactive and non-radioactive metals in the context of nuclear waste disposal, the production of energy in nuclear power plants and of processes along the value chain of metalliferous raw materials.

The present Annual Report contains results explicitly related to the radiochemical and radio-ecological research aspects "Long-lived Radionuclides in Biosystems" and "Long-lived Radionuclides at Permanent Disposal Sites".

I would like to thank the visitors, German and international ones, for their interest in our research and for their participation in the institute seminars. We would also like to thank our scientific collaborators and the visiting scientists for coming to Dresden/Rossendorf in 2011 to share their knowledge and experience with us. We continue to strongly encourage the collaborations and visits by scientists in the future. Special thanks are due to the Executive Board of the Helmholtz-Zentrum Dresden-Rossendorf, the Ministry of Science and Arts of the State Saxony, the Federal Ministry of Education and Research, the Federal Ministry of Economics and Technology, the Deutsche Forschungsgemeinschaft, the European Commission, and other organizations for their support.

Prof. Dr. Gert Bernhard
Director of the Institute of Resource Ecology

Contents

SCIENTIFIC CONTRIBUTIONS

PART I – LONG-LIVED RADIONUCLIDES IN BIOSYSTEMS

PART II – LONG-LIVED RADIONUCLIDES AT PERMANENT DISPOSAL SITES

PUBLICATIONS

SCIENTIFIC ACTIVITIES

PERSONNEL

ACKNOWLEDGEMENTS

INDEX OF AUTHORS

LONG-LIVED RADIONUCLIDES IN BIOSYSTEMS

Interaction of U(VI) with the Äspö strain *P. fluorescens* studied by potentiometric titration

L. Lütke, H. Moll, G. Bernhard

Using potentiometric titration *Pseudomonas fluorescens* cells could be characterized in terms of surface functional group densities and the corresponding pK_a values. Subsequently this method was successfully applied for the determination of relevant U(VI) surface complexes and their stability constants.

Since microbes are well known to affect the mobility of actinides, dominant microbial strains from sites destined for future nuclear waste deposition have to be investigated regarding their interaction mechanisms with soluble actinyl ions. The investigated subsurface groundwater strain *Pseudomonas fluorescens* has been isolated from the Äspö site, Sweden [1].

EXPERIMENTAL. *P. fluorescens* CCUG 32456A was grown in NB medium. Culture purity was ensured by light microscopy and *in situ* PCR with subsequent RFLP. Cells were harvested in the mid-exponential growth phase, washed in a solution containing 0.099 M NaCl and 0.001 M HCl and then suspended in the same solution for titrations of only *P. fluorescens*. In case of simultaneous titration of *P. fluorescens* and U(VI), the cells were washed and suspended in 0.1 M $NaClO_4$ and the pH was adjusted to 3 by adding $HClO_4$. The titrations were carried out under N_2 atmosphere. CO_2-free 0.042 M NaOH was used as titrant. Titration curves were evaluated using the program HYPERQUAD2008 [2].

RESULTS. Data resulting from titration of solutions containing solely *P. fluorescens* were fitted using a three-site model. Calculated pK_a values and site densities of the binding sites were 4.65 ± 0.13 (0.82 ± 0.06 mmol/$g_{dry\ weight}$), 6.62 ± 0.13 (0.36 ± 0.09 mmol/$g_{dry\ weight}$), and 9.18 ± 0.02 (0.78 ± 0.24 mmol/$g_{dry\ weight}$). Comparing these values to the pK_a ranges of different functional groups reported in Cox et al. [3], the respective surface functional groups can be attributed to carboxyl, phosphate and amine moieties. The parameters determined for surface functional groups of *P. fluorescens* (CCUG 32456 A) are comparable to those obtained for another strain of this bacterium, *P. fluorescens* (ATCC 55241) [4].

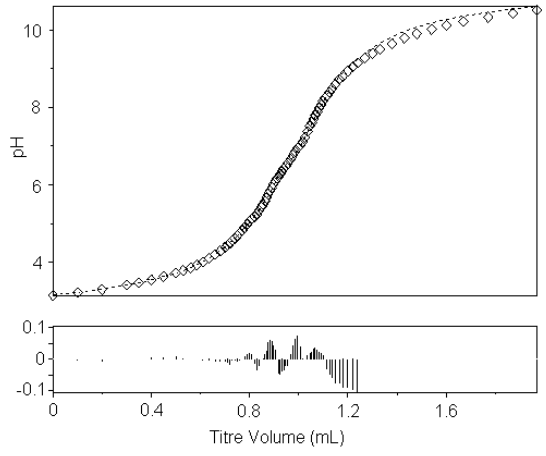

Fig. 1: Titration of $1 \cdot 10^{-4}$ M UO_2^{2+} and 0.3 g/L cells in 0.1 M $NaClO_4$ with 0.042 M NaOH (data ◊, fit ---).

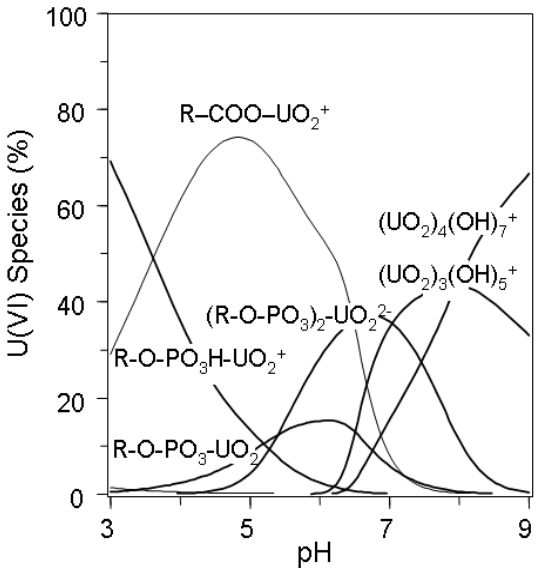

Fig. 2: U(VI) species distribution in dependence on pH, [U(VI)] = $1 \cdot 10^{-4}$ M, [dry biomass] = 0.2 g/L.

Figure 1 illustrates the titration curve of U(VI) with *P. fluorescens* and the fit with HYPERQUAD.
Besides the determined pK_a values and site densities of the bacteria, the following hydrolytic uranyl species were included in the fit: $(UO_2)_2(OH)_2^{2+}$, $(UO_2)_3(OH)_5^{+}$, $(UO_2)_4(OH)_7^{+}$. Extracted U(VI) surface complexes and stability constants using HYPERQUAD are given in the following table:

Tab. 1: Calculated U(VI) surface complexes and stability constants.

Complex	xyz	log β (± SD)
R-COO-UO_2^{+}	110	6.66 ± 0.05
R-O-PO_3-UO_2	110	7.54 ± 0.18
R-O-PO_3H-UO_2^{+}	111	12.73 ± 0.06
$(R\text{-}O\text{-}PO_3)_2$-$UO_2^{2-}$	120	12.97 ± 0.07

Based on the calculated stability constants (Tab. 1) and the stability constants of relevant U(VI) hydrolytic species, the U(VI) species distribution in dependence on the pH (Fig. 2) was calculated for a given [U(VI)] and [dry biomass] using the software HySS2009.
This species distribution shows that in the acidic pH range below pH 3.5 U(VI) binds to the cell surface mainly via protonated phosphoryl groups. The complexation by carboxylic groups plays a role over a wide pH range up to around pH 7. At pH 7, fully deprotonated phosphoryl groups are mainly responsible for U(VI) binding. If the pH is increased further uranyl hydroxides dominate the U(VI) speciation in aqueous solution (in a CO_2-free system).

ACKNOWLEDGEMENTS. The authors thank the BMWi for financial support (contract no.: 02E10618).

[1] Pedersen, K. et al. (1997) *FEMS Microbiol. Rev*. **20**, 399–414.
[2] Gans, P. et al. (1996) *Talanta* **43**, 1739–1753.
[3] Cox, J.S. et al. (1999) *Environ. Sci. Technol.* **33**, 4514-4521.
[4] Yoshida, T. et al. (2004) *Radiochim. Acta* **92**, 749-753.

Curium(III) speciation studies with the Äspö-strain *Pseudomonas fluorescens*

H. Moll, L. Lütke, G. Bernhard

The interaction between soluble species of Cm(III) and cells of the Äspö-strain *P. fluorescens* was studied at trace Cm(III) concentrations (0.3 µM) using time-resolved laser-induced fluorescence spectroscopy (TRLFS). Extraction studies have shown that the biosorption of Cm(III) is a reversible process and the Cm(III) is bound by surface complexation.

The interaction between bacteria and metals influences the speciation of hazardous actinides in the environment. Pseudomonads, ubiquitous soil and groundwater bacteria, can interact with actinides by both direct (with planktonic cells [1]) and indirect (with secreted pyoverdins [2]) pathways. The goal of this work was a systematic study to explore the unknown speciation of Cm(III) with pyoverdin-free cells of the Äspö-strain *P. fluorescens* (CCUG 32456A) by TRLFS. The strain was isolated from groundwater from borehole KR0013, 70 m underground in the Äspö Hard Rock Laboratory tunnel [3].

EXPERIMENTAL. TRLFS measurements were performed under N_2 atmosphere at 25 °C. As a background electrolyte, analytical grade 0.1 M $NaClO_4$ was used. The Cm(III) concentration was fixed at 0.3 µM. In two runs, the biomass concentration was kept constant at 0.2 $g_{dry\ weight}$/L, while varying pH between 8.0-1.4 and 1.5-8.0, respectively. In two runs, the biomass concentration was changed at pH 3.05 and 6.08, respectively. Desorption studies were performed with 0.01 M EDTA solution (pH 5) as described in [4]. TRLFS spectra were recorded using a unique pulsed flash lamp pumped Nd:YAG-OPO laser system (Powerlite Precision II 9020 laser equipped with a Green PANTHER EX OPO from Continuum, Santa Clara, CA, USA). Further details about the laser system can be found in [2].

RESULTS. TRLFS is an established experimental technique for characterizing the Cm(III) speciation in a variety of systems, based on quantifying the various Cm(III) species by deconvoluting the total emission spectra.
The spectroscopic speciation indicated strong interactions between Cm(III) and *P. fluorescens* cells as shown in Fig. 1. A strong decrease in the emission band of the free Cm^{3+} at 593.7 nm could be detected already at pH 1.43 and a biomass concentration of 0.2 $g_{dry\ weight}$/L. The dependencies found in the TRLFS spectra (Fig. 1A, B) suggested the occurrence of two individual Cm(III)–*P. fluorescens* species having emission maxima at ca. 599.6 (species 1) and 601.6 nm (species 2).
Luminescence data were evaluated by the factor analysis technique. Input parameters for the data fitting were the known and calculated total concentrations of Cm^{3+} and of the functional groups located at the cell envelope of *P. fluorescens* (pK_a's and corresponding site densities [5]), the pH of each sample, the known stability constants of the curium(III) hydroxides, and the normalized sample spectra. Due to the strong interactions detected in the acidic pH region a protonated Cm(III) phosphoryl complex is likely to occur followed by a carboxyl complex at higher pH (Fig. 2). The best fits were obtained with two 1 : 1 complexes, R–O–PO_3H–Cm^{2+} ($\log \beta_{111} = 12.7 \pm 0.6$) and R–COO–$Cm^{2+}$ ($\log \beta_{110} = 6.1 \pm 0.5$).

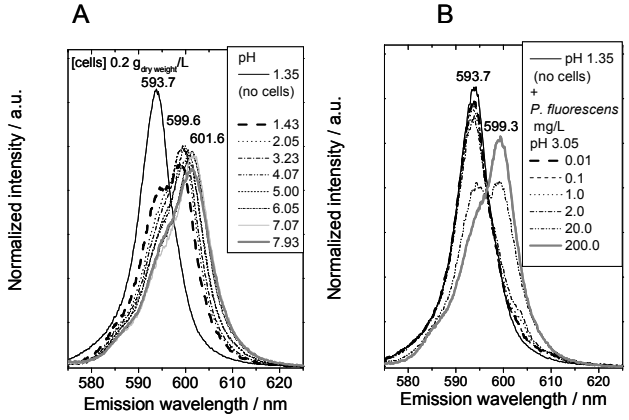

Fig. 1: TRLFS data of 0.3 µM Cm(III) in 0.1 M $NaClO_4$ measured: A) as a function of pH at a fixed biomass concentration of 0.2 $g_{dry\ weight}$/L; and B) as a function of the biomass concentration at pH 3.05. The spectra are scaled to the same peak area.

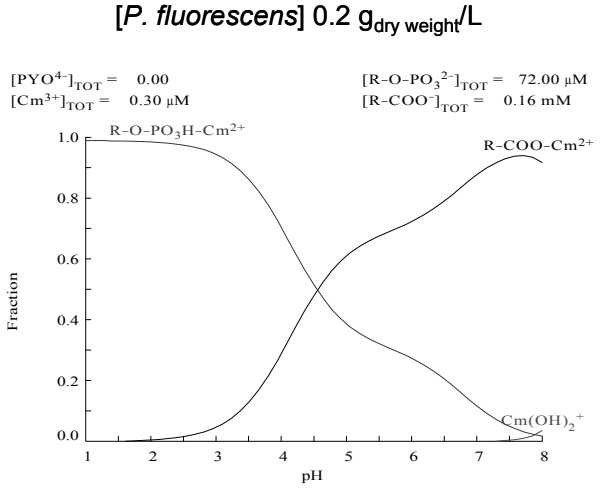

Fig. 2: Speciation of Cm(III) in aqueous solutions as a function of pH providing 800-fold (0.2 $g_{dry\ weight}$/L) excess of functional groups from the *P. fluorescens* cell envelope.

We extracted the cell-bound Cm(III) with 0.01 M EDTA solution (pH 5). Between 90 and 100% of the Cm(III) was released from the cells. These results show that the biosorption is reversible and confirms the formation of surface complexes with functional groups of the cell envelope.

ACKNOWLEDGEMENTS. This work was funded by the BMWi under contract number 02E10618.

[1] Moll, H. et al. (2012) in preparation.
[2] Moll, H. et al. (2008) *Biometals* **21**, 219-228.
[3] Pedersen, K. et al. (1997) *FEMS Microbiol. Rev.* **20**, 399-414.
[4] Panak, P.J. et al. (2001) *Radiochim. Acta* **89**, 499-504.
[5] Lütke, L. et al. (2012) this report, p. 9

Influence of low uranium concentrations on *Peanibacillus* sp. JG-TB8 using calorimetric metabolic monitoring

M. H. Obeid, A. Geissler, K. Fahmy, J. Oertel

The transition of industrially caused metal contaminations into the food chain constitutes a serious risk for the environment and human health. It is particularly a major challenge to develop ecotoxicological biomonitors that provide a physical readout based on measurable metabolic effects. We have used long term calorimetry to study how europium and uranium at environmentally relevant concentrations affect the metabolic activity of *Peanibacillus* sp. JG-TB8, a gram-positive bacterium isolated from a uranium mining waste pile. The data show that calorimetric metabolic monitoring opens a new route of biological sensing for the quantitative assessment of metal / radiometal toxicity in the environment.

The qualitative and quantitative risk assessment of radiotoxicity in contaminated sites plays a key role in radioecological monitoring and for environmental protection. High doses of radioactivity are physically measurable in the near field of nuclear waste disposals. However, it is a major challenge to develop methods for low dose risk assessments typical for the far field, where transmission of radionuclides into the food chain may lead to health risks that are not detectable by conventional methods.

Here, a novel approach using metabolic monitoring of bacterial cell growth was established using the Thermal Activity Monitor (TAM III; TA instruments) as a multichannel microcalorimeter. Almost all physical and chemical processes involve exchange of heat, rendering the measurement of thermal effects an attractive non-invasive method to assess the turnover of chemical reactions independently of their complexity to access the underlying thermodynamics [1]. Here we demonstrate that long term microcalorimetry can detect the metabolic effects of low dose heavy metal exposure during bacterial growth. The heat effects normally encountered with biological samples are generally quite small due to the small enthalpy changes associated with the underlying biomolecular interactions. The high sensitivity and thermal stability of the TAMIII calorimeter provide the monitoring of such small changes of heat releases within 0.0001 °C.

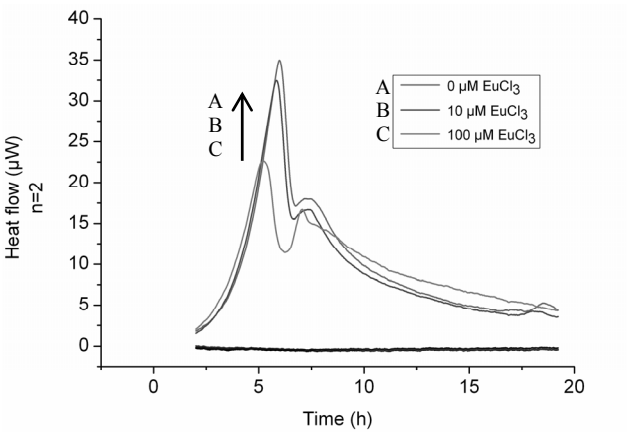

Fig. 1: Thermogramm of *Peanibacillus* sp. JG-TB8 grown in R2A media at 30 °C with different $EuCl_3$ concentrations (10 µM and 100 µM). Pure R2A-media with and without $EuCl_3$ were used as negative controls (zero-line).

Tab. 1: Summary of growth rate constant (K) and evaluation of the first max. heat flow depending on the $EuCl_3$ concentration.

$EuCl_3$ [µM]	0	10	100
K [min^{-1}]	0.01324	0.01252	0.01161
first max. heat flow [µW]	34.88	32.45	22.62

The objective in this approach is the identification of the minimal dose of radionuclides that generates a measurable change in metabolic heat release. Therefore, the toxicity of a radionuclide was defined as a measurable effect on the metabolic activity of *Peanibacillus* sp. JG-TB8, a gram-positive bacterium isolated from a soil sample of the uranium mining waste pile "Haberland" (Johanngeorgenstadt, Germany) [2, 3].

EXPERIMENTAL. Liquid cultures of *Peanibacillus* sp. JG-TB8 grown in R2A media at 30 °C were exposed to micromolar concentrations (0, 10, 50, 100 µM) of uranium (VI) salts and the metabolic heat release measured as a function of time and temperature. The non-radioactive "heavy metal stress" exerted by europium (Eu(III)) served as reference under the same conditions.

RESULTS. First results showed distinct and reproducible effects of europium on the time-dependent heat release already at 10 µM concentration. The toxicity of uranium and europium caused a decrease of maximal heat flow compared to control samples.

In contrast to europium, for which the inhibitory action scales with concentration, uranium influences bacterial growth in a more complicated manner which strongly depends on temperature and pH, probably as a consequence of its different speciations (data not shown).

The results demonstrate that microcalorimetric monitoring is an extremely sensitive tool to investigate the influence of low heavy metal and radionuclide concentrations on the metabolic activity of microorganisms as shown here for *Peanibacillus* sp. JG-TB8. The bacterial growth rates were determined with high accuracy continuously in real time. The proven long-term stability will also allow the monitoring of higher living organisms (e.g. C. *elegans*).

This project established by state-of-the-art calorimetric experiments a novel strategy to detect biological responses to low doses of heavy metal and radiometal contaminants. It provides standardized methods for biological toxicity assessment particularly at low doses, which cannot be ranked by existing assays which are based on lethality.

[1] Cooper, A. (2007) in: *Handbook of Biosensors and Bioships*, John Wiley & Sons, Ltd., London.
[2] Reitz, T. (2011) *PhD Thesis*, TU Bergakademie Freiberg.
[3] Pollmann, K. et al. (2006) *Biotechnol Adv.* **24**, 58-68.

Study of the impact of europium(III) on the viability of FaDu cells

S. Sachs, G. Bernhard

The impact of Eu(III) on the viability of FaDu cells has been studied as a function of Eu(III) concentration and time as well as in the absence and presence of fetal bovine serum (FBS). The Eu(III) toxicity onto the cells is significantly influenced by its chemical speciation. FBS constituents in nutrient medium enhance the solubility of Eu(III) by complexation, thus, decreasing its toxicity.

In case of the accidental release of long-lived radionuclides, such as actinides, into the environment, knowledge about their behavior in bio-systems is necessary to asses and prevent health risks. This includes knowledge about the interaction of actinides with eukaryotic cells and their impact on the cell viability.
Objective of our work is the study of interaction processes of actinides with mammalian cells on a cellular level by combination of biochemical and spectroscopic techniques. This includes the cultivation of cell lines, the determination of the cellular tolerance against relevant metals as a function of time, concentration and nutrient composition as well as the correlation between the metal ion uptake into cells and their chemical speciation, thus enabling a better understanding of their bioavailability and toxicity.
In the present study we investigated the impact of Eu(III), an analog for trivalent actinides, on the viability of FaDu cells. Simultaneously, we investigated the speciation of Eu(III) in cell culture medium [1].

EXPERIMENTAL. FaDu cells (human squamous cell carcinoma cell line) were grown in 175 cm^2 flasks (CELLSTAR®, Greiner) in Dulbecco's modified eagle medium (DMEM; w/o sodium pyruvate, with stabile glutamin, 4.5 g/L D-glucose; Biochrom) supplemented with 10% fetal bovine serum (FBS; Sigma), 0.7 mmol/L non-essential amino acids, 20 mmol/L HEPES buffer, penicillin/streptomycin (100 U/mL/100 µg/mL), and 1 mmol/L sodium pyruvate (all from Biochrom) [2]. Cells were incubated at 37 °C, 5% CO_2 and 95% humidity. At confluence, cells were subcultured in 96 well plates (CELLSTAR®, Greiner) and seeded at 3000 cells/well.
To study the Eu(III) toxicity onto the cells, Eu(III) was added to the cells after two days of incubation. Eu(III) solutions with initial concentrations of 5-1200 µM were prepared by dissolution of $EuCl_3$ stock solutions with complete cell culture medium or with cell culture medium w/o FBS (pH 7.8 ± 0.2). All solutions were prepared just before exposure. The Eu(III) concentration was measured by ICP-MS. Before Eu(III) addition, the wells were emptied and 100 µL of the respective Eu(III) solution was added to the cells (12 wells/concentration). In case of the studies w/o FBS, the cells were rinsed before the addition of the FBS-free Eu(III) solutions using 100 µL phosphate buffered saline solution (PBS; w/o Ca^{2+}, Mg^{2+}; Biochrom). After Eu(III) addition, the cells were incubated for 24, 48, and 72 h.
The toxicity of Eu(III) was analyzed by the MTT assay [3]. After the exposure time, 10 µL MTT solution (3-(4,5-dimethylthiazol-2-yl)-2,5-diphenyl tetrazolium bromide; Duchefa; 5 mg/mL in PBS) were added to each well and incubated for 3 h. Then, wells were emptied and 100 µL 0.04 M HCl in isopropanol (Merck/Roth) were added to dissolve the blue formazan crystals. After slight agitation for 10 min at room temperature, the absorbance at 620 nm was measured using a microplate reader (Mithras LB940, Berthold). Data were normalized to cell control samples.

RESULTS. As an example, the viability of FaDu cells after 48 h incubation with 5-1200 µM Eu(III) in the presence and absence of FBS is shown in Fig. 1. In the presence of FBS, the viability of FaDu cells is still in the range of the control samples up to about 800 µM Eu(III). With further increasing Eu(III) concentration the cell viability decreases. Comparable results were reported for the impact of Eu(III) and other lanthanide ions on a human osteosarcoma cell line [4]. In the absence of FBS, the cell viability is significantly influenced by Eu(III). It decreases significantly with increasing Eu(III) concentration, starting already at low Eu(III) concentrations. In the absence of FBS, the cell viability shows a very slight dependence on the incubation time with Eu(III). It decreases slightly with increasing incubation time.

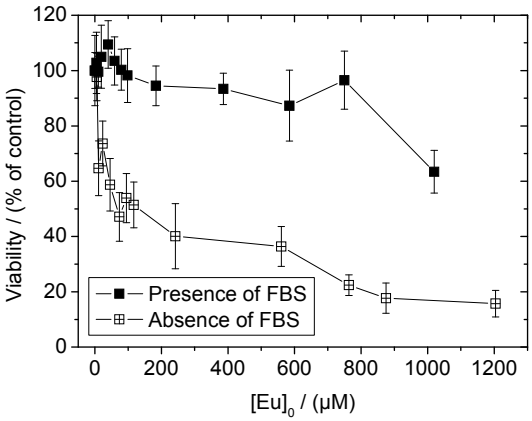

Fig. 1: Viability of FaDu cells after 48 h incubation with Eu(III) in the presence and absence of FBS.

The differences in the Eu(III) toxicity are caused by a different chemical speciation of Eu(III) in solution. Results of Eu(III) solubility studies in the used media after 24-72 h of incubation (37 °C, 5% CO_2, 95% humidity) have shown, that the solubility of Eu(III) in cell culture medium is high in the presence of FBS. For an initial Eu(III) concentration of 1 mM, about 70% of Eu(III) is still dissolved after 72 h. In contrast to that, nearly all Eu(III) is precipitated in the absence of FBS over the whole studied concentration range. These results point to a stabilization of Eu(III) in solution by complexation with FBS constituents, most probably serum proteins, which was confirmed by TRLFS [1]. In spite of the low Eu(III) solubility in nutrient media in the absence of FBS, its toxicity onto FaDu cells and probably its bioavailability is higher than in the absence of FBS.

ACKNOWLEDGEMENTS. We thank E. Leßmann (Institute of Radiation Physics) for providing FaDu cells and FBS and training in cell cultivation techniques.

[1] Heller, A. et al. (2012) this report, p. 13.
[2] Leßmann, E., personal communication.
[3] Mosmann, T. (1983) *J. Immunol. Methods* **65**, 55-63.
[4] Feyerabend, F. et al. (2010) *Acta Biomater.* **6**, 1834-1842.

Luminescence spectroscopic investigation of the dominant europium(III) species in cell culture media

A. Heller, S. Sachs, G. Bernhard

The dominant binding form of Eu(III) in Dulbecco's modified eagle medium (DMEM) and FaDu cell culture medium has been investigated by TRLFS. In DMEM two different Eu(III) species, which have yet to be identified, exist simultaneously. In contrast, in FaDu cell culture medium only one Eu(III) species, which includes carbonate, a component of fetal bovine serum (FBS) and possibly phosphate as ligands, dominates. Furthermore, calcium is required for charge neutralization.

To asses health risks of actinides(III) released into the environment, knowledge about their behavior in different biosystems is necessary. In particular, this includes knowledge about the incorporation of actinides into eukaryotic cells and their impact on the cell viability [1]. These processes are mainly influenced by their chemical speciation, which, in turn, strongly depends on the composition of nutrients. In the present study we, therefore, investigated the Eu(III) speciation in two cell culture media by TRLFS. Table 1 summarizes the inorganic ions contained in DMEM [2], the main component of FaDu cell culture medium [1]. Besides several amino acids, these inorganic ions are the main constituents of DMEM.

Tab. 1: Inorganic components of DMEM (all concentrations in mM).

Na^+	K^+	Mg^{2+}	Ca^{2+}	Fe^{3+}
132.5	4.6	6.9	1.5	0.2
Cl^-	NO_3^-	SO_4^{2-}	CO_3^{2-}	PO_4^{3-}
102.2	0.6	6.9	38.0	0.9

EXPERIMENTAL. Due to the radiotoxicity of actinides(III), Eu(III) was used as an analog. Different Eu(III) solutions with a constant metal concentration of $1 \cdot 10^{-5}$ M and varying composition of inorganic constituents of the nutrients (see Table 1) with and without FBS were studied in addition to the Eu(III) reference solutions with DMEM and complete FaDu cell culture medium. The pH and ionic strength were kept constant at pH = 7.4 and I = 0.1 M (NaCl), respectively. TRLFS measurements were carried out under normal atmosphere and room temperature with an excitation wavelength of 394 nm.

RESULTS. The reference luminescence spectra and decay curves of Eu(III) in DMEM and FaDu cell culture medium are depicted in Figure 1.
Important spectroscopic parameters are the intensity ratio of the electric dipole transition $^5D_0 \rightarrow {}^7F_2$ over the magnetic dipole transition $^5D_0 \rightarrow {}^7F_1$ ($R_{E/M}$), the luminescence lifetime (τ) and the number of water molecules in the first hydration shell of the Eu^{3+} ion (n_{H2O}) [3]. Comparing these parameters of Eu(III) in both nutrient media reveals a nearly identical fine structure of the steady state spectra but a slightly higher $R_{E/M}$ in DMEM than in FaDu cell culture medium. Furthermore, the luminescence of Eu(III) in DMEM decays in a bi-exponential mode indicating the existence of two Eu(III) species, whereas in FaDu cell culture medium only a mono-exponential decay curve was measured indicating one dominant Eu(III) species.
To compare all sample spectra with those of the references, a coordination-environment (CE) diagram [4] was created by plotting the $R_{E/M}$ against the number of water molecules that have been replaced upon complexation (Fig. 2).

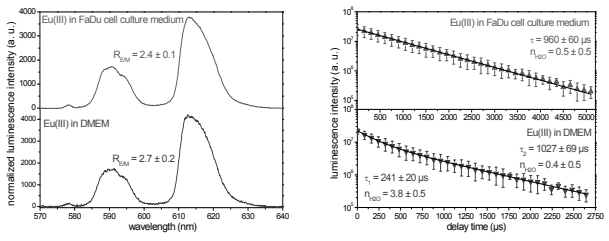

Fig. 1: Average steady state spectra (left) and luminescence decay curves (right) of Eu(III) in DMEM and FaDu cell culture medium.

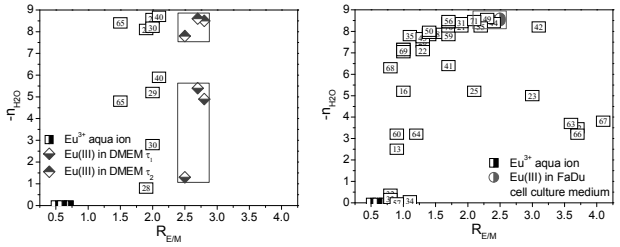

Fig. 2: CE-diagrams for determination of the dominant Eu(III) species in DMEM (left) and FaDu cell culture medium (right)

For Eu(III) in DMEM none of the sample spectra measured so far really match that of the reference. Indeed, the luminescence decay of Eu(III) in sample 65 containing CO_3^{2-}, PO_4^{3-} and Ca^{2+} is very similar but the $R_{E/M}$ is to small. Therefore, the dominant Eu(III) binding forms in DMEM have yet to be identified and are the subject of ongoing studies.
In case of Eu(III) in FaDu cell culture medium three spectra (samples 44, 49 and 71) were found to closely match the $R_{E/M}$, τ and n_{H2O} of the reference spectrum (see Table 2). FBS and CO_3^{2-} were contained in all of these samples, Ca^{2+} and PO_4^{3-} each in two of them. In contrast, none of the spectra measured in binary solutions of Eu(III) with solely one of these ligands fits the spectroscopic parameters of the reference spectrum. Therefore, we conclude that a ternary Eu(III) species is formed in FaDu cell culture medium. This complex definitely contains CO_3^{2-} and a component of FBS. Ca^{2+} is needed for charge equalization. The involvement of PO_4^{3-} has yet to be confirmed.

Tab. 2: Comparison of spectroscopic parameters of Eu(III) in FaDu cell culture medium and sample solutions.

Sample	$R_{E/M}$	τ [µs]	n_{H2O}
Eu(III) in FaDu medium	2.4	960 ± 60	0.5 ± 0.5
sample 44	2.4	861 ± 40	0.6 ± 0.5
sample 49	2.3	1019 ± 20	0.4 ± 0.5
sample 71	2.1	934 ± 32	0.5 ± 0.5

[1] Sachs, S. et al. (2012) this report, p. 12.
[2] BIOCHROM product information, www.biochrom.de.
[3] Kimura, T. et al. (1996) *Radiochim. Acta* **72**, 61-64.
[4] Ozaki, T. et al. (2002) *Anal. Bioanal. Chem.* **374**, 1101-1104.

Study on the influence of microorganisms on the water chemistry in flooded underground uranium mines

C. Gagell, T. Arnold, U. Jenk,[1] I. Röske[2]
[1]Wismut GmbH, Chemnitz, Germany; [2]Institute of Microbiology, Dresden University of Technology, Dresden, Germany

A research program was started in which the influence of microorganisms, living underground, on the migration behaviour of uranium in flooded former uranium mines in East Germany is studied. For this, suitable sampling sites representing different stages of flooding, i.e. newly (< 3 years), intermediate (15-25 years) and long-term (> 50 years) flooded were selected and appropriate devices to grow biofilms on were designed, constructed and mounted in the mine sites.

Uranium mining operated by the Wismut GmbH (formerly known as SDAG Wismut) was carried out in Saxony and Thuringia from 1946 till 1990. In 1991, the company started to remediate the mining relics, which often included the flooding of the whole pit body. The mine water still contains elevated amounts of toxic metals such as uranium, radium, arsenic which have to be removed by expensive classical waste water treatment systems.
Microorganisms may play an important role for geochemical processes such as metal immobilization. Their influence on the water chemistry in flooded uranium mines is studied in this project. The expected results may contribute to improved remediation measures.

RESULTS. Due to the flooding of the underground mines, which is a common remediation strategy, the sampling sites are not directly accessible. Therefore, suitable sampling devices adapted to the respective conditions on site had to be designed, assembled and installed. Their performance had and has to be refined in the course of the research project. The purpose of the sampling devices is to obtain biological material at sites which represent the conditions underground.
Four former uranium mines were selected, each characteristic for a certain flooding stage. These mines, shown in Fig. 1, are: Königstein, Pöhla, Schlema and Zobes. The mine Königstein was flooded in 2010 and the mine water is characterized by an acidic pH with oxic conditions. A detailed characterization of the aqueous chemistry is described in [1]. In addition, there are data available describing the microbiological diversity before the pit flooding [2,3]. Thus, it is expected that Königstein should represent a dynamic sampling site in which changes in the microbial diversity are expected to occur within the next years. The mines Pöhla and Schlema have been flooded in 1990. The mine waters show slightly alkaline pH values. In Pöhla reducing conditions with low concentration of uranium are currently observed, indicating that the geochemical milieu has been dramatically changed during the last 20 years. Schlema still shows higher uranium concentrations. Here, it is expected that the uranium concentration will decrease within the next years to reach concentrations comparable to those found in Pöhla. Zobes is an example for abandoned uranium extraction site with stable geochemical conditions, since the flooding already started in 1963.

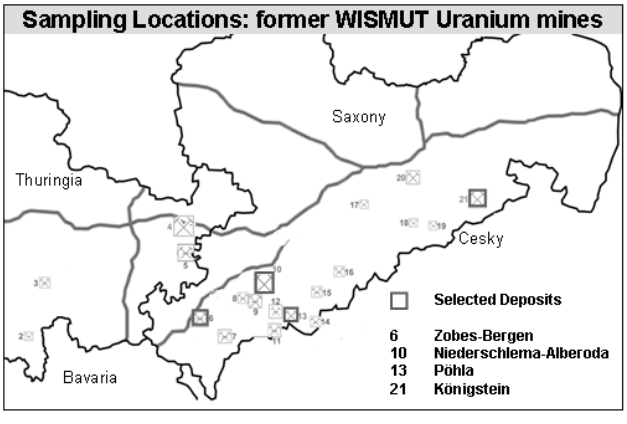

Fig. 1: Geographical position of sampling locations. Four different former uranium mines in Saxony were selected for microbial analysis of mine water.

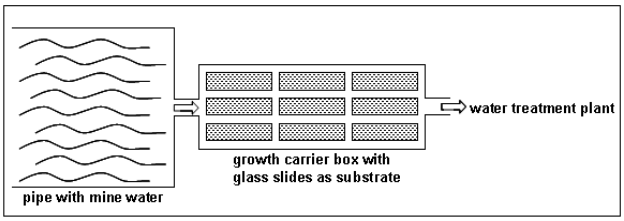

Fig. 2: Schematic illustration of a flow cell system.

The sampling devices on which biofilms should grow were specifically constructed and adapted to the respective conditions on site to enable the microorganisms to form biofilms in their natural habitat. The growth carrier boxes were optimized with respect to degassing. Two examples are described below. The flow cell shown in Fig. 2 was placed ahead of the water treatment system in Schlema. A similar system was also installed in Pöhla and Königstein. In addition, a sampling device specifically designed for the very deep shaft in Schlema was developed. This immersion system has the advantage to collect biofilm materials grown in situ on three different water levels in the flooded Schlema mine site. The collected water and biofilm samples are then used to determine the microbial diversity of the respective sites. Genomic DNA was extracted and will be sequenced in the next weeks. State of the art techniques such as pyrosequencing will be applied. The data will give an overview of present bacteria, archaea and eukaryotic species. In addition, the metabolic activity of the present microorganisms will be studied by e.g. the DNA-SIP technique. The interaction of uranium with microorganisms will be clarified by a combination of confocal laser scanning microscopy and spectroscopy.

ACKNOWLEDGEMENTS. We thank Dirk Falkenberg for assembling the growth carrier boxes.

[1] Arnold, T. et al. (2011) *Geochim. Cosmochim. Acta.* **75**, 2200-2212.
[2] Brockmann, S. et al. (2010) *J. Fluoresc.* **20**, 943-951.
[3] Zirnstein, I. et al. (2012) submitted.

Uranium contents in plants and mushrooms grown on a uranium contaminated site

N. Baumann, T. Arnold

Uranium concentration in plants, plant compartments and mushrooms, grown on test site Gessenwiese within a former uranium mining heap in eastern Thuringia, was determinate and compared.

Test site Gessenwiese is located near Ronneburg between the villages Grobsdorf and Kauern. All samples were collected on this test site. The test site was installed on the ground of a former and now removed uranium mining tailing heap from the SDAG WISMUT Company. This test site is a part of a research program of the Friedrich-Schiller-University Jena for investigations on acid mining drainage (AMD) and heavy metals retention, especially uranium as well as heavy metal uptake and accumulation into plants and there compartments [1]. Bioavailability of uranium to vegetation in general is discussed e.g. in [2].

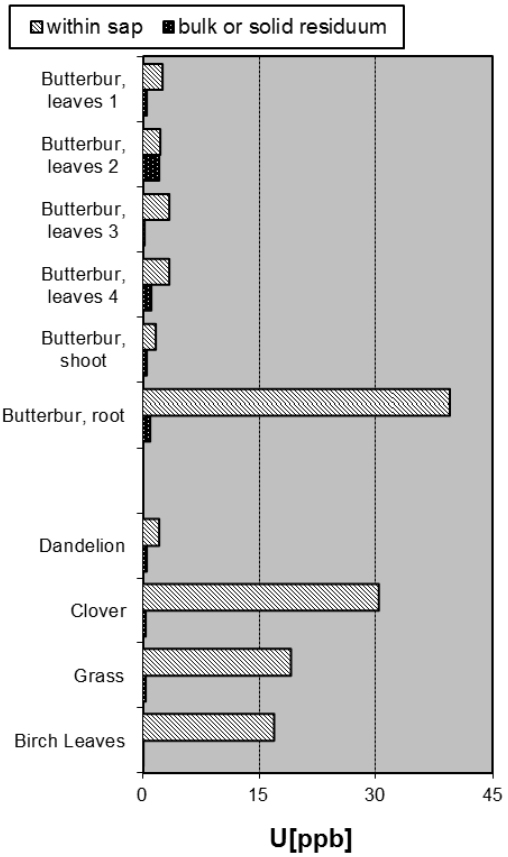

Fig. 1: Uranium contents in plants and plant compartments from the test site Gessenwiese.

EXPERIMENTAL. To find out, if the incorporated uranium from the plants and mushrooms is more in the plant saps or rather accumulated in the cell material, plants and mushrooms after washing the samples were separated into sap and residuum by using a centrifuge at 40,000 rpm. In case it was not possible to get sap by centrifugation at those conditions, e. g. for the mushroom earthfan (Fig. 2) only bulk sample analyses were carried out. After acid digestion, elementary analyzes were made with ICP-MS (Perkin Elmer ELAN 9000) from the gained saps, and from the solid residuum.

RESULTS. In case of the plant compartments, the highest uranium concentration was in the roots, as shown in

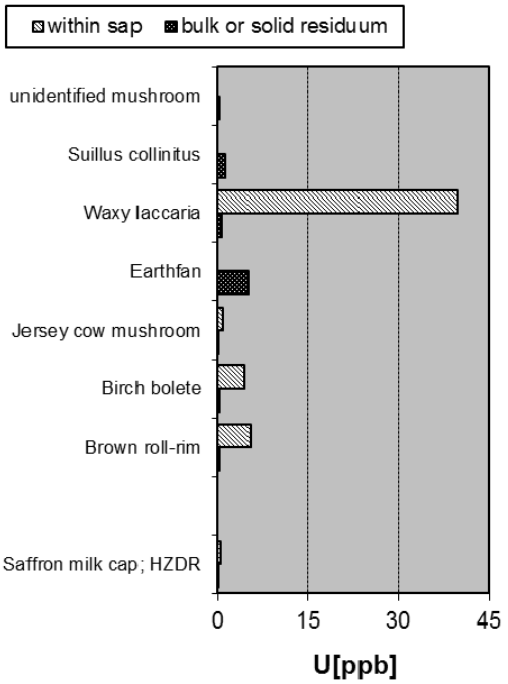

Fig. 2: Uranium contents of various mushrooms from the test site Gessenwiese, compared with a mushroom grown in HZDR grounds terrain (saffron milk cap).

case of butterbur (Fig. 1). The uranium concentration in mushrooms in general was still lower than in plants, except in case of waxy laccaria sap. In both, plants and mushrooms, the uranium concentration in the saps was higher than in the residue, in general. Consequently, only a small part from the incorporated uranium could be bound on the cell material. The uranium concentrations found in plants and mushrooms in general always were lower than the uranium concentration in the surrounding soil water samples from this region [3].

$UO_2SO_{4(aq)}$, the dominant uranium species in the soil water samples [3], does not enter to an adequate extend into the plants, so that it would be reasonable to use the investigated plants and mushrooms for uranium phytoremediation.

To get more uranium into the plant, organic ligands have to be added to the soil, as organic acids e. g. citric acid [4] – if those acids will be able to crack the uranium sulfate complex, which was detected as the main uranium species by TRLFS in the surface water and soil water from this test site, were the investigated plants and mushrooms comes from [3].

ACKNOWLEDGEMENTS. The authors thank U. Schaefer and S. Weiß for technical support, E. Kothe und G. Büchel (both Friedrich-Schiller-Universität Jena) for getting access to test site "Gessenwiese" and the EU for funding within the UMBRELLA project.

[1] Baumann, N. et al. (2010) *Report FZD-530*, p. 47.
[2] Pushon, T. et al. (2003) *Environ. Toxicol. Chem.*, **22**, 1146-1154.
[3] Baumann, N. et al. (2012) *J. Radioanal. Nucl. Chem.*, in press.
[4] Ebbs, D.S. et al. (1998) *J. Exp. Bot.*, **324**, 1183-1190.

Uranium immobilization in biofilms from the underground rock characterization facility tunnel ONKALO (Finland)

E. Krawczyk-Bärsch, H. Lünsdorf,[1] T. Arnold

[1]Helmholtz Centre for Infection Research, Department of Vaccinology and Applied Microbiology, Braunschweig, Germany

In an underground rock characterization facility, the ONKALO tunnel in Finland, massive 5-10 mm thick biofilms were observed attached to tunnel walls where groundwater was seeping from bedrock fractures at a depth of 70 m. In laboratory experiments performed in a flow cell with detached biofilms to study the effect of uranium on the biofilm, uranium was added to the circulating groundwater obtained from the fracture feeding the biofilm. The final uranium concentration was adjusted to $4.25 \cdot 10^{-5}$ M, in the range expected from a leaking spent nuclear fuel (SNF) canister in a future underground repository. EF-TEM studies indicated that uranium in the biofilm was immobilized intracellularly in microorganisms by the formation of metabolically mediated uranyl phosphate, similar to needle-shaped autunite ($Ca[UO_2]_2[PO_4]_2 \cdot 2\text{-}6H_2O$) or meta-autunite ($Ca[UO_2]_2[PO_4]_2 \cdot 10\text{-}12H_2O$).

EXPERIMENTAL. At a depth of 70 m of the ONKALO tunnel in Finland, 771 m from the tunnel entrance, massive biofilms were observed attached to the tunnel walls where groundwater was seeping from bedrock fractures. Biofilm samples were taken for laboratory experiments in flow cells. Uranium was added to the circulating groundwater until a final concentration of $4.25 \cdot 10^{-5}$ M during 42 h was obtained. Biofilm samples were prepared for EF-TEM and EELS studies by fixing them with 1% (vol/vol). In the TEM laboratory, portions of the biofilm were excised and processed further, following the routine embedding protocol, with minor modifications, described in [1]. Ultrathin sections of the biofilm samples, 30 nm thick, were analyzed by means of electron spectroscopy using an in-column filter EF-TEM (LIBRA 120 PLUS; Zeiss, Oberkochen, Germany) at magnifications ranging from 4,000 to 50,000, and micrographs were registered using a bottom-mount 2048×2048 CCD camera (SharpEye; Tröndle, Moorenweis, Germany). Overall ultrastructure in the elastic bright field-mode was acquired from 90 nm sections. Hardware settings were generally used for EELS acquisition, described in [2].

RESULTS. In the cytoplasm of numerous small rod-shaped microorganisms (Ø = 0.4 µm), needlelike crystals with high electron density could be observed (Fig. 1). EELS analysis of these crystals unequivocally identified uranium as a main constituent, based on ionization intensity peaks of O- and/or N-edges ($O_{4,5}$ = 93.5 eV; $N_{6,7}$ = 380.0 eV). In addition, intensity peaks of phosphorus and calcium $L_{2,3}$-edges were obtained as well. The presence of these elements in one crystal is clearly indicated in the elemental distribution analysis of uranium, calcium and phosphorus, which was performed over a selected area of the biofilm. The results provide spectroscopic evidence for the existence of a U-phosphate mineral, similar to autunite ($Ca[UO_2]_2[PO_4]_2 \cdot 2\text{-}6H_2O$ or meta-autunite $Ca[UO_2]_2[PO_4]_2 \cdot 10\text{-}12H_2O$), which formed intracellularly in the small rod-shaped microorganism cells during the experiment. Previous studies have described the formation of meta-autunite as precipitates on the cell surface of numerous microorganism strains isolated from extreme habitats such as uranium waste piles and groundwater from radioactive waste depositories [3, 4]. The formation of intracellular polyphosphate-mediated autunite or meta-autunite was detected in microorganisms isolated from uranium mine wastes as electron-dense granules [3]. The literature explains the formation as the cells' response to the heavy metal stress caused by the release of inorganic phosphate ($H_2PO_4^-$) from the cellular polyphosphate and the subsequent precipitation of uranium as uranyl phosphate ($UO_2[H_2PO_4]_2$) [5]. Microorganisms are known to possess several uranium-resistance mechanisms, often involving precipitation to reduce toxicity. We found that the potential toxicity of uranyl was avoided by the uranium forming strong complexes with phosphate in the cytoplasm of these strains of microorganisms. The phosphate released from the cellular polyphosphate was used, since analysis of the original groundwater indicated negligible amounts of phosphate.

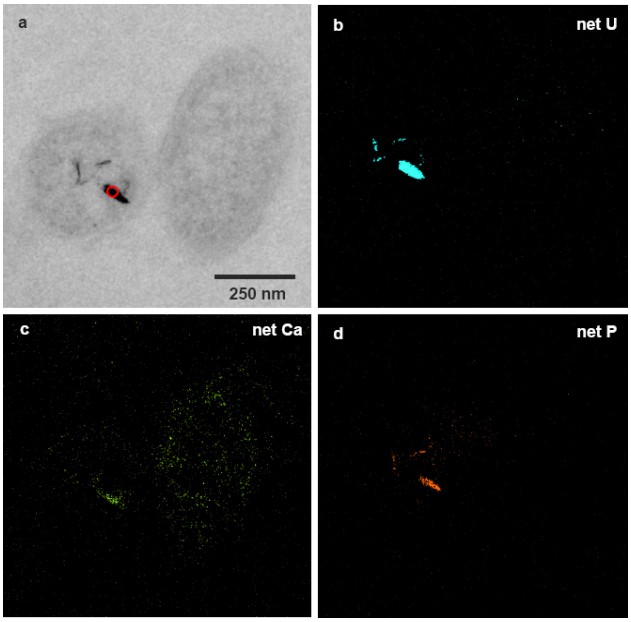

Fig. 1: Needlelike crystals with high electron density, observed in small rod-shaped microorganisms of the biofilm by EF-TEM (a). Distribution analysis of uranium (b), calcium (c) and phosphorus (d) after uranium sorption experiments.

ACKNOWLEDGEMENTS. The European Atomic Energy Community Seventh Framework Programme [FP7/2007-2013] under grant agreement n° 212287, Collaborative Project ReCosy is thanked for financial support.

[1] Lünsdorf, H. et al. (2001) *Methods Enzymol.* **331**, 317-331.
[2] Krawczyk-Bärsch, E. et al. (2012) submitted.
[3] Merroun, M. et al. (2006) *Radiochim. Acta* **94**, 723-729.
[4] Nedelkova, M. et al. (2007) *FEMS Microbiol. Ecol.* **59**, 694-705.
[5] Francis, A.J. et al. (2004) *Radiochim. Acta* **92**, 481–488.

Eukaryotic diversity of biofilms in the underground uranium mine Königstein (Saxony, Germany)

I. Zirnstein, E. Krawczyk-Bärsch, T. Arnold, I. Röske[1]
[1]Institute of Microbiology, Dresden University of Technology, Dresden, Germany

Biofilms grow underground in the uranium mine Königstein (Germany) either as stalactite-like slime communities or as acid streamers in the drainage channels. The eukaryotic diversity of these biofilms was analyzed by microscopic investigations and by molecular methods (PCR, cloning, sequencing). The biofilm communities of the Königstein environment consist of a variety of groups belonging to nine major taxa: ciliates, flagellates, amoebae, heterolobosea, fungi, apicomplexa, stramenopiles, rotifers, arthropoda and a large number of uncultured eukaryotes.

EXPERIMENTAL. Biofilms grow underground in the mine galleries in a depth of 250 m (50 m above sea level) of the Königstein mine. The underground uranium mine Königstein (Saxony, Germany) represents conditions comparable with an acid mine drainage, i.e. low pH 2.86 ± 0.05, high concentrations of heavy metals (iron 47-90 mg/L), and in addition absence of light and high concentrations of uranium (9.3-69.5 mg/L) [1].
The mine habitat offers two types of ecological niches associated with copious biofilm growth. The first one grows in the drainage channels as gelatinous filament streamers called acid streamers. The second type of biofilm was collected in a parallel gallery by breaking off stalactite-like structures from the ceiling (Fig. 1).

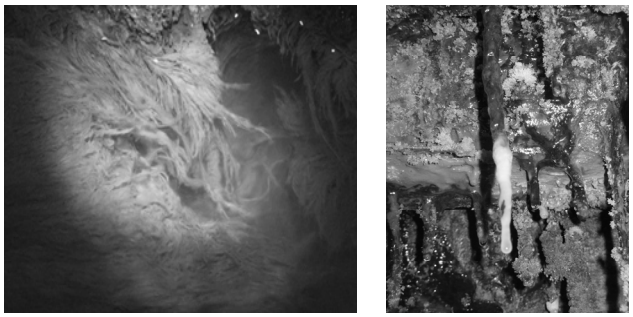

Fig. 1: Left: Acid streamer biofilms growing in the drainage channel of the gallery 390 in a depth of 250 m of the former uranium mine Königstein (Germany), Right: Stalactite-like biofilms hanging from the ceiling.

For analyzing eukaryotic diversity two methods were selected: microscopical study and molecular analyses of the biofilm samples. For microscopical investigations a TCS-SP2 CLSM (Leica Microsystems) was used.
The second used method based on extracted total DNA with the extraction method by Johnson [2]. After that the DNA fragments were amplified by 18S-rDNA-PCR using the primer 515F and 1209R [3]. Amplification was performed for 30 cycles with an annealing temperature of 55 °C using the 5'-Prime MasterMix from Eppendorf. The purified amplified 18S rDNA fragments were cloned into *E. coli* (chemical competently TOP 10 F') using the pMBL T/A Cloning Kit (Genaxxon BioScience) following the manufacturers' recommendations. The recombinant clones (103 clones) were selected by blue-white colony selection. Representative clones were selected for sequencing to enable the phylogenetic classification and compared to sequences available in the data base of National Center for Biotechnology using BLASTN.

RESULTS AND DISCUSSION. The biofilm communities of the Königstein environment showed a low eukaryotic biodiversity due to the extreme conditions in the underground mine (no light, high concentrations of iron and uranium, low pH). It consists of a variety of groups belonging to nine major taxa: ciliates (*Oxytricha sp. Vorticella sp.*,), flagellates (*Bodo saltans, Bodo angustus, Rhynchomonas sp*.), amoebae (*Vannella sp., Thecamoebae sp*.), heterolobosea (*Vahlkampfia sp*., *Naegleria sp., Paravahlkampfia sp*.), fungi, apicomplexa (*Eimeriidae*), stramenopiles (*Diplophrys archeri*), rotifers (*Rotaria sp*.), arthropoda (*acari*) and a large number of uncultured eukaryotes, denoted as acidotolerant eukaryotic cluster (AEC). Almost a third of all sequences belong to the AEC group. Most (9 of 13) of these uncultured sequences are similar to uncultured eukaryote species isolated from Rio Tinto site (Spains river of fire) [4].

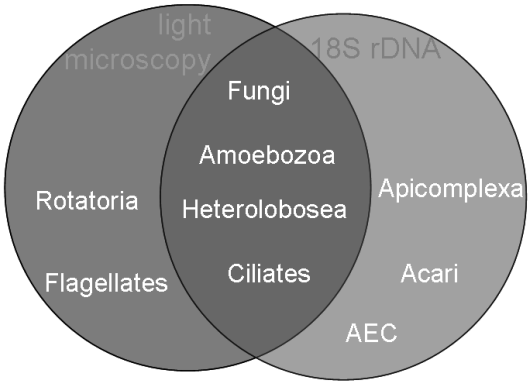

Fig. 2: Identification of eukaryotic groups detected by light microscopy and 18S rRNA gene analyses. Species of groups in the circle colored grey were detected by light microscopy, groups in the blue circle determined by genetic analyses. Groups situated in the overlapping part were analyzed by both investigations.

The results obtained showed that there were differences by the two used methods (Fig. 2). Species of fungi, amoebozoa, heterolobosea and ciliates were detected by both methods. Only genetic analyses identified the presence of apicomplexa, acari and a cluster of AEC in the uranium mine Königstein. Additional to these results, flagellates and rotatoria were only visualized by light microscopy.
Flagellates, stramenopiles and rotifers were detected for the first time in milieus characterized by high concentrations of uranium. This study shows that not only bacteria and archaea may live in extreme environments, but also several species of eukaryotes, clearly showing their potential influence on carbon cycling and metal immobilization within biofilms.

ACKNOWLEDGEMENTS. We would like to thank Dr. K. Hänel (former: VVB Wasserversorgung und Abwasserbehandlung, Leipzig) for their help in microscopic characterization of the flagellates and the Wismut GmbH for their admission for sampling.

[1] Arnold, T. et al. (2011) *Geochim. Cosmochim. Acta*, **75**, 2200-2212.
[2] Johnson, D.B. et al. (2005) *J. Microbiol. Methods* **60**, 299-313.
[3] Baker, B.J. et al. (2009) *Appl. Environ. Microbiol.* **75**, 2192-2199.
[4] Amaral-Zettler, L.A. et al. (2011) *ISME J.* **5**, 42-50.

Bacterial isolates from pore water of the Mont Terri Rock laboratory

A. Geissler

The bacterial diversity in a porewater sample from the Mont Terri rock laboratory was studied by a culture-dependent method under anaerobic conditions. The retrieved bacterial isolates were analysed by 16S rRNA gene analysis and affiliated with *Betaproteobacteria* especially *Acidovorax* spp. and *Cupriavidus* spp. and *Gammaproteobacteria* especially *Pseudomonas* spp.

EXPERIMENTAL. The Mont Terri Rock Laboratory is situated in the north-west part of Switzerland. The pore water sample HTW3 was collected until June 2011. Immediately after arriving, the sample was successively filtered through a 0.45 µm, 0.22 µm and 0.1 µm sterile filter. The filters were frozen at −20 ºC for further analysis and the filtrates as well as a portion of the original water were used for the culture-dependent analysis. 0.1 mL aliquots of the water were spread on 50% R2A plates or G1M1 plates [1] and incubated at room temperature or 30 ºC under anaerobic conditions.

RESULTS. By using these two different media, we were able to enrich and isolate bacteria from the pore water of the Mont Terri rock laboratory. After 4 weeks of incubation the observed colonies were picked and transferred to new plates. The colonies were white or yellow coloured, circular shaped but with different size.

The 16S rRNA gene of the isolates was amplified, sequenced and phylogenetic analyzed to get some information about these isolates.

All the isolates enriched and isolated from 50% R2A media were affiliated with *Betaproteobacteria* (Fig. 1).

The 16S rRNA gene of isolate HTW3-12 was 99% similar to the 16S rRNA gene of the uncultured *Acidovorax sp.* A19, which was retrieved from a low-grade copper bioleaching heap, and *Acidovorax facilis* 228. Interestingly, 16S rRNA genes of *Acidovorax* spp. were also detected in the clone library of sample MT-2 (see clones MT-2-81 and MT-2-113 in Fig. 1) [2]. The sample MT-2 is an Opalinus clay sample taken from the Mont Terri rock laboratory by drilling. Both samples, MT-2 and HTW3, were taken from the same location in the rock laboratory. In this case, we could identify *Acidovorax* spp. by a culture-dependent method in the porewater and a culture-independent method in the clay sample.

In addition, the isolate HTW3-8 (Fig. 1) was closely affiliated with the betaproteobacterium *Cupriavidus campinensis* WS2, the type strain of *Cupriavidus campinensis* [3].

From the MT-2 sample were also bacteria isolated on R2A media but with a slightly different method [4]. *Bacilli* and *Clostridia* were in comparison to our results detected in the Opalinus clay sample [4].

A nitrite reducing media (G1M1) was also used to isolate bacteria from the pore water. In comparison to the R2A media, only representatives of Gammaproteobacteria were enriched on the G1M1 media. The 16S rRNA genes of these isolates were similar to the 16S rRNA gene of *Pseudomonas stutzeri*, a well known denitrifier.

The limited bacterial diversity observed by the culture-dependent method in the pore water from the Mont Terri rock laboratory can be explained by the unfavorable living conditions in the Opalinus clay. In addition, we could demonstrate that it also depends on the used media, what kind of bacteria can be enriched and isolate from the sample. The used R2A media is specific for oligotrophic microorganisms, whereas the G1M1 media is specific for nitrite reducing bacteria.

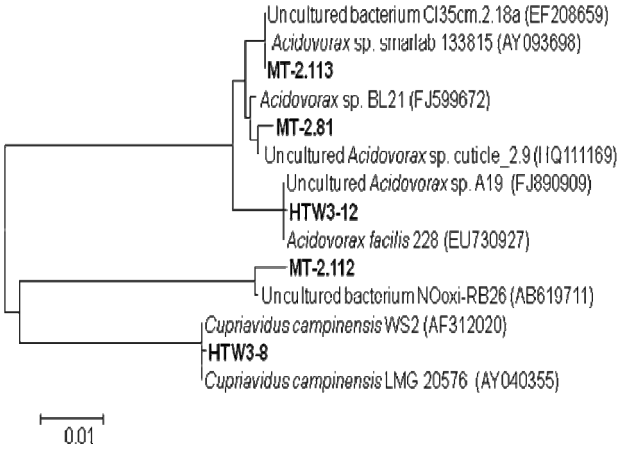

Fig. 1: Phylogenetic dendrogramm of the 16S rRNA genes of the betaproteobacterial isolates obtained from the Mont Terri pore water HTW3 and sequences retrieved from the clone library of sample MT-2 [2].

The further morphological and biochemical characterization of the observed isolates as well as the study of their interactions with radionuclides are in progress.

Our results improve the knowledge of the bacterial diversity in pore water of Opalinus clay which is a potential host rock for a nuclear waste repository.

ACKNOWLEDGEMENTS. This work was funded by BMWi through contract 02E10618.

[1] Heylen, K. et al. (2006) *Appl. Environ. Microbiol.* **72**, 2637-2643.
[2] Bachvarova, V. et al. (2011) *Report HZDR-001*, p. 30.
[3] Goris, J. et al. (2001) *Int. J. Syst. Evol. Microbiol* **51**, 1773-1782.
[4] Bachvarova, V. et al. (2010) *Report FZD-530*, p.18.

Nutrient induced changes in natural bacterial community of the Opalinus clay of Mont Terri

S. Selenska-Pobell, V. Bachvarova

The 16S rRNA gene retrieval revealed unexpected high diversity in unperturbed Opalinus clay samples, collected from the Mont Terri underground laboratory. Treatments of the samples with R2A medium, commonly used for recovery and cultivation of bacteria from oligotrophic environments, resulted in strong propagation of two bacterial groups, not identified in the original samples. These groups masked the natural bacterial diversity in the Opalinus clay.

During the last decade it was demonstrated that bacteria are distributed in almost all extreme habitats, including also the deep subsurface geological layers [1]. It was also demonstrated that bacteria strongly influence many geochemical processes in nature, including the behavior of heavy metals and radionuclides as well [2]. For this reason, it is important to study bacterial community in the Mont Terri underground laboratory foreseen for deposition of highly radioactive wastes. On one hand, it is important to define the biological potential of this environment. On the other hand, it may help to predict the influence of bacteria on the migration of radionuclides which may be released there in case of accidental seep out from the depository.

EXPERIMENTAL. Two 16S rDNA clone libraries were constructed by using $16SrRNA_{7F}$ and $16SrRNA_{1513R}$ primers as described in [2]. The first library was constructed by using total DNA recovered from the unperturbed sample corresponding to the inner part of the drilling core BHT-1, refereed further as MT-2 [3]. For the second library total DNA recovered from the parallel sample, MT-2-R2A, corresponding also to the inner part of the core, but treated with R2A medium for two weeks [3], was used as a template. The analysis of the constructed libraries was performed as described in [2].

RESULTS. As evident from the results presented in Fig. 1, nine different bacterial groups were identified in the unperturbed MT-2 sample. The largest group found in the sample includes rather diverse representatives of *Clostridia,* which were affiliated with five distinct clostridial families. The second largest group in the MT-2 sample was, in contrast, very uniform and it was closely related to *Acidovorax* sp., belonging to the Beta subclass of Proteobacteria. Representatives of *Acidovorax* are nitrate reducers able to reduce U(VI) to U(IV) as well [4]. The third predominant group was affiliated with *Bacteroidetes*, which are widely distributed in water, soils and sediments and are characterized as a bacterial group which is most adaptive to changes in the nutrient conditions in the environment [5]. Small populations of Alpha-, Gamma-, and Deltaproteobacteria were identified in the MT-2 sample as well.

Treatments with R2A medium lead to stimulation of only two groups of *Firmicutes* which completely overgrew in the sample MT-2-R2A the rest of the bacterial populations characteristic for the unperturbed original sample MT-2 (Fig. 1). About 50% of the retrieved genes in the MT-2-R2A sample were affiliated with *Paenibacillus* sp. and 45% with the non-pathogenic clostridial group of

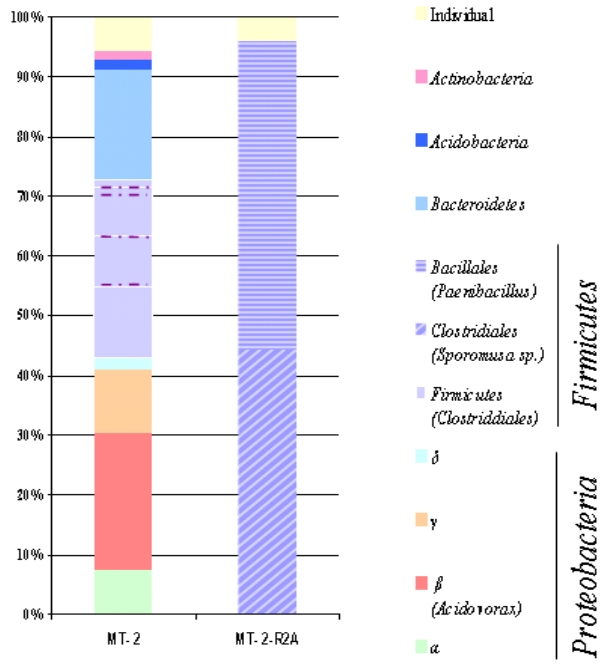

Fig. 1: Comparison of the bacterial diversity in the unperturbed MT-2 sample and the R2A medium treated sample.

Sporomusa sp. It is noticeable that both these species were not identified in the unperturbed sample MT-2.

Only about 5% of the clones of the MT-2-R2A library were categorized as individual.

The strong propagation of only two big groups of bacteria in MT-2-R2A looks in contradiction with the earlier demonstrated increased number of RISA fragments in the same sample [3]. However, one can explain these conflicting results by the fact that the two mentioned groups of *Firmicutes,* shown to predominate the sample MT-2-R2A, possess very high number of ribosomal RNA (*rrn*) operons (up to 10) which contain the most variable bacterial intergenic spacers (IGSs) between their 16S and 23S rRNA genes [6]. The mentioned author demonstrated that in *Paenibacillus* the IGSs vary even in one and the same strain [6]. Moreover, *Paenibacillus* is the only bacterial genus in which some representatives may contain the 5S rRNA gene integrated in their IGS regions. For this reason, the appearance of many bands of the RISA pattern of the sample MT-2-R2A shown in [3] confirms the strong proliferation of *Firmicutes* possessing extremely variable IGSs. Our results demonstrate that using of a combination of methods is required for reliable analysis of such complex samples as those collected from the Mont Terri. In addition, we demonstrate that the bacterial community is easy to activate by changes of the nutrient conditions.

ACKNOWLEDGMENTS. This work was funded by BMWi, contract 02E10618.

[1] Nedelkova, M. et al. (2005) *Underground Injection Science and Technology,* p. 521-536, Elsevier, Amsterdam.
[2] Geissler, A. et al. (2009) *Geobiology* **7**, 282-294.
[3] Bachvarova, V. et al. (2011) *Report HZDR*-001, p. 30.
[4] Cardens, E. et al. (2008) *Appl. Env. Microb.* **74**, 3718–3729.
[5] Lebaron, P. et al. (2001) *FEMS Microbiol. Ecol.* **34**, 255-266.
[6] Dingman, D.W. (2004) *Can. J. Microbiol.* **50**, 779-791.

Bacterial communities in pore water of Mont Terri found before and after injection of nitrate

S. Selenska-Pobell, G. Radeva,[1] A. Geissler, H. Moors,[2] N. Leys[2]
[1]Institute of Molecular Biology, Bulgarian Academy of Science, Sofia, Bulgaria; [2]Belgian Nuclear Research Centre SCK•CEN, Mol, Belgium

Potential activity of natural bacterial community in opalinus clay pore water was studied in the frames of the Bitumen-Nitrate (BN) experiment running at the Mont Terri underground laboratory. Applying direct molecular methods we demonstrate a strong shifting in the indigenous bacterial community after injection of nitrate into one of the packed-of intervals of the BN-experiment.

The goal of the BN experiment is to understand the influence of nitrate and organic degradation products of bitumen on safety of burying bituminized intermediate-level radioactive wastes in opalinus clay. This *in situ* experiment takes place in the international underground experimental laboratory Mont Terry in Switzerland. It is based on treatments and analyses of the pore water inside of a tube inserted in the opalinus clay. The latter is separated in three packed–off intervals each supplied with a filter screen and its own recirculation solution [1]. In this report bacterial community in one of the BN intervals and its response to increased nitrate concentrations were studied.

EXPERIMENTAL. Total DNA was recovered from two samples: the first one, called BN1, represented artificial pore water (APW) which was circulating for 3 months in the interval I of the BN test system. The second one (BN1+N) was collected from the interval I 24 hours after the addition of APW supplemented with 93 mg/L nitrate. Analyses of bacterial communities, established in the two samples, were performed by ribosomal intergenic amplification (RISA) using universal bacterial primers 16S $rDNA_{968}$ and 23S $rRNA_{130}$, consequent cloning and sequencing of the 16S rRNA gene parts of the amplicons as described in [2].

RESULTS. As evident from the results presented in Fig. 1, only 24 hours after the addition of nitrate, the RISA profile of the BN1 sample was significantly changed. Some of the bands of this original untreated sample were not found in the profile of the nitrate supplemented sample BN1+N. Moreover, new bands appeared in the latter sample.
These results indicate that the nitrate treatment stimulated strong proliferation of bacterial groups which replaced the populations predominating the initial sample. In order to clear which are the members of the untreated natural opalinus clay pore water bacterial community and to find out which bacterial groups were stimulated by the nitrate addition, the RISA fragments of the samples BN1 and BN1+N were subjected to further cloning and sequencing analyses. Results of these analyses are presented in Fig. 2.
As shown in the figure natural bacterial community of interval 1 (sample BN1) is strongly predominated by representatives of *Clostridiales* which belong to the *Firmicutes* division. In addition to the clostridial populations, two smaller groups, one of *Betaproteobacteria* (limited to the *Acidovorax* species) and a second one of *Bacteroidetes* are characteristic for this community. Interestingly, *Clostridiales* and *Acidovorax* sp. were found to predominate also in unperturbed rock opalinus clay samples [3].
The nitrate addition stimulated in the sample BN1+N strong proliferation of *Bacteroidetes* and also of *Alpha-* and *Deltaproteobacteria* which were not identified in the untreated samples, most probably due to their presence there in low numbers which were below the detection limit of the applied method.
The stimulated bacterial groups in the BN1+N sample contain oligotrophic and/or chemolithoautotrophic representatives, able to reduce and respire nitrate.

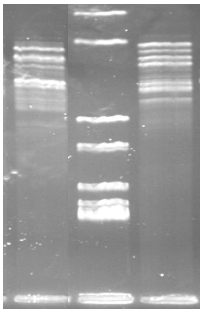

Fig. 1: RISA profiles of the samples collected from interval I before (BN1) and 24 hours after the addition of nitrate (BN1+N).

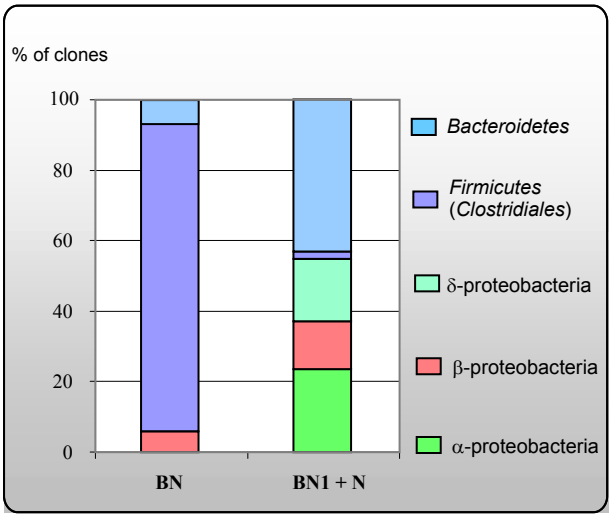

Fig. 2: Nitrate induced shifting in bacterial community structure in the pore water of interval I.

This finding indicates that the natural pore water bacterial community possesses a potential to "sense" and consume nitrate even without addition of organic matter. Experiments including addition of nitrate + organic matter (acetate) are in progress in the frames of the BN experiment. These experiments will allow to make conclusions about the safety of bituminization of intermediate-level radioactive wastes for their deposition.

[1] http://www.mont-terri.ch/Work_Programme/WP_Ph15_web.pdf International Research Project Mont Terri.
[2] Radeva, G. et al. (2005) *Can. J. Microb.* **51**, 910-923.
[3] Selenska-Pobell, S. et al. (2012) this report, p. 19.

Bacterial diversity in Spanish clays

M. López Fernández,[1] M. L. Merroun,[1] A. Geissler
[1]Department of Microbiology, University of Granada, Granada, Spain

In this work, we studied the differences in the bacterial community in several bentonite samples from clay formations located in different regions of Cabo de Gata, Almeria, Spain, using the Ribosomal Intergenic Spacer Amplification (RISA) approach and molecular methods based on 16S rRNA gene analysis.

A reliable performance assessment of radioactive waste repository depends on a better knowledge on the interactions of radionuclides and natural microorganisms of geological formations (salts, granitic and clays) used as host rock candidate for these disposal systems. In Spain, Clay deposits from Cabo de Gata region, Almeria have been well characterized [1] and considered in this study as host rock candidate for geological disposal of radioactive wastes. In the current work we characterize the bacterial diversity in Bentonite samples from Cabo de Gata, Spain.

EXPERIMENTAL. The bentonite samples used in this study were collected in March 2011 from Cabo de Gata, Almeria, Spain. The sample called Bentonite I, consisting of BI-2 (aerobic sample) and BI-3 (anaerobic sample recovered from a depth of 20 cm), was taken from El Cortijo de Archidona; the sample called Bentonite II was collected from El Toril and finally sample Bentonite IV (BIV-2, aerobic sample and BIV-3, anaerobic sample from a depth of 20 cm) from Los Trancos (Fig. 1). To recover total DNA from the Spanish Clay we took 5 g and used a method previously described [2] with small modifications [3].

Fig. 1: Bentonite sampling.

For a quick estimation of the bacterial community structure the Ribosomal Intergenic Spacer Amplification (RISA) approach was used as described earlier, using the primer pair $16S_{969F}$-$23S_{130R}$ [3]. After that from each sample a bacterial clone library was constructed. 16S rRNA gene fragments were amplified and cloned by using bacterial universal primers ($16S_{8f}$ and $16S_{1513r}$) and analysed by Restriction Fragments Length Polymorphism (RFLP) analysis. The resulting RFLP patterns of 100 clones per library were grouped together and one representative of each RFLP group was selected for sequencing.

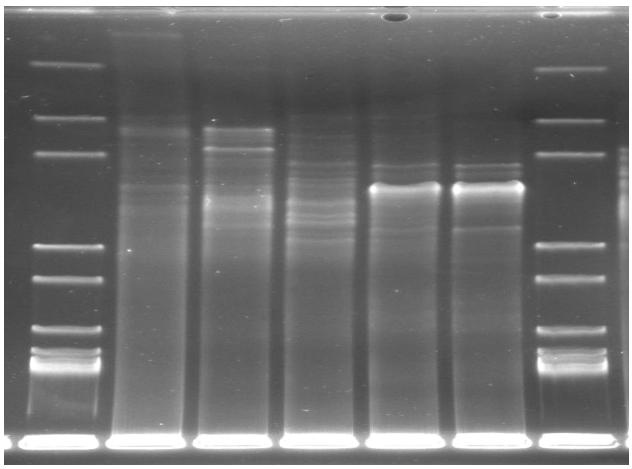

Fig. 2: RISA analysis of the samples: (1) BI-2; (2) BI-3; (3) BIV-2; (4) BIV-3; (5) BII-2; (M) 1kb DNA Ladder.

RESULTS. As evident from the results presented in Fig. 2, the RISA patterns obtained are different for each sample, which represent different bacterial communities in the analyzed Spanish Clay samples.
The reason for this could be that the samples were taken from different locations and/or from different depths. But there are also some similarities between the pattern of sample BIV-3 and BII-2. Differences between the samples were also obtained by RFLP analysis (Tab. 1). As shown in table 1 samples BI-3 and BIV-2 are the most diverse while sample BII-2 and BIV-3 present the lowest diversity.

Tab 1: RFLP analysis of the clone libraries from the samples BI-2, BI-3, BII-2, BIV-2 and BIV-3.

Sample	Groups		Individuals
	nº	nº of clones	nº of clones
BI-2	20	52	47
BI-3	8	25	75
BII-2	14	86	14
BIV-2	14	40	60
BIV-3	7	88	12

So far, preliminary results indicate that the main population in the studied samples are Proteobacteria. But the full analysis of all obtained sequences will give us more information about the bacterial diversity in the studied Spanish clay samples and the differences between these samples.

ACKNOWLEDGEMENTS. This work was supported by grants EEBB-I-2011-02430 and CGL2009- 09760 from the Spanish Ministry of Sciences and Innovation.

[1] Villar, M.V. et al. (2006) *J. Iber. Geol.* **32**, 15-36.
[2] Selenska-Pobell, S. et al. (2001) *Antonie Van Leeuwenhoek* **79**, 149-161.
[3] Bachvarova, V. et al. (2011) *Report HZDR-001,* p. 30.

Production of recombinant S-layer proteins using different expression systems

F. Lederer, S. Kutschke, K. Pollmann

Surface layer (S-layer) proteins are wide spread bacterial structures which are part of the cell envelope of many bacteria and nearly all archaea. These proteins exhibit the ability to form two-dimensional crystal lattice at the cell surface and technical surfaces. In addition to their beneficial features for bacteria such as working as a molecular sieve, S-layer proteins are able to bind toxic heavy metals. Depending on the S-layer variants they bind with high affinities huge amounts of metals such as uranium, gold or palladium. Genetic modifications of S-layer proteins enable the design of proteins for specific purposes. Here we compared three different protein expression systems for synthesis of recombinant S-layer proteins in order to find the most effective host organism.

EXPERIMENTAL. The S-layer genes of *Bacillus* spec. JG-B12 (2586 bp), *Lysinibacillus sphaericus* JG-A12 (*slfB*-3712 bp, *sllB*-3303 bp) and *Lactobacillus acidophilus* 4356 (1485 bp) were amplified with polymerase chain reaction and cloned into three different expression vectors pET-30 Ek/LIC (*Escherichia coli* expression vector) [1,2], pNZ8148 (*Lactococcus lactis* expression vector) and LIC 2151K SUMO3 (*Pichia pastoris* expression vector). These S-layer gene vector constructs were transformed into the including host organisms and incubated at different adapted temperatures for 24-48 hours. The S-layer protein expression rates of positive clones were analyzed in appropriate medium with different inductor quantities combined with protein purification and SDS PAGE analyzes.

RESULTS. The four different S-layer protein genes of three different organisms were successfully cloned in *E. coli* and *L. lactis*. In contrast, the preparation of *P. pastoris* clones failed completely. *E. coli* exhibited high protein expression rates in the cytoplasm of the cells (up to 26% of bacterial biomass are recombinant S-layer proteins) while the expression rate in *L. lactis* cells was significantly lower. The recombinant proteins produced by *L. lactis* were secreted to the medium. The S-layer protein SllB expressed with the pET-30 Ek/LIC expression vector in *E. coli* BL21(DE3) was partly secreted to the medium. In Table 1 we compared the three different expression systems regarding their efficiency to produce recombinant S-layer proteins. In principal, the production of recombinant S-layer proteins in *E. coli* was successful. However, the subsequent protein preparation did not show the typical S-layer structures. In contrast, light microscopic images of purified S-layer proteins produced and secreted by *L. lactis* point to the formation of typical S-layer structures. The successful heterologous expression of three different S-layer proteins in two different expression systems was demonstrated by SDS-PAGE and is shown in Fig. 1.

Tab. 1: Comparison of three different protein expression systems regarding their characteristics in S-layer protein expression.

Expression system/ characteristics	*E. coli*	*Lactococcus lactis*	*Pichia pastoris*
Organism	Gram neg. bacteria	Gram pos. bacteria	yeast
Vector	pET-30 Ek/LIC (Novagen)	pNZ8148 (MoBiTec)	LIC 2151K (Life sensor)
Secretion	typically not	yes	yes
Analyzed S-layer genes	*slfB*, *sllB*	*sllB*, *slfB*, SL B12, SL *L. acidophilus*	*sllB*, *slfB*
S-layer structure	denatured	intact	–
Cultivation costs	economic	cost-intensive	cost-intensive

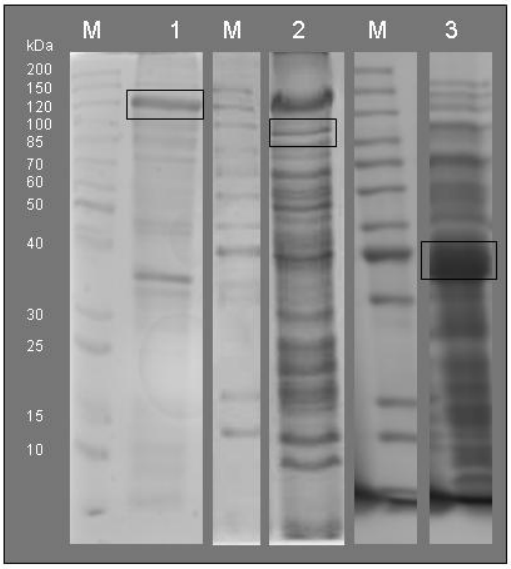

Fig. 1: Expression of the S-layer protein SllB of *L. sphaericus* JG-A12 (lane 1, 116 kDa) in *E. coli*, the functional S-layer protein of *Bacillus* spec. B12 (lane 2, 91 kDa) and the functional S-layer protein of *L. acidophilus* (lane 3, 52 kDa) in *L. lactis* cells demonstrated by SDS-PAGE analyses of the cell extract. M, molecular mass standard. The black boxes mark the expressed S-layer protein bands.

DISCUSSION. The identification of a well adapted S-layer protein expression system is essential for the development of genetically modified S-layer proteins with defined characteristics. Important parameters for recombinant protein production and design are low cultivation costs, chosen host, secretion potential, purification abilities and functionality of S-layers. With the presented analyses we identified *Lactococcus lactis* in combination with the pNZ8148 vector as the most suitable S-layer protein expression system. This system enabled protein secretion as well as formation of native-like S-layer structures.

ACKNOWLEDGEMENTS. The work was supported by the German Federal Ministry of Education and Research (BMBF); project BIONA (BMBF/DLR 01RB0805A).

[1] Pollmann, K. et al. (2007) *Appl. Microbiol. Biotechnol.* **75**, 1079-85.
[2] Lederer, F. et al. (2010) *Microbiology* **75**, 3584-95.

Influence of different preparation and storage possibilities on the thermal stability of the S-layer protein of *Bacillus* JG-B58

U. Kummer, N. Eslami,[1] K. Fahmy, S. Kutschke
[1]Faculty of Pharmacy, Behesty University of Medical Science, Teheran, Iran

In this study, Differential Scanning Calorimetry (DSC) was used to analyse the influence of different preparation methods and storage conditions on S-layer stability of *Bacillus sp.* JG-B58.

EXPERIMENTAL. The *Bacillus* sp. JG-B58 was cultivated in NB medium and harvested at the exponential growth phase.
The preparation of S-layer protein was performed using a method M1 based on cell disruption [1] and method M2 using chaotropic salt [2]. After quantification of protein content one part of the sample was stored in standard buffer with and without NaN_3 and one part was lyophilized.
The idea for using DSC was the possibility to describe the thermostability of organic polymers. The DSC measurements were performed using 0.2 mg/mL S-layer protein in a temperature range from 30 to 80 °C by NanoDSC (TA Instruments) and the baseline difference method.

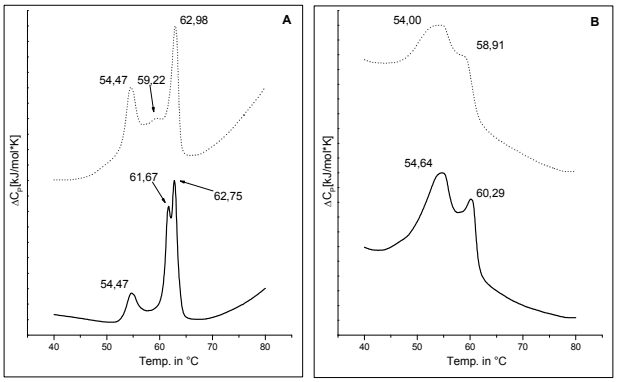

Fig. 1: DSC spectra of S-layer proteins prepared by M1 and M2 (A); DSC-spectra of proteins after storage using two different methods (dotted line M2, compact line M1) (B).

RESULTS. The results of DSC measurements document qualitative differences in thermal stability of S-layer proteins. Figure 1 shows differences in the thermal stability of S-layer after the preparation by using different methods. Three melting temperatures could be defined in the DSC spectra, which may assigned to unfolding monomers (Tm_1) and paracrystalline protein arrays (Tm_2, Tm_3).
Figure 1A shows that Tm_2 is shifted from 61.67 °C after preparation according M1 to lower temperatures (59.22 °C) when using preparation method M2. In contrast, Tm_1 stayed constant at 54.47° C. Additionally, Tm_3 shifted from 62.75 °C to higher temperatures (62.98 °C) in samples prepared by M2. A sharper Tm_1 peak points to changes in protein structure during preparation using method M2. Especially the shift of Tm_2 indicates changes of the protein structure caused by different preparation conditions. Moreover, the ratio of the heights of Tm_2 and Tm_3 peak is changed depending on the preparation method.
Figure 1B compares DSC-spectra of proteins stored in standard buffer in the fridge or lyophilized. In comparison to the buffered samples, the spectra of the lyophilized sample are slightly shifted to lower temperatures. The peaks of the spectrum of the buffered sample are sharper

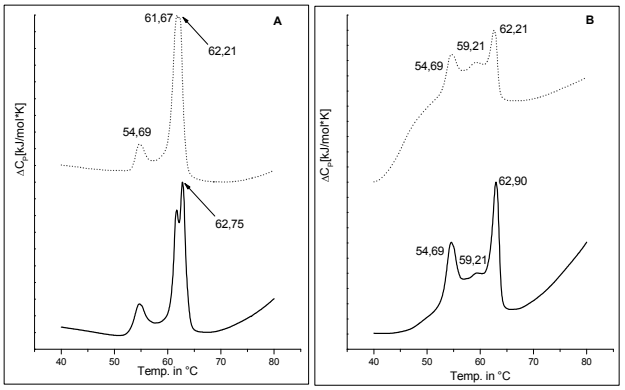

Fig. 2: The DSC spectra show the influence of NaN_3 in French press sample (dotted line without and compact line with NaN_3) (A), and the influence of NaN_3 after preparation [2] (dotted line without and compact line with NaN_3) (B).

than those of the lyophilized sample. In summary, the spectra in Fig. 1B are relatively similar, indicating that the different storage methods have no significant influence on the protein behavior. However, it is necessary to determine possible differences in the secondary structures and changes in the physical and chemical characteristics by other methods like CD.
In another experiment, the influence of NaN_3 during the storage of S-layer proteins on structure and characteristics of the proteins was examined using DSC. The results of these measurements are shown in Fig. 2. Especially differences that are detected at Tm_3 demonstrate a strong influence of NaN_3 during storage of S-layer prepared by M1. This peak is shifted from 62.75 °C in case of NaN_3 containing sample to 62.21 °C in the case of NaN_3 free sample. A second difference between the spectra of the two samples is visible at Tm_2. This peak occurs in both spectra at the same temperature, but the ratio of the height in comparison to Tm_3 is clearly changed. This peak is sharper in the sample containing NaN_3. Figure 2B shows the DSC-spectra of NaN_3-containing or NaN_3-free S-layer samples proteins prepared by M2. The results are similar to the results shown in Fig. 2A. However, the differences between the samples are less significant. In addition, a small shift of the Tm_3 peak from 62.21 °C to 62.90 °C is detectable.
In summary, the differences between the Tm_3 values of the samples are small. The DSC measurements give a preliminary estimate of the stability of S- layers. More detailed information on S-layer stability will be obtained from CD or IR spectroscopy.

[1] Raff, J. (2002) *Report FZR-358*.
[2] Lortal, S. et al. (1991) *J. Gen. Microbiol.* **137**, 549-59.

Effect of various storage conditions on the survival of gram-positive bacteria

S. Fischer, M. Suhr, S. Kutschke, K. Pollmann, A. Barkleit, J. Raff

Storage conditions sustainably affect properties of bacterial biomass and have thus an important influence on their behavior regarding e.g. the interaction with metals. For reproducible results in studies it is absolutely necessary to use microorganisms from one single cultivation batch having same properties. The present investigation demonstrates the impact of different storage conditions on the vitality and stability of bacterial biomass in a time scale of 3 weeks.

Storage of biomass is not trivial. Optimal conditions highly depend on the kind of the biological material, so it is necessary to vary different parameters like pH, ionic strength, nutrients and temperature [1]. In the present study, different temperatures during storage were tested. The aim was to verify the presence of surface-layer (S-layer) proteins and the vitality of the cells to choose optimal storage conditions, allowing many experiments with identical biomass. For the investigation a gram-positive isolate from the uranium mining waste pile "Haberland" nearby Johanngeorgenstadt (Saxony) is used. Like many other bacteria and archaea, the chosen strain possesses an S-layer which covers as outermost envelope the cell and protects it against environmental impacts. S-layer proteins also self-assemble on different technical surfaces in regularly structured 2-D lattices, maintaining their high heavy metal binding capacities [2]. To study the biosorption of toxic and rare metals by living bacterial cells and parts thereof, all studied objects have to be isolated from one batch.

EXPERIMENTAL. *Bacillus* sp. JG-B53 was cultivated in a 5 L bioreactor at 30 °C in nutrient broth (NB) medium (5 g/L peptone, 3 g/L meat extract). Cells were harvested under sterile conditions in the late exponential phase and washed in 0.9% NaCl (pH = 6). Aliquots of the wet biomass were prepared and stored as a thin film under the following conditions: (1) standard buffer (50 mM Tris, 1 mM $MgCl_2$, pH 7.5) at 4 °C, (2) standard buffer (50 mM Tris, 1 mM $MgCl_2$, 3 mM NaN_3, pH 7.5) at 4 °C, (3) 0.9% NaCl, 4 °C, (4) 15% glycerin, −20 °C, (5) 15% glycerin, −70 °C, (6) without any additive at −20 °C and (7) without any additive at −70 °C. A fresh reference sample was directly analyzed after the harvest. The stored samples were investigated after time periods of 2 days, 1, 2, and 3 weeks.
The frozen samples were incubated for 3 minutes in a 30 °C prewarmed water bath and washed three times with 0.9% NaCl.
To get information about the morphology, light microscopic pictures of the cells were taken with an Olympus BX61 microscope in phase contrast mode. The vitality of the bacteria was verified with LIVE/DEAD staining (SYTO® 9 green-fluorescent nucleic acid stain and red-fluorescent nucleic acid stain with propidium iodide) and microscopic analyses with the fluorescence filters U-MNU and U-MSWB (Olympus BX61 microscope), done according to [3]. Proteins were extracted by an incubation with 10% SDS for 10 minutes at 95 °C. The determination of the total protein content in the supernatant was performed according to Lowry [4]. The protein profile and the presence of S-layers were analyzed by SDS-PAGE using a 10% polyacrylamide separating gel, with a normalized amount of 2 µg protein per slot [5].

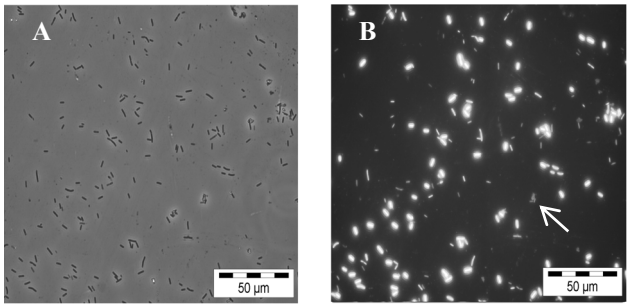

Fig. 1: Cells of the fresh *Bacillus sp.* JG-B53 sample.

RESULTS. The first step was to analyze the fresh reference sample of *Bacillus sp.* JG-B53. A micrograph of such cells in phase contrast mode is shown in Fig. 1A and after LIVE/DEAD staining in Fig. 1B. Alive and dead cells can be identified as bright and dim (arrow) dots, respectively. The figures show vital cells without any spores.
The storage experiments with bacterial biomass of *Bacillus sp.* JG-B53 showed no significant change in the protein profile by means of SDS-PAGE under frozen conditions and over a storage time of 3 weeks compared to liquid samples stored at 4 °C.
In frozen samples, the LIVE/DEAD staining showed that the amount of living cells decreases by 5-10% per week. However, there is no difference between samples frozen at different temperatures and samples with or without glycerin (sample conditions 4-7). The cells showed also their typical morphology (Fig. 2).
Liquid samples stored at 4 °C (sample conditions 1-3), contained almost 80% dead cells after a storage time of one week. In addition, the morphology changes after one week compared to reference cells of *Bacillus sp.* JG-B53.

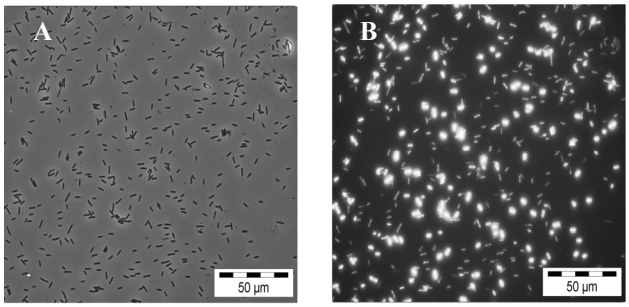

Fig. 2: Cells of *Bacillus sp.* JG-B53 sample after storage of 3 weeks, −70 °C without any additive.

CONCLUSION. The results demonstrate that storage of living bacterial biomass is possible for a time period of 3 weeks under frozen conditions and without losing their properties. First tests show that the bacterial biomass from one single cultivation leads to reproducible results during biosorption experiments with different metals.

[1] Costa, C.P. et al. (1991) *Rev. De Microbiol.* **22**, 263-268.
[2] Sleytr, U.B. et al. (2001) *Prog. Surf. Sci.* **68**, 231-278.
[3] LIVE/DEAD® BacLight™ Bacterial Viability Kits.
[4] Lowry, O.H. et al. (1951) *J. Biol. Chem.* **193**, 265-275.
[5] Laemmli, U.K. (1970) *Nature* **227**, 680-685.

Photocatalytic decomposition of diclofenac by ZnO-nanoparticles immobilized on different S-layer coated carriers

M. Vogel, F. Lehmann,[1] K. Pollmann,[1] J. Raff
[1]Helmholtz Institute Freiberg for Resource Technology, Freiberg, Germany

ZnO-nanoparticles were synthesized on different S-layer coated carriers. These biocomposite materials were used for photocatalytical decomposition of the pharmaceutical diclofenac.

This work contributes to the development of stable photocatalytically active composite materials, which can be used for decomposition of pharmaceuticals in (waste) waters. For this application, nanotechnology is combined with biotechnology. Nanoparticles from the semiconductors ZnO and TiO_2 are known to be promising photocatalysts for the degradation of environmental contaminants because of their high photosensitivity, stability and large band gap. These nanoparticles should be reliably and permanently immobilized for their use in technical applications. In our approach, bacterial surface layer proteins (S-layer) are used as a basis for the synthesis of nanoparticles of defined size and to establish a nanoparticle fixation with long-term stability on carrier materials.
The pharmaceutical diclofenac (DCF) is frequently found in surface waters and was therefore chosen as a model compound for the test of photocatalytic activity. The produced biocomposites were tested for decomposition of DCF during irradiation with UV-light.

EXPERIMENTAL. As carriers for the immobilization of ZnO-nanoparticles different materials were chosen (for details see Tab. 1). Prior to use, the carriers were cleaned by rinsing with deionized water (1, 2), by RCA-cleaning (3) and by sonication in isopropanol (4). The surface of the carriers was modified by three alternating layers of the polyelectrolytes polyethyleneimine and polystyrenesulfonate using the layer-by-layer technique [1]. S-layer proteins of *Bacillus* sp. JG-B53 were isolated according to the protocol in reference [2]. For recrystallization of S-layer proteins on the polyelectrolyte coated carriers, the carriers were incubated for 24 h in 1.5 mM TRIS, 10 mM $CaCl_2$ at pH = 8 with a protein concentration of 0.5 mg/mL. After washing, the ZnO-nanoparticles were synthesized on the S-layer surface according to a method described in [3]. Therefore, the coated carriers were shaken in 30 mM TRIS-buffer with 20 mM $Zn(NO_3)(H_2O)_6$ at pH = 8 for 4 h. Zn bound on the carriers was determined by dissolution of Zn with 20% acetic acid for 2 h and ICP-MS measurement. For irradiation experiments, different amounts of coated carriers (Tab. 1) were covered with a solution of 100 µM diclofenac.
Suspensions were irradiated with UV-light (365 nm; 8 W) (3UV-lamp, Ultra-Violet products) in a closed box while shaking. Samples of 200 µL were taken at defined time points. For monitoring the degradation of DCF, HPLC-analyses were performed [4].

Tab. 1: Specification of the used carrier materials.

Carrier	(Particle) size	Amount
1 Silica gel	0.5-1 mm	10 g
2 Quartz sand	0.4-0.8 mm	10 g
3 Glass foam	0.6-2 mm	1 g
4 Stainless steel disc	∅ 50 mm	1 disc

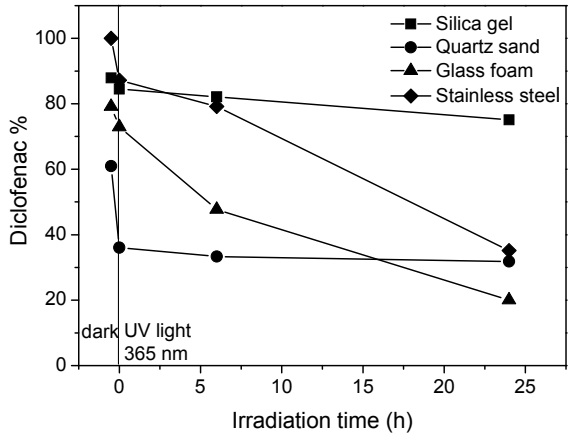

Fig. 1: Decomposition of DCF by ZnO-nanoparticles (3.7 ± 0.6 mg) immobilized on different S-layer coated carriers under UV irradiation.

RESULTS. On all S-layer coated carrier materials, ZnO-nanoparticles were successfully immobilized. The photocatalytic activity of these biocomposites was tested by monitoring the DCF decomposition during irradiation with UV-light. As shown in Fig. 1, the degradation of DCF differs in dependence on the used biocomposite under the given experimental conditions. The biocomposites with glass foam and stainless steel as carriers show a degradation of DCF to 20% and 35% of initially applied DCF, respectively. In contrast to that, nearly no decomposition and no degradation products (not shown) were detected in experiments with composites using silica gel and quartz sand as carriers. In case of all tested carriers, a decrease of DCF concentration could be detected also when incubated in the dark for 0.5 h. This decrease can be attributed to a sorption of DCF to the photocatalytically active material, because there are no peaks of degradation products in the HPLC-diagrams. Biocomposites with silica gel and quartz sand as carriers showed no decomposition of DCF and in case of quartz sand also a huge not reproducible sorption and were therefore excluded for further experiments. The glass foam and especially the stainless steel discs are promising carrier materials for the immobilization of S-layer/ZnO-nanoparticles. Both of these S-layer coated carrier materials are chosen and further used for an optimization of the ZnO-synthesis regarding stability and activity of the photocatalytic nanoparticle layer.

ACKNOWLEDGEMENTS. This work was supported by the Federal Ministry of Education and Research (BMBF 03X0094G).

[1] Decher, G. et al. (1997) *Science* **277**, 1232-1237.
[2] Raff, J. et al. (2003) *Chem. Mater.* **15**, 240-244.
[3] Bauermann, L.P. et al. (2007) *Int. J. Mat. Res.* **98**, 879-883.
[4] Pollmann, K. et al. (2009) *Report FZD-511*, p. 24.

QCM-D, a versatile tool for analyzing thin layer deposition: surface layer protein recrystallization on modified SiO_2 surfaces

M. Suhr, T. Günther, J. Raff, K. Pollmann

The formation of sheets of bacterial surface layer (S-layer) proteins can be monitored by quartz microbalance with dissipation monitoring (QCM-D) in the nano-scale range providing a detailed understanding of the self-assembling process and its kinetic. Subsequent atomic force microscopy (AFM) studies enable the imaging of these nanostructures and allow exact statements of structural properties.

The quartz crystal sensor in the QCM-D system oscillates at resonance frequency. In relation to the Sauerbrey equation ($\Delta m = -C \cdot 1/n \cdot \Delta f$), the change in mass can be measured in dependence of the frequency change. Statements to viscoelastic properties can be made by the dissipation parameter ($\Delta D = E_{loss}/(2 \pi E_{stored})$) [1]. S-layer proteins with their remarkable properties like self-assembling in highly ordered lattices, high metal binding capacities and high stability make them interesting for several technical applications in nanobiotechnology [2, 3]. In this study, the influence of surface modifications with adhesion promoters like polyelectrolytes on adsorption kinetics and stability of the protein layer should be determined.

EXPERIMENTAL. *Sensor surface modification.* The quartz crystals were modified with alternating layers of polyelectrolytes (PE) e.g. polyethylene imine (PEI) and polystyrene sulfonate that were applied via dip coating using the Layer by Layer technique (LbL) [4].
S-layer recrystallization. S-layer proteins of the *Bacillus* species JG-B53 were used. Protein monomers (0.2 g/L) were recrystallized on polyelectrolyte modified and unmodified sensor surfaces inside the flow module using a buffer system (1.5 mM TRIS, 10 mM $CaCl_2$, pH = 8).
QCM-D measurements were carried out with a Q-Sense E4 module equipped with flow modules QFM 401 (Q-Sense AB, Gothenburg, Sweden). For the experiments, QSX 303 SiO_2 sensors with a fundamental frequency of ~5 MHz were used. The crystals were cleaned by using alkaline swelling agents rinsing with ultrapure water and placing in an ozone cleaning chamber. The shifts in frequency (Δf) and dissipation (ΔD) were recorded using Q-Soft 401 software. The data modeling based on the Voigt model for viscoelastic molecules was done with the Q-Tool 3. All experiments were performed with a constant flow of 125 µL/min and at a temperature of 25 °C.
AFM-characterization. Imaging was done with an Asylum Research MFP3D Bio AFM using Olympus OMCL AC40 or OMCL TR400 cantilever in AC mode in liquid.

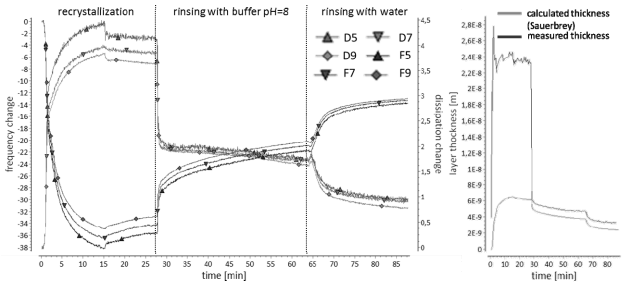

Fig. 1: QCM-D diagram of deposition of JG-B53 S-layer proteins on SiO_2 coated gold crystals (a); layer thickness profile (b).

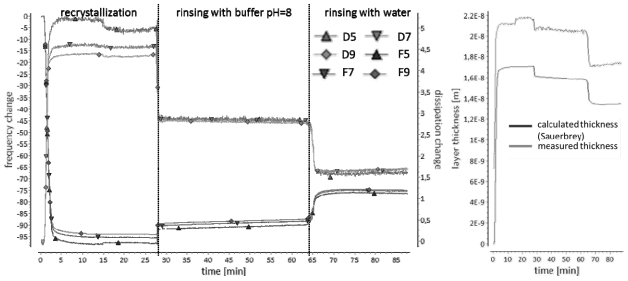

Fig. 2: QCM-D diagram of deposition of JG-B53 S-Layer proteins on modified SiO_2 coated gold crystals (a); layer thickness profile (b).

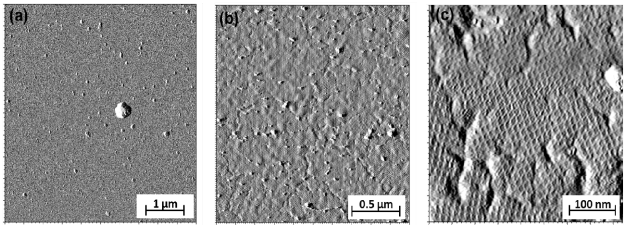

Fig. 3: AFM images of recrystallized JG-B53 S-layer on SiO_2; unmodified (a), PE modified surfaces (b), and scan of S-layer lattice (c).

RESULTS. QCM-D measurements indicate that the protein coating is accelerated on PE modified surfaces in comparison to unmodified surfaces (Fig. 1, 2). In case of PE modified sensors, the recrystallization process of JG-B53 S-layer was finished within 25 min. The stable signals of Δf (blue) and ΔD (orange), shown in Fig. 2, verify the formation of a nearly fully closed and stable protein layer. Accordingly, QCM-D (Fig. 1) and previous AFM studies [5] showed that a fully closed protein layer could not be obtained within 12-24 h without any modification of the technical surface. The lower Δf in Fig. 1 can be explained by a smaller amount of adsorbed protein. In both figures the parameter ΔD show an increasing signal that is probably caused by the elastic property of the protein biomolecules within the first 25 min. The stable Δf and ΔD signal of the PE modified sensors (Fig. 2) during rinsing proved both, a complete coverage with protein and a higher stability of the formed protein layer.
The visualization of the sensor surface by AFM (Fig. 3) verifies the QCM-D measurements. An almost completely closed protein layer could be detected that cover the surface of the PE modified sensor. Figure 3c shows the detailed AFM scan of the S-Layer lattices of JG-B53 with its typical p4 symmetry exhibiting a measured height of ~10 nm (compared calculated QCM-D thickness ~13 nm).

CONCLUSION. The combination of QCM-D and AFM technique allows the detection of protein layer formation on a nanometer scale. With QCM-D it is possible to investigate not only structural properties but also adsorption kinetics. We have shown that the modification of technical surfaces is crucial for a fast and stable S-layer coating.

[1] Product instructions of the companies L.O.T. Oriel/ Q-Sense.
[2] Sleytr, U.B. et al. (2001) *Progr.Surf. Sci.* **68**, 231-278.
[3] Lopez, A.E. (2010) *small* **6**, 396-403.
[4] Decher, G. et al (1994) *Biosens. Bioelect.* **9**, 677-684.
[5] Günther, T. et al. (2010) *Report FZD-530*, p. 23.

High resolution AFM imaging of microorganisms

T. Günther, M. Suhr, J. Raff, K. Pollmann

Atomic force microscopy (AFM) is a versatile tool for exploring the nano-world. Originally used for material research, AFM becomes more and more interesting also for other fields, e.g. microbiology. For the analysis of biological surfaces with high resolution, a stable immobilization of the samples on a flat surface is crucial. Here, a new method is described for a variety of single cell organisms.

Biological AFM is a fast growing field. The power of AFM opens up the possibility to investigate biological samples under native conditions. In case of AFM analyses, this includes imaging, manipulation and interaction force measurements and some other methods [1]. AFM can be used at least over two orders of magnitude ranging from intact cells down to single proteins. One challenge of bio-imaging is the reliable immobilization of the sample material on a flat surface. Especially larger samples like intact cells can be detached by the probe tip. Many procedures were developed to avoid this problem but mostly for a small selection of organisms [2, 3]. The presented new method allows the immobilization of single cell organisms of different kingdoms and was tested with prokaryotes as well as eukaryotic single cell organisms.

EXPERIMENTAL. Organisms were cultivated in their respective medium (*Bacillus sp.* – nutrient broth (NB) media, 30 °C; *E. coli* – Luria Bertami (LB) media, 37 °C; *Chlorella vulgaris* – minimal media; *Pichia pastoris* – yeast extract peptone dextrose (YPD) media). Immobilization was achieved by centrifugal deposition of cells at polyelectrolyte (polyethyleneimine PEI and polystyrenesulfonate PSS) coated silicon dioxide wafers. Cells were washed two times with PBS. Optical density (600 nm) was adjusted to 0.1. The wafers were spin coated with 15 alternating layers of polyelectrolytes (2.5 k rpm, $[PEI/PSS]_7/PEI$). Cell suspensions and wafers were deposited in specially prepared reaction tubes with tilted bottom. Cells were sedimented at the wafer surface at 15,000 g for at least 30 min.

RESULTS. The investigations were focused on the reliable immobilization of the organisms. Multiple scans were performed on single cells of *E. coli*, *Pichia pastoris*, *Chlorella vulgaris* (results not shown) and *Bacillus sp.* JG-B53 in order to prove the coating stability and to demonstrate the possibility of repeated scanning of one target cell. The quality of suchlike produced images is visible in Fig. 1A that shows an AFM height image of *Bacillus sp.* Such an overview scan helps to determine the position of single cells and facilitates their imaging. The most interesting application of this method is the detailed investigation of the surface of a microbe. Figure 1B is an AFM amplitude image of *Bacillus sp.* The cells were immobilized and showed no movement or altering during the scan. A flagellum as well as a part of the cell can be clearly identified. The area in the white frame is magnified in Fig. 1C. In this image, the rectangular structure of the cell covering surface layer is visible. The possibility to image structures in the range of micrometers down to a few nanometers demonstrates the rigidity of the produced samples and the advantage of the developed method.

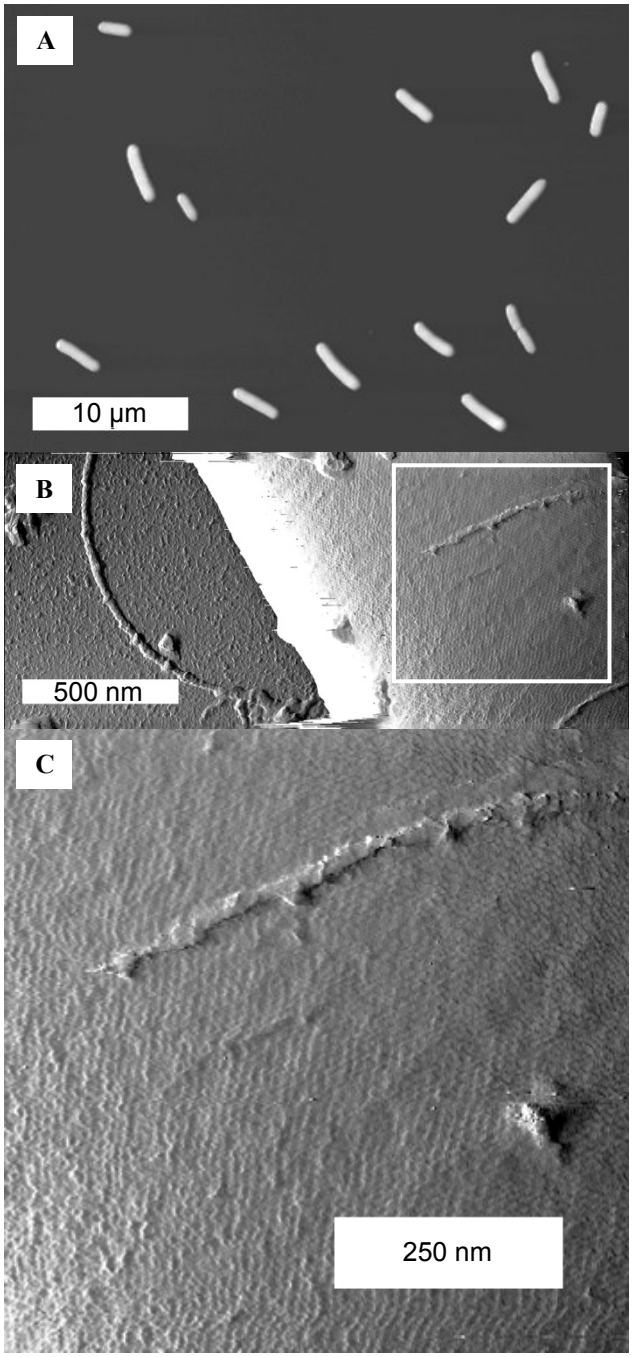

Fig. 1: A – Overview scan (AFM height image) of immobilized *Bacillus* sp. JG-B53; B – Detail scan (AFM amplitude image) of a single cell; C – Detail scan (AFM amplitude image) of the structured cell surface (surface-layer protein envelope with p4 symmetry).

[1] Casuso, I. et al. (2011) *J. Mol. Recognit.* **24**, 406-413.
[2] Doktycz, M. et al. (2003) *Ultramicroscopy* **97**, 209-216.
[3] Bolshakova, A.V. et al. (2004) *Biotechnol. Progr.* **20**, 1615-1622.

Steady state and time resolved measurements for the evaluation of a FRET-biosensor

U. Weinert, K. Pollmann,[1] J. Raff

[1] Helmholtz Institute Freiberg for Resource Technology, Freiberg, Germany

Fluorescence resonance energy transfer (FRET) is a powerful tool to monitor interactions on a molecular level. In this work, a FRET pair composed of a green and red fluorescence dye combined with a receptor is used as optical transducer for a sensory system. Therefore, components were chemically linked to Surface(S)-layer proteins to obtain a defined sensory layer. For evaluation of the system two methods were used and their suitability is discussed.

EXPERIMENTAL. S-layer proteins from strain *Lysinibacillus sphaericus* JG A12 were used for all experiments and were applied in their polymer form. For the coupling of fluorescence dyes to COOH groups of S-layer proteins, 20 mM 1-Ethyl-3-(3-dimethylamino-propyl)carbodiimid was used and for coupling to NH_2 groups NHS ester modified fluorescence dyes were used. The molar ratio of protein to fluorescence dye was 1 : 1. Reaction buffer was 0.1 M MES (pH 5.6). Proteins were modified either with only green fluorescence dye as donor or with green and red fluorescence dye as FRET pair, where the red fluorescence dye represents the acceptor.

For steady state measurements, samples were diluted 1 : 10 in 0.1 M MES (pH 5.6). For time resolved measurements, undiluted proteins were applied and the lifetime of donor dye was determined. Experimental parameters are listed in Tab. 1. All measurements were performed with the system Quantamaster 40-Q25 (Birmingham, U.S.A.).

Tab. 1: Chosen parameters for steady state and time resolved fluorescence measurements.

Parameter	Steady state	Time resolved
Excitation	450 nm	450 nm
Emission	500−700 nm	520 nm
Slit width	2 nm	12 nm

RESULTS. S-layer proteins were successfully modified with both fluorescence dyes. The modification rate was between 30 and 40 mol%. This means that nearly two fluorescence dyes are coupled to one unit cell of the S-layer protein. The size of a unit cell is 13x13 nm consisting of 4 monomers and coordinated in p4 symmetry.

Steady state measurements. Samples were excited at a wavelength of 450 nm, and the emission spectra from 500 to 650 nm were measured (Fig. 1). In case of proteins modified with only donor dye, one distinct peak at 530 nm can be determined. In case of samples modified with a FRET pair, two distinct peaks of the donor and acceptor were determined. Thus, it can be assumed that a FRET occurs between the green and red fluorescence dye. A reference of protein modified with only acceptor dye was also measured in order to exclude excitation of acceptor dye at 450 nm. Results show that the red acceptor dye is not excited at 450 nm which additionally proves that the emission peak at 570 nm is caused by an energy transfer.

Lifetime measurements. With the help of time resolved measurements, lifetimes of fluorescence dyes can be determined. Fluorescence lifetime is controlled by quenching effects. In case of a FRET, the lifetime of a donor dye will decrease due to the energy transfer to an acceptor. Table 2 shows the determined lifetime of donor dye linked to S-layer proteins. If an acceptor is additionally linked to the protein, the lifetime of donor dye decreases from 2.0 ns to 1.8 ns. This decrease indicates a quenching of the fluorescence dye and, hence, energy transfer.

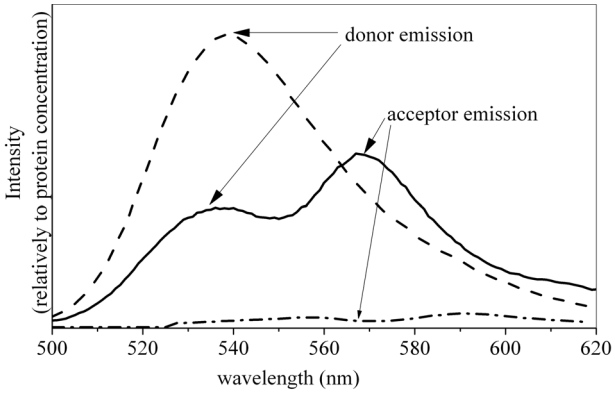

Fig. 1: Emission spectra of protein polymers modified with only donor dye (dashed line) or both fluorescence dyes (black line), also shown is an example of proteins modified with only acceptor dye (dot-and-dashed line); excitation wavelength is 450 nm.

Tab. 2: Lifetime of donor dye linked to proteins in presence and absence of acceptor dye, also linked to S-layer protein; values are means of 5 measurements, accuracy of one calculated lifetime was at least better than 0.03 ns.

Donor dye	Lifetime [ns]
In absence of acceptor	2.03 ± 0.08
In presence of acceptor	1.82 ± 0.13

DISCUSSION. With the help of both methods, an energy transfer between two fluorescence dyes which are linked to S-layer proteins could be verified. Thereby, steady state and lifetime measurements showed their advantages and disadvantages. Emission spectra from steady state measurements are easy to analyze, and the detection of a potential FRET is rapidly generated. However, fluorescence signals are influenced by on protein concentration. Further static quenching, e.g. originated from different buffer solutions, may occur. Both effects − the intensity of emission spectra and static quenching − will influence the results. In comparison to that, time resolved measurements are independent from static quenching and to some extend from concentration of the sample. This is due to the fact that the calculated decay curve represents the lifetime and is independent from initial intensity. The very small differences in lifetime necessitate a high accuracy of calculated lifetime constituting a considerable drawback.

Trehalose renders the "dauer" larva of *Caenorhabditis elegans* resistant to extreme desiccation

H. Khesbak, C. Erkut,[1] T. Kurzchalia,[1] K. Fahmy
[1]Max-Planck-Institute of Cell Biology and Genetics, Dresden, Germany

The soil nematode *Caenorhabditis elegans* is a well established model organism in developmental biology and genetically fully described. We have performed preliminary experiments to explore its potential for the assessment of low dose metal and radiotoxicity. Investigation of a dehydrated non-metabolic state that can be revitalized by rehydration, the "dauer", is of particular interest as high concentrations of previously solvated ions are produced. This includes the increase of ingested toxic metals with biomolecule under anhydrobiotic conditions. We have studied the role of trehalose, a protective sugar synthesized in response to desiccation, which maintains reversibility of dehydration-induced physical changes but at the same time is known to bind metal ions [1]. Living organisms where investigated by infrared spectroscopy. For trehalose-producing strains, full reversibility of the desiccation-induced changes of vibrational modes was observed but not for a trehalose-defficient strain. We have assigned the spectral changes to altered responses of lipids to desiccation in the presence or absence of trehalose [2].

EXPERIMENTAL. Equal amounts of daf-2 (reference strain of *C. elegans*) and daf-2;ΔΔtps (a trehalose deficient strain) dauers were preconditioned on the surface of a diamond attenuated total reflection (ATR) cell (Resultec, Germany) and absorption changes were monitored by IR spectroscopy (IFS 66v, Bruker, Germany). In order to obtain a stable baseline, the sample was first exposed to 97% RH by equilibrating through the gas phase with a saturated Na_2HPO_4 solution in a reservoir which was separated from the sample compartment by a dialysis membrane. Subsequently, samples were desiccated at ambient humidity (ca. 50% RH) and rehydrated at 97% RH by removing or re-connecting the reservoir, respectively. During desiccation and rehydration, spectra were recorded continuously (128 scans, 2 cm^{-1} resolution, 4000 to 800 cm^{-1}) for 1 h. Difference spectra were generated by subtracting the absorption of the appropriate initial reference state.

RESULTS. Figure 1 shows the absolute infrared absorption spectra of living *C. elegans* dauers for the reference strain daf-2 (a) and the trehalose-deficient strain daf-2;ΔΔtps (e) in the region of CH stretching vibrations, revealing indistinguishable spectral properties before desiccation. Reducing the relative humidity from 97% to ~50% produces frequency shifts in the CH stretching modes as a consequence of reduced H-bonding and or changes in free packing volume of hydrocarbon chains. Part of these changes occurs at regions that coincide with the corresponding hydration-dependent changes in native *C. elegans* phospholipds extracted by organic solvents. Remarkably, the physical changes that are responsible for the altered vibrational properties are fully reversible upon rehydration in the case of the trehalose-synthesizing strain daf-2. In contrast, the trehalose-defficient strain exhibits an additional spectral feature at 2858 cm^{-1}, generated during desiccation, that is not reversed upon rehydration. The

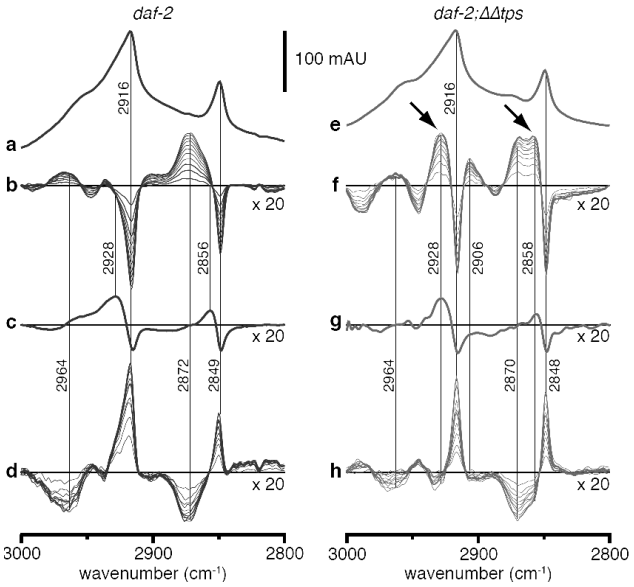

Fig. 1: Total infrared absorption (a, e) and hydration-dependent absorption difference spectra (b-d, f-h) in the CH_2 stretching range for daf-2 and daf-2;ΔΔtps dauers. Total absorption spectra of preconditioned dauers (a, e). Absorption changes induced by water loss from preconditioned dauers relative to the absorption at 97% RH (b, f). Arrows indicate irreversible changes that are assigned to lipids. Absorption changes induced by water loss of a hydrated film of extracted lipids (c, g). Absorption changes induced by the reuptake of water by rehydrated dauers relative to their initial absorption at w45% RH (d, h). Scale bar represents 100 milliabsorption units (mAU).

2848/2858 cm^{-1} frequency shift matches that of the extracted phospholipid extract, when exposed to a humidity change. Therefore, we assign the irreversible spectral change to an irreversible desiccation-induced structural transition in lipidic acyl-chains. Their CH-stretching frequencies are known to respond to changes in free volume.

DISCUSSION. We have shown that *in vivo* infrared spectroscopy can reveal subtle physical differences in the life nematodes that exhibit a true anhydrobiotic state. This state renders them suitable to address the environmentally important question of transiently very high intracellular concentrations of toxic substances such as heavy metals in seasonally dry soils and their impact on reactivation of metabolic activity.

[1] Oku, K. et al. (2005) *Biosci. Biotechnol. Biochem.* **96**, 7-12.
[2] Erkut, C. et al. (2011) *Curr. Biol.* **21**, 1331-1336.

Complexation of U(VI) with model tetrapeptides in the presence and absence of phosphorylgroups

R. Husar, K. Heine, S. Weiß, A. Barkleit, H. Zänker, T. Henle[1]

[1]Department of Chemistry and Food Chemistry, Dresden University of Technology, Dresden, Germany

The complexation of uranium(VI) with a model tetrapeptide, modified or not modified by phosphorylation, was investigated at pH 2 to 8 by time-resolved laser-induced fluorescence spectroscopy (TRLFS) and potentiometric titration. Phosphorylic groups proved to form stronger complexes than carboxylic groups.

A study on the interaction of U(VI) with milk proteins had shown that whey proteins exhibit lower adsorption affinity then caseins [1]. The absence of phosphorylgroups in whey proteins is assumed to cause this difference. Here we further verify this hypothesis by experiments with model oligopeptides. The amino acid sequence of the peptides in this study complies with that of amino acids 13-16 in the milk protein β-casein. The model peptide structures of L-valinyl-L-alanyl-L-seryl-L-leucine (H_2N-Val-Ala-Ser-Leu-OH, VASL) and L-valinyl-L-alanyl-L-phosphoseryl-L-leucine (H_2N-Val-Ala-PSer-Leu-OH, VAS^PL) are shown in Fig 1.

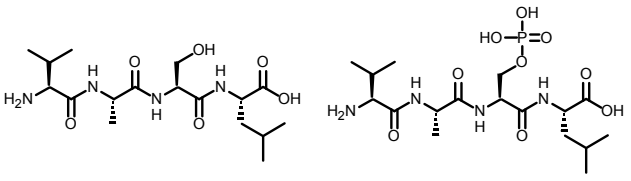

H_2N-Val-Ala-Ser-Leu-OH, VASL H_2N-Val-Ala-PSer-Leu-OH, VAS^PL

Fig. 1: Structure of model of the tetrapeptides VASL and VAS^PL.

EXPERIMENTAL. The tetrapeptides were synthesized by solid-phase peptide synthesis using Fmoc protection group strategy on Wang resin and purified by reversed phase HPLC described elsewhere [2, 3]. For complexation experiments the ionic strength was set to 0.1 M ($NaClO_4$) under carbonate free inert gas atmosphere at room temperature. pH values between 2 to 8 were adjusted with $HClO_4$ and NaOH. The potentiometric titration experiments were performed with a Mettler Toledo titration system [3] at two U(VI) concentrations ($1 \cdot 10^{-3}$ and $1.5 \cdot 10^{-3}$ M) and one ligand concentration ($3 \cdot 10^{-3}$ M). TRLFS measurements were carried out at a fixed U(VI) concentration of $1 \cdot 10^{-5}$ M and at ligand concentrations varied between $2 \cdot 10^{-6}$ and $15.6 \cdot 10^{-5}$ M. Set up and parameters of measurement by TRLFS and potentiometric titration are described elsewhere [3-5].

RESULTS. The luminescence spectra of U(VI) solutions at pH 4.5 are exemplarily shown in Fig. 2. Luminescence data are given in Tab. 1. The complexation of U(VI) with the phosphorylated peptide VAS^PL is indicated by an increase in luminescence intensity and a 9 nm red shift of the emission maxima, compared to the free U(VI) ion. They suggest the formation of UO_2^{2+}-phosphoryl species. In the absence of phosphorylic groups the complexation of U(VI) is characterized by a decrease in luminescence intensity and a slight red shift of the peak maxima by 2 nm caused by the interaction with carboxylic groups. Interaction of amino and hydroxyl groups can be neglected because of their strong protonation in the investigated pH range [5]. The luminescence lifetimes of the

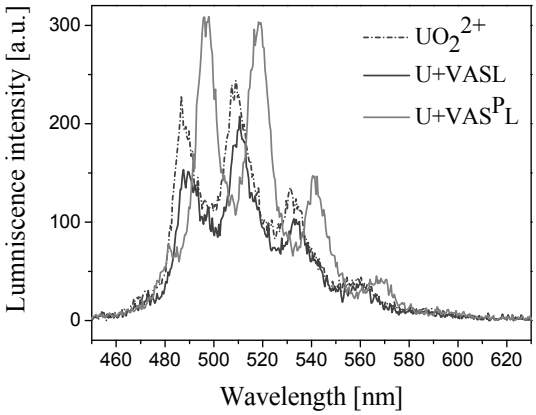

Fig. 2: Luminescence spectra of U(VI) solutions in the presence and absence of phosphoryl groups ([U(VI)] = $1 \cdot 10^{-5}$ M. [Ligand] = 15.6 eq.; I = 0.1M. pH = 4.5, 25 °C).

Tab. 1: Luminescence properties of the U(VI) solutions.

System	Luminescence maxima [nm]					Lifetimes [µs]
UO_2^{2+}	488	509	532	558	585	1.3/8.9
U+VASL	491	511	533	560	580	1.4/7.7
U+VAS^PL	497	518	541	567	595	0.4/1.2

phosphoryl complex species are significantly shorter than the lifetimes of the free uranyl cation.

The complex formation constants were determined with the programs SPECFIT [6] (TRLFS) and Hyperquad [7] (potentiometric titration). Table 2 exhibits the species identified and the calculated results. The latter demonstrate that U(VI) complexation due to phosphorylic groups results in higher complex formation constants than complexation due to carboxylic groups. The species determined and their properties are in accordance with similar data of U(VI) complexation with amino acids [5].

Tab. 2: Complex formation constants log β_{MHL} of U(VI) ligand systems.

System	log β_{111}
UO_2 VASL	10.77 ± 0.05
UO_2 VAS^PL	15.98 ± 0.37
UO_2 $HThr^{2-}$ [5]	10.33 ± 0.26
UO_2 $HPThr^{2-}$ [5]	15.02 ± 0.23

The results allow the conclusion that amino acid sequences with phosphoryl groups will play a more important role for the complexation of uranium and other actinides in protein matrices than sequences carrying solely carboxylic groups. This also holds for real milk proteins.

[1] Schreppel, K. et al. (2009) *Report FZD-511*, p. 56.
[2] Schreppel, K. et al. (2010) *Report FZD-530*, p. 12.
[3] Husar, R. (2011) Diploma thesis, Dresden University of Technology, Dresden.
[4] Koban A. et al. (2003) *Radiochim. Acta* **91**, 391-396.
[5] Guenther, A. et al. (2006) *Radiochim. Acta* **94**, 845-851.
[6] Binstead, R.A. et al. (2006) SPECFIT – Global analysis system, Version 3.0.37, Spectrum software associates, Malborough, U.S.A.
[7] Gans, P. et al (2003) Hyperquad 2003, Version 3.0.25, Protonic Software, Leeds, U.K.

The role of water H-bond imbalances in B-DNA sub state transitions and peptide recognition revealed by time-resolved FT-IR spectroscopy

H. Khesbak, O. Savchuk, S. Tsushima, K. Fahmy

Conformational substrates BI and BII of the phosphodiester backbone in B-DNA contribute to DNA flexibility and protein recognition. We studied the BI-BII transition on its intrinsic time scale by rapid scan FT-IR spectroscopy [1]. Correlation analysis of IR absorption changes, occurring within seconds after an incremental growth of the DNA hydration shell, identifies water populations w_1 (PO_2-bound) and w_2 (non-PO_2-bound), exhibiting weaker and stronger H-bonds, respectively, than those dominating in bulk water. The BII substrate is stabilized by w_2. The water H-bond imbalance of 4 kJ/mol is equalized at little enthalpic cost upon formation of a contiguous water network at 12-14 H_2O molecules per DNA phosphate. In this state, hydration water cooperatively stabilizes the BI conformer *via* the entropically favored replacement of w_2 DNA interactions by additional w_2 water contacts. Such water rearrangements determine the recognition of DNA by peptides and particularly by strongly water-coordinated ions such as lanthanides.

EXPERIMENTAL. Dried films of salmon testes DNA where rehydrated at defined relative humidity and then exposed to a hydration pulse (4 s), thereby, increasing the number Γ of H_2O molecules / PO_2 by less than 1. The relaxation to basal humidity was followed by rapid scan FT-IR spectroscopy. Different water populations and their DNA binding sites were identified from the synchronicity/asynchronicity of the water OH stretching and the DNA PO_2-stretching absorptions.

RESULTS. DNA films respond to transient hydration by increased absorption in the OH stretching region (due to water uptake) and by shifts of vibrational frequencies of the chemical groups of the DNA backbone. The antisymmetric PO_2-stretching mode (PO_{as}) shifts down upon increased H-bonding (1245/1205 cm^{-1} difference band) (Fig. 1A). We compared the relaxation kinetics of this absorption change with the kinetics of the water ν(OH) absorptions at high and low frequencies in the broad OH stretching range (3800-3000 cm^{-1}) during dissociation of the added water from the hydration shell. Thereby, the coupling of weakly and strongly bound water populations (w_1 and w_2 absorbing at high and low OH-stretching frequencies, respectively) to H-bond changes at the DNA-phosphate groups could be studied. Surprisingly, only the high frequency OH stretching mode is synchronized with the PO_2-H-bond changes, whereas the stronger H-bonded water population w_2 (lower ν(OH)) dissociates more slowly from the DNA (Fig. 1C). Therefore, the w_2 population must reside in the DNA grooves, rather than in the PO_2-hydration shell. Kinetic differences have been analyzed by correlation, resulting in the disrelation spectra shown in Fig. 1B. When all spectral changes are correlated with that of w_2, a large disrelation amplitude is obtained for the PO_2 difference band (red trace), whereas no disrelation is found when correlated with the w_1 population (black). Other pair-wise comparisons are shown in the 2D map (Fig. 1D) in color code, evidencing the heterogeneity in H-bond changes in the DNA hydration shell.

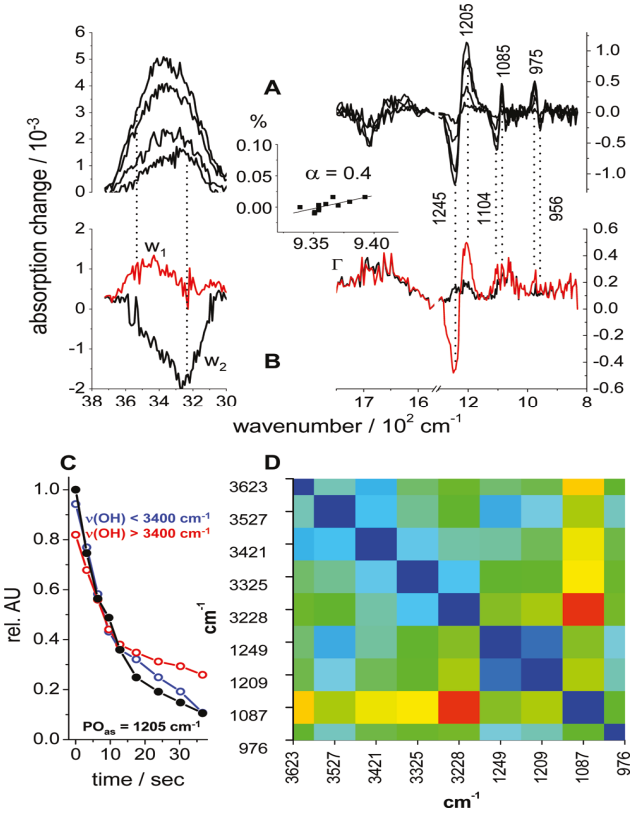

Fig. 1: Hydration-induced difference spectra at Γ = 9.33. (A) The water ν(OH) absorption (3800-3000 cm^{-1}) decreases over time (1.5, 4.6,14.2, and 38.1 s) upon release of excess water to the gas phase. H-bond changes to the DNA backbone cause frequency shifts in the 1300-800 cm^{-1} range dominated by increased H-bonding to the PO_2 groups (down shift of the PO_{as}: 1245/1205 cm^{-1} difference band) but showing little BI state formation (small changes at 1085, 1060, and 975 cm^{-1}). (B) Disrelation spectra referenced to the water ν(OH) at 3530 cm^{-1} (w_1, black) and 3230 cm^{-1} (w_2, red) showing the large kinetic similarity of the PO_{as} and the w_1 (small amplitudes) but not the w_2 absorption (large disrelation amplitudes). Inset: linear relation between water content (Γ = mol H_2O/mol DNA-phosphate) and sample expansion. The coefficient R is the slope of the linear regression line. (C) Time course at high and low frequency half of the water ν(OH) absorption and of the PO_{as} (black). The disrelation spectra represent the root square deviation of the absorption changes from those of the ν(OH) of w_1 and w_2. (D) Disrelation map showing similarity (blue) and dissimilarity (red) of the time dependencies in pairwise comparisons of selected infrared bands. The inhomogeneity of the DNA hydration water is qualitatively obvious from the different coloring.

DISCUSSION. The data reveal heterogeneous water clusters in the DNA grooves and at the PO_2 groups. Although the latter are primary hydration sites, their H-bonds are weaker than those of water H-bonds to the bases. We have shown that these clusters merge into a contiguous hydration shell with 12-14 water molecules per PO_2 group. Under these conditions, hydration couples cooperatively to the BI-BII substate transition in an entropically driven process that can compensate the entropically unfavorable induction of structure in DNA-bound peptides [1]. Water relocation is further critical in lanthanide binding where the highly ordered DNA hydration shell competes with inner sphere coordination water.

[1] Khesbak, H. et al. (2011) *J. Am. Chem. Soc.* **133**, 5834-42.

Eu^{3+}-mediated polymerization of benzenetetracarboxylic acid studied by spectroscopy, temperature-dependent calorimetry, and density functional theory

A. Barkleit,[1,2] S. Tsushima, O. Savchuk, J. Philipp, K. Heim, M. Acker,[3] S. Taut,[3] K. Fahmy

[1]Institute of Resource Ecology, Helmholtz-Zentrum Dresden-Rossendorf, Dresden, Germany; [2]Division of Radiochemistry, Department of Chemistry and Food Chemistry, Dresden University of Technology, Dresden, Germany; [3]Central Radionuclide Laboratory, Dresden University of Technology, Dresden, Germany.

Thermodynamic parameters for the complexation of Eu^{3+} with pyromellitic acid (1,2,4,5-benzenetetracarboxylic acid, BTC) as a model system for polymerizable metal-complexing humic acids were determined using isothermal titration calorimetry (ITC). At low metal and ligand concentrations (< 50 µM Eu^{3+}, < 1 mM BTC), a 1 : 1 monomeric Eu-BTC complex was identified in the range of 25-60 °C. At elevated concentrations (> 500 µM Eu^{3+} and BTC) a temperature-dependent polymerization was observed, where BTC monomers are linked via coordinating shared Eu^{3+} ions. With the onset of polymerization, time-resolved laser fluorescence (TRLFS) can still reveal the water coordination number of the lanthanide, whereas calorimetry is superior in determining the thermodynamic data in this regime. Evaluating the heat uptake kinetics, the monomer and polymer formation steps could be separated by "time-resolved" ITC, revealing almost identical binding enthalpies for the sequential reactions.

EXPERIMENTAL. ITC measurements were done with a Microcal VP-ITC calorimeter (GE Healthcare, Buckinghamshire, U.K.) at different temperatures (25, 40, and 60 °C). A total of 56 aliquots (5 µL of 10 mM BTC in 0.1 M $NaClO_4$, pH 5.7) was injected in 1.412 mL of 1 mM $EuCl_3$ (0.1 M $NaClO_4$, pH 5.7) in 5 min intervals at 25 °C, and in 27 min intervals at 40 and 60 °C to allow the completion of slow polymerization reactions. Measurements were analyzed with the associated software Origin™ 7.5.

RESULTS. ITC trace of Eu^{3+}-BTC complex formation at 25, 40 and 60 °C showed endothermic binding with stoichiometries of 1.0, 1.2 and 0.9, respectively. At 25 °C, the reaction was complete within less than 2 min (Fig. 1A, inset) with a reaction enthalpy $\Delta H = 16.5$ kJ mol^{-1} and $\Delta S = 130$ J mol^{-1} K^{-1} (from data in Fig. 1A). At higher temperature, the reaction showed a "tailing heat uptake" resulting in an apparent doubling of both ΔH and ΔS (Fig. 1B, lower panel). Figure 1B exemplifies the biphasic behavior at 40 °C by decomposing the ITC signal into a fast component with similar kinetics as measured at 25 °C and a slower phase for the additional heat uptake at higher temperatures. We have assessed the reaction heat in these different time windows resulting in two isotherms (Fig. 1B, lower panel). The early and late phase of the transient can be modeled with enthalpies of 14.6 and 16.3 kJ mol^{-1} (entropies of 138 and 160 J mol^{-1} K^{-1}, respectively, and a stoichiometry of 0.8-0.9) very similar to the 1 : 1 binding at 25 °C. The additional Eu^{3+} coordination appears to be crucial for the formation of polymeric states (and precipitation). However, an overall 1 : 1 stoichiometry also holds for the polymerized Eu-BTC complexes. This hints at a polymerization process with previously bound Eu^{3+} ions in monomeric complexes being shared between BTC molecules in a polymeric network.

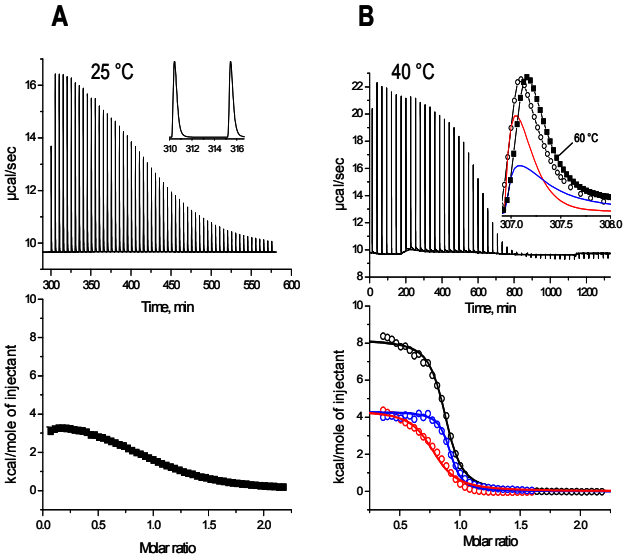

Fig. 1: Heat uptake during Eu-BTC complex formation measured by isothermal titration calorimetry. A) Injection of BTC at 25 °C is characterized by a fast heat transients (upper panel, less than 2 minutes (inset)). Integrated heats (lower panel) are consistent with a 1 : 1 stoichiometry and ΔH and ΔS values of 16.5 ± 0.1 kJ mol^{-1} and 130 ± 5 J mol^{-1} K^{-1}, respectively. B) Upper panel: injection of BTC at 40 °C shows prolonged heat uptake (inset, open circles) which can be decomposed into a fast (inset, red) and slow (inset, blue) component. Lower panel: total integrated heats (black) can be reproduced from the sum of the fast (red) and slow contribution (blue). The resulting curves are both consistent with a 1 : 1 stoichiometry. ΔH values for the fast and slow reaction are 14.6 ± 0.4 and 16.3 ± 0.4 kJ mol^{-1} with ΔS of 138 ± 4 and 160 ± 4 J mol^{-1} K^{-1}, respectively. All experiments were carried out with an initial concentration of 1 mM Eu^{3+}.

DISCUSSION. Calorimetry has been successfully applied to cover the energetics of Eu^{3+}-BTC complex formation in the monomeric and polymeric regime, where binding constants cannot be deduced from TRLFS (not shown). Energetics of monomer and polymer formation are remarkably similar and thus independent of the overall charge state of BTC (~3.5 at pH 5.7) or Eu-BTC (about neutral to anionic at pH 5.7). We ascribe the entropic changes to water release from the inner coordination shell because it scales with the release of ~2 and ~4 water molecules in the mono- and polymeric states, respectively (TRLFS, data not shown). The initial speciation of lanthanides and actinides is thus a key determinant in their environmental immobilization by polymerizing humic acids with little structural or electrostatic constraints.

[1] Barkleit, A. et al. (2011) *Inorg. Chem.* **50,** 5451-5459.

Complex formation of U(VI) with acetylacetone investigated by TRLF and ATR FT-IR spectroscopy

A. Günther, G. Geipel, H. Foerstendorf, G. Bernhard

The complexation of uranyl ions with acetylacetone in aqueous solution was investigated. The formed complexes showed no significant fluorescence signal, whereas IR spectroscopic results suggest the formation of 1 : 1, 1 : 2 and possibly 1 : 3 complexes.

1,3-β-diketones, such as acetylacetone, are very well chelating ligands and can bind different metals. Some solid uranyl complexes with 1,3-β-diketones are known from the literature e.g. [1, 2]. The complexation is possible due to a keto-enol-tautomerism and in the case of acetylacetone an enol-mesomerism (Fig 1.)

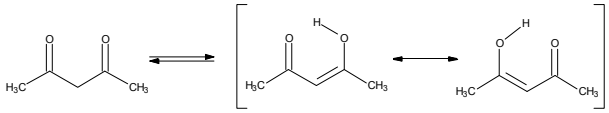

Fig. 1: Chemical structure of acetylacetone (acac) and the enol-forms.

EXPERIMENTAL. The experiments were performed at a fixed uranyl perchlorate concentration of $5 \cdot 10^{-5}$ M (TRLFS) and at a fixed uranyl chloride concentration of $1 \cdot 10^{-3}$ M (IR). The acetylacetone (acac) concentration was varied between 0 and $2.5 \cdot 10^{-3}$ M (TRLFS) and between 0 and $5 \cdot 10^{-2}$ M (IR). All experiments were performed at an ionic strength of 0.1 M $NaClO_4$ (TRLFS) or 0.1 M NaCl (IR) in the pH range from 2 to 6. The luminescence of the U(VI) ion was measured after excitation with laser pulses at 266 nm (Minilite laser, Continuum, USA) and at averaged pulse energy of 250 µJ. For the measurements of the luminescence of the acac, a fs-laser-pulse-based TRLFS system was applied as described in detail in [3]. The ATR FT-IR measurements were performed with a Bruker Vertex 80/v instrument using a diamond ATR accessory equipped with a flow cell. Spectral resolution was 4 cm^{-1}.

RESULTS. Figure 2A exemplarily shows the uranium fluorescence spectra as a function of the total acac concentration in aqueous solution at pH 6. We observed a decrease in the luminescence intensity with increasing ligand concentration, but no shifts of the main emission bands were detected at each investigated pH value. Only the lifetimes of the initial uranyl species were obtained, changing significantly with increasing acac concentration. After first analysis of the spectroscopic data we assume that the dynamic luminescence quenching (radiationless transitions in the energetic ground state) predominates, and statements regarding the complexation cannot be drawn on base of this data. The time-resolved luminescence decay of the pure acac in aqueous solution at pH range from 4 to 6 is mono-exponential, and the lifetime is in the range from 1.65 to 1.81 ns. After addition of uranium(VI) to the acac solution (see Fig. 2B), no differences to the emission properties of acac without uranium(VI) were found. The obtained lifetimes for the mono-exponential decay are in the range from 1.60 to 1.75 ns.
From TRLFS results we conclude that the formed U(VI)/acac complexes show no appropriate fluorescence signal under the given experimental conditions.

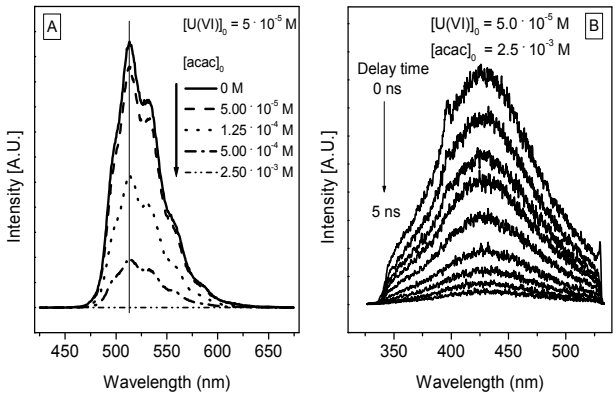

Fig. 2: Luminescence spectra of U(VI) recorded at pH 6 as a function of the acac-concentration (A) and of acatylacetone (time-resolved) in a U(VI)/acac complex solution (B).

Figure 3 shows the obtained ATR FT-IR difference spectra between the measured spectra of the respective U(VI)/acac complex solutions (positive bands) and those of the pure ligands (negative bands) at a constant U(VI)/acac concentration ratio and at different pH values. Complexation of the ligand molecules is reflected by the minima > 1690 cm^{-1} representing the keto groups and by the bands at 1525 and 1350 cm^{-1}, which are due to an increasing binding of U(VI) by acac and formation of a chelating system in the solution. The frequency of the $\nu_{as}(UO_2)$ mode is shifted from 963 to 912 cm^{-1} with increasing pH, suggesting an enhanced U(VI) complexation starting from free uranyl ion (963 cm^{-1}), via a 1 : 1 (945 cm^{-1}), 1 : 2 (932 cm^{-1}) to a 1 : 3 complex (912 cm^{-1}).

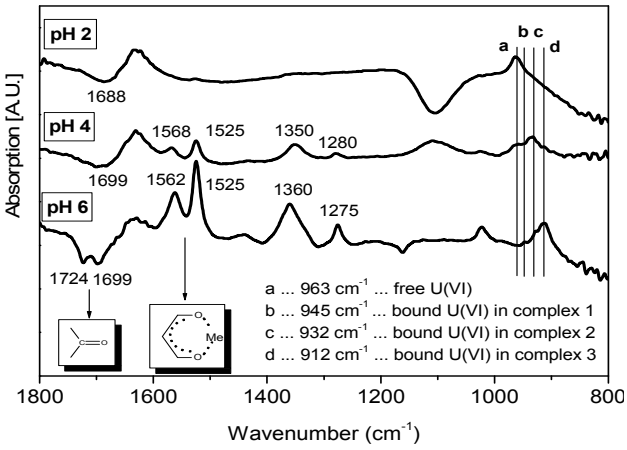

Fig. 3: IR difference spectra of U(VI)/acac complex solutions at pH 2, 4 and 6, $[U(VI)] = 1 \cdot 10^{-3}$ M, $[acac] = 5 \cdot 10^{-3}$ M.

ACKNOWLEDGEMENTS. The authors thank K. Heim for the IR measurements. This work was supported by the Federal Ministry of Education and Research under the contract number 02NUK014B.

[1] Alcock, N.W. et al. (1987) *Acta Cryst.* **C43**, 1480–1483.
[2] Tellez, C.S. et al. (1995) *Spectrochim. Acta* **51A**, 395–404.
[3] Geipel, G. et al. (2004) *Spectrochim. Acta* **60**, 417-424.

UV-vis investigation of the complexation of U(VI) and Eu(III) with Schiff bases in methanolic solution

K. Lindner, A. Günther, G. Bernhard

The complexation of uranium(VI) and europium(III) with N-benzylidenaniline (NBA), 2-(2-Hydroxybenzylidenamino)-phenol (HBAP) and Alpha-(4-hydroxyphenylimino)-p-cresol (HPIC) was studied by UV-vis spectroscopy. All Schiff bases form complexes with the metal ions in methanolic solution.

Schiff bases have a wide application in biological, clinical and analytical field [1-3]. In particular, they constitute an important class of chelating ligands in coordination chemistry. The used Schiff bases of this work (Fig. 1) represent important basic structures for supramolecular molecules, which are potentially suitable for extraction of metal ions from contaminated areas.

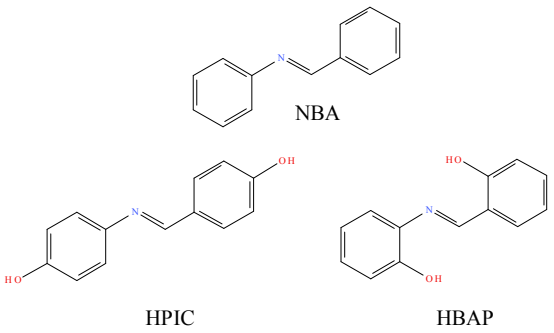

Fig 1: Structure of the used Schiff bases: N-benzylidenaniline (NBA), Alpha-(4-hydroxyphenylimino)-p-cresol (HPIC), 2-(2-Hydroxybenzylidenamino)-phenol (HBAP).

EXPERIMENTAL. The UV-vis measurements were performed using a CARY5G spectrometer (Varian Co.). The absorption spectra were recorded from 200 to 600 nm with a step size of 0.1 nm. The experiments were carried out with a 1 mm quartz glass cuvette (Hellma) at a temperature of 22 ± 1 °C. The complexation studies were performed in methanol at 120 mV. The metal concentration of uranium(VI) and europium(III) were fixed at 0.1 mM. The Schiff bases concentration was varied between 0 and 2 mM. The ionic strength in all samples was set to 0.1 M ($NaClO_4$).

RESULTS. Figure 2 exemplarily shows the UV-vis absorption spectra of U(VI) as a function of the NBA concentration at 120 mV. An increased absorption with increasing NBA concentration is observed. A hypsochromic shift from 242 (free ligand not shown here) to 237 nm indicates the complex formation of U(VI) and NBA. The same results are obtained in the Eu(III)-NBA-system. Investigations with the ligand HBAP show a bathochromic effect to 281 nm for both metals (Fig. 3). In addition, the absorption maxima increase with the rising concentration. The UV-vis absorption spectra of HPIC show neither with U(VI) nor with Eu(III) a spectral shift (Fig. 4). With both metal ions, the complexation of this ligand can only be observed through a decrease of the double band at 283 and 332 nm in comparison with the free HPIC.
The calculations of the complex formation constants based on the presented spectroscopic data are in progress.

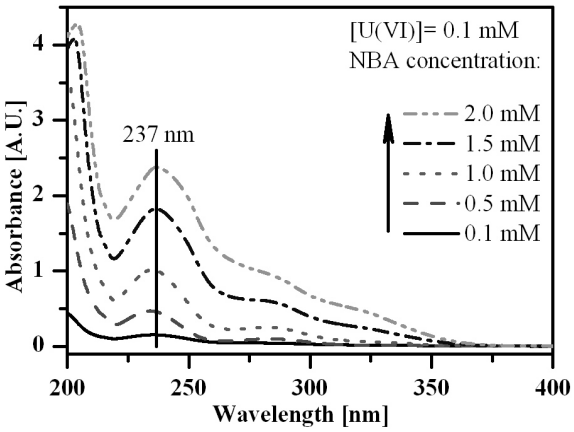

Fig. 2: UV-vis spectra of 0.1 mM U(VI) as a function of the N-benzylidenaniline concentration (NBA) at 120 mV and I = 0.1 M ($NaClO_4$).

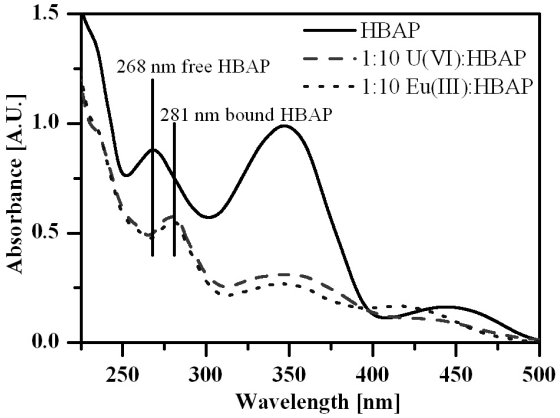

Fig. 3: UV-vis spectra of the free and bound HBAP at 120 mV and I = 0.1 M ($NaClO_4$), [U(VI)]=[Eu(III)]=0.1 mM, [HBAP] = 1 mM.

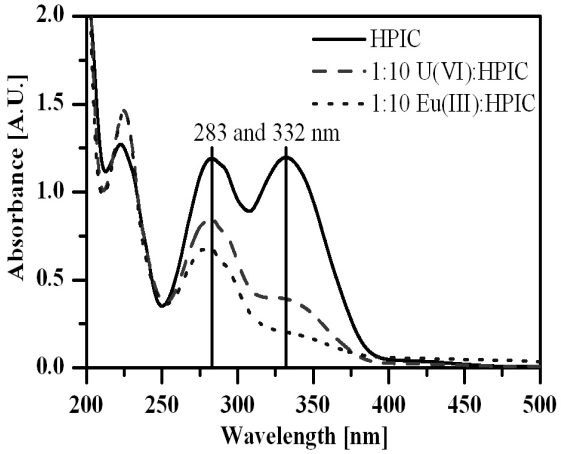

Fig. 4: UV-vis spectra of the free and bound HPIC at 120 mV and I = 0.1 M ($NaClO_4$), [U(VI)]=[Eu(III)]=0.1 mM, [HPIC] = 1 mM.

ACKNOWLEDGEMENTS. This work was supported by the Federal Ministry of Education and Research under contract number 02NUC014B.

[1] Cheng, L.-X. et al. (2010) *Bioorg. Med. Chem. Lett.* **20**, 2417-2420.
[2] Hemmateenejad, B. et al. (2010) *Spectrochim. Acta Part A* **75**, 340-346.
[3] Ibrahim, M.N. et al. (2006) *E-J. Chem.* **3**, 257-261.

LONG-LIVED RADIONUCLIDES AT

PERMANENT DISPOSAL SITES

Structure-stability relationship of thorium(IV)/silica colloids

C. Hennig, S. Weiß, D. Banerjee, A. C. Scheinost, G. Bernhard, H. Zänker

Thorium(IV) and silica form meta-stable colloids in aqueous solution at pH ≥ 7. The internal structure consists of [Th(O, OH)$_n$] polyhedra coordinated by [SiO$_4$] polyhedra. Silica is significantly enriched at the colloid surface if the concentration of the initial solutions is above the silica solubility limit.

EXPERIMENTAL. Th/silica colloids were prepared by rapid dilution of thorium carbonate in silicic acid solution. Solutions with silicic acid concentrations below and above the silica solubility limit of $2 \cdot 10^{-3}$ M were prepared to obtain both monomeric as well as polymeric silicic acid species.

RESULTS. Immediately after adding the silicic acid to the thorium carbonate solution, a strong increase of scattered light intensity was observed as shown in Fig. 1, indicative of the formation of colloids.

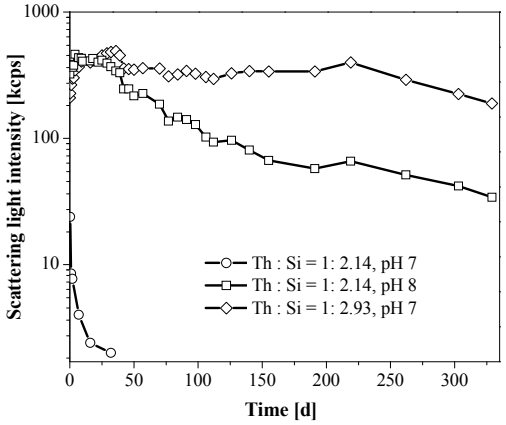

Fig. 1: Long-term stability of the Th/silica colloids. Initial [Th] = 0.8 mM, [HCO_3^-] = 50 mM.

The scattering intensity of a suspension containing colloids with a molar Si/Th ratio of 2.14 at pH 7 drops down within 32 days followed by sedimentation of the precipitate. A suspension with the same molar Si/Th ratio at pH 8 shows an increased colloid stability. A colloid suspension with a molar Si/Th ratio of 2.93 is stable at pH 7 over nearly one year.

Figure 2 shows the dependence of the zeta potential of Th/silica colloids on pH and silicate concentration. The measurement indicates that the particles carry positive charge at acidic pH and negative charge at alkaline pH. The isoelectric point of a pure Th(IV) oxyhydroxide colloid lies at pH 8.1, but is shifted to significantly lower pH values in the presence of silica. For example, a silicate concentration of $1.1 \cdot 10^{-2}$ M shifts the zeta potentials to lower values, i.e. a negative charge of the particles at pH 7 which supports electrostatical stabilization of the colloid suspension at near-neutral pH. Furthermore, it shifts the isoelectric point to pH 4.7.

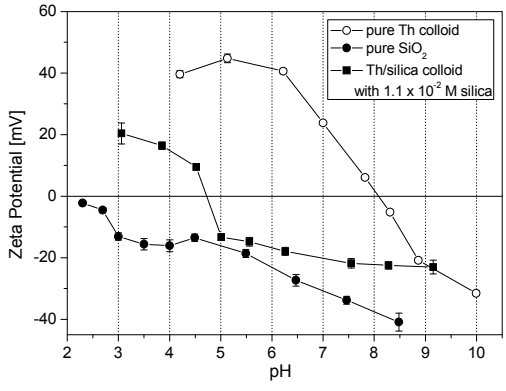

Fig. 2: Zeta potential of Th(IV) colloids/resuspensions as function of pH, [Th] = $1 \cdot 10^{-3}$ M; initial [CO_3^{2-}] = $5 \cdot 10^{-3}$ M, I = $5 \cdot 10^{-2}$ M $NaClO_4$. Error bars indicate 95% confidence level.

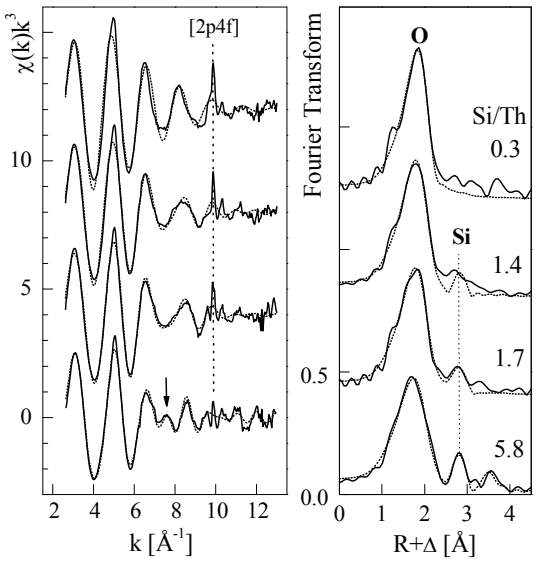

Fig. 3: Thorium L_3 edge EXAFS (left) and their corresponding Fourier transform (right) of colloid samples with Si/Th ratios noted in the figure.

EXAFS spectra of the colloid samples show silicon atoms in the environment of thorium with a Th-Si distance of ~3.25 Å. This short distance is characteristic for silica in bidentate coordination and reveals coordination of Th and silica. Additionally, high-energy X-ray scattering indicate short Th-Th distances of 3.98 Å. The colloid structure is not homogenous. To clarify this issue, the bulk Si/Th ratio of the colloids, determined by ICP-MS, and the surface Si/Th ratio, determined by X-ray photoelectron spectroscopy (XPS), were compared. XPS is a surface sensitive technique with an excitation depth of 5-10 Å. The size of U/silica colloids, which are regarded as equivalent to the Th/silica colloids, is < 20 nm [1]. Samples with low Si/Th ratios show a good agreement between the volume and the surface composition. In contrast, a sample with a Si/Th ratio of 1.45 in the volume reveals, when tested by with XPS, a Si/Th ratio of 2.77. This indicates an enrichment of silica at the colloid surface. The enrichment of silica at the particle surface is most likely related with the reaction kinetics. Th shows a fast kinetics and polymerizes in the first minutes of the reaction with Th and/or Si. With decreasing Th concentration this kinetics becomes slower and is determined by the kinetics of silicic acid and oligomeric silica species. The light scattering measurements show fast initial formation of colloids, determined by polymerization of Th. Subsequently, the scattering light intensity increases slowly and reaches a steady state after ~7 days. Further Th polymerization is most likely limited by silica enrichment at the particle surface.

[1] Dreissig, I. et al. (2011) *Geochim. Cosmochim. Acta* **75**, 352-367.

Zeta potentials of amorphous Th(IV) oxyhydroxide and Th(IV) carbonate solid phases

S. Weiß, R. Husar, H. Zänker

The zeta potentials and the isoelectric points of Th(IV) carbonate solids are significantly lower than those of Th(IV) oxyhydroxide. Leaching the Th(IV) carbonate solids with carbonate-free water makes them more similar to Th(IV) oxyhydroxide.

Thorium(IV) can be precipitated from acidic solutions by increasing the pH toward the near-neutral region which is well documented in the literature [1, 2]. However, it can also be precipitated from carbonate-containing alkaline solutions (where the solubility of Th is strongly enhanced due to the formation of the pentacarbonate complex $[Th(CO_3)_5]^{6-}$) by decreasing the pH. We precipitated Th(IV) from both acidic and alkaline solutions. The zeta potential of the precipitates was determined, which is a measure of the surface charge of the products and which is crucial for the colloidal behavior of the nanoparticles. The charge behavior of the two types of precipitate is discussed.

EXPERIMENTAL. Th oxyhydroxide (Th hydrous oxide) was produced by adding degassed NaOH to a 1 mM Th(IV) solution in 0.1 M $HClO_4$ (pH 4). The Th(IV) carbonate solids were prepared by neutralizing solutions of 1 mM Th in 50 mM $NaHCO_3$ using 0.1 M $HClO_4$. Aliquots of the carbonate-containing samples were leached with pure water (4 and 10 times) by centrifugation and resuspension. Preparation and leaching of the samples were done under inert gas. Aliquots of the tenfold leached sample were freeze-dried and the carbonate content was determined by deliberating the CO_2 from the solids at 800 °C and determining it using IR detection (Multi N/C, Analytik Jena). The error of the method is about ± 10%. Laser Doppler electrophoresis in disposable capillary cells was applied to measure the zeta potential of the precipitates (Zetasizer Nano ZS, Malvern Instruments). Zeta potential measurements on aliquots of the suspensions, equilibrated at pH 3 to 10 for 3 days, were performed.

RESULTS. As mentioned above, the precipitation of dissolved thorium from acidic solutions results in the formation of Th(IV) oxyhydroxide [1, 2]. However, the precipitation of Th(IV) from carbonate-containing alkaline solutions provides a more complex product. Even after tenfold leaching, this product still contains 20 wt.-% carbonate. Its composition would relatively well comply with the stoichiometry of thorium hydroxo carbonate, $Th(OH)_2CO_3$, which has a carbonate content of 18.4 wt.-%. However, the existence of this compound could only be proved in a dissolved form according to the literature, not in the form of a solid [3]. We therefore assume that our precipitate most likely consists of a non-stoichiometric Th(IV) hydroxo carbonate which possibly also contains Na (cf. [3]).

Figure 1 shows the results of the zeta potential measurements. Curve (a) represents the Th(IV) oxyhydroxide precipitated by the neutralization of an acidic Th(IV) solution. Its isoelectric point, pH(IEP), was found at 8.3 which is in good accordance with the value of 7.5-8.5 found for crystalline thorium dioxide, ThO_2(cr), by potentiometric titration at I = 0.01 to 0.1 M $NaClO_4$ [4]. Curve (b) gives the zeta potential of the solid precipitated from a

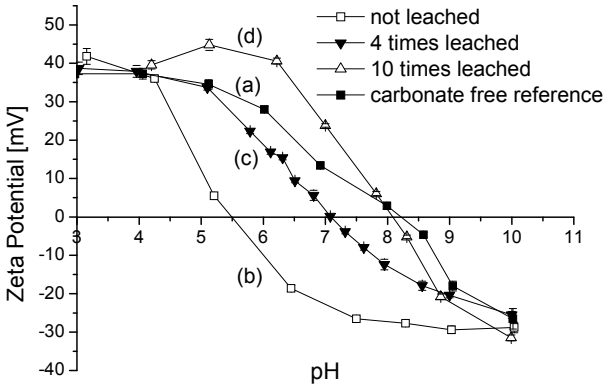

Fig. 1: Zeta potential vs. pH for Th(IV) oxyhydroxide samples before and after leaching and carbonate free reference.

carbonate-containing alkaline solution in dependence on pH. These zeta potentials are much lower than those of curve (a) which results in a pH(IEP) of only 5.5. The leaching of the carbonate-containing precipitate causes an increase of the zeta potential and, consequently, an increase of the pH(IEP) (curves (c) and (d)). After tenfold leaching the pH(IEP) of Th oxyhydroxide is reached.

There are essentially two influences that govern the electric charge and thus the zeta potential of a nanoparticle at a given solution composition:

(i) ions adsorbed at the particle/water interface,
(ii) the properties of the solid phase of the particles.

Two alternative hypotheses might explain the results of Fig. 1:

1.) The zeta potential curve of the Th(IV) carbonate solid (curve (b)) is determined by adsorbed bicarbonate. Washing the nanoparticles removes the adsorbed bicarbonate and "reveals" the true zeta potentials of the Th(IV) carbonate solid. The pH(IEP) of this substance happens to be the same as that of Th(IV) oxyhydroxide.
2.) The "true" zeta potentials and the pH(IEP) of the Th(IV) carbonate solid are significantly lower than those of Th(IV) oxyhydroxide. Leaching attacks the Th(IV) carbonate solid surfaces. A thin surface layer is converted into pure Th(IV) oxyhydroxide due to the leaching. Zeta potential measurement, therefore, finds values close to the zeta potential of Th oxyhydroxide. This is conceivable because Th(IV) oxyhydroxide might be a more stable compound than a Th(IV) hydroxo carbonate.

We are not yet able to decide which one of the two hypotheses is the correct one.

[1] Rothe, C. et al. (2002) *Inorg. Chem.* **41**, 249-258.
[2] Bitea, C. et al. (2003) *Coll. Surf. A* **217**, 63-70.
[3] Rand, M. et al. (2008) in: *Chemical Thermodynamics 11, Thorium*, p. 345, Elsevier, Amsterdam.
[4] Olsson, M. et al. (2002) *J. Colloid Interf. Sci.* **256**, 256-261.

Surface complexes of U(VI) on gibbsite studied by EXAFS spectroscopy

K. Gückel, H. Foerstendorf, A. Rossberg

In continuation to ATR FT-IR experiments [1], results from EXAFS spectroscopy illustrate as well the influence of carbonate on the sorption of uranium onto gibbsite. In the absence of atmospheric CO_2 a mononuclear inner-sphere complex is formed on the surface, whereas a uranium dimer containing carbonate and hydroxyl ions is formed on the surface in the presence of CO_2 in air.

EXPERIMENTAL. Gibbsite suspensions were adjusted to pH 6 and equilibrated in a Heidolph Promax 2020 shaker for one day under inert gas or ambient atmosphere. Then a 18.8 mM (air) or 200 mM (N_2) U(VI) stock solution was added to obtain the desired concentration. During the contact time the samples were placed back in the shaker at room temperature for 60 h, followed by centrifugation at 187,000 g for 45 min. The supernatant was decanted and the precipitates were placed in the EXAFS sample holders. The samples were subsequently frozen and stored in liquid nitrogen until the measurement.
EXAFS measurements were carried out at the ROBL beamline (BML20) at the ESRF, Grenoble. Uranium L_{III}-edge spectra of frozen sorption samples were collected in fluorescence mode using a 13-element-germanium detector and a helium cryostat at 15 K [2].

RESULTS. The Fourier-transform (FT) spectra (Fig. 1, left panel) of the k^3-weighted U L_{III}-edge EXAFS spectra (not shown) with the best fits and the FT of the residuals are shown in Fig. 1.
For all samples, the values for R_{Oax}, R_{Oeq}, the coordination numbers CN_{Oax}, CN_{Oeq} and σ_{Oax}, σ_{Oeq} are quite similar and typical for uranyl aqueous complexes .
Peak 2 (Fig. 1, right panel) is assigned to one coordinated Al at a distance of ~3.4 Å and occurs in all FT spectra. This value is concordant with the results for U–Al distances found for complexes of uranyl on gibbsite , imogolite and montmorillonite .
In the FT spectra of the carbonate containing samples, peak 2 has a shoulder at position 1 (Fig. 1, left panel). This shoulder at $R + \Delta R = 2.63$ Å can be assigned to an atom at a distance of 2.92 Å. In order to increase the sensitivity on the spectral changes the residual between the experimental spectra and the fit of the first two shells (O_{ax}, O_{eq}) is calculated (Fig. 1, right panel). For the carbonate containing samples the intensity of peak 1 correlates clearly with the intensity of peak 3 (Fig. 1, right panel) and the experimental conditions. Peak 1 (Fig. 1, right panel) at ~$2.4 + \Delta R$ is an indicator of the presence of bidentately coordinated CO_3^{2-} groups. For the carbonate-free samples peak 1 has low amplitude near the detection limit, which is not three times higher than the mean background. Hence the carbonate interactions with U(VI) can be ruled out. Only the carbonate containing samples show a higher peak 1 amplitude, therefore suggesting a U-CO_3^{2-} interaction. Accordingly, the shoulder of peak 2 (Fig. 1, right panel) at $R + \Delta R = 2.63$ Å can be assigned to a carbon atom of carbonate at a distance of 2.92 Å.
The presence of bidentately coordinated CO_3^{2-} implies the presence of a peak at ~$3.65 + \Delta R$ in the FT (Fig. 1, right panel). Peak 3 occurs only in the FT spectra of the carbonate containing samples (Fig. 1, both panels). This peak

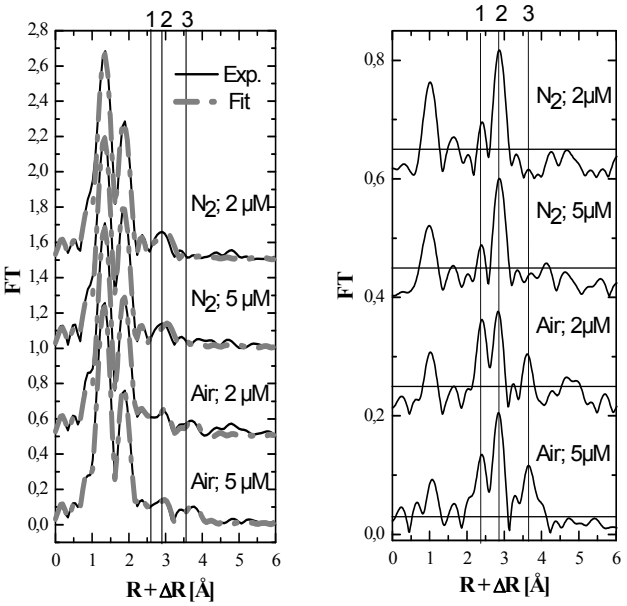

Fig. 1: FT (solid line) and best-fit of the first two shells (dot-dash-line) of the sorption samples (left panel). FT of the residual (right panel). The black horizontal lines are the estimated levels of the limit of detection.

can be attributed to U–U interactions with a U–U distance of 3.92 Å. This R_U is in line with the distance observed for the species like $(UO_2)_2(OH)_2^{2+}$ [6] and the $(UO_2)_2(CO_3)(OH)_3^-$ complex [7].
In summary, the EXAFS results illustrate the influence of carbonate on the sorption of uranium onto gibbsite. In the absence of atmospheric carbonate, a mononuclear inner-sphere complex is formed (Fig. 2, right). This is evidenced by a U–Al distance of 3.4 Å and the lack of peaks that belong to other bound atoms. Due to the speciation, uranium hydroxides are bound to the surface of gibbsite. In the presence of carbonate U–U and U–C interactions are proven by U–U distances of 3.9 Å and U–C distances of 2.92 Å. Due to the calculated speciation a uranium dimer containing carbonate and hydroxyl ions is proposed to be formed on the surface (Fig. 2, left).

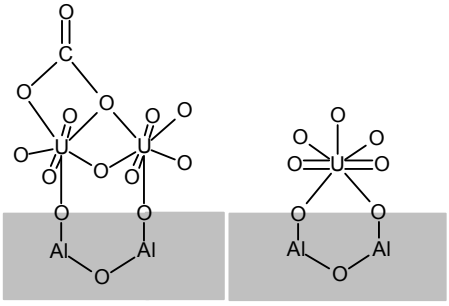

Fig. 2: Possible structures of the two complexes: $(UO_2)_2(CO_3)(OH)_3^-$ (left), mononuclear (right).

[1] Gückel, K. et al. (2011) *Report HZDR-001*, p. 60.
[2] Rossberg, A. et al. (2009) *Environ. Sci. Technol.* **43**, 1400-1406.
[3] Hattori, T. et al. (2009) *Geochim. Cosmochim. Acta* **73**, 5975-5988.
[4] Arai, Y. et al. (2006) *Geochim. Cosmochim. Acta* **70**, 2492-250.
[5] Hennig, C. et al. (2002) *Radiochim. Acta* **90**, 653-657.
[6] Tsushima, S. et al. (2007) *Inorg. Chem.* **46**, 10819-10826.
[7] Szabo, Z. et al. (2008) *Dalton Trans.* **18**, 3158-3161.

Uranium(VI) sorption complexes at the γ-Al_2O_3 water interface

A. Rossberg, K. Müller, H. Foerstendorf, K. Gückel, A. C. Scheinost

Aluminium(hydr)oxides in natural sediments and mine waste may influence the migration of uranium due to their high surface area and sorption capacity. While several studies investigated the macroscopic sorption to Al minerals studies, only few investigated the sorption mechanisms at the molecular level. Here, we report the structures and the speciation of three U(VI)/γ-Al_2O_3 sorption complexes as a function of the surface loading determined by factor analysis of U-L_{III} EXAFS spectra.

EXPERIMENTAL. Nine sorption samples (sample 3-11) where prepared from aqueous solutions with different initial U(VI) concentrations (0.07-18.9 mg/L) and γ-Al_2O_3 equilibrated at pH 6 (pH 7 for sample 10). Surface loadings (Γ) between 1.4 and 18.8 mg/g were obtained. Reference samples are: sample 1 – edge sharing complex of U(VI) sorbed on freshly prepared $Al(OH)_3$ without carbonate (ES), sample 2 – aqueous $UO_2(CO_3)_3^{4-}$ complex (TC), sample 12 – schoepite. Fluorescent UL_{III} EXAFS spectra where measured at 15 K using a 13-element Ge-detector and a closed-cycle He-cryostat at ROBL. The aqueous sample 2 was measured in absorption mode at room temperature. The spectra were analyzed with iterative target transformation factor analysis (ITFA) [1].

RESULTS. For samples 3-11, three spectral distinct components, enabling a reasonable reproduction of the spectral mixtures (Fig. 1, left), were detected by ITFA. These three components refer to the spectra of three structurally different sorption complexes. Target testing [2] was applied in order to identify the components by introducing spectra of possible U(VI) references. The spectral mixtures 3-11 can be reproduced by linear combinations of the spectra of the three reference samples (ES, TC, schoepite). For each sorption sample, ITFA yields the relative concentrations of the identified reference samples (Fig. 1, right). Note that the error of the relative concentrations is approximately ± 6%. For Γ < 3.5 mg/g (samples 3 and 4), ES and TC complexes are present in nearly equal shares (Fig. 1, right). For higher surface loadings, the TC complex disappears and the ES complex reaches its maximum at Γ = 4.3 mg/g (sample 6). For even higher loadings, the schoepite-like component becomes predominant. The EXAFS structural parameters such as interatomic distances (R) and Debye-Waller factors (DW) of the three components are: ES – inner sphere sorption complex with $R_{U–Oeq}$ = 2.36 Å, $DW_{U–Oeq}$ = 0.01 $Å^2$, $R_{U–Al}$ = 3.39 Å, TC – three bidentately coordinated carbonato groups with R_{U-Oeq} = 2.44 Å, $DW_{U–Oeq}$ = 0.005 $Å^2$, $R_{U–C}$ = 2.91 Å, and schoepite – polynuclear species with $R_{U–Oeq}$ = 2.33 Å, $DW_{U–Oeq}$ = 0.03 $Å^2$, $R_{U–U}$ = 3.88 Å. Other structural features, like the U–O_{ax} signal, are constant or have no significant influence so that they do not contribute to the variations. The radial distances of structural key features such as the signal of the distal oxygen atoms arising from bidentately coordinated carboxylic groups and the signal of the U–U interaction arising from polynuclear species are highlighted in Fig. 1.

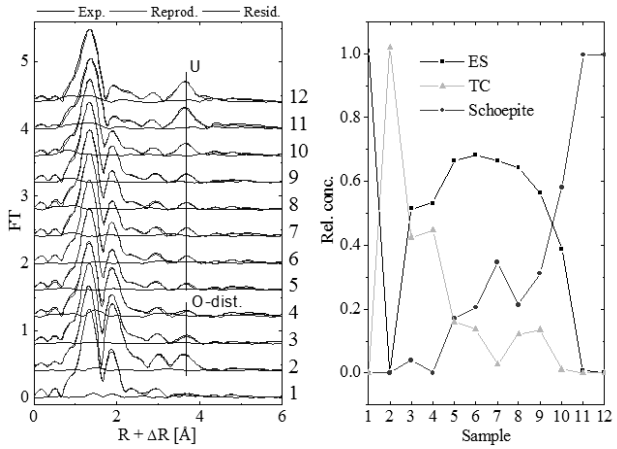

Fig. 1: FT of EXAFS spectra (left panel) of the sorption samples 3-11 and references (sample 1, 2 and 12, see text) with their ITFA reproduction and residuals. The sorption samples are sorted with increasing U(VI) loading (range: 1.4-18.8 mg/g). The vertical line shows the radial position of the distal oxygen atom (O–dist.) and the U–U interaction. Relative concentrations of the three reference samples (right panel).

The presence of a sorbed TC complex is confirmed by subtracting 51% of the ES complex from spectrum 3 and renormalization to 100%.
The spectra of the carbonato surface complex and of the aqueous TC complex are in agreement (Fig. 2).

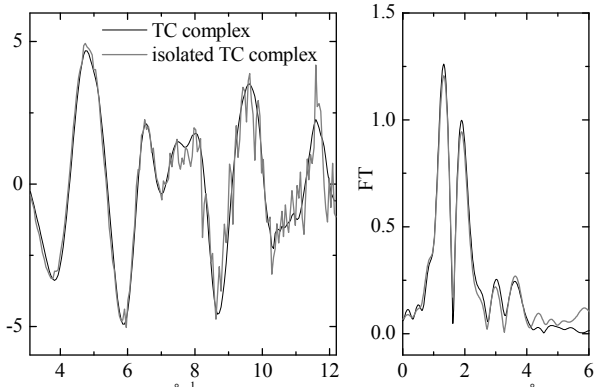

Fig. 2: Spectrum of the aqueous TC complex compared with the isolated spectrum of the carbonato surface complex.

For all sorption samples showing an U–U interaction and for schoepite the fitted $R_{U–U}$ do not deviate more than 0.02 Å from the average value of $R_{U–U}$ = 3.88 Å. Note that this distance is also observed for the aqueous dimeric hydrolysis species $(UO_2)_2(OH)_2^{2+}$ [3]. Hence, the formation of dimeric sorption complexes which might be a precursor for schoepite at higher surface loadings cannot be excluded.

[1] Rossberg, A. et al. (2003) *Anal. Bioanal. Chem.* **376**, 631-638.
[2] Malinowski, E.R. (1978) *Anal. Chim. Acta* **103**, 339-354.
[3] Tsushima, S. et al. (2007) *Inorg. Chem.* **46**, 10819-10826.

Influence of organic ligands on U(VI) sorption onto Opalinus Clay between 10 and 50 °C

K. Schmeide, C. Joseph

The influence of low molecular weight organic acids on the U(VI) sorption onto Opalinus Clay (OPA) was studied in the temperature range 10 to 50 °C using OPA pore water as background electrolyte. Especially citrate and tartrate decrease the U(VI) sorption. With increasing temperature, U(VI) sorption increases both in the absence and in the presence of clay organics.

In addition to salt and crystalline rock, argillaceous rock is considered as potential host rock and backfill material for nuclear waste repositories in deep geological formations. Most natural clays are closely associated with natural organic matter. Low molecular weight organic acids such as acetate, lactate, propionate and formate as well as fulvic and humic acids can be released from the clay under certain conditions [1, 2]. Organics can influence the transport of actinides in the environment [3]. Due to radioactive decay, elevated temperatures of up to 100 °C are expected for the disposal of high-level nuclear waste in clay formations [4]. Thus, the influence of clay organics on the U(VI) sorption onto OPA from the underground rock laboratory in Mont Terri, Switzerland, was studied in the temperature range from 10 to 50 °C.

EXPERIMENTAL. Conditions of sorption experiments: $[^{233}U(VI)] = 1 \cdot 10^{-6}$ M; [ligand] = 0-$1 \cdot 10^{-2}$ M; S/L = 60 g/L; OPA (BHE-24/1); pore water: I = 0.36 M, pH 7.6; $pCO_2 = 10^{-3.5}$ atm; 10-50 °C. The OPA suspensions were pre-equilibrated for 7 d. After that, aliquots of U(VI) and ligand stock solutions were added simultaneously. The sorption time was 7 d. The samples were analyzed by liquid scintillation counting.

RESULTS. The influence of low molecular weight organic acids on the U(VI) sorption onto OPA at 25 °C is given in Fig. 1. The results show that the low U(VI) sorption onto OPA in the absence of ligands (K_d = (0.0222 ± 0.0004) m^3/kg [5]) further decreases with increasing concentration of organic ligands ($1 \cdot 10^{-5}$-$1 \cdot 10^{-2}$ M) due to complex formation in aqueous solution. The mobilizing effect of the organic ligands on U(VI) increases in the following sequence: formate < lactate ~ acetate ≤ propionate < tartrate < citrate. For instance, in the presence of citrate ($1 \cdot 10^{-2}$ M), which has been identified as important ligand in radioactive waste problems, the K_d value for U(VI) amounts to only (0.0011 ± 0.0003) m^3/kg. This shows that citric acid indeed has to be taken into account for safety assessment for nuclear waste repositories. The influence of the organic ligands on the U(VI) sorption onto OPA correlates with the stability of the respective U(VI) ligand complexes in solution. In contrast, humic acid (≤ 50 mg/L) does not change the amount of U(VI) sorbed onto OPA (cf. [5]). In the presence of the low molecular weight organic acids, a reduction of U(VI) to U(IV) was not detected.

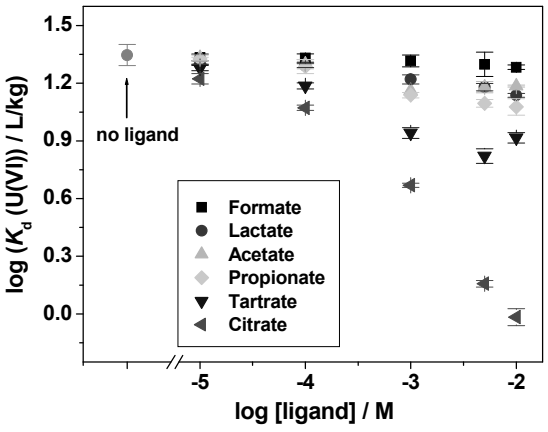

Fig. 1: Influence of low molecular weight organic acids on the U(VI) sorption onto OPA at 25 °C.

In a second series of experiments, the influence of temperature on the U(VI) sorption onto OPA in the absence of ligands and in the presence of lactate or citrate was studied. In the absence of organic ligands, the U(VI) sorption increases with increasing temperature (Fig. 2). For U(VI), an apparent endothermic sorption enthalpy was determined with 34 ± 1 kJ/mol. The entropy amounts to ΔS = 139 ± 3 J·mol^{-1}·K^{-1}. An increased sorption with increasing temperature was also observed for the sorption of Ni^{2+} and Ln^{3+} onto montmorillonite [6] as well as for the sorption of Eu^{3+} and NpO_2^+ onto OPA [7, 8]. Furthermore, an increased interaction of U(VI) with OPA at 60 °C was also detected by diffusion experiments [9].

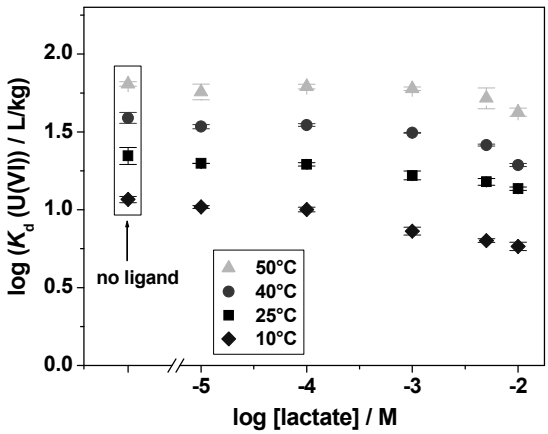

Fig. 2: Influence of temperature on the U(VI) sorption onto OPA in the absence of ligands and in the presence of lactate.

The stronger U(VI) sorption onto OPA with increasing temperature is maintained also in the presence of lactate (cf. Fig. 2) and citrate, when present in the concentration range from $1 \cdot 10^{-5}$ to $1 \cdot 10^{-2}$ M.

ACKNOWLEDGEMENTS. This work was funded by the BMWi under contract number 02E10156.

[1] Courdouan, A. et al. (2007) *Appl. Geochem.* **22**, 2926-2939.
[2] Claret, F. et al. (2003) *Sci. Total Environ.* **317**, 189-200.
[3] Schmeide, K. et al. (2010) *Appl. Geochem.* **25**, 1238-1247.
[4] Brasser, T. et al. (2008) *Report GRS-247*.
[5] Joseph, C. et al. (2011) *Chem. Geology* **284**, 240-250.
[6] Tertre, E. et al. (2005) *Geochim. Cosmochim. Acta* **69**, 4937-4948.
[7] Schott, J. et al. (2012) *Radiochim. Acta*, in press, DOI: 10.1524/ract.2012.1921.
[8] Fröhlich, D.R. et al. (2012) *Appl. Clay Sci.*, submitted.
[9] Joseph, C. et al. (2012) this report, p. 43.

Influence of humic acid on U(VI) diffusion through Opalinus Clay

C. Joseph, L. Van Loon,[1] A. Jakob,[1] K. Schmeide, S. Sachs
[1]Laboratory of Waste Management, Paul Scherrer Institute, Villigen, Switzerland

Diffusion experiments with U(VI) in Opalinus Clay (OPA) were performed in the absence and presence of humic acid (HA). The influence of HA on U(VI) diffusion was found to be not significant.

Natural clay is discussed as potential host rock for nuclear waste repositories. Thus, it is of high interest to investigate its interaction with actinides such as uranium. Organic matter, such as HA, is ubiquitous in nature and presents also a part of natural clay [2]. HA has a variety of functional groups which enables it to complex metal ions like uranium. Thus, HA can influence the migration of actinides through natural clay. Therefore, the U(VI) diffusion through the natural clay OPA was investigated in the absence and presence of HA.

EXPERIMENTAL. OPA bore core samples (BLT-14) from Mont Terri, Switzerland (thickness: 1.1 cm, diameter: 2.55 cm) were inserted in diffusion cells described in [3]. Two cells were applied. In the first cell the U(VI) diffusion was investigated, in the second cell the simultaneous diffusion of U(VI) and HA (type M42, batch M180A [4]) was studied ($[^{233}U(VI)] = 1 \cdot 10^{-6}$ mol/L, $[^{14}C\text{-HA}] = 10$ mg/L). A confining pressure of 5 MPa was on both cells applied. The experimental set-up used for the diffusion experiments is described in [3]. The experiments were performed under anaerobic conditions (N_2, 0% CO_2) at 25 °C. The cells were coupled with a source (200 mL) and receiving reservoir (20 mL) filled with OPA pore water (pH 7.6, $I = 0.36$ M) [5]. The source reservoirs were tracered with $^{233}U(VI)$ and ^{14}C-HA. The U(VI) diffusion experiments were carried out for three months. After that, the clay samples were removed from the cells. With the abrasive peeling technique [6] U(VI) diffusion profiles in OPA were determined. The profiles were evaluated using the commercial software COMSOL Multiphysics 3.5a.

RESULTS. Within the duration of diffusion experiments no $^{233}U(VI)$ could be detected in the receiving reservoirs of both cells. However, diffused HA colloids were found. The diffusive flux J [mol/(m^2·s)] of a solute can be described by Fick's first law Eq. (1), where D_e represents the effective diffusion coefficient [m^2/s], C [mol/m^3] the tracer concentration in the mobile phase and x [m] denotes the spatial coordinate.

$$J = -D_e \cdot \frac{\partial C}{\partial x} \quad (1)$$

The apparent diffusion coefficient D_a [m^2/s] considers the tracer interaction with the clay. Both diffusion coefficients are linked by the rock capacity factor α [-] according to:

$$D_a = \frac{D_e}{\alpha} . \quad (2)$$

The rock capacity factor α is defined as:

$$\alpha = \varepsilon + \rho \cdot K_d \quad (3)$$

where ε [-] is the diffusion-accessible porosity, ρ [kg/m^3] the dry bulk density and K_d [m^3/kg] the sorption distribution coefficient.

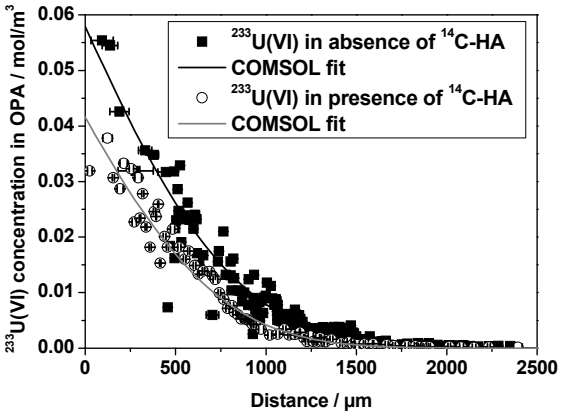

Fig. 1: Concentration profiles of $^{233}U(VI)$ in OPA in the absence and presence of ^{14}C-HA.

In Fig. 1 the U(VI) diffusion profiles determined in the absence and presence of HA are shown. The comparison of the two data sets leads to the conclusion that in the presence of HA U(VI) penetrates the clay less than in the absence of HA. Such a reduced metal ion diffusion was already described for the U(VI) diffusion in compacted kaolinite in the presence of HA [7]. The respective diffusion parameter values determined by fitting the U(VI) profiles are summarized in Tab. 1.

Tab. 1: Determined values for the U(VI) diffusion in the absence and presence of HA.

	U(VI)	U(VI) (+HA)
D_e [10^{-12} m^2/s]	1.9 ± 0.4	1.2 ± 0.3
D_a [10^{-14} m^2/s]	3.1 ± 0.3	2.5 ± 0.3
K_d [m^3/kg]	0.025 ± 0.003	0.020 ± 0.003
K_d [m^3/kg]*	0.0222 ± 0.0004	

*determined by sorption experiments [1].

Also the comparison of the K_d as well as D_e values determined for U(VI) in the absence and presence of HA confirm the conclusion. However, based on the experimental uncertainties, it is concluded that HA does not have a significant effect on U(VI) diffusion through compacted water-saturated OPA. In a previous study, the system U(VI) / HA / OPA was investigated by means of batch sorption experiments [1]. There, also no influence of HA on the U(VI) interaction with OPA was observed. This result is confirmed by the diffusion experiments with intact OPA bore core samples.

ACKNOWLEDGEMENTS. The BMWi funded this work (02E10156).

[1] Joseph, C. et al. (2011) *Chem. Geol.* **284**, 240-250.
[2] Claret, F. et al. (2003) *Sci. Total Environ.* **317**, 189-200.
[3] Van Loon, L.R. et al. (2003) *J. Contam. Hydrol.* **61**, 73-83.
[4] Sachs, S. et al. (2004) *Report FZR-399.*
[5] Pearson, F.J. (1998) *PSI Internal report TM-44-98-07.*
[6] Van Loon, L.R. et al. (2005) *Appl. Radiat. Isot.* **63**, 11-21.
[7] Mibus, J. et al. (2006) *Report FZR-443,* p. 60.

Influence of temperature on U(VI) diffusion through Opalinus Clay

C. Joseph, L. Van Loon,[1] A. Jakob,[1] K. Schmeide, S. Sachs
[1]Laboratory of Waste Management, Paul Scherrer Institute, Villigen, Switzerland

Diffusion experiments with U(VI) in Opalinus Clay (OPA) were performed at 25 and 60 °C. The U(VI) diffusion is comparable to the Np(V) diffusion at 25 °C in OPA. At 60 °C, no significant influence of temperature on U(VI) diffusion was observed. However, two diffusion profiles of U(VI) were observed and attributed to a colloidal and aqueous U(VI) species.

Natural clay is discussed as potential host rock for nuclear waste repositories. Thus, it is of high interest to investigate its interaction with actinides such as uranium. Due to the radioactive decay of the actinides and their fission products elevated temperatures of up to 100 °C are expected close to the waste containers in the repository [1]. Thus, the migration of U(VI) through the natural clay OPA was investigated at 25 and 60 °C.

EXPERIMENTAL. OPA bore core samples (BLT-14) from Mont Terri, Switzerland (thickness: 1.1 cm, diameter: 2.55 cm) were inserted in diffusion cells described in [4]. A confining pressure of 5 MPa was on both cells applied. The experimental set-up used for the diffusion experiments at 25 and 60 °C is described in [4, 5]. The experiments were performed under anaerobic conditions (N_2, 0% CO_2). The cells were coupled with a source (200 mL) and receiving reservoir (20 mL) filled with OPA pore water (pH 7.6, $I = 0.36$ M) [6]. The source reservoir additionally contained the tracer ^{233}U(VI) ($1 \cdot 10^{-6}$ M). The U(VI) diffusion experiments were carried out for three months. After that, the clay samples were removed from the cells. With the help of the abrasive peeling technique, U(VI) diffusion profiles in OPA were determined [7]. The profiles were evaluated using the commercial software COMSOL Multiphysics 3.5a.

RESULTS. Within the duration of diffusion experiments no ^{233}U(VI) could be detected in the receiving reservoirs of the cells at 25 and 60 °C. The determined U(VI) diffusion profiles in the OPA samples are shown in Fig. 1.
The theoretical background of the diffusion process has been described in [4, 8]. The respective diffusion parameter values determined by fitting the U(VI) profiles are summarized in Tab. 1.
At 25 °C, the K_d value for U(VI) determined by diffusion studies agrees well with the K_d value determined by means of sorption experiments [3]. In contrast, Wu et al. [2] determined for the Np(V) / OPA system a larger K_d value by diffusion than by batch sorption experiments. The authors concluded that during the diffusion experiment Np(V) was partially reduced to Np(IV). Since in the present study the K_d values determined for the U(VI) / OPA system by batch sorption and diffusion experiments are comparable, a reduction of U(VI) to U(IV) can be excluded.

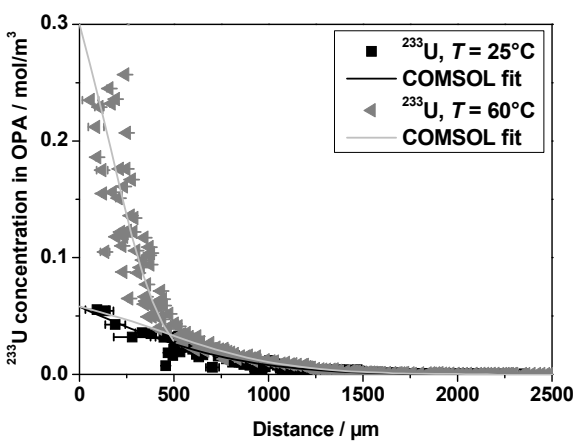

Fig. 1: Concentration profiles of ^{233}U(VI) in OPA at 25 °C and 60 °C.

Tab. 1: Determined values for the U(VI) diffusion at 25 and 60 °C.

	25 °C		60 °C	
	U(VI)	Np(V) [2]	U(VI) coll.	U(VI) aq.
D_e [10^{-12} m^2/s]	1.9 ± 0.4	6.9 ± 1.1	3 ± 1	3 ± 0.5
D_a / [10^{-14} m^2/s]	3.1 ± 0.3	2.8 ± 0.4	0.50 ± 0.07	2.8 ± 0.2
K_d [m^3/kg]	0.025 ± 0.003	0.1 ± 0.01	0.25 ± 0.05	0.045 ± 0.005
K_d [m^3/kg]*	0.0222 ± 0.0004	0.025 ± 0.005		

*determined by sorption experiments [3].

The D_e of U(VI) is smaller than the D_e for the Np(V) diffusion in OPA. That means, U(VI) diffuses with a smaller flux through OPA than Np(V). However, the comparison of the D_a values, which consider the tracer interaction with the clay, shows that the Np(V) diffusion in OPA is in the same range as that of U(VI). This leads to the conclusion that the migration of both actinides through OPA is similar.
Fitting the U(VI) diffusion profile at 60 °C, it became obvious that at least two different U(VI) species are involved in the diffusion process (Fig. 1). These two species were attributed to a diffusing colloidal and aqueous U(VI) species, respectively. The colloidal U(VI) species diffused only about 500 µm into the OPA sample. The aqueous U(VI) species could be detected up to a diffusion distance of about 2.5 mm.
In comparison to the U(VI) diffusion at 25 °C, the interaction of U(VI) with OPA is stronger at 60 °C for both U(VI) species, which is reflected in higher K_d values. With increasing temperature also D_e increases. However, the D_a values for U(VI) at 25 °C and 60 °C (aqueous U(VI) species) are almost equal. This leads to the conclusion, that the migration of U(VI) through OPA is similar at both investigated temperatures.

ACKNOWLEDGEMENTS. The BMWi funded this work (02E10156).

[1] Brasser, T. et al. (2008) *Report GRS – 247*.
[2] Wu, T. et al. (2009) *Environ. Sci. Technol.* **43**, 6567-6571.
[3] Joseph, C. et al. (2011) *Chem. Geol.* **284**, 240-250.
[4] Van Loon, L.R. et al. (2003) *J. Contam. Hydrol.* **61**, 73-83.
[5] Joseph, C. et al. (2012) in preparation.
[6] Pearson, F.J. (1998) *PSI Internal report TM-44-98-07*.
[7] Van Loon, L.R. et al. (2005) *Appl. Radiat. Isot.* **63**, 11-21.
[8] Joseph, C. et al. (2012) this report, p. 42.

Multi-method spectroscopic approach for the uranium(VI) hydrolysis at temperatures up to 60 °C. Part 1: ATR FT-IR spectroscopic measurements

K. Müller, R. Steudtner, T. Meusel

The speciation of 10 mM U(VI) in the pH range from 3.0 to 5.0 was investigated at elevated temperatures by *in situ* ATR FT-IR spectroscopy. A shift of the formation of hydrolysis products to lower pH values and a decrease of the U(VI) solubility can be derived from the spectroscopic data.

The formation and distribution of U(VI) hydrolysis species is predicted to depend strongly on the temperature. In particular the stability of U(VI) polynuclear hydroxo complexes, which are dominant species at 25 °C may change. According to experimental studies of other metal ions, namely Al(III) and La(III), the nuclearity decreases upon increasing temperature [1, 2].
At 25 °C, several spectroscopic techniques, namely UV-vis, TRLFS, EXAFS and vibrational spectroscopy have been applied for identification and structural characterization of U(VI) hydroxo species [3-6]. However, approaches to examine alterations in the thermodynamic data at elevated temperatures are rare.

EXPERIMENTAL. Sample preparation and analysis were done under normal atmosphere and at 25, 40, and 60 °C. The diluted U(VI) solutions were prepared from a 0.05 M UO_2Cl_2 stock solution using Milli-Q water. Ionic strength was 0.1 M (NaCl). Solution pH was adjusted by adding NaOH or HCl. The pH meters were calibrated at each temperature using standard buffers (WTW).

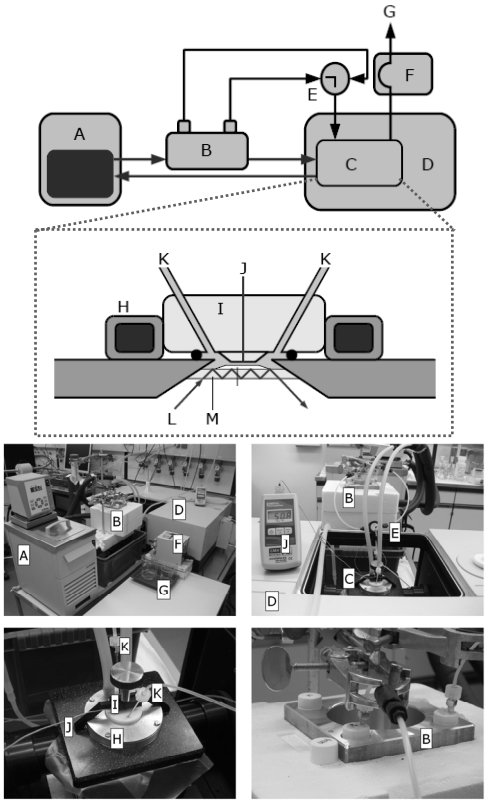

Fig. 1: ATR FT-IR spectroscopic set-up for temperatures up to 70 °C. A) thermostat; B) sample preparation and storage box; C) ATR unit; D) FT-IR spectrometer; E) three-way valve; F) peristaltic pump; G) waste; H) ATR unit heating system; I) flow cell; J) temperature sensor; K) needle; L) IR beam; M) ATR crystal.

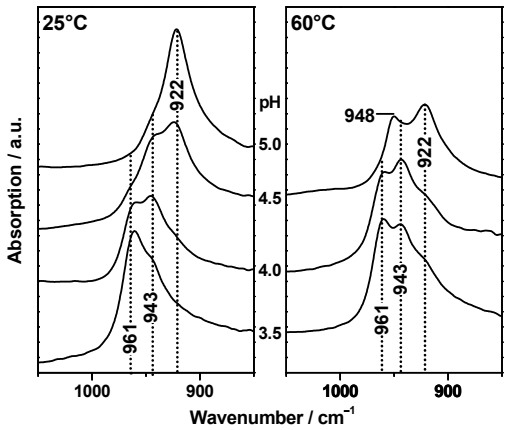

Fig. 2: ATR FT-IR spectra of aqueous 10 mM U(VI) solutions (0.1 M NaCl, air) in the pH range from 3.5 to 5.0 (from bottom to top) at 25 °C (left) and 60 °C (right).

The ATR FT-IR accessory and the procedure of *in situ* experiments were described previously [6]. The upgraded system for measurements at elevated temperatures, consisting of thermostatic controllable sample holder and flow cell is illustrated in Fig. 1.

RESULTS. In Fig. 2 the IR absorption bands representing the $\nu_3(UO_2)$ mode of aqueous U(VI) solutions at 25 °C (left) and 60 °C (right) are shown. The U(VI) concentration was constant at 10 mM, and pH ranged from 3.5 to 5.0 (from bottom to top). At 25 °C, the transition of three distinct band positions at 961, 943, and 922 cm^{-1} is detected as a function of pH. They can be assigned to the free UO_2^{2+} cation (1,0), predominantly at lower pH ($pH \leq 3.5$), the dimer hydroxo (2,2) complex dominating at $pH \sim 4.0$, and the trimer hydroxo (3,5) complex ($pH \geq 4.5$) [6, 7]. At 60 °C, the course of U(VI) hydrolysis is considerably changed. Although all three species were redetected, the transition between them was found to be faster and hydrolysis starts already at lower pH compared to 25 °C. Additionally, the solubility seems to be reduced at higher temperature, because the formation of an U(VI) precipitate with absorption maximum at 948 cm^{-1} is detected in the spectrum at pH 4.5. In contrast, at 25 °C precipitation in freshly prepared 10 mM occurs only at $pH > 5.0$. At the reduced concentration level of 0.1 mM U(VI) in TRLFS experiments the formation of U(VI) precipitate was not observed at all [8].
In summary, the obtained spectral infrared spectroscopic data strongly evidences a modified speciation in millimolar U(VI) aqueous solutions at different temperatures. The formation of U(VI) hydroxo complexes shifts to lower pH at 60 °C. No indication for decrease in nuclearity of the polynuclear complexes was observed at the investigated concentration.

[1] Mesmer, R.E. et al. (1971) *Inorg. Chem.* **10**, 2290-2296.
[2] Ciavatta, L. et al. (1987) *Polyhedron* **6**, 1283-1290.
[3] Meinrath, G. (1997) *J. Radioanal. Nucl. Chem.* **224**, 119-126.
[4] Moulin, C. et al. (1998) *Appl. Spectrosc.* **52**, 528-535.
[5] Tsushima, S. et al. (2007) *Inorg. Chem.* **46**, 10819-10826.
[6] Müller, K. et al. (2008) *Inorg. Chem.* **47**, 10127-10134.
[7] Quilès, F. et al. (2000) *Vib. Spectrosc.* **23**, 231-241.
[8] Steudtner, R. et al. (2012) this report, p. 45.

Multi-method spectroscopic approach for the uranium(VI) hydrolysis at temperatures up to 60 °C. Part 2: TRLF spectroscopic measurements

R. Steudtner, K. Müller

The speciation of 0.1 mM U(VI) in the pH range from 3.0 to 5.0 was investigated at elevated temperature by TRLF spectroscopy. A change in the formation of hydrolysis products can be derived from the spectroscopic data.

EXPERIMENTAL. Sample preparation and analysis were done as described elsewhere [1]. The diluted U(VI) solutions (0.1 mM) were prepared from a 0.05 M $UO_2(ClO_4)_2$ stock solution and ionic strength was adjusted by adding $NaClO_4$. The luminescence of U(VI) was measured after excitation with laser pulses at 266 nm (Minilite laser system, Continuum) and an averaged pulse energy of 300 µJ. The emitted fluorescence light was detected using a spectrograph (iHR 550, HORIBA Jobin Yvon) and an ICCD camera (HORIBA Jobin Yvon). The TRLF spectra were recorded from 400 to 650 nm by accumulating 50 laser pulses using a gate width of 20 µs. For the time-resolved measurements 101 spectra were recorded until a maximum delay time of 100 µs. The first time step started 50 ns after the excitation pulse.

RESULTS. In Fig. 1 the luminescence spectra between 400 and 650 nm of aqueous U(VI) solutions at 25 °C (left) and 60 °C (right) are shown. The U(VI) concentration was constant at 0.1 mM, and pH ranged from 2.0 to 5.0 (from bottom to top).

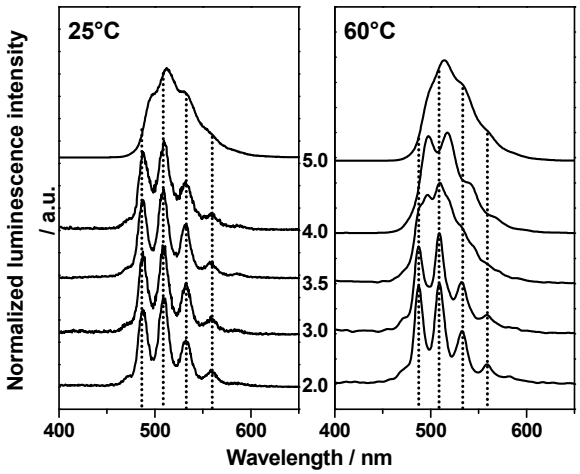

Fig. 1: TRLF spectra of aqueous 0.1 mM U(VI) solutions (0.1 M $NaClO_4$, air) in the pH range from 2.0 to 5.0 (from bottom to top) at 25 °C (left) and 60 °C (right).

In the strong acidic pH range the free UO_2^{2+} cation dominates the U(VI) speciation at both temperatures. The luminescence spectra ($\leq$ pH 3.0) are characterized by the typical emission bands at 487.8, 508.7, 532.2 and 558.9 nm for the free UO_2^{2+} [2]. At higher pH, the luminescence spectra at 25 °C and 60 °C are considerable different. At 60 °C, the spectra at pH $\geq$ 3.5 are strongly influenced by the formation of a U(VI) hydroxo complex. The respective peak maxima at 497.8, 518.0, 542.2 and 568.1 nm are attributed to the U(VI) dimer hydroxo complex [2]. In contrast, the dimeric hydroxo complex does not contribute significantly to the spectra obtained at the same pH at 25 °C. At pH 5.0 both luminescence spectra at 25 °C and 60 °C present characteristic spectral features (fluorescence decay time and band position) of the U(VI) trimer hydroxo complex [3], predominating the speciation at near neutral conditions.

For determination of the complex formation constant the luminescence as well as the infrared spectra [4] were analyzed with SPECFIT [5, 6]. Table 1 summarizes the complex formation constants resulting from the experiments and estimated by the van't Hoff equation [7]. Ionic strength corrections to 0.1 M were made by using the SIT (specific ions interaction theory) method [7] with the ionic interaction coefficients considered to be temperature independent.

The equilibrium constants of the two U(VI) hydroxo complexes at 60 °C show small discrepancies to the values obtained by applying the van't Hoff equation. In accordance to the ATR FT-IR results, the formation of U(VI) hydroxo complexes onsets at lower pH at 60 °C in comparison to 25 °C.

Tab. 1: Experimental and calculated complex formation constant at 60 °C for the reaction:
$m\ UO_2^{2+} + n\ OH^- \rightleftharpoons (UO_2)_m(OH)_n^{2m-n}$.

$\log K_{0.1\ M}$	$(UO_2)_2(OH)_2^{2+}$	$(UO_2)_3(OH)_5^{+}$
TRLFS	4.99 ± 0.19	14.14 ± 0.08
ATR FT-IR	4.63 ± 0.41	14.80 ± 0.41
Van't Hoff equation*	5.29 ± 0.08	13.84 ± 0.04

$$* \log K_{0.1\ M}(T) = \left(\frac{298.15\,K}{T}\right) \log K_{0.1\ M}(298.15\,K) + \Delta_r S_m \left(\frac{T - 298.15\,K}{RT\ln(10)}\right)$$

[1] Günther, A. et al. (2011) *Radiochim. Acta* **99**, 535-541.
[2] Moulin, C. et al. (1998) *Appl. Spectrosc.* **52**, 528-535.
[3] Sachs, S. et al. (2007) *Radiochim. Acta* **95**, 103-110.
[4] Steudtner, R. et al. (2011) *Dalton Trans.* **40**, 11920-11925.
[5] Binstead, R.A. et al. (2005) SPECFIT - Global analysis system, Version 3.0.37, Spectrum Software Associates, Marlborough, U.S.A.
[6] Gampp, H. et al. (1985) *Talanta* **32**, 257-264.
[7] Guillaumont, R. et al. (2003) *Update on the chemical thermodynamics of uranium, neptunium, plutonium, americum and technetium,* Elsevier, Amsterdam.

Sorption and interfacial redox of Sn(II) under anoxic conditions: magnetite vs. anatase

S. Dulnee, D. Banerjee, A. Rossberg, A. C. Scheinost

The long-lived fission product ^{126}Sn is of substantial interest in the context of nuclear waste disposal in deep underground repositories. However, the redox state (di- or tetravalent) under the expected anoxic conditions is still a matter of debate. We, therefore, investigated the stability of Sn(II) in the presence of a highly redox-reactive mineral, magnetite ($Fe^{II}Fe^{III}_2O_4$), in comparison to a non-redox-reactive, anatase (TiO_2).

EXPERIMENTAL. Mineral synthesis and sorption experiments were performed in the dark under strictly anoxic conditions in a glovebox at < 2 ppm O_2. The nanoparticulate magnetite, synthesized as described in [1], was characterized by TEM, XRD, BET, Zeta-sizer, and Mössbauer spectroscopy (MS) before using in sorption experiments.
Kinetic uptake experiments were conducted with 10 µM $[Sn(II)]_{ini}$ at pH 6.5 ± 0.05, using either 2 g/L magnetite or 2 g/L anatase (SSA ~234 m²/g) suspended in 0.01 M NaCl. pH edges were monitored with 2 mL of 2 g/L magnetite and 25 (1.03% Sn) and 5 (0.21% Sn) mL of 10 µM $[Sn(II)]_{ini}$ held for 24 h before pH was verified again. Sn sorbed were expressed as $(Sn_i–Sn_s)*100/Sn_i$, where Sn_i and Sn_s represent initial concentration and supernatant concentration of Sn investigated by ICP-MS.

RESULTS. Added Sn(II) is strongly sorbed between pH 3 to 9 by magnetite, and between 3 to 7 by anatase (Fig. 1). At low pH and positive surface charge, decreased sorption is in line with the predominance of Sn^{2+} (or Sn^{4+}) cation (< pH 3), while at pH > 3 uncharged Sn(II) and negatively charged Sn(IV) species prevail. The decrease of sorption at high pH is related to the charge reversal of the mineral surfaces, which happens at higher pH for magnetite than for anatase.

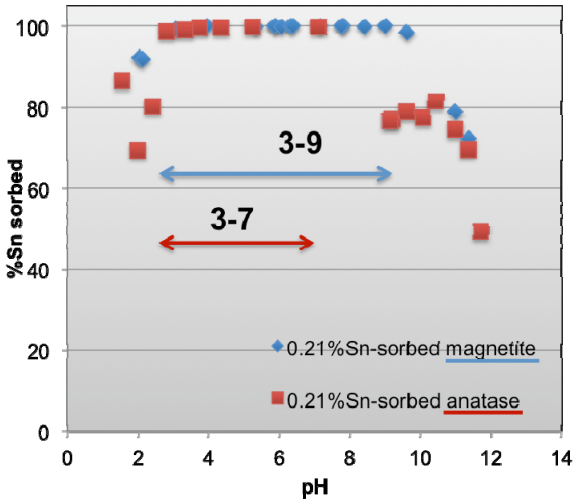

Fig. 1: Sorption of Sn onto magnetite and anatase as a function of pH.

We found a rapid (< 30 min) oxidation of Sn(II) to Sn(IV) in the presence of magnetite (data not shown). Although solubility calculation predicted the precipitation of SnO_2, the local structure determined by XA showed two Sn-Fe distances of about 3.15 and 3.60 Å in line with edge and corner sharing arrangements between octahedrally Sn(IV) and the magnetite surface, indicative of inner-sphere complexation (Fig. 2). The complex structure remains invariant between pH 3 and 9 (Fig. 2).

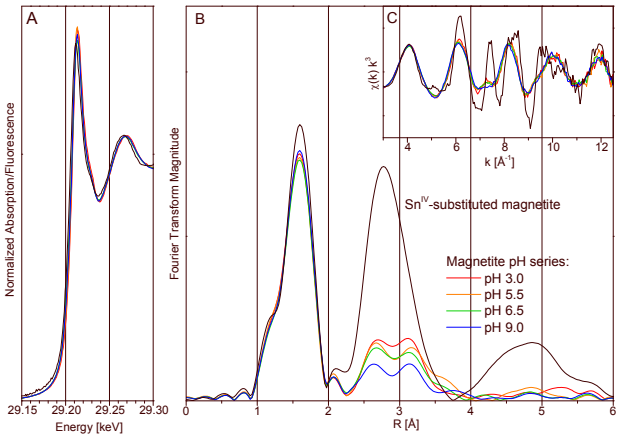

Fig. 2: Sn-K edge XANES and EXAFS of Sn sorbed to magnetite as a function of pH. The spectrum of Sn(IV)-substituted magnetite is shown for comparison.

After 30 min reaction with anatase, Sn(II) was conserved. However, even with the redox-inert anatase, Sn(II) oxidized to Sn(IV) over time, forming an Sn(IV) inner-sphere complex with Sn-Ti distances at 3.24 and 3.53 Å (Fig. 3).

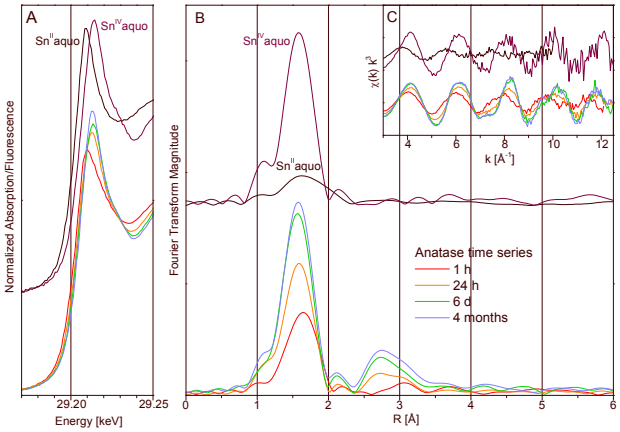

Fig. 3: Sn-K edge XANES and EXAFS of Sn sorbed to anatase as a function of time.

Our results clearly indicate that Sn(IV) is the most relevant oxidation state to be considered even under reducing conditions, and that inner-sphere complexation is a relevant retention mechanism.

[1] Kirsch, R. et al. (2011) *Environ. Sci. Technol.* **45**, 7267-7274.

X-ray photoelectron spectroscopy investigation of Sn(II) reaction with magnetite and goethite

D. Banerjee, S. Dulnee, A. C. Scheinost

XPS investigation of reaction of Sn(II) with magnetite and goethite surfaces under varying pH conditions revealed oxidation of Sn(II) to Sn(IV) on both mineral surfaces. Formation of Fe(II) as a reaction product was also observed. However, the ratio of Sn to Fe(II) produced as reaction product is approximately 1, suggesting transfer of electrons from the bulk to the surface of the minerals to oxidize part of the Fe(II) to Fe(III).

EXPERIMENTAL. Mineral synthesis [1] and sorption experiments were carried out under strictly anoxic conditions in a Jacomex glovebox (< 2 ppmv O_2). For the sorption experiments 2 g/L mineral suspension was initially pH adjusted and equilibrated for 24 h. Subsequently, 10 µM Sn(II) solution was added and the resulting suspension was further equilibrated for 24 h. For the goethite series, two samples at pH 3 and 9 and for the magnetite series three samples at pH 3, 6.5 and 9 were analyzed with XPS. The supernatant was analyzed for dissolved Fe using ICP-MS.

X-ray Photoelectron Spectroscopy (XPS) spectra of frozen wet pastes of reacted samples were collected with a cryogenic KRATOS Axis Ultra electron spectrometer under monochromatic Al Kα radiation (1486.6 eV). The samples were analyzed in the liquid nitrogen cooled (−155 °C) analytical chamber of the instrument. All the elemental spectra were fitted using CasaXPS software.

RESULTS. The Sn $3d_{5/2}$ XPS spectra of the reacted samples for both goethite and magnetite series exhibit a single peak at a binding energy of 486.8 eV which is in excellent agreement with that of SnO_2 as obtained from available database [2]. This suggests that the sorbed Sn(II) is readily oxidized to Sn(IV) at the surfaces of goethite and magnetite.

The Fe $2p_{3/2}$ spectrum of the pristine goethite sample is fitted with four multiplet peaks [3] corresponding to Fe(III) with the leading peak position around 710 eV (Fig. 1A, top). A rigorous fitting routine was employed, where the peak parameters of all other peaks of the multiplet set, such as peak position, intensity and full width at half maximum (fwhm) were constrained with respect to the leading peak. In the reacted samples, however, a small contribution (~ 5% of total Fe) around 708 eV is identified which corresponds to Fe(II) (Fig. 1A, middle and bottom). This suggests that Fe(II) is produced as a reaction product at the surface of goethite.

For the pristine magnetite sample (Fig. 1B, top) the Fe $2p_{3/2}$ spectrum exhibits presence of both Fe(III) and Fe(II) at the surface. In the Sn-reacted sample at pH 3, only minor increase in the surface Fe(II) proportion is observed (Fig. 1B, middle). A similar result of only minor increase in surface Fe(II) proportion was also observed for the sample at pH 6.5. At pH 9, however, a more substantial increase in the surface Fe(II) proportion is observed (Fig. 1B, bottom).

XPS quantification table (Tab. 1) shows that the atomic ratio between Sn and Fe(II) produced as a reaction product is approximately 1 for both goethite and magnetite series samples. Assuming that for the oxidation of each atom of Sn(II) to Sn(IV), two atoms of Fe(III) are reduced to Fe(II), one would expect a ratio of 1 : 2 for Sn : Fe(II). Since there is no evidence of Fe(II) being dissolved from the surface from the dissolved Fe data, it is likely that electrons are transferred from the bulk of the minerals to the surface to oxidize Sn(II). Such structural electron transfer process has been documented in case of goethite, ferrihydrite and hematite in recent studies [4].

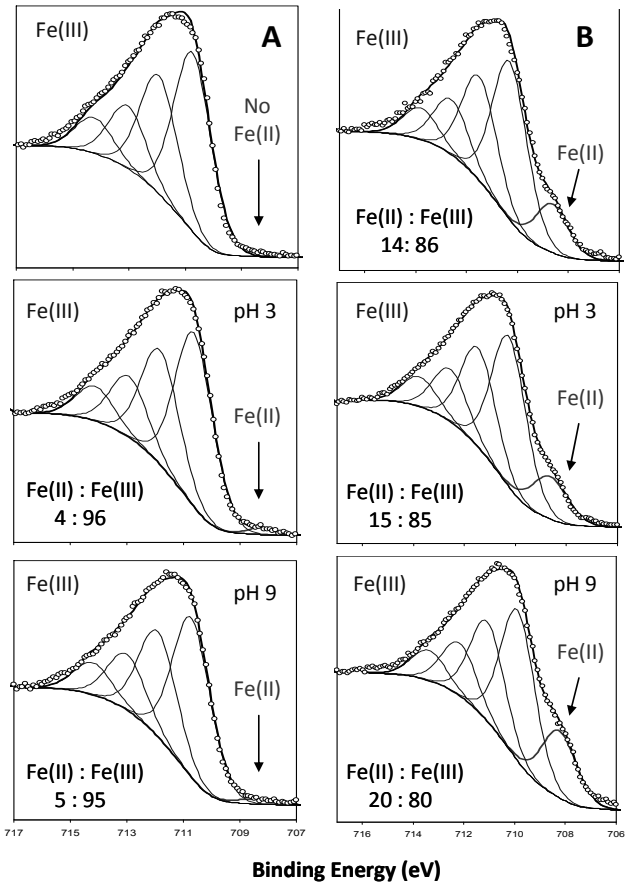

Fig. 1: Fe $2p_{3/2}$ XPS spectra of pristine (top) and Sn-reacted samples at pH 3 and 9 for the goethite series on the left column (A) and those of the magnetite series on the right column (B). The Fe(III) multiplet peaks used in the fitting of the spectra are shown as thin lines, Fe(II) contributions are indicated by arrows.

Tab. 1: XPS quantification table (values in atomic %; error ± 5%).

	Goe	Sn-Goe pH 3	Sn-Goe pH 9	Mag	Sn-Mag pH 3	Sn-Mag pH 6.5	Sn-Mag pH 9
Sn	0.0	0.6	0.7	0.0	0.5	0.5	0.8
Fe(II)	0.0	0.8	1.0	4.2	4.4	4.6	5.5

[1] Kirsch, R. et al. (2008) *Mineral. Mag.* **72**, 185-189.
[2] Wagner, C.D. et al. (2000) NIST XPS Database, version 3.5.
[3] Renock, D. et al. (2009) *Chem. Geol.* **268**, 116-125.
[4] Williams, A.G.B. et al. (2004) *Environ. Sci. Technol.* **38**, 4782-4790.

Influence of temperature on the sorption of selenate onto anatase

C. Franzen, N. Jordan, K. Müller

The sorption of Se(VI) onto anatase was investigated at different temperatures (25 °C, 40 °C, and 60 °C) by batch experiments and *in situ* ATR FT-IR spectroscopy. A decrease in sorption at higher temperatures could be observed and assigned to a change in the surface properties of anatase.

EXPERIMENTAL. Batch experiments were conducted at a solid-to-solution ratio of 0.5 g L^{-1} and an initial Se(VI) concentration of 10^{-5} mol L^{-1}. The suspensions were equilibrated for 48 hours in a thermostatically controlled head-over-head shaker. All preparations were conducted in N_2-atmosphere. After thermostatically controlled centrifugation during two hours at 12,000 g, the remaining selenium concentration in the supernatant was determined by ICP-MS.
The selenate sorption reactions onto anatase were investigated by *in situ* ATR FT-IR spectroscopy, in comparison to a recent study at 25 °C [1]. A dedicated flow set-up with integrated temperature monitoring of the solutions and the ATR crystal was used.
The impact of temperature (25 °C and 60 °C) on the variable surface charge of anatase (pH 3.5-11) was evaluated by zeta potential measurements using laser Doppler electrophoresis.

RESULTS. The sorption of Se(VI) onto anatase as a function of pH was similar at 25 °C and 60 °C, i.e. sorption decreased with increasing pH (Fig. 1). However, the sorption capacity of anatase towards Se(VI) was lowered at a higher temperature. Furthermore, the pH value above which no Se(VI) sorption occurs was shifted to lower pH values.

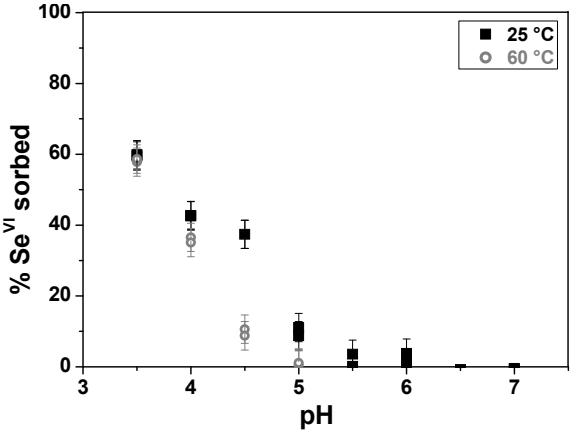

Fig. 1: Se(VI) sorption edges onto anatase at 25 °C and 60 °C ($[Se(VI)]_{ini}$ = 10^{-5} mol L^{-1}, m/v = 0.5 g L^{-1}, I = 0.1 M NaCl).

As shown in Fig. 2, the isoelectric point of anatase (pH_{IEP}) was located at pH 6.3 at 25 °C. At higher temperatures, the pH_{IEP} was shifted towards lower pH with a value of 5.5 at 60 °C; being in good agreement with data from literature where the pH_{PZC} of different oxides and hydroxides were experimentally determined and calculated at different temperatures [2, 3]. In addition, the absolute values of the zeta potential were lowered at higher temperatures. Both findings were in good agreement with the batch experiments.

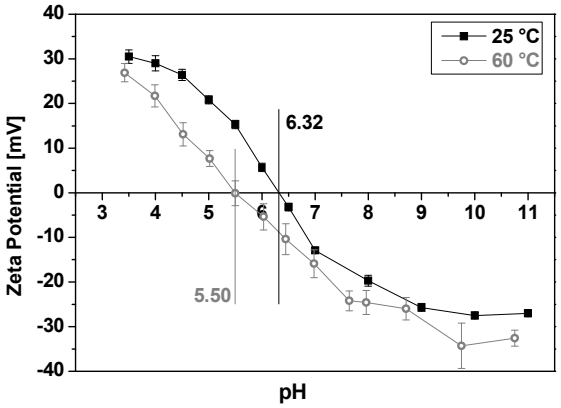

Fig. 2: Zeta potential of the neat surface of anatase at 25 °C and 60 °C (m/v = 0.5 g L^{-1}, I = 0.1 M NaCl).

ATR FT-IR spectroscopy at 25 °C showed a blue shift of the asymmetric ν_3(Se-O) stretching mode of the sorbed Se(VI) onto anatase (880 cm^{-1}) compared to the ν_3 mode of the free SeO_4^{2-} species in solution (867 cm^{-1}), indicating the formation of outer-sphere complexes on the anatase surface [1].
At higher temperatures, IR measurements showed a reduction of the band intensity of the ν_3(Se-O) mode, providing evidence for an overall decrease of selenium(VI) sorption capacity onto anatase (Fig. 3), in agreement with the batch experiments. However, since only a very small blue shift (885 cm^{-1}) of the ν_3(Se-O) mode was observed, no significant structural changes on the sorbed selenium(VI) surface complexes are predicted at higher temperature.

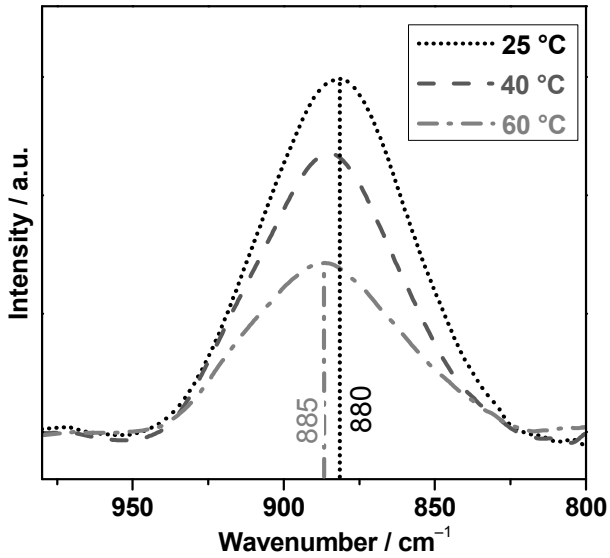

Fig. 3: IR spectra of the Se(VI) sorption onto anatase ($[Se(VI)]_{ini}$ = 500 µM; pH = 3.5, I = 0.1 M NaCl).

ACKNOWLEDGEMENTS. This work is part of the VESPA project, funded by BMWi through contract 02E10790.

[1] Jordan, N. et al. (2011) *Geochim. Cosmochim. Acta* **75**, 1519-1530.
[2] Kulik, D. (2000) *Geochim. Cosmochim. Acta* **64**, 3161-3179.
[3] Vlasova, N.N. et al. (2004) in: *Water-Rock Interaction 2*, p. 1017-1021, Balkema Publ., Leiden.

Adsorption mechanism of Se(VI) onto maghemite

N. Jordan, A. Ritter, H. Foerstendorf, A. C. Scheinost, S. Weiß, K. Heim, J. Grenzer,[1] A. Mücklich,[1] H. Reuther[1]
[1]Institute of Ion Beam Physics and Materials Research, Helmholtz-Zentrum Dresden-Rossendorf, Dresden, Germany

Sorption of Se(VI) onto maghemite has been investigated. Both increase in pH and ionic strength led to a decrease of Se(VI) sorption. Zeta potential measurements showed that the pH_{IEP} of maghemite was not significantly impacted upon Se(VI) sorption, but the net positive surface charge at pH < pH_{IEP} was decreased. *In situ* ATR FT-IR measurements revealed the formation of bidentate outer-sphere (OS) complexes (C_{2v} symmetry) during the sorption process. EXAFS showed the additional presence of ~ 15% of inner-sphere (IS) complexes in binuclear corner-sharing geometry.

In the context of nuclear waste management, ^{79}Se could be one of the major isotopes contributing to the global radioactivity potentially reaching the biosphere. Maghemite (γ-Fe_2O_3) is a ubiquitous iron oxide in the environment and is also part of the corrosion products of stainless steel canisters. In addition, maghemite ability to remove inorganic pollutants like As(V), Cr(VI), Mo(VI) was already shown and its magnetic properties eases the separation process. Thus, this study was aiming at characterizing at both macroscopic and microscopic levels the sorption process of Se(VI) onto maghemite.

EXPERIMENTAL. Maghemite (Alfa Aesar) is a polycrystalline powder with a high purity (> 99%) and a specific surface area of 38 $m^2\ g^{-1}$. The detailed description of the performance of batch sorption studies, zeta potential measurements and *in situ* ATR FT-IR sorption experiments is given elsewhere [1].

RESULTS. Se(VI) sorption onto maghemite is at maximum in the acidic pH range and decreases with increasing pH and ionic strength (Fig. 1). EXAFS evidenced the absence of heterogeneous reduction of Se(VI) at the maghemite surface, showing that only sorption processes are responsible for its withdrawal from the liquid phase to the solid phase.
The zeta potential is strongly pH-dependent, ranging from ~ 43.3 mV at pH 3.5 to ~ −32.8 mV at pH 11.0 (Fig. 2). The net negative charge of maghemite correlates with pH. Upon Se(VI) sorption, the pH_{IEP} of maghemite was not significantly shifted. However, the net positive charge of maghemite is decreased at pH < 8.0. Both observations are strong indications of an electrostatic interaction process between the maghemite surface and SeO_4^{2-} ions [1, 2].

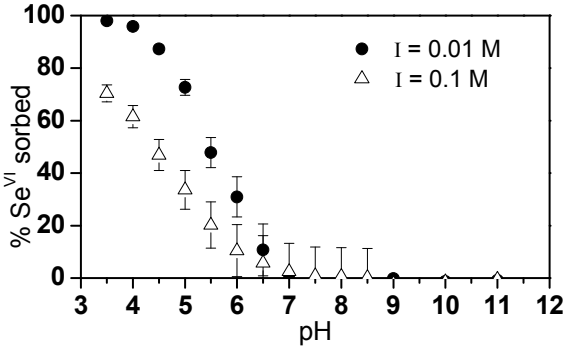

Fig. 1: Sorption edges of Se(VI) onto maghemite. m/V = 1 g L^{-1}, 0.1 and 0.01 M NaCl, $[Se^{VI}]_{initial}$ = 1·10^{-5} M, 2 days of stirring.

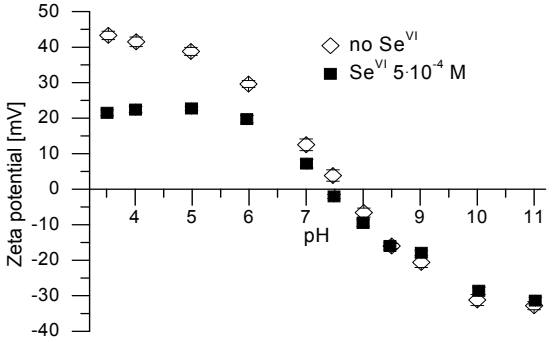

Fig. 2: Zeta potential of maghemite (open diamonds) and the effect of Se(VI) sorption (filled squares), m/V = 0.75 g L^{-1}, $[Se^{VI}]_{initial}$ =5·10^{-4} M, 0.1 M NaCl, 2 days of stirring.

IR measurements (Fig. 3) revealed a fast formation of outer-sphere (OS) complexes, easily removed by flushing with blank solution. Because of the vibrational band pattern, the tetrahedral symmetry (T_d) of the aqueous SeO_4^{2-} ions is significantly changed upon OS complexation [3]. Similar surface complexes were observed at higher pH and lower ionic strength (data not shown). However, EXAFS (data not shown) revealed the additional presence of a small portion (~15%) of inner-sphere (IS) complexes at acidic pH.

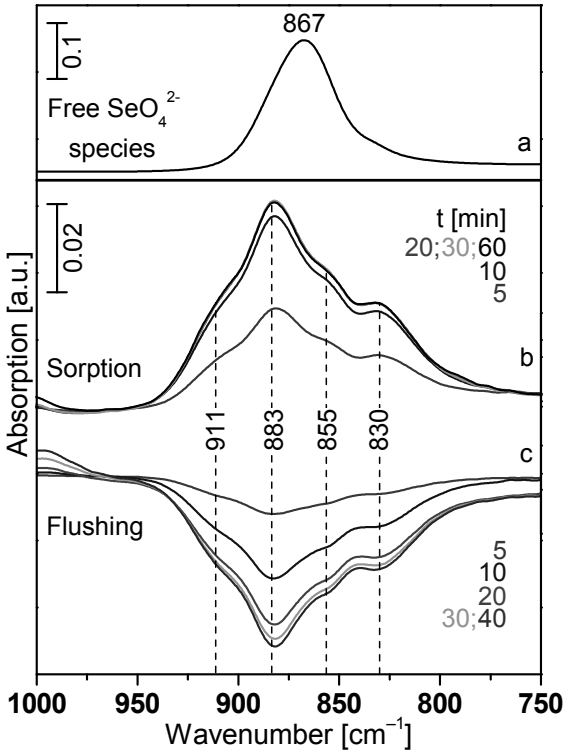

Fig. 3: *In situ* ATR FT-IR spectra of 0.1 M Se(VI) in aqueous solution (a), 500 µM sorbed on γ-Fe_2O_3 (b), desorbed from γ-Fe_2O_3 (c) (D_2O, pD 3.5, 0.1 M NaCl, N_2). Indicated values are in cm^{-1}.

[1] Jordan, N. et al. (2011) *Geochim. Cosmochim. Acta* **75**, 1519-1530.
[2] Elzinga, E.J. et al. (2009) *J. Colloid Interf. Sci.* **340**, 153-159.
[3] Foerstendorf, H. et al. (2012) this report, p. 50.

Different types of outer-sphere complexes of selenate ions on mineral surfaces

H. Foerstendorf, N. Jordan, K. Heim, A. Ritter

The intrinsic correlation between the molecule symmetry and its vibrational modes allows the discrimination between different types of outer-sphere complexes of selenate anions on mineral surfaces by *in situ* IR spectroscopy.

Recently, the classification of outer-sphere complexation was differentiated for cationic surface species by introducing a so-called "extended outer-sphere" (EOS) surface complex. In contrast to the "classical" outer-sphere complex (OS), the EOS is characterized by interactions with the surface *via* a sustained hydration shell of the surface [2]. In this comparative work, we demonstrate that such a discrimination can also be valid for surface species of selenate ions on different minerals.

EXPERIMENTAL. The performance of the *in situ* ATR FT-IR sorption experiments of selenate are described in detail elsewhere [1].

RESULTS. During outer-sphere complexation, water molecules separate the sorbed species and the functional surface groups. This is referred to non-specific adsorption. Indeed, during the formation of outer-sphere surface complexes, the oxyanions retain their hydration shell and do not form chemical (covalent) bonds with the surface sites. Rather, the attraction is done by electrostatic forces. Therefore, the symmetry of outer-sphere complexes is expected to be very similar to those of the free selenate ions in solution, i.e. T_d. Figures 1A and B show the band of the $\nu_3(SeO_4)$ mode of the tetrahedral aqueous SeO_4^{2-} ion and the surface species formed on the anatase surface, respectively. In both spectra, the overall shape of this band is nearly unchanged reflecting the same molecular symmetry. The slightly shifted frequency of the surface species

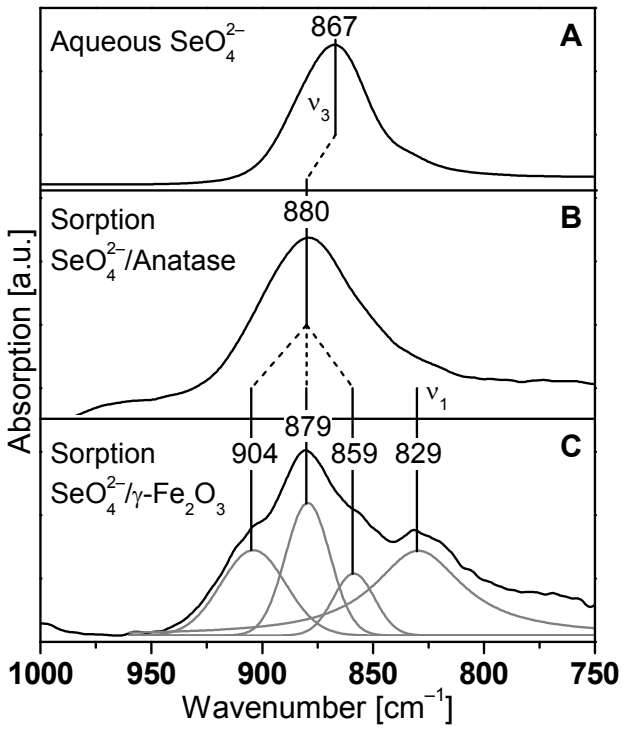

Fig. 1: IR spectra of aqueous selenate species. Aqueous SeO_4^{2-} (A), surface complex on anatase [1] (B) and on maghemite [5] (C).

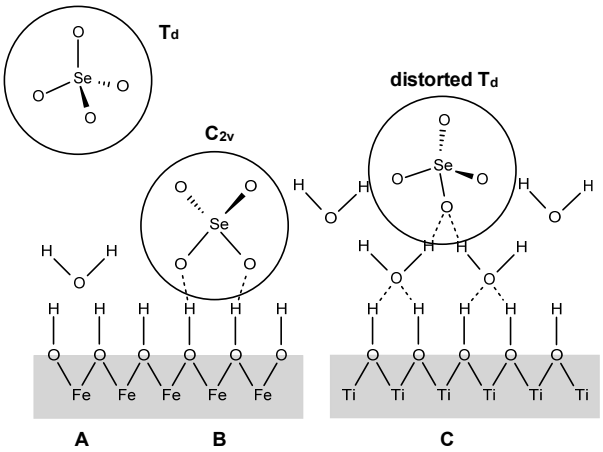

Fig. 2: Scheme of SeO_4^{2-} surface species. Aqueous species (A), outer sphere complex as derived for maghemite surfaces (B) and extended outer sphere complex as derived for anatase surfaces (C).

represents the weak interaction with the surface which might result in a somehow distorted tetrahedral geometry [1]. A coordination to functional groups *via* one or two of their oxygen atoms is expected to result in a lower molecular symmetry compared to the free aqueous species. In addition, such a change of the molecule's symmetry should be reflected by significant alterations in the vibrational spectra. Generally, because of the symmetry change vibrational modes might split due to their multiple degenerated character and/or become IR active. In fact, the selenate sorption species on maghemite show completely different spectral characteristics, that is a split of the $\nu_3(SeO_4)$ mode into three bands and the appearance of the $\nu_1(SeO_4)$ mode which becomes IR active indicating a significantly changed symmetry (Fig. 1C). Such a change of the band pattern is in agreement with a C_{2v} symmetry instead of T_d [3]. A close association of these outer-sphere complexes to the maghemite surface could take place *via* H-bonds, as it was recently suggested from sorption experiments of atmospherically derived carbonate onto ferrihydrite [4].

With respect to results from batch experiments on a macroscopic level and from X-ray absorption spectroscopy demonstrating outer-sphere complexation of selenate on both anatase [1] and maghemite [5], the molecule symmetry of the surface species is completely different on the different surfaces. This implies that selenium(VI) forms outer-sphere complexes onto maghemite, explaining the symmetry reduction of the sorbed species from T_d (Fig. 2A) to C_{2v} (Fig. 2C), whereas selenate is sorbed as extended outer-sphere complexes onto anatase (Fig. 2B).

[1] Jordan, N. et al. (2011) *Geochim. Cosmochim. Acta* **75**, 1519-1530.
[2] Lee, S.S. et al. (2010) *Langmuir* **26**, 16647-16651.
[3] Nakamoto, K. (2002) *Handbook of Vibrational Spectroscopy*, p. 1872-1892, Wiley, Chichester.
[4] Hausner, D.B. et al. (2009) *J. Coll. Interface. Sci.* **337**, 492-500.
[5] Jordan, N. et al. (2012) this report, p. 49.

Identifying causes of kinetic processes involved in metal-humate complexation

H. Lippold, S. Eidner,[1] M. U. Kumke,[1] J. Lippmann-Pipke
[1]Department of Chemistry, Physical Chemistry, University of Potsdam, Golm, Germany

The applicability of equilibrium models for humic-bound transport of toxic or radioactive metals is limited by kinetic processes. Increasing inertness observed for metal-humate complexes conflicts with the assumption of their dissociation under changing geochemical conditions. This work aimed at gaining more insight into the chemical background of such processes, focusing on time-dependent changes in the competition effect of Al(III) with respect to humate complexation of Tb(III) and Eu(III).

EXPERIMENTAL. Tb(III) and Eu(III) were employed both as analogues of trivalent actinides (using ^{160}Tb and ^{152}Eu as short-lived radioactive tracers to allow studies at low concentrations) and as sensitive spectroscopic probe metals. Their humic-bound fractions were determined by the anion exchange method [1] for systems of Al(III) and humic acid (HA) that had been allowed to pre-equilibrate for different time periods before. Laser-induced fluorescence spectroscopy (steady-state and time-resolved) was employed to detect structural alterations as a function of contact time.

RESULTS. Time-dependent studies on complexation of Tb(III) with pre-equilibrated Al(III)/HA systems (Fig. 1) uncovered that the "blocking effect" of Al(III) increased within a period of ~2 days. As the amount of bound Al(III) was constant during that time, the trend must be based on qualitative changes.

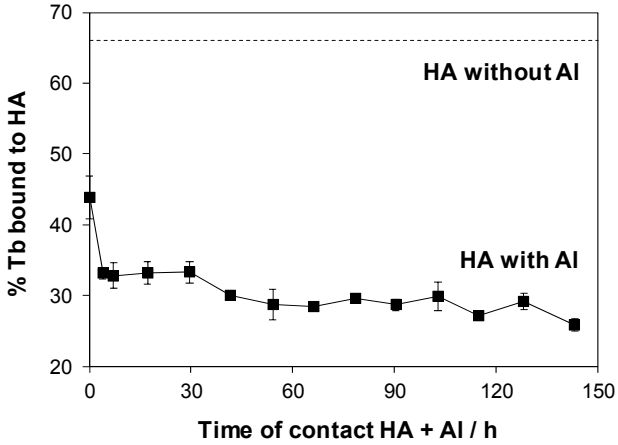

Fig. 1: Increasing competition of Al(III) on complexation of Tb(III) with HA (10^{-7} M [^{160}Tb]Tb, 10^{-5} M Al, 5 mg L^{-1} HA, 0.1 M $NaClO_4$, pH 4.0) [2].

A delayed degradation of polynuclear hydrolysis species (observed for Fe(III) [3], illustrated in Fig. 2a) does not occur, which was concluded from time-dependent pH measurements.

The time scale of the stabilization process corresponds to the kinetics of an increase in complex inertness found in dissociation experiments. Based on these studies, a "diffusion theory" has been established [4, 5], where it is assumed that bound metals penetrate the humic molecule, moving from weak peripheral sites to strong internal sites which are not directly accessible (Fig. 2b). However, in view of our competition experiments, we object to this theory. The increase in the blocking effect is not explicable with a movement away from the ("initial") binding sites for competing metals.

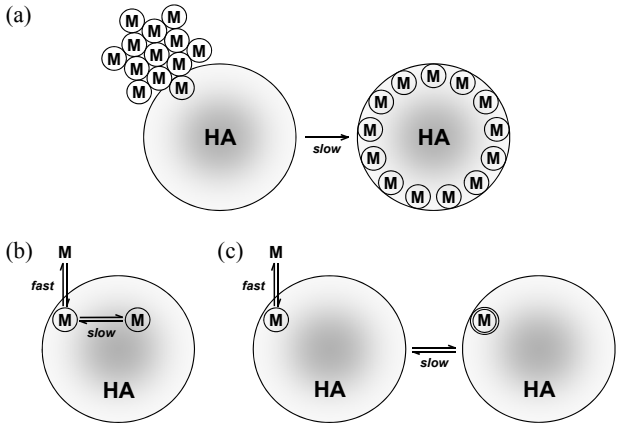

Fig. 2: Schematic illustration of possible stabilization processes leading to an increase in the inertness of metal-humate complexes.

Instead, it appears that an on-site stabilization as depicted in Fig. 2c is the only possible explanation, i.e., bound metals do not change sites but the sites themselves get stronger. We suppose that structural rearrangements are induced in the vicinity of Al(III), causing it to be more and more trapped. In this way, it becomes less exchangeable for competing metals, and also the access to free binding sites may be increasingly hindered.

With the objective of providing evidence of such alterations, fluorescence spectra and fluorescence decay curves were recorded for Tb(III) and Eu(III) as spectroscopic probe metals. They were contacted with Al(III)/HA systems that had been pre-equilibrated for different time periods, covering the time frame of the increase in the competition effect (Fig. 1). In fact, it turned out that significant structural changes were induced by complexation of Al(III). They occurred, however, immediately. Subsequent processes on the time scale of the kinetic effect could not be detected. It cannot be excluded that they were overlain by alterations caused by the probe metals, which had to be applied at rather high concentrations (10^{-5} M) to obtain sufficient fluorescence intensities. In addition, however, fluorescence spectra of Al(III)/HA systems, recorded in the absence of probe metals, did not show any time-dependent trend. One may conclude that the kinetic effect is based on comparatively moderate structural changes. Nonetheless, for assessing the mobility of contaminant metals in natural systems with humic carriers, these processes must be taken into account. That means, in complexation studies with purified humic substances, equilibration times must be long enough to cover these phenomena.

ACKNOWLEDGEMENTS. This work was funded by the Federal Ministry of Economics and Technology (BMWi), Project Management Agency PTKA-WTE, contract no. 02 E 10176.

[1] Hiraide, M. et al. (1985) *Anal. Chim. Acta* **172**, 215-221.
[2] Lippold, H. et al. (2012) *Appl. Geochem.* **27**, 250-256.
[3] Lippold, H. et al. (2007) *Chemosphere* **67**, 1050-1056.
[4] Choppin, G.R. et al. (1991) *Mar. Chem.* **36**, 27-38.
[5] Rao, L. et al. (1994) *Radiochim. Acta* **66/67**, 141-147.

Complexation of Eu(III) with salicylate at elevated temperatures studied by TRLFS

A. Barkleit, M. Acker[1]

[1]Central Radionuclide Laboratory, Dresden University of Technology, Dresden, Germany

We present the investigation of the complexation behavior of Eu(III) with salicylate at ambient and elevated temperatures with time-resolved laser-induced fluorescence spectroscopy (TRLFS) and the resulting thermodynamic data (stability constants, reaction enthalpies).

Organic matter like the ubiquitous humic acids influences the migration behavior of radionuclides and heavy metals. Different substituted benzoic acids like salicylic acid (2-hydroxobenzoic acid) can mimic the main functionalities and are often used as model compounds for humic substances.

The understanding of the complexation behavior of radionuclides and heavy metals with such natural organic matter and the thermodynamic quantification of the interaction especially at elevated temperatures is of great importance to simulate and predict their migration behavior in the environment.

EXPERIMENTAL. Spectrophotometric TRLFS titrations at different temperatures between 25 °C and 60 °C ($3 \cdot 10^{-5}$ M Eu^{3+}, $1 \cdot 10^{-5}$-0.1 M ligand, 0.1 M $NaClO_4$, pH 5) were carried out with a pulsed flash lamp pumped Nd:YAG-OPO laser system from Continuum (Santa Clara, CA, U.S.A.), combined with a spectrograph and an ICCD camera (Andor iStar) from LOT-Oriel. The excitation wavelength was 394 nm. The temperature was adjusted using a stirred temperature-controlled cuvette holder (Flash 300TM, Quantum Northwest, U.S.A.).

RESULTS. The luminescence spectrum of Eu^{3+} shows the typical changes upon ligand addition which indicate a complexation: The intensity of the hypersensitive $^5D_0$-$^7F_2$ transition at about 615 nm increases strongly, the symmetry-forbidden $^5D_0$-$^7F_0$ transition appears (see Fig. 1), and the luminescence lifetime prolongs. The luminescence lifetime of the Eu^{3+} aquo ion remains nearly constant within the studied temperature range (112 ± 5 µs). The lifetime corresponds to a number of nine water molecules in the first spherical coordination shell of Eu^{3+}, provided that the empirical linear relationship between lifetime and number of water molecules discovered by Horrocks et al. [1] is temperature independent. The luminescence lifetime is prolonged with ligand addition up to 305 ± 5 µs. This corresponds to a number of three remaining water molecules in the first coordination shell of Eu^{3+}; six water molecules have been substituted by coordination sites of ligand molecules. A similar lifetime (about 300-340 µs) was found by Kuke et al. [2] for a concentrated Eu^{3+} salicylate mixture at decreased temperatures.

The substitution of up to six water molecules in the first coordination shell of Eu^{3+} suggests the formation of more than a 1 : 1 complex. Also complexes with 1 : 2 and 1 : 3 metal-to-ligand stoichiometry seem to be formed. Furthermore, the high water substitution rate implies the formation of chelate coordination with carboxylate and (protonated) hydroxyl. These assumptions are underlined by a crystal structure of $Eu(Sal)_3$ where both the carboxylate and hydroxyl group coordinate the metal ion in a chelating manner [2].

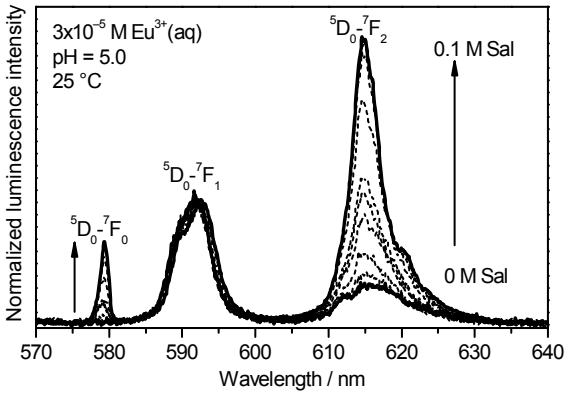

Fig. 1: Luminescence emission spectra of the spectrophotometric titration of Eu^{3+} with salicylate.

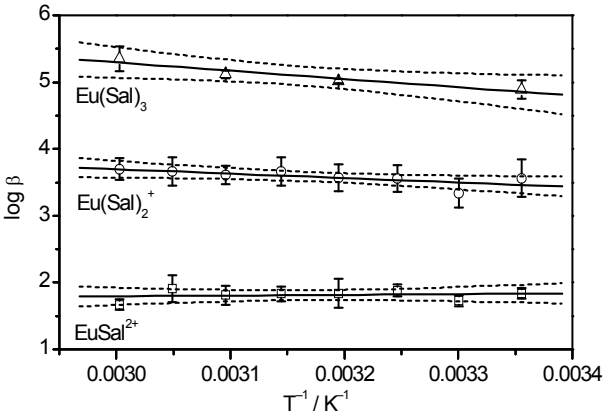

Fig. 2: Van´t Hoff plot of the Eu salicylate complex formation.

In the studied temperature range between 25 °C and 60 °C, the total complex stability constants log β_{MLH} for these 3 complexes could be determined with the computer program SPECFIT. Up to date only the stability constants for the 1 : 1 and 1 : 2 complexes have been determined at room temperature [3-5]. The literature values are somewhat higher than ours. This is possibly due to a small amount on 1 : 3 complex which was not detected there but enlarged the constants of the 1 : 1 and 1 : 2 complexes.

The thermodynamic data were graphically obtained from the complex stability constants at different temperature by means of the modified linear form of the van´t Hoff equation (Fig. 2). The formation of the 1 : 1 complex is nearly temperature independent. The reaction enthalpy $\Delta_R H$ with -2.14 ± 4.9 kJ mol^{-1} is close to zero within the error bars, which is in accordance with the literature [6]. The formation of the 1 : 2 complex is found to be slightly endothermic ($\Delta_R H = 12.7 \pm 4.8$ kJ mol^{-1}) similar to literature data [6], whereas those of the 1 : 3 complex is considerably enhanced ($\Delta_R H = 23.7 \pm 4.9$ kJ mol^{-1}). This might explain why this complex was not characterized in solution so far at room temperature.

[1] Horrocks, W.D. et al. (1979) *J. Am. Chem. Soc.* **101**, 334-340.
[2] Kuke, S. et al. (2010) *Spectrochim. Acta A: Mol. Biomol. Spectrosc.* **75**, 1333-1340.
[3] Hasegawa, Y. et al. (1989) *Bull. Chem. Soc. Jpn.* **62**, 1486-1491.
[4] Aoyagi, N. et al. (2004) *Radiochim. Acta* **92**, 589-593.
[5] Irving, H. et al. (1970) *Anal. Chim. Acta* **49**, 449-454.
[6] Hasegawa, Y. et al. (1990) *Bull. Chem. Soc. Jpn.* **63**, 2169-2172.

Aqueous uranium(VI) complexes with acetic acid: Combining multi-spectroscopic methods with factor analysis and quantum chemical calculations

C. Lucks, A. Rossberg, S. Tsushima, H. Foerstendorf, A. C. Scheinost, G. Bernhard

UV-vis, EXAFS and IR spectra of aqueous U(VI) complexes with acetic acid (ac) were recorded as a function of pH. By means of iterative transformation factor analysis (ITFA), it was possible to isolate the spectrum of each individual U(VI) complex and to determine the pH-speciation of the complexes. The uranium acetate complexes show exclusively bidentate coordination of the carboxylic group. The distance to complexed water was reduced for the 1 : 1 complex.

EXPERIMENTAL. Solutions of 50 mM U(VI) in 1 M ac were prepared at pH 0.5-3.9. UV-vis data were recorded in the spectral range from 700 to 350 nm. EXAFS measurements at the U L_{III}-edge were performed in transmission mode at the Rossendorf Beamline BM20 (ROBL). For IR spectroscopy, solutions of the same composition were prepared. Additionally, reference solutions of water and the ligand dissolved in water were made at each pH.

RESULTS. ITFA applied to the UV-vis data in the range of 400 to 470 nm and to the IR spectra in the range of the antisymmetric stretching vibration mode of the uranyl moiety, $\upsilon_3(UO_2)$, univocally yield the spectra of the thermodynamically expected 1 : 1, 1 : 2, and 1 : 3 U(VI)-ac complexes. For both spectroscopic methods, the ITFA derived speciation is in line with thermodynamic calculations using literature data [1]. With rising pH, the IR spectra show strong bands at 1535 and 1465 cm^{-1}, which can be attributed to the antisymmetric $\nu_{3,as}(COO)$ and symmetric $\nu_{3,s}(COO)$ stretching mode of bidentately coordinated carboxylate groups [2]. According to DFT calculations, monodentate complexation should give comparable strong signals at 1590 and 1340 cm^{-1}. For all measured samples, no signal was detected around 1590 cm^{-1}. Hence, monodentate coordination can be ruled out.

The EXAFS spectra were fitted using single backscattering paths for O_{ax}, O_{eq}, C, and the 4-legged MS-path of O_{ax}. The distance of O_{eq} ($R(U–O_{eq})$), its Debye-Waller term ($DW(O_{eq})$) and the U–C distance ($R(U–C)$) are plotted against the number of coordinated ligands calculated according to the experimentally confirmed thermodynamic speciation (Fig. 1).

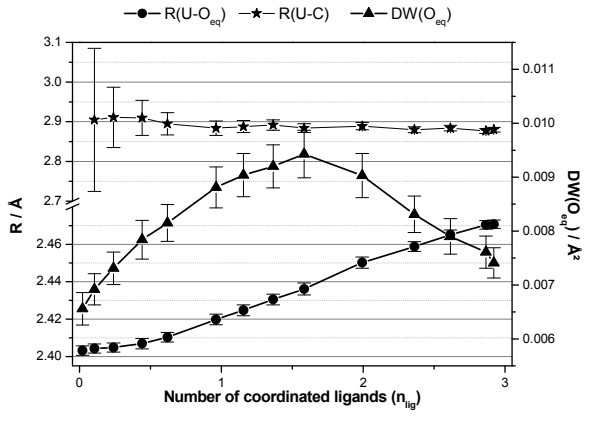

Fig. 1: $U–O_{eq}$ distance (circles), corresponding DW (triangles) and U–C distance (stars) as a function of the number of coordinated ligands for the U(VI)-ac system.

The $U–O_{eq}$ bond length rises continuously with the number of coordinated ligands (Fig. 1). This rise in distance generally implies bidentate coordination of the carboxylic groups. The DW rises steadily until a maximum is reached at an average n_{lig} of 1.6 and decreases then continuously. The lowest values of the DW of O_{eq} are observed when either no ac ligand or three ac ligands are coordinated, corresponding to the aquo complex of the uranyl ion (uranyl hydrate) and to the 1 : 3 U-ac complex, respectively. As uranyl hydrate is expected to show a uniform coordination of water molecules because of the low structural disorder, the 1 : 3 complex should show a uniform coordination of acetate molecules as well. The highest DW appears at 1.6 coordinated ac ligands which corresponds to pH) 2.57 where in average ~2 O_{eq} belong to the coordinated water molecules and ~3 O_{eq} to the carboxylic group. At this pH, the fractions of the U-ac complexes are distributed nearly equally (33% 1 : 1 U-ac, 28% 1 : 2 U-ac, 23% 1 : 3 U-ac). Hence, the high DW can be explained by the high structural disorder due to the presence of structurally different complexes and/or by the presence of different coordinating ligands in nearly equal shares. Unlike the investigations of Jiang et al. [3], we found at the highest pH a relatively long $U–O_{eq}$ distance of ~ 2.47 Å which is in line with the $U–O_{eq}$ distance of 2.48 Å found for three bidentately coordinated acetate groups in a solid sample of $Na[UO_2ac_3]$ measured using EXAFS [4]. This quite simple shell fitting approach gives already strong evidence that in the case of the 1 : 3 U-ac complex all acetate groups are connected in a bidentate manner. Over the whole pH range, the measured U–C distances are in average 2.89 ± 0.01 Å (Fig. 1), a value which is expected in case of bidentate coordination of the carboxylic group.

In contrast to UV-vis and IR, only three components could be isolated after application of ITFA to the EXAFS spectra. After the comparison of the thermodynamic speciation and the ITFA results, the succeeding components can be assigned to uranyl hydrate, the 1 : 1 and the 1 : 3 U(VI)-ac complexes. All structural parameters of the 1 : 3 complex ($R(U–O_{eq})$ = 2.47 Å, $R(U–C)$ = 2.88 Å, $R(U–C_{dis})$ = 4.36 Å) are in line with a solid sample of $Na[UO_2ac_3]$ [4]. In contrast, the 1 : 1 complex shows $R(U–O_{eq})$ = 2.41 Å, which is significantly lower than the weighted average of the involved structural entities (three complexing water molecules and one bidentately coordinated acetate: $R(U–O_{eq})$ = 2.43 Å).

A possible explanation for this behavior is that $R(U–O_{water})$ and $R(U–O_{carboxvlate})$ are different for all complexes formed. A method that calculates theoretical spectra under variation of the involved structural entities and compares them with the measured data was then applied. At its optimum $R(U–O_{water})$ was reduced to 2.36 Å for the 1 : 1 complex while $R(U–O_{carboxvlate})$ remained at 2.47 Å.

[1] Ahrland, S. (1951) *Acta Chem. Scand.* **5**, 199-219.
[2] Kakihana, M. et al. (1987) *J. Phys. Chem.* **91**, 6128-6136.
[3] Jiang, J. et al. (2002) *J. Chem. Soc. Dalton Trans.*, 1832-1838.
[4] Denecke, M. et al. (1998) *J. Alloys Compd.* **271-273**, 123-127.

Effect of ligand coordination to the "yl"-bond in uranyl(VI) complexes

S. Tsushima, H. Foerstendorf, A. Rossberg, C. Lucks, K. Fahmy

The π and/or σ donation from the coordinating ligand was found to be the origin of the U–O_{yl} bond weakening in uranyl(VI) complexes.

The uranyl(VI) aquo ion $UO_2(H_2O)_5^{2+}$ has a Raman active O–U–O symmetric stretching band (ν_1) at 870 cm^{-1}. The band is red-shifted upon a replacement of the first shell water with ligand due to the weakening of the "yl"-bond. For the 1 : 1 uranyl complexes, Nguyen-Trung et al. [1] found the U–O_{yl} bond to weaken in the order OH^- > CO_3^{2-} > $C_2O_4^{2-}$ > F^- > SO_4^{2-}, $CH_3CO_2^-$ > Cl^- > Br^-, NO_3^-. DFT calculations has been used to study the origin of the U–O_{yl} bond weakening in uranyl(VI) coordination complexes.

CALCULATIONS. DFT calculations were performed using Gaussian 09. Structures were optimized in aqueous phase using CPCM solvation model at the B3LYP level. The small-core effective core potential and the corresponding basis set were used for all elements except for H. For H, the 6-311++G** basis was used.

RESULTS. Figure 1 gives the relationship between O–U–O ν_1 frequencies obtained by Raman spectroscopy [1] and those obtained by B3LYP calculations. A linear correlation between experimental and B3LYP values can be clearly seen. When wrong coordination modes are used for geometry optimization and vibrational frequency calculations, which are plotted in Fig. 1 as triangles, they show larger deviations from the linear fitting. It demonstrates that the DFT calculations well reproduce the trend of "yl"-bond weakening in various uranyl coordination complexes.

We have analyzed this point further by looking into molecular orbitals of the uranyl coordination complexes. In UO_2Cl^+(aq), the HOMO-3 is the σ_u orbital, the HOMO-8 and the HOMO-9 are the π_u, the HOMO-10 is the σ_g, the HOMO-11 and the HOMO-12 are the π_g MOs. However there is hardly any mixing of the chlorine orbital with any of the uranyl bonding MOs. The ligand coordination seems to have minimal influence on the uranyl bond and in fact the difference in U–O_{yl} distance in UO_2^{2+}(aq) and UO_2Cl^+(aq) is very small with only 0.003 Å at the B3LYP level. In UO_2F^+(aq), the HOMO is the σ_u, the HOMO-6 is the π_u, the HOMO-9 is the σ_g, the HOMO-10 and the HOMO-12 are the π_g orbitals. There is contribution from the fluorine orbital to the HOMO, but it has antibonding character with respect to the uranyl σ_u MO and, therefore, does not affect the strength of the U–O_{yl} bond (Fig. 2, left). There is also a fluorine π contribution to the HOMO-12 which mixes with the uranyl π_g orbital (Fig. 2, right). From Fig. 2, it is clear that there is a bonding interaction between the U 6d orbital and the F 2p orbital in the HOMO-12, resulting in a "π competition" between the fluorine and the uranyl oxygen over the U 6d orbital. This leads to the weakening of the U–O_{yl} π bond in UO_2F^+(aq) which makes a modest lengthening of the U–O_{yl} distance of 0.013 Å compared to the UO_2^{2+}(aq) ion at the B3LYP level.

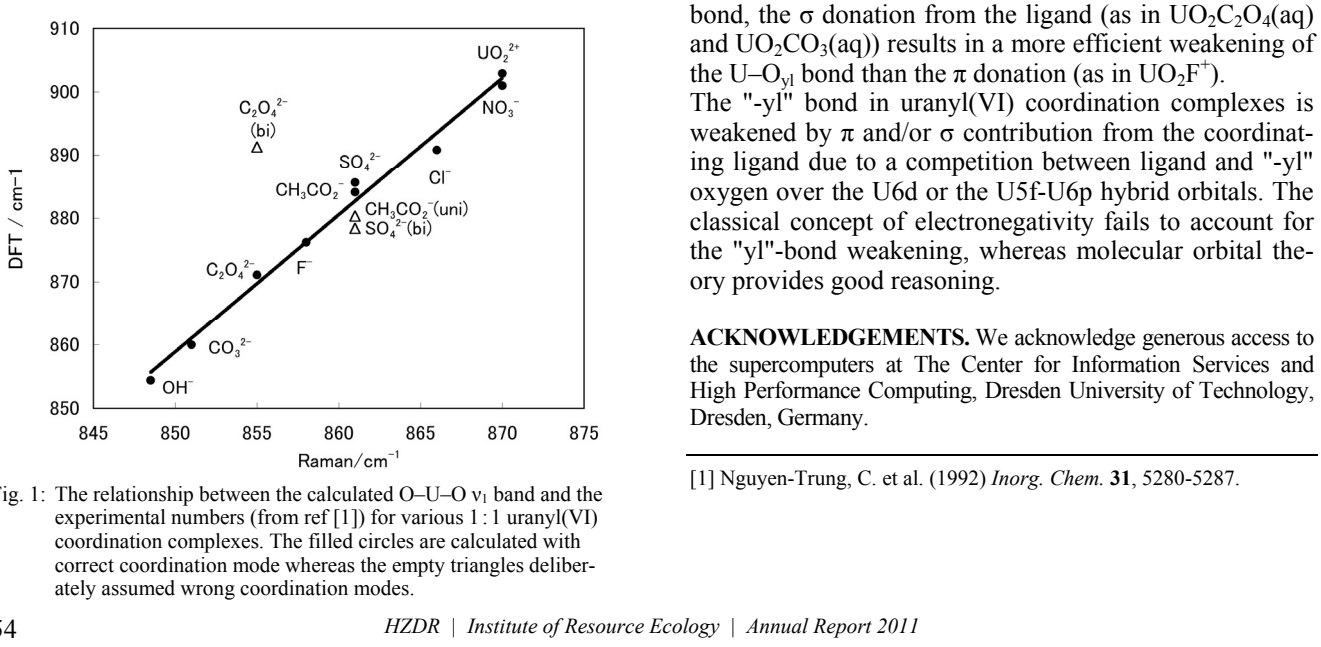

Fig. 1: The relationship between the calculated O–U–O ν_1 band and the experimental numbers (from ref [1]) for various 1 : 1 uranyl(VI) coordination complexes. The filled circles are calculated with correct coordination mode whereas the empty triangles deliberately assumed wrong coordination modes.

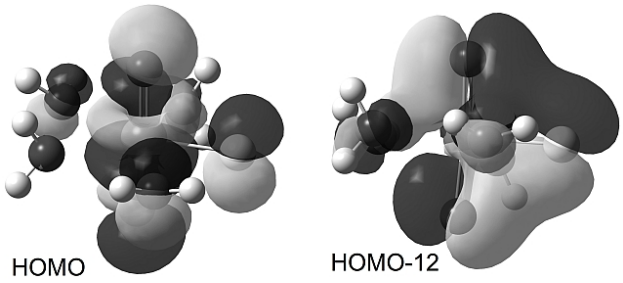

Fig. 2: The HOMO and HOMO-12 of the UO_2F^+(aq). The F 2p orbital has antibonding character with respect to the uranyl σ_u orbital (HOMO, left) whereas it makes significant π donation to the uranyl π_g orbital (HOMO-12, right) resulting in the "π competition" between "yl"-oxygen and fluorine.

In $UO_2C_2O_4$(aq), the HOMO-11 is the uranyl π_u MO which has significant σ contribution from the ligand MO. Similarly in UO_2CO_3(aq), the HOMO-10 is the uranyl π_u MO and it has also significant σ contribution from the ligand MO. In both complexes, U5f-U6p hybrid orbitals make bonding interaction with ligand MO, and there is competition between the "yl"-oxygen and the ligand over the uranyl MOs. The U–O_{yl} bond lengthening compared to UO_2^{2+}(aq) in these complexes are 0.016 Å and 0.021 Å, respectively. Since the σ bond is much stronger than the π bond, the σ donation from the ligand (as in $UO_2C_2O_4$(aq) and UO_2CO_3(aq)) results in a more efficient weakening of the U–O_{yl} bond than the π donation (as in UO_2F^+).

The "-yl" bond in uranyl(VI) coordination complexes is weakened by π and/or σ contribution from the coordinating ligand due to a competition between ligand and "-yl" oxygen over the U6d or the U5f-U6p hybrid orbitals. The classical concept of electronegativity fails to account for the "yl"-bond weakening, whereas molecular orbital theory provides good reasoning.

ACKNOWLEDGEMENTS. We acknowledge generous access to the supercomputers at The Center for Information Services and High Performance Computing, Dresden University of Technology, Dresden, Germany.

[1] Nguyen-Trung, C. et al. (1992) *Inorg. Chem.* **31**, 5280-5287.

Thermodynamic reference database THEREDA: 3. WWW interface and first releases of data to the public

A. Richter, V. Brendler, H. Moog,[1] C. Marquardt,[2] M. Altmaier,[2] W. Voigt,[3] S. Wilhelm[4]

[1]GRS mbH, Braunschweig, Germany; [2]Institute for Nuclear Waste Disposal, Karlsruhe Institute of Technology, Karlruhe, Germany; [3]Institut für Anorganische Chemie, TU Bergakademie Freiberg, Freiberg, Germany; [4]AF-Consult, Baden, Switzerland

The cooperative project THEREDA aims at the establishment of a centrally administered and maintained database of verified thermodynamic parameters as it is required for environmental applications in general and radioactive waste in particular. The website "www.thereda.de" is developed in parallel with the database. It shall serve users as a portal to the database and as an information and discussion platform on issues concerning the database. In June 2011, the first data could release to the public *via* this website.

THEREDA is a project dedicated to a THErmodynamic REference DAtabase [1-5]. The main objective is to establish a comprehensive and internally consistent thermodynamic database for the geochemical modeling of near-field and far-field processes occurring in the different rock formations currently under discussion in Germany to host a repository for radioactive waste. This database is to be accessed in an uncomplicated way.

WWW INTERFACE. THEREDA is available *via* commonly available internet browsers under the address . This web presence is based on the Content Management System Joomla!. The website offers a public area (without previous authentification) where general information about the project, news, public documents, a forum and contact forms are hosted. Various modules and components are installed to enable the aforementioned offers, such as "JoomFish" for multiple languages, "DocMan" as document administration tool, "Kunena" for the user forum, "JoomlaStats" for website statistics or "jNews" to show news.

Another module is an extension specifically programmed for the data access for external users (registration required). This offers important benefits with respect to extension of user group and access possibilities, omitting problems with different software versions and country-specific installations, a hierarchically stepped access to data or data input and auditing (user authorization) and the simplification of database maintenance and persistence.

After login, various possibilities are offered for data access:

- Single data query: query for specific data with interactively defined selection criteria (thermodynamic data, interaction coefficients, temperature range, ion-ion interaction model - Extended Debye-Hückel, SIT or Pitzer).
- Complex systems: stepwise construction of a query for more than one elements (temperature range, ion-ion-interaction model), query result presented as an ASCII file (JSON format), in the future: selection of a geochemical speciation code will be possible.
- Tailored databases: issue of fixed ready-to-use parameter files, specific for an ion interaction model, can be exported in various formats to suit the needs of a variety of geochemical speciation code (PhreeqC, ChemApp, EQ3/6, GWB and the generic format JSON).

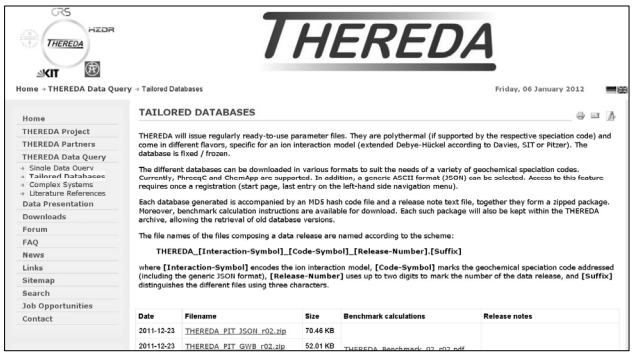

Fig. 1: Screenshot of the THEREDA website: Access to tailored databases.

The website also serves as an intranet for the project partners to provide documents (e.g., drafts of technical paper, protocols and presentations of meetings) and to give access to test versions of the database.

RELEASES OF DATA. On June 30 and December 23, 2011, the management board of THEREDA announced the first and second release of data, respectively. These releases cumulatively cover systems made up by the primary species

- Na^+, K^+, Mg^{2+}, Ca^{2+}, Cl^-, SO_4^{2-}, H^+, and $H_2O(l)$ for the temperature range between 273.15 and 383.15 K (some ranges are extended to 523.15 K, dependent on the specific system)
- Na^+, K^+, Mg^{2+}, Ca^{2+}, Cl^-, Am^{3+}, Nd^{3+}, Cm^{3+} and $H_2O(l)$ for the temperature range 298.15 K.

Currently, the geochemical codes ChemApp and PhreeqC and the generic format JSON are supported.

The released data represent only a small part of all data already stored in THEREDA. As documentation, assessment, amendment and testing of data is an ongoing process, there will be further releases in the future covering more elements, reactions and interactions.

The next release will be parameter files for the system:

- Na^+, K^+, Mg^{2+}, Ca^{2+} ,Cl^-, SO_4^{2-}, $CO_2(g)$, CO_3^{2-}, $H_2O(l)$ for the temperature range 298.15 K and the supported codes ChemApp and PhreeqC.

While THEREDA can store data for various models of non-ideal interactions in the aqueous phase, the present release is valid only for the well known Pitzer formalism, which allows for the calculation of solution-mineral equilibria at high ionic strengths.

ACKNOWLEDGEMENTS. Financial support of project stage 2 by the Federal Office for Radiation Protection (BfS) is gratefully acknowledged.

[1] Richter, A. et al. (2007) *Report FZD-459*, p. 71.
[2] Richter, A. et al. (2009) *Report FZD-511*, p. 57.
[3] Gester, S. et al. (2009) *Report FZD-511*, p. 58.
[4] THEREDA – Thermodynamic Reference Database (2011), *Report GRS-265*.
[5] Altmaier, M. et al. (2008) *ATW* **53**, 249-253.

The consequences of different thermodynamic databases for geochemical modeling: a short comparison using in-house examples

F. Bok, A. Richter, E. Krawczyk-Bärsch, K. Schmeide

The results of geochemical calculations vary, depending on the geochemical code, interaction model and thermodynamic database (TDB) applied. For calculations using the same data and conditions, different databases can lead to significantly different results. The role of thermodynamic databases is shown in two scenarios using different databases under identical conditions.

EXPERIMENTAL. Two scenarios were taken for the calculation of Eh-pH-diagrams: one uranium-containing groundwater seep from the granitic ONKALO tunnel wall [1] and one synthetic Np solution, which was used for the study of the contribution of reduced sulfur functionalities to the redox behavior of humic acid [2]. The calculations were performed with "Geochemist's Workbench" (Rockware®, Release 8.0.12). For each solution, three daifferent E_h-pH-diagrams were calculated (Fig. 1), using a prerelease of the "Thermodynamic Reference Database" (THEREDA) [3], the JAEA TDB [4], and the LLNL TDB, which comes with "Geochemist's Workbench" [5]. Mineral formation was suppressed because no solid phases were found in [1, 2]. The missing log K value for a spectroscopically verified aqueous ($Ca_2UO_2(CO_3)_3^0$) species was taken from [6], which was included only in the calculation with the LLNL TDB for reasons of clarity.

RESULTS. One of the most common problems is the lack of thermodynamic data for individual species in the TDB, effectively excluding such species from calculations. For instance, the aqueous species $Ca_2UO_2(CO_3)_3^0$ is missing in all three TDBs so far. It does not occur in the calculation results, although it is a predominant species under the given conditions. Including the species log K value into the calculation, the stability regions of $UO_2(CO_3)_2^{2-}$ and $UO_2(CO_3)_3^{4-}$ are completely displaced by $Ca_2UO_2(CO_3)_3^0$ (Fig. 1, left bottom). Therefore, it is necessary to examine whether the TDB contains the data of all the expected species.

On the other hand, there is the problem of questionable species in the TDBs, such as $Np(OH)_5^-$ which is only found in the LLNL TDB. The existence of this complex is doubtful, especially since $NpO_2(am)$ shows no increase in solubility with increasing pH [9]. In addition, thermodynamic parameters for $Np(OH)_5^-$ species are explicitly rejected from the NEA TDB [10] and THEREDA.

Other common problems are inconsistencies in TDBs: log K values for the included species are often collected from various sources or measured with different methods, leading to incompatible thermodynamic data. For example, the log K values for the reaction:

$$Np(OH)_3^+ + 3H^+ \rightarrow Np^{4+} + 3H_2O \qquad (1)$$

differ significantly in the THEREDA (log K = 2.80, orig. taken from [7]), the JAEA TDB (log K = −4.30, orig. taken from [8]) and the LLNL TDB (log K = 5.85). This causes very different regions of stability for the $Np(OH)_x$ species or even the complete disappearance of some species (Fig. 1, top-/center-right).

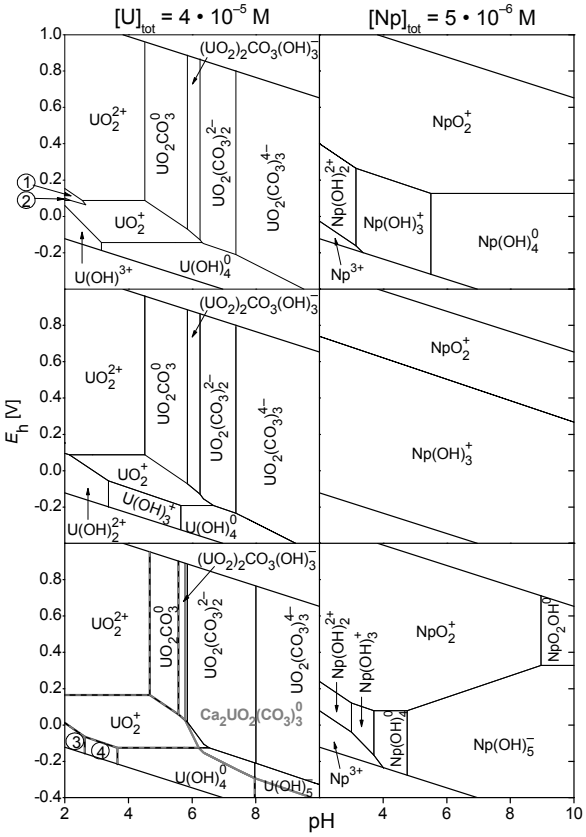

Fig. 1: E_h-pH-diagrams of uranium [1] (left) and neptunium [2] (right) solutions calculated using different TDBs: THEREDA [3] (top), JAEA TDB [4] (center), LLNL TDB (bottom); gray: calculation including log K value of $Ca_2UO_2(CO_3)_3^0$ formation reaction [6]; (1) $U(SO_4)_2^0$, (2) $U(SO_4)^{2+}$, (3) $U(OH)_2^{2+}$, (4) $U(OH)_3^+$.

It is always important to check the aims and validity limits of the TDBs. For instance, thermodynamic data for the SIT model will not work properly in high-saline (> 4 molal) fluids and, therefore, the predicted predominance of aqueous species may not reflect reality.

When entering thermodynamic data of additional species into the database file, it is necessary to check the correct way of defining the new species/reaction. Otherwise, the inserted species will be ignored in the calculation.

[1] Krawczyk-Bärsch, E. et al. (2012) submitted.
[2] Schmeide, K. et al. (2012) *Sci. Total Environ.*, in press, DOI: 10.1016/j.scitotenv.2011.12.052.
[3] THEREDA http://www.thereda.de (accessed 2011-11-08).
[4] JAEA Thermodynamic DataBase http://migrationdb.jaea.go.jp/english.html (accessed 2011-07-20).
[5] Geochemist's Workbench Homepage (Aqueous Solutions LLC™). http://www.gwb.com/thermo.htm (accessed 2011-12-08).
[6] Bernhard, G. et al. (2001) Radiochim. Acta 89, 511-518.
[7] Neck, V. et al. (2001) Radiochim. Acta **89**, 1-12.
[8] Fujiwara, K. et al. (2010) JAEA-Review 2009-059.
[9] Neck, V. et al. (2001) Radiochim. Acta 89, 1-16.
[10] Guillaumont, R. et al. (2003) *Chemical Thermodynamics of Uranium, Neptunium, Plutonium, Americium and Technetium. Chemical Thermodynamics Vol. 5*, Elsevier, Amsterdam.

Generation and analysis of smart K_d-values: I. Coupling of PhreeqC, UCODE and SimLab

J. Schikora, M. Stockmann, V. Brendler

Within the project ESTRAL (Realistic Integration of Sorption Processes in Transport Programs for long-term Safety Analysis), pre-computed distribution coefficients (K_d) that are able to reflect changing geochemical conditions are implemented in the existing 3D transport program r³t [1]. The so-called smart K_d-values are calculated as a function of important environmental parameters [2,3] by coupling of different computer codes.

TOOLS AND METHODOLOGY. It is important to know how the variation in the output of a model (here: smart K_d-values) can be apportioned, qualitatively or quantitatively, to different sources of variation. This can be done by a sensitivity analysis (SA), which helps to identify key parameters of a model. Additionally to a SA, an uncertainty analysis (UA) aims to quantify and describe the overall uncertainty associated with the model output as a result of uncertainties in the model input (error propagation).
To do both analyses in a consistent manner we have coupled three computer codes to form one tool: SimLab, UCODE and PhreeqC. The information flow between these codes is described in the following sections.
(1) SimLab 2.2 [4]. It is used for sensitivity and uncertainty analysis. Within SimLab the defined model parameters are varied according to the selected sampling method and their assigned error distribution functions. The generated parameter combinations are written to a UCODE input-file and saved.
Extended Fourier Amplitude Sensitivity Test (eFAST) or replicated Latin Hypercube Sampling (rLHS) were used as sampling methods for global variance-based SA. The use of rLHS as sampling method allows it to introduce correlations between the parameters. This is useful as chemical systems often contain correlations between the governing parameters. An example for the system under investigation is the correlation between ionic strength and calcium concentration.
SimLab provides histograms, cumulative distribution functions and inverse cumulative distribution functions for the purpose of UA. It also calculates statistical descriptors like mean, variance, standard deviation or skewness of the distribution of the simulation results.
(2) UCODE 3.062 [5]. This program is used as 'middle shell'. It processes the varied environmental parameters. To do this UCODE takes each parameter vector E_i and converts it, with the help of a template file, into a valid input for the respective geochemical code PhreeqC. After PhreeqC has completed the simulation UCODE processes the next vector E_i. This is done for all parameter combinations.
(3) PhreeqC 2.17 [6]. This geochemical code is used for modeling the sorption of contaminants onto site-specific mineral phases of various sediments. The necessary thermodynamic data for these calculations are provided by a specific ESTRAL-database, which is developed within the project. The so-called smart K_d-values are calculated for each parameter combination, extracted from the PhreeqC output via batch-file and saved for further interpretation in a separate results-file. This file is also used by SimLab for sensitivity and uncertainty analysis.
Through combination of the UCODE input-file and the results-file with the K_d-values one is able to generate a K_d-matrix which can be accessed from the 3D transport program r³t.
As a result the strategy to couple the three codes SimLab, UCODE and PhreeqC has a fivefold benefit:

- One can calculate smart K_d-values for a given number of parameter combinations.
- It is possible to perform an UA on the smart K_d-values.
- SimLab provides in contrast to UCODE also methods for global SA.
- Both analyses, SA and UA, can be done inside SimLab, without switching the interface.
- Parameter correlations can be dealt with.

APPLICATION CASE. Table 1 shows the environmental parameters with their ranges and error distribution functions for the upper aquifer of Gorleben site (a potential repository site in Germany), covering all relevant radionuclides.

Tab. 1: Environmental parameters E_i with minimum, maximum and error distribution function for the upper aquifer of Gorleben site (a potential repository site in Germany).

E_i	Range*		Distribution
	Min	Max	
E_1: **pH**	6.40	8.68	uniform
E_2: **DIC** [mol/L]	3.53E-04	9.05E-03	log-uniform
E_3: **IS** [mol/L]	9.58E-04	1.77E-02	log-uniform
E_4: **Al** [mol/L]	7.68E-07	4.29E-06	log-uniform
E_5: **Ca** [mol/L]	2.40E-04	4.84E-03	log-uniform
E_6: **RN** [mol/L]			
Am, Cm, Th	1.00E-14	1.00E-8	log-uniform
Cs, Ni, Se, U	1.00E-12	1.00E-6	log-uniform
Np, Pu, Ra	1.00E-13	1.00E-7	log-uniform

*based on field data [7] with the exception of E_6.

An actual example for the use of the three mentioned codes to generate and analyse a smart K_d-matrix for U(VI) based on Tab. 1 is given in [8].

ACKNOWLEDGEMENTS. This project is funded by the German Federal Ministry of Economics and Technology (BMWi) under contract number 02 E 10518.

[1] Fein, E. (2004) *Report GRS-192*.
[2] Stockmann, M. et al. (2010) *Report FZD-530*, p. 33.
[3] Stockmann, M. et al. (2011) *Report HZDR-001*, p. 71.
[4] JRC Ispra. Simlab (2011) Software package for uncertainty and sensitivity analysis. http://simlab.jrc.ec.europa.eu/
[5] Poeter, E.P. et al. (2006) *U.S.G.S. Techniques and Methods 6-A11*.
[6] Parkhurst, D.L. et al. (1999) *U.S.G.S. Report 99-425*.
[7] Klinge, H. et al. (2004) *Project Gorleben. Documentation of basic hydrogeological data*, BGR, Hannover.
[8] Stockmann, M. et al. (2012) this report, p. 58.

Generation and analysis of smart K_d-values: II. Uranium(VI)

M. Stockmann, J. Schikora, V. Brendler

In the framework of the ESTRAL project, the existing transport program r³t [1] has been improved towards a more realistic description of the radionuclide migration by implementing the smart K_d-concept based on surface complexation [2,3]. In this article, results exemplarily for the sorption of uranium(VI) in the upper aquifer (UAF) at the Gorleben site are presented.

The distribution coefficients (K_d) for contaminants and their uncertainty and sensitivity analysis can be calculated as function of important environmental parameters such as pH, ionic strength (IS), dissolved inorganic carbon (DIC) by coupling of the computer programs PhreeqC, UCODE and SimLab [4]. The Gorleben site (as a potential nuclear waste repository site in Germany) was selected as an exemplary case of application for a proof-of-concept, here we present results for UO_2^{2+}.

UNCERTAINTY ANALYSIS. The uncertainty analysis focuses on the description of the resulting total variance. A suitable tool for characterization is the frequency or distribution function. This allows to determine the probability of the parameters to fall in a certain interval. Figure 1 shows the frequency distribution of the pre-calculated smart K_d-values for UO_2^{2+} based on extended Fourier Amplitude Sensitivity Test sampling (eFAST) over all environmental parameters according to [4].
The log K_d-values for the sorption of UO_2^{2+} onto mineral surfaces in the UAF at Gorleben site are between −6.8 and 0.75. Comparing to literature (see Tab. 1), especially to the temporally constant conservative K_d-value from [5], which was previously used in r³t for the retention of uranium at Gorleben site, the resulting mean Kd shows good agreements.

SENSITIVITY ANALYSIS. Multidimensional matrices of smart K_d-values (representing the variation of the different geochemical conditions) are generated and stored a-priori to any r³t run. As a result of the sensitivity analysis, the importance of the environmental parameters can be identified. Figure 2 shows the 3-D plot for the K_d-matrix for UO_2^{2+} as a function of pH, [Ca], and [DIC] (logarithmic scale).
The ranking list of first order sensitivity indices is presented in Tab. 2. Indices ranked highest are the most sensitive parameters. It is obvious that pH mainly influences the sorption of UO_2^{2+} in UAF, followed by [Ca], [DIC], and [U].

ACKNOWLEDGEMENTS. This project is funded by the German Federal Ministry of Economics and Technology (BMWi) under contract number 02 E 10518.

[1] Fein, E. (2004) *GRS-Report 192.*
[2] Stockmann, M. et al. (2010) *Report FZD-530*, p. 33.
[3] Stockmann, M. et al. (2011) *Report HZDR-001*, p. 71.
[4] Schikora, J. et al. (2012) this report, p. 57.
[5] Suter, D. et al. (1998) *Proceedings DisTec 98*, Kontec, Hamburg.
[6] Joseph, C. et al. (2011) *Chem. Geol.* **284,** 240-250.
[7] Zavarin, M. et al. (2004) *LLNL Report UCRL_TR-204713*, Livermore, U.S.A.

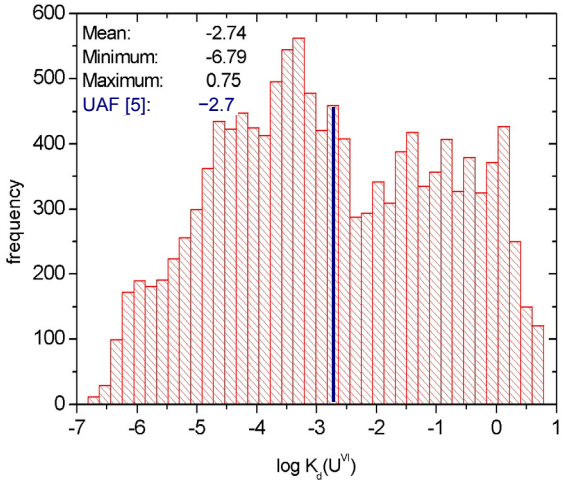

Fig. 1: Frequency distribution of 13,000 pre-calculated log K_d-values for UO_2^{2+} (K_d in m³/kg).

Tab. 1. Comparison of mean smart K_d for UO_2^{2+} with literature values (K_d in m³/kg and logK_d).

	ESTRAL	[5]	[6]	[7]
K_d [m³/kg]	0.0015	0.002	0.02	
log K_d	−2.82	−2.70	−1.7	−6.07 to −1.17

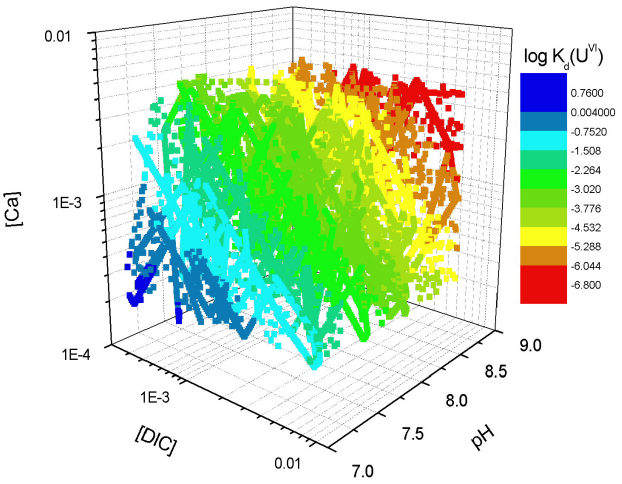

Fig. 2: Multidimensional K_d-matrix for UO_2^{2+} as a function of pH, [Ca], and [DIC] (K_d in m³/kg, logarithmic scale).

Tab. 2: Sensitivity indices for log K_d-values for UO_2^{2+} calculated with eFAST (13,000 parameter samples).

E_i	Sensitivity Index	Rank
pH	0.804	1
[Ca]	0.145	2
[DIC]	0.053	3
[U]	0.001	4

Laboratory measurements on fresh terrestrial gas hydrate bearing sediments

J. Kulenkampff, E. Spangenberg[1]

[1]Helmholtz Zentrum Potsdam, Deutsches GeoForschungsZentrum GFZ, Potsdam, Germany

Physical properties (saturation, grain size distribution, porosity, permeability, resistivity, ultrasonic velocity and attenuation) of terrestrial gas hydrate bearing core samples from the Mallik 5L-38 Gas Hydrate Research Well (Mackenzie Delta, Northwest Territories, Canada) have been investigated in the field laboratory under simulated in situ conditions with a specially designed core analysis system (FLECAS).

EXPERIMENTAL. The Mallik 5L-38 well has been drilled in the frame of an international gas hydrate production test program [1] which included complete coring of the gas hydrate section. Experimental procedure and results from petrophysical measurements on core samples have been published recently [2].
Twenty samples were prepared immediately after core retrieval and mounted into the pressure vessel of FLECAS [3] at deep frozen conditions. Electrical resistivity, ultrasonic P-wave and S-wave velocities and amplitudes were recorded while the samples were brought to in situ pressure and temperature and subsequently allowed to disintegrate under controlled P-T conditions.

RESULTS. A strong decrease of all parameters, especially of the P-wave and S-wave amplitudes, could be observed at the melting point of ice (~1 h). Smaller changes occurred later, apart from the loss of mechanical strength and a distinct recovery of the ultrasonic amplitudes, when the gas hydrate decomposition was initialized by the release of the pore pressure or by heating above the stability threshold (~3.5 h). The gas hydrate decomposition started instantaneously when the pore pressure was released, took about 20 min., and was accompanied by a temperature drop of about 3 °C at the sample surface (Fig. 1).
Only small variations were found in the bulk parameters of the unconsolidated sand samples remaining after gas hydrate decomposition. This explains the uniform behavior of all samples from the gas hydrate zone of the Mallik well.
This data set provides an experimental basis for formation evaluation and serves as a reference for realistic studies with gas hydrates which are synthetically grown in sediments in the laboratory.

ACKNOWLEDGEMENTS. This project was funded by the German Ministry of Education and Science (BMBF) within the framework of the GEOTECHNOLOGIEN program. We acknowledge the international partnership that undertook the Mallik 2002 Gas Hydrate Production Research Program.

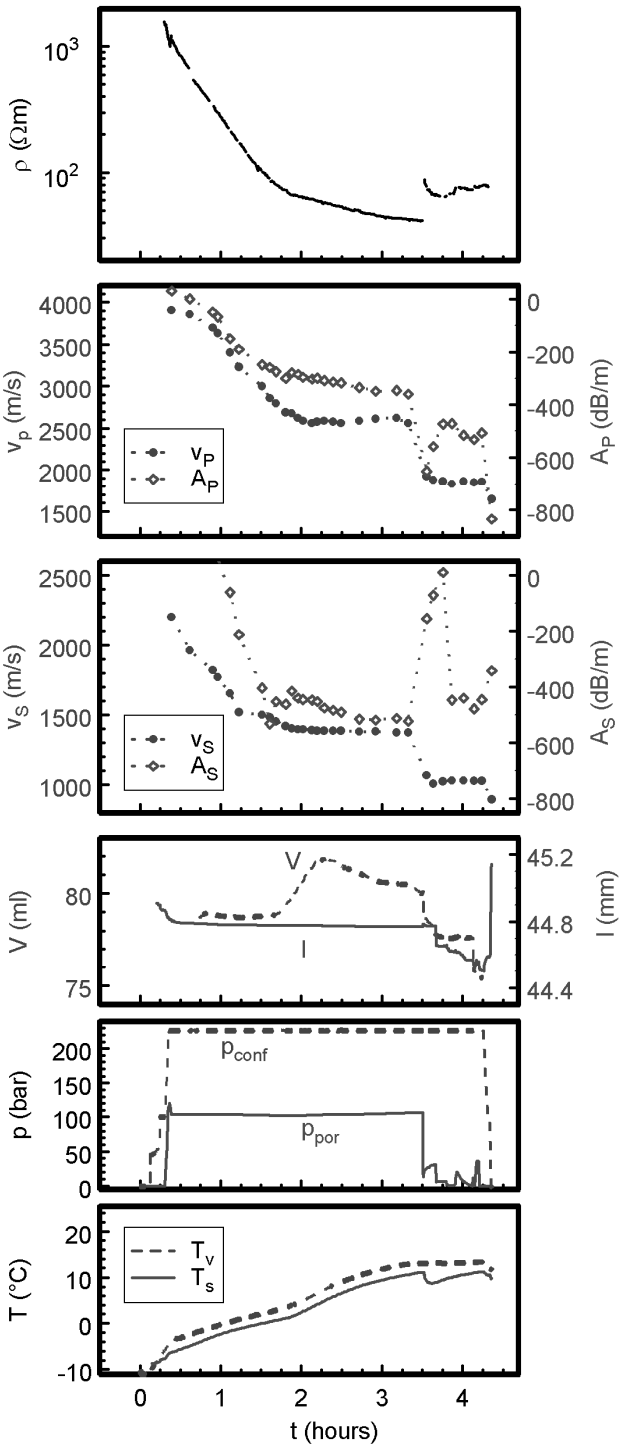

Fig. 1: Measurement record of a gas hydrate sample from 1078 m depth. (ρ: Electrical resistivity; A_P, A_S: Compressional / shear ultrasonic amplitude loss; V_P, V_S: Compressional / shear wave velocity; V: Sample volume; l: Sample length; p_{conf}, p_{por}: Confining / pore pressure; T_V, T_S: Vessel / sample temperature).

[1] Dallimore, S R et al. (2005) *Scientific Results from the Mallik 2002 Gas Hydrate Production Research Well Program, Mackenzie Delta, Northwest Territories, Canada,* Geological Survey of Canada, Bulletin 585, Ottawa.
[2] Kulenkampff, J. et al. (2010) in: *Geophysical Characterization of Gas Hydrates*, p. 321-328, SEG, Tulsa.
[3] Kulenkampff, J. et al. (2005) Proceedings World Geothermal Congress 2005, paper 1610, 1-9.

A new radiolabeling method for commercial Ag^0 nanopowder with ^{110m}Ag for sensitive nanoparticle detection

H. Hildebrand, K. Franke

Nanoparticle (NP) tracking in complex media is still a challenge since NP concentrations are expected to be low compared to elemental background levels as it can be found in environmental matrices. We present a new method for radiolabeling of commercial silver nanopowder (Ag^0-NPs) with ^{110m}Ag ($t_{1/2}$ = 250 d). This radionuclide provides an adequate time frame for particle detection, localization and tracking under various experimental conditions. The radiolabeling procedure ensures high efficiency, stability and consistency of particle properties. Detection of Ag^0-NP in concentrations as low as 125 ng kg^{-1} could be reached. For the first time, an appropriate tool for life-cycle studies of commercial Ag^0-NPs is provided without changing chemical composition of the material. This is of great importance, e.g. for research in the field of nanotoxicology.

EXPERIMENTAL. Radiolabeling was conducted by adding $[^{110m}Ag]AgNO_3$ aqueous stock solution to powdered Ag^0-NPs (Sigma-Aldrich, dp < 100 nm) followed by a low temperature annealing procedure (50-105 °C). $[^{110m}Ag]Ag^0$-NPs with specific activities of up to 1 MBq mg^{-1} were prepared. $[^{110m}Ag]Ag^0$-NPs were dispersed in ultrapure water by sonication and afterwards centrifuged to separate NPs from supernatant. The washing procedure was conducted to remove unbound $^{110m}Ag^+$ from $[^{110m}Ag]Ag^0$-NPs. $^{110m}Ag^+$ was measured in the supernatant and in the sediment to determine radiolabeling yield using a gamma counter. Chemical stability of $[^{110m}Ag]Ag^0$-NPs radiolabeling was tested as a function of pH of the dispersion and time.

RESULTS. Radiolabeling of the Ag^0-NPs was conducted via self-diffusion (or isotope exchange) of radionuclides into the NPs crystal structure. First successful radiolabeling tests were carried out at room temperature. A fast ^{110m}Ag introduction or isotope exchange within the first couple of seconds of the radiolabeling procedure applies to about 5 atomic layers of the Ag^0-NPs; elevated temperatures lead to a slow diffusion within the crystal structure over time [1].
For a more stable labeling and efficient handling, low temperature annealing at 50 °C for 3 hours was found to be the best alternative. The important NP properties such as particle size distribution (Fig. 1), morphology and chemical composition remained unaltered within the labeling process. The radiolabeling yield was tested by applying several washing steps to the freshly prepared $[^{110m}Ag]Ag^0$-NPs. Only trace levels of unbound $^{110m}Ag^+$ could be detected. Therefore, it can be concluded that > 99% of the applied ^{110m}Ag could be introduced into the $[^{110m}Ag]Ag^0$-NPs.

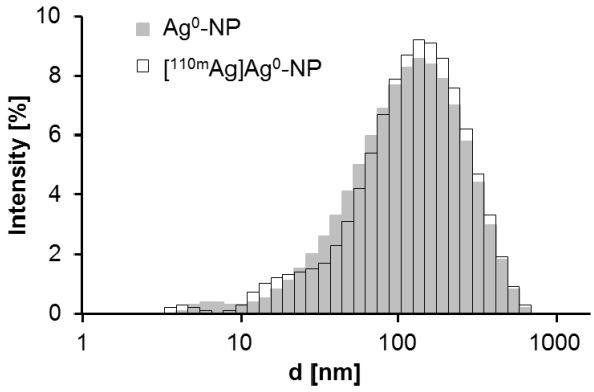

Fig. 1: Particle size distribution by intensity of aqueous Ag^0-NP dispersions, original Ag^0-NPs (grey histogram), radiolabeled $[^{110m}Ag]Ag^0$-NPs, annealed at 50 °C for 3 h (white histogram).

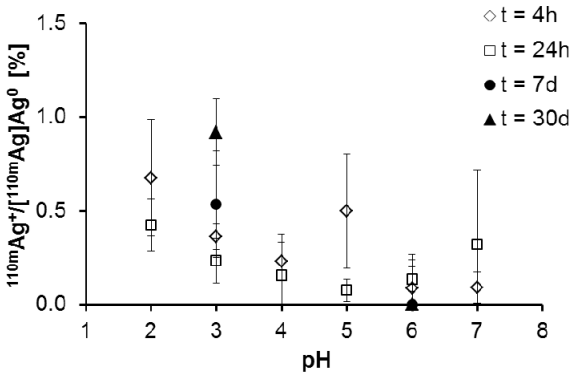

Fig. 2: $^{110m}Ag^+$ leaching from $[^{110m}Ag]Ag^0$-NPs as a function of time and pH of the dispersions (c_{NP} = 1 g L^{-1}).

Ag^0-NPs tend to slowly dissolve in aqueous media. For applicability of $[^{110m}Ag]Ag^0$-NPs in environmental process studies it is essential to have knowledge about radiolabel stability in comparison to the Ag^+ release from the NPs. The results show that Ag^0-NPs dissolution increases with decreasing pH of the dispersion. At pH 3, about 1.25 wt.-% of the initial Ag^0 is detected as Ag^+ in solution after exposure times of 30 days. $^{110m}Ag^+$ release from $[^{110m}Ag]Ag^0$-NPs follows the same dissolution characteristics as the Ag^0-NPs (Fig. 2). This indicates that the radionuclides are not loosely adsorbed on the Ag^0-NP surface but included in the NP inner structure.
A specific activity of 0.2 kBq mg^{-1} for $[^{110m}Ag]Ag^0$-NPs is sufficient for sensitive particle detection via measurement of gamma radiation. A limit of quantification of 62.5 mg kg^{-1} $[^{110m}Ag]Ag^0$-NPs could be reached. For higher specific activities (1 MBq mg^{-1}) quantification of 125 ng kg^{-1} $[^{110m}Ag]Ag^0$-NPs is possible which is very close to predicted environmental concentrations [2].

CONCLUSIONS. Radiolabeling of commercial Ag^0 nanomaterial provides numerous advantages for research projects. The radiolabel gives visibility to NPs at very low concentrations and in complex media such as soil, sediments, organisms, surface coatings or daily life products. The natural background of silver can be clearly distinguished from particular silver which is not possible in the case of complete digestion of samples and analyses of target ions. Allocation of NPs due to filtration, sorption or sedimentation can be studied in detail and unintended effects such as sorption e.g. on walls of reaction vessels can be clearly quantified. The presented radiolabeling strategy provides the great advantage to maintain the all-important Ag^0-NP characteristics such as chemical composition, size and morphology.

[1] Gerischer, H. et al. (1954) *Z. Elektrochem.* **10**, 819-827.
[2] Ferreira da Silva, B. et al. (2011) *Trends Anal. Chem.* **30**, 528-540.

Neon identifies two billion year old fluid component in Kaapvaal Craton

J. Lippmann-Pipke, B. Sherwood Loolar,[1] S. Niedermann,[2] N. A. Stroncik,[3] R. Naumann,[3] E. van Heerden,[4] T. C. Onstott[4]

[1]Department of Geology University of Toronto, Toronto, Canada; [2]Helmholtz-Zentrum Potsdam, Potsdam, Germany; [3]Department of Microbiology, University of the Free State, Bloemfontein, South Africa; [4]Department of Geosciences, Princeton University, Princeton, U.S.A.

Crustal fracture fluids and fluid inclusions from nine South African ultra-deep gold mines were analyzed for their dissolved gases (including noble gases) and isotopic compositions. A group of fracture waters shows highest ever observed $^{21}Ne/^{22}Ne$ isotope ratios and strong correlations of this enriched neon signal with high contents of dissolved H_2, CH_4 and higher hydrocarbons of proposed abiogenic origin (water rock interaction reactions). The end-member of the enriched neon signal was identified as a > two billion year old metamorphic fluid hydrogeologically isolated in inclusions.

EXPERIMENTAL. We analyzed shallow (to ~1 km) and deep fracture waters (to > 3 km) from the Witwatersrand Basin, South Africa, for their gas and noble gas isotopic composition. Gas and water sampling procedures, compositional and isotopic analysis of the dissolved gases components in fracture fluids and fluid inclusions, and for the major and trace element analysis of various rock samples are described in [1] and references therein.

RESULTS. The neon signature clearly differentiates a group of typical crustal fracture fluids (Fig. 1, open diamonds) from another group with a significantly enriched nucleogenic neon signal (filled diamonds) with the highest $^{21}Ne/^{22}Ne$ ratios (0.160 ± 0.003) ever reported in groundwater [1]. Fluid inclusions in adjacent rocks (filled triangles) yield even higher $^{21}Ne/^{22}Ne$ ratios between 0.219 and 0.515, consistent with an extrapolated $^{21}Ne/^{22}Ne$ value of 3.3 ± 0.2 at $^{20}Ne/^{22}Ne = 0$. The significant neon offset from air composition is interpreted as due to nucleogenic neon production by $^{17,18}O(\alpha,n)^{20,21}Ne$, $^{19}F(\alpha,n)^{22}Na(\beta^+)^{22}Ne$ and $^{19}F(\alpha,p)^{22}Ne$ reactions [2] in the local Achaean formations with observed unusual high O/F ratios [1]. We show that this nucleogenic end-member represents a fluid component that was produced in the fluorine-depleted Achaean formations and trapped in fluid inclusions more than two billion years ago [1].

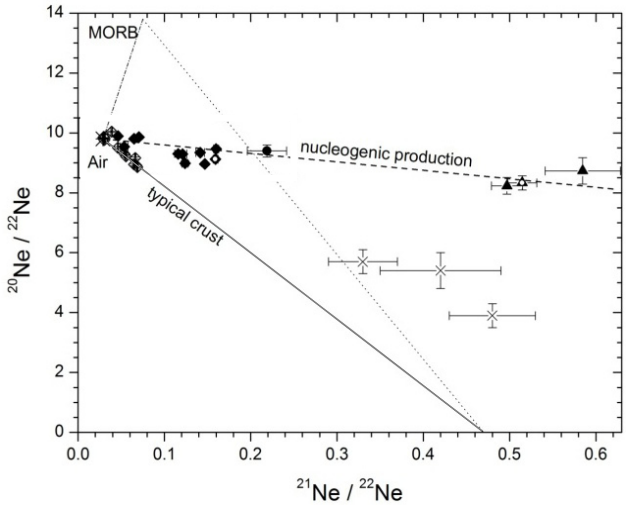

Fig. 1: Neon isotope signatures ($^{20}Ne/^{22}Ne$ *vs.* $^{21}Ne/^{22}Ne$) of fracture waters (open and filled diamonds), fluid inclusions in bulk rock (filled circle), and fluid inclusions in vein quartz (filled triangles) from the Witwatersrand Basin. Fluid inclusion data from an Achaean anorthosite from Western Greenland (crosses) are plotted for comparison [3]. More details see text.

The observation of enriched nucleogenic neon signatures in deep fracture water implies the release of this billion year old neon component from the fluid inclusions and its accumulation in exceptionally isolated fracture water systems.

The observed association of this Achaean neon signature with H_2- and hydrocarbon-rich geogases of proposed abiogenic origin [4] dissolved in the same deep groundwater suggests that the fracture systems have also allowed for the accumulation of various products of water-rock reactions throughout geologic times. One of these fracture systems contained a chemolithotrophic, single species ecosystem surviving on radiolytically produced H_2 and sulfate completely independent of the surface photosphere [5,6].

CONCLUSIONS. The fracture systems that host the fluids with the enriched neon signal are hydrogeologically isolated reservoirs, virtual "time capsules", which over timescales of several million years [7] progressively accumulate fluids released from a variety of processes. These include the leakage of fluid inclusions (with ≥ two billion year old metamorphic fluids representing the enriched nucleogenic neon end-member) and extensive water-rock-interactions producing the mmol/L levels of H_2, hydrocarbons of proposed abiogenic origin and dissolved solutes that enhance the salinity. Significantly, the bulk of the fracture fluid, the enriched nucleogenic neon isotopic signature and the dissolved H_2 and hydrocarbons are not necessarily all of the same age. We suggest only that the enriched nucleogenic neon in the fluid inclusions is a ≥ two billion year old metamorphic fluid component resulting from production by natural nuclear reactions in F-depleted Achaean formations with subsequent accumulation in hydrogeologically isolated fracture fluids (with minimum bulk residence time estimates of millions of years [7]) that are characterized by significant quantities of accumulated products of potentially much later water-rock reactions.

[1] Lippmann-Pipke, J. et al. (2011) *Chem. Geol*. **283**, 287-296.
[2] Wetherill, G.W. (1954) *Phys. Rev.* **96**, 6578-6583.
[3] Zadnik, M.G. and Jeffrey, P.M. (1985) *Chem. Geol.* **52**, 119-125.
[4] Sherwood Lollar, B. et al. (2002) *Nature* **416**, 522-524.
[5] Lin L.-H. et al. (2006) *Science* **314**, 479-482.
[6] Chivian, D. et al. (2008) *Science* **322**, 275-278.
[7] Lippmann, J. et al. (2003) *Geochim. Cosmochim. Acta* **67**, 4597-4619.

Geogas transport in fractured hard rocks – correlations with mining seismicity at 3.54 km depth, TauTona gold mine, South Africa

J. Lippmann-Pipke, J. Erzinger,[1] M. Zimmer,[1] C. Kujawa,[1] M. Boettcher,[2] E. van Heerden,[3] A. Bester,[3] H. Moller,[4] N. A. Stroncik,[5] Z. Reches[6]

[1]Helmholtz-Zentrum Potsdam, Potsdam, Germany; [2]Department of Earth Sciences, University of New Hampshire, Durham, U.S.A.; [3]Department of Microbiology, University of the Free State, Bloemfontein, South Africa; [4]Rock Engineering, TauTona Gold Mine, AngloGold Ashanti, Carletonville, South Africa; [5]Integrated Ocean Drilling Program, Texas A&M University, College Station, U.S.A.; [6]School of Geology and Geophysics, Oklahoma University, Norman, U.S.A.

An on-site gas monitoring study has been conducted in the framework of an international earthquake laboratory (NELSAM-DAFSAM projects) at the TauTona gold mine, South Africa. Five up to 60 m long boreholes were drilled in 3.54 km depth into the highly fractured Pretorius Fault Zone for multi-year chemical and 3D seismic monitoring. The major gas concentrations are constant and air like. The geogas components show most interesting trends and variations on the minute-by-minute basis and correlate with blasting induced seismicity. The current set-up of the gas monitoring system is sensitive enough to quantify geogas transport during periods of intensive blasting activities (including recorded blasts with seismic moment ≤ $1 \cdot 10^9$ Nm located within 1000 m off the borehole). These system specifications should comply with requirements for quantitative interrelation studies between (blasting induced) earth quakes and fluid flow at earthquake focal depth – the final goal of the project.

EXPERIMENTAL. Details on the technical challenges for conducting comprehensive and high temporal resolution online (trace) gas monitoring in an active mine, the various realizations of the analytical devices (quadrupole mass spectrometry (QMS): N_2, O_2, Ar, H_2, CO_2, He, CH_4; ^{222}Rn detection; offline noble gas isotope analysis (^{3,4}He, ^{36,40}Ar), sensor based gas analysis (H_2, CO_2); borehole temperature and pressure) and their continuous improvement is described in full detail in [1] and references therein. Details on the 3D seismic network (seismometers, strain meters) are provided in [2].

RESULTS. Highly sensitive detection of geogas compositional changes in a highly fractured fault zone could be obtained during the cause of four years [1]. While the earlier QMS based system allowed for the parallel monitoring of a wide suite of gas components the final sensor based device provided much sharper and higher signals (Fig. 1) – due to a significantly smaller dead volume.

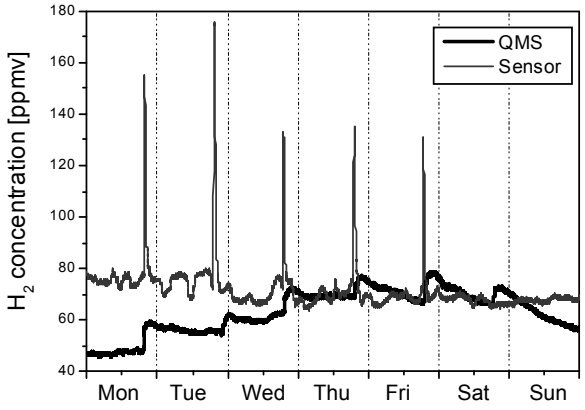

Fig. 1: Comparison of QMS and sensor-based analytical results of H_2 concentration measurements in the course of one week.

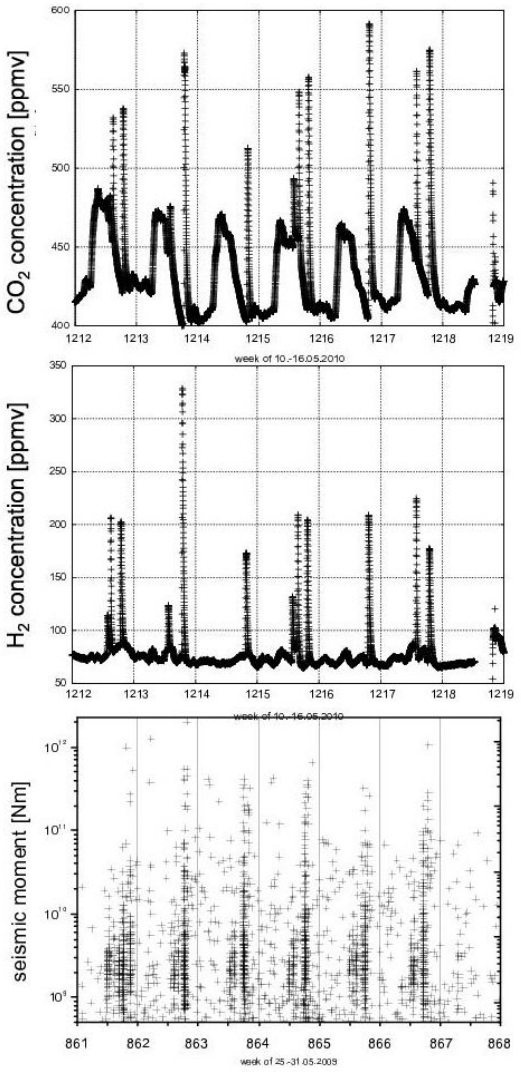

Fig. 2: *Top & center:* Typical multiple CO_2 and H_2 peaks per weekday, sensor based analysis (2010). *Bottom*: Typical seismic moments in a week in 2009.

Geogas concentration variations in the borehole (Fig. 2, top & center) are caused by fault fracture permeability changes during blasting activities on weekday afternoons with individual seismic moments even ≤ $1 \cdot 10^{11}$ Nm (Fig. 2, bottom). Single stronger, far distant seismic events (> $1 \cdot 10^{13}$ Nm, ~ 1 km) are likely not affecting the borehole gas composition. Unfortunately, *isochronal* high resolution gas and seismic data could never be obtained.

CONCLUSION. Quantification of geogas transport during mining induced seismic events has become possible. Next project phase shall provide also isochronal seismic and geogas data (DFG Li872/6-1).

[1] Lippmann-Pipke, J. et al. (2011) *Appl. Geochem.*, **26**, 2134-2146.
[2] Boettcher, M. et al. (2009) *Geophys. Res. Lett.*, **36**, L10307.

- Articles (peer-reviewed)
- Extended Abstracts, Reports, Contributions
- Lectures, Oral Presentations
- Posters
- Patent
- Theses
- Master, Diploma, Bachelor

ARTICLES (PEER-REVIEWED)

Anderson, C.; Johnsson, A.; Moll, H.; Pedersen, K.
Radionuclide geomicrobiology of the deep biosphere
Geomicrobiology Journal 28, 540-561 (2011).

Arnold, T.; Baumann, N.; Krawczyk-Bärsch, E.; Brockmann, S.; Zimmermann, U.; Jenk, U.; Weiß, S.; Wobus, A.; Zirnstein, I.
Identification of the uranium speciation in an underground acid mine drainage environment analysed by laser fluorescence spectroscopy
Geochimica et Cosmochimica Acta 75, 2200-2212 (2011).

Barkleit, A.; Foerstendorf, H.; Li, B.; Rossberg, A.; Moll, H.; Bernhard, G.
Coordination of uranium(VI) with functional groups of bacterial lipopolysaccharide studied by EXAFS and FT-IR spectroscopy
Dalton Transactions 40, 9868-9876 (2011).

Barkleit, A.; Geipel, G.; Acker, M.; Taut, S.; Bernhard, G.
First fluorescence spectroscopic investigation of Am(III) complexation with an organic carboxylic ligand, pyromellitic acid
Spectrochimica Acta Part A 78, 549-552 (2011).

Barkleit, A.; Tsushima, S.; Savchuk, O.; Philipp, J.; Heim, K.; Acker, M.; Taut, S.; Fahmy, K.
Eu^{3+}-mediated polymerization of benzenetetracarboxylic acid studied by spectroscopy, temperature-dependent calorimetry, and density functional theory
Inorganic Chemistry 50, 5451-5459 (2011).

Chakraborty, S.; Bardelli, F.; Mullet, M.; Greneche, J.M.; Varma, S.; Ehrhardt, J.J.; Banerjee, D.; Charlet, L.
Spectroscopic studies of arsenic retention onto biotite
Chemical Geology 281, 83-92 (2011).

Comarmond, M.J.; Payne, T.E.; Harrison, J.J.; Thiruvoth, S.; Wong, H.K.; Aughterson, R.D.; Lumpkin, G.R.; Müller, K.; Foerstendorf, H.
Uranium sorption on various forms of titanium dioxide – influence of surface area, surface charge and impurities
Environmental Science & Technology 45, 5536-5542 (2011).

Davidson, M.M.; Silver, B.J.; Onstott, T.C.; Moser, D.P.; Gihring, T.M.; Pratt, L.M.; Boice, E.A.; Sherwood Lollar, B.; Lippmann-Pipke, J.; Pfiffner, S.M.; Kieft, T.L.; Seymore, W.; Ralston, C.
Capture of planktonic microbial diversity in fractures by long-term monitoring of flowing boreholes, Evander Basin, South Africa
Geomicrobiology Journal 28, 275-300 (2011).

Dreissig, I.; Weiss, S.; Hennig, C.; Bernhard, G.; Zänker, H.
Formation of uranium(IV)-silica colloids at near-neutral pH
Geochimica et Cosmochimica Acta 75, 352-367 (2011).

Dupouy, G.; Bonhoure, I.; Conradson, S.D.; Dumas, T.; Hennig, C.; Le Naour, C.; Moisy, P.; Scheinost, A.C.; Simoni, E.; Den Auwer, C.
Local structure in americium and californium hexacyanoferrates. Comparison with their lanthanide analogues
European Journal of Inorganic Chemistry 10, 1560-1569 (2011).

Erkut, C.; Penkov, S.; Khesbak, H.; Vorkel, D.; Verbavatz, J.M.; Fahmy, K.; Kurzchalia, T.V.
Trehalose renders dauer larva of *Caenorhabditis elegans* resistant to extreme desiccation
Current Biology 21, 1331-1336 (2011).

Frost, L.; Geipel, G.; Viehweger, K.; Bernhard, G.
Interaction of uranium(VI) towards glutathione - an example to study different functional groups in one molecule
Proceedings in Radiochemistry 1, 357-362 (2011).

Gaona, X.; Dähn, R.; Tits, J.; Scheinost, A.C.; Wieland, E.
Uptake of Np(IV) by C-S-H phases and cement paste: an EXAFS study
Environmental Science & Technology 45, 8765-8771 (2011).

Götz, C.; Geipel, G.; Bernhard, G.
The influence of the temperature on the carbonate complexation of uranium(VI) - a spectroscopic study
Journal of Radioanalytical and Nuclear Chemistry 287, 961-969 (2011).

Günther, A.; Steudtner, R.; Schmeide, K.; Bernhard, G.
Luminescence properties of uranium(VI) citrate and uranium(VI) oxalate species and their application in the determination of complex formation constants
Radiochimica Acta 99, 535-541 (2011).

Heberling, F.; Scheinost, A.C.; Bosbach, D.
Formation of a ternary neptunyl(V) biscarbonato inner-sphere sorption complex inhibits calcite growth rate
Journal of Contaminant Hydrology 124, 50-56 (2011).

Heine, K.B.; Clegg, J.K.; Heine, A.; Gloe, K.; Karsten, G.; Henle, T.; Bernhard, G.; Cai, Z.L.; Reimers, J.R.; Lindoy, L.F.; Lach, J.; Kersting, B.
Complexation, computational, magnetic, and structural studies of the Maillard reaction product isomaltol including investigation of an uncommon π interaction with copper(II)
Inorganic Chemistry 50, 1498-1505 (2011).

Heller, A.; Barkleit, A.; Bernhard, G.
Chemical speciation of trivalent actinides and lanthanides in biological fluids: the dominant in vitro binding form of curium(III) and europium(III) in human urine
Chemical Research in Toxicology 24, 193-203 (2011).

Jeazet, H.B.T.; Mizera, J.; Doert, T.; Gloe, K.; Heine, A.; Bernhard, G.; Gloe, K.
Coordination chemistry of bis(2-pyridylimine) ligands with Ag(I): formation of two structurally different coordination polymers and one metallocycle controlled by linker and the solvent system
Journal of Inclusion Phenomena and Macrocyclic Chemistry 71, 343-352 (2011).

Jordan, N.; Foerstendorf, H.; Weiß, S.; Heim, K.; Schild, D.; Brendler, V.
Sorption of selenium(VI) onto anatase: macroscopic and microscopic characterization
Geochimica et Cosmochimica Acta 75, 1519-1530 (2011).

Joseph, C.; Schmeide, K.; Sachs, S.; Brendler, V.; Geipel, G.; Bernhard, G.
Sorption of uranium(VI) onto Opalinus clay in the absence and presence of humic acid in Opalinus clay pore water
Chemical Geology 284, 240-250 (2011).

Khesbak, H.; Savchuk, O.; Tsushima, S.; Fahmy, K.
The role of water H-bond imbalances in B-DNA substate transitions and peptide recognition revealed by time-resolved FTIR spectroscopy
Journal of the American Chemical Society 133, 5834-5842 (2011).

Kirsch, R.; Fellhauer, D.; Altmaier, M.; Neck, V.; Rossberg, A.; Fanghänel, T.; Charlet, L.; Scheinost, A.C.
Oxidation state and local structure of plutonium reacted with magnetite, mackinawite, and chukanovite
Environmental Science & Technology 45, 7267-7274 (2011).

Kottmeier, K.; Günther, T. J.; Weber, J.; Kurtz, S.; Ostermann, K.; Rödel, G.; Bley, T.
Recombinant expression of surface active hydrophobin HFB1 from *Trichoderma reesei* in *Pichia pastoris*
Engineering in Life Sciences 91, 133-141 (2011).

Krawczyk-Bärsch, E.; Lünsdorf, H.; Arnold, T.; Brendler, V.; Eisbein, E.; Jenk, U.; Zimmermann, U.
The influence of biofilms on the migration of uranium in acid mine drainage (AMD) waters
Science of the Total Environment 409, 3059-3065 (2011).

Křepelová, A.; Sachs, S.; Bernhard, G.
Influence of humic acid on the Am(III) sorption onto kaolinite
Radiochimica Acta 99, 253-260 (2011).

Lederer, F.; Günther, T.; Raff, J.; Pollmann, K.
***E. coli* filament formation induced by heterologous S-layer expression.**
Bioengineered Bugs 2, 1-4 (2011).

Lippmann-Pipke, J.; Erzinger, J.; Zimmer, M.; Kujawa, C.; Boettcher, M.; van Heerden, E.; Bester, A.; Moller, H.; Stroncik, N.A.; Reches, Z.
Geogas transport in fractured hard rock - correlations with mining seismicity at 3.54 km depth, TauTona gold mine, South Africa
Applied Geochemistry 26, 2134-2146 (2011).

Lippmann-Pipke, J.; Sherwood Lollar, B.; Niedermann, S.; Stroncik, N.; Naumann, R.; van Heerden, E.; Onstott, T.C.
Neon identifies two billion year old fluid component in Kaapvaal Craton
Chemical Geology 283, 287-296 (2011).

Liu, J.; Lippold, H.; Wang, J.; Lippmann-Pipke, J.; Chen, Y.
Sorption of thallium(I) onto geological materials: influence of pH and humic matter
Chemosphere 82, 866-871 (2011).

Merroun, M.; Nedelkova, M.; Ojeda, J.J.; Reitz, T.; Fernandez, M.; Arias, J.M.; Romero-Gonzalez M.; Selenska-Pobell, S.
Bio-precipitation of uranium by two bacterial isolates recovered from extreme environments as estimated by potentiometric titration, TEM and X-ray absorption spectroscopic analyses
Journal of Hazardous Materials 197, 1-10 (2011).

Moll, H.; Brendler, V.; Bernhard, G.
Aqueous curium(III) phosphate species characterized by time-resolved laser-induced fluorescence spectroscopy
Radiochimica Acta 99, 775-782 (2011).

Müller, K.; Lefèvre, G.
Vibrational characteristics of outer-sphere surface complexes: example of sulfate ions adsorbed onto metal (hydr)oxides
Langmuir 27, 6830-6835 (2011).

Payne, T.E.; Brendler, V.; Comarmond, M.J.; Nebelung, C.
Assessment of surface area normalisation for interpreting distribution coefficients (K-d) for uranium sorption
Journal of Environmental Radioactivity 102, 888-895 (2011).

Planer-Friedrich, B.; Scheinost, A.C.
Formation and structural characterization of thioantimony species and their natural occurrence in geothermal waters
Environmental Science & Technology 45, 6855-6863 (2011).

Prieur, D.; Martin, P.M.; Jankowiak, A.; Gavilan, E.; Scheinost, A.C.; Herlet, N.; Dehaudt, P.; Blanchart, P.
Local structure and charge distribution in mixed uranium-americium oxides: effects of oxygen potential and Am content
Inorganic Chemistry 50, 12437-12445 (2011).

Reitz, T.; Merroun, M.L.; Rossberg, A.; Steudtner, R.; Selenska-Pobell, S.
Bioaccumulation of U(VI) by *Sulfolobus acidocaldarius* at moderate acidic conditions
Radiochimica Acta 99, 543-553 (2011).

Sachs, S.; Bernhard, G.
Humic acid model substances with pronounced redox functionality for the study of environmentally relevant interaction processes of metal ions in the presence of humic acid
Geoderma 162, 132-140 (2011).

Sachs, S.; Bernhard, G.
Influence of humic acids on the actinide migration in the environment: suitable humic acid model substances and their application in studies with uranium – a review
Journal of Radioanalytical and Nuclear Chemistry 290, 17-29 (2011).

Seitz, F.; Pollmann, K.; Mackenzie, K.; Opiolka, S.
Photooxidation in combination with nanotechnologies - principles, developments and R&D approaches of an advanced technology for water and air treatment - Uviblox®
Journal of Advanced Oxidation Technologies 14, 260-265 (2011).

Selenska-Pobell, S.; Reitz, T.; Schönemann, R.; Herrmannsdörfer, T.; Merroun, M.; Geißler, A.; Bartolomé, J.; Bartolomé, F.; Garcia, L.M.; Wilhelm, F.; Rogalev, A.
Magnetic Au nanoparticles on archaeal S-layer ghosts as templates
Nanomaterials and Nanotechnology 1, 8-16 (2011).

Sobolev, O.; Cuello, G.J.; Scheinost, A.C.; Johnson, M.R.; Nikitenko, S.; Le Forestier, L.; Brendle, J.; Charlet, L.
The short range order of ions in clay minerals: Sm^{3+} coordination
Physica Status Solidi (C) 208, 2293-2298 (2011).

Sornein, M.O.; Cannes, C.; Le Naour, C.; Mendes, M.; Hennig, C.
Electrochemical behaviour of tetrachloro and tetrabromo uranyl complexes in room temperature ionic liquids
Journal of Electroanalytical Chemistry 661, 49-56 (2011).

Steudtner, R.; Müller, K.; Schmeide, K.; Sachs, S.; Bernhard, G.
Binary and ternary uranium(VI) humate complexes studied by attenuated total reflection Fourier-transform infrared spectroscopy
Dalton Transactions 40, 11920-11925 (2011).

Steudtner, R.; Sachs, S.; Schmeide, K.; Brendler, V.; Bernhard, G.
Ternary uranium(VI) carbonato humate complex studied by cryo-TRLFS
Radiochimica Acta 99, 687-692 (2011).

Tits, J.; Geipel, G.; Mace, N.; Eilzer, M.; Wieland, E.
Determination of uranium(VI) sorbed species in calcium silicate hydrate phases: A laser-induced luminescence spectroscopy and batch sorption study
Journal of Colloid and Interface Science 359, 248-256 (2011).

Tsushima, S.
On the "yl" bond weakening in uranyl(VI) coordination complexes
Dalton Transactions 40, 6732-6737 (2011).

Viehweger, K.; Geipel, G.; Bernhard, G.
Impact of uranium (U) on the cellular glutathione pool and resultant consequences for the redox status of U
BioMetals 24, 1197-1204 (2011).

Voegelin, A.; Jacquat, O.; Pfister, S.; Barmettler, K.; Scheinost, A.C.; Kretzschmar, R.
Time-dependent changes of zinc speciation in four soils contaminated with zincite or sphalerite
Environmental Science & Technology 45, 255-261 (2011).

▶ EXTENDED ABSTRACTS, REPORTS, CONTRIBUTIONS

Acker, M.; Barkleit, A.; Müller, M.; Schott, J.; Bernhard, G.
Joint project: Interaction and transport of actinides in natural clay rock with consideration of humic substances and clay organics - Investigations of temperature dependence of complexation and sorption of trivalent actinides (Am(III)) in the system actinide-NOM-natural clay rock-aquifer
Final Report, Dresden University of Technology, Dresden, Germany (2011).

Altmaier, M.; Brendler, V.; Bube, C.; Marquardt, C.; Moog, H.C.; Richter, A.; Scharge, T.; Voigt, W.; Wilhelm, S.
THEREDA – Thermodynamic reference database
Report GRS-265, Summary of Final Report (63 p.) and Abschlussbericht (876 p.), Gesellschaft für Anlagen- und Reaktorsicherheit, Braunschweig, Germany (2011).

Barkleit, A.; Heller, A.; Baraniak, L.; Bernhard, G.
Comparison of spectroscopic investigation and computer modelling of lanthanide(III) and actinide(III) speciation in human biological fluids
Proceedings of Third European IRPA Congress June 14−16, 2010, Helsinki, Finland, STUK – Radiation and Nuclear Safety Authority, 2318-2327 (2011).

Frost, L.; Osman, A.A.A.; Geipel, G.; Viehweger, K.; Moll, H.; Bernhard, G.
Interaction of U(VI) with some bioligands or the influence of different functional groups on complex formation
The New Uranium Mining Boom, Challenge and lessons learned (Merkel, B.; Schipek, M. eds.), Springer, Heidelberg, 595-606 (2011).

Geipel, G.; Günther, A.; Viehweger, A.; Bernhard, G.
Uranium – transfer from soil to plant cells
The New Uranium Mining Boom, Challenge and lessons learned (Merkel, B.; Schipek, M. eds.), Springer, Heidelberg, 821-826 (2011).

Joseph, C.; Van Loon, L.R.; Jakob, A.; Schmeide, K.; Sachs, S.; Bernhard, G.
Effect of temperature and humic acid on the U(VI) diffusion in compacted Opalinus Clay
The New Uranium Mining Boom, Challenge and lessons learned (Merkel, B.; Schipek, M. eds.), Springer, Heidelberg, 617-626 (2011).

Kaempf, N.; Scheinost, A. C.; Schulze, D. G.
Oxide minerals in soils
Handbook of Soil Sciences: Properties and Processes, Part III: Soil Mineralogy (Huang, P. M.; Li, Y.; Sumner, M. E. eds.), CRC Press, Boca Raton (2011).

Krawczyk-Bärsch, E.
Report and evaluation of the redox potential measurements during the intercomparison exercise of ReCosy
ReCosy ICE Report - Assessment of ReCosy Intercomparison Exercise. Intercomparison of Redox Determination Methods on Designed and Near-Natural Aqueous Systems (Altmaier, M.; Buckau, G.; Fellhauer, D.; Gaona, X. eds.), KIT Scientific Reports 7572, KIT Sientific Publishing, Karlsruhe, 1-24 (2011).

Krawczyk-Bärsch, E.; Arnold, T.; Eisbein, E.; Brendler, V.; Jenk, U.; Zimmermann, U.
The application of microsensors for the determination of redox processes in biofilms from uranium contaminated acidic mine drainage waters
3rd Annual Workshop Proceedings of the Collaborative Project "Redox Phenomena Controlling Systems" (7th EC FP CP RECOSY), KIT Scientific Reports 7603, KIT Scientific Publishing, Karlsruhe, 117-122 (2011).

Kulenkampff, J.; Spangenberg, E.
Laboratory measurements on fresh terrestrial gas-hydrate-bearing sediment cores
Geophysical Characterization of Gas Hydrates (Riedel, M.; Willoughby, E.C.; Chopra, S. eds.) Society of Exploration Geophysicists, Tulsa, 321-328 (2011).

Lippold, H.; Kulenkampff, J.; Gründig, M.; Zakhnini, A.
Contributions to modelling actinide transport in potential host rock formations: Elementary processes and influence of heterogeneous structures.
Final Report, Helmholtz-Zentrum Dresden-Rossendorf, Leipzig, Germany (2011).

Pollmann, K.; Raff, J.; Kutschke, S.
Biotechnologische Verfahren zur Sicherung von Rohstoffen
Acamonta – Zeitschrift für Freunde und Förderer der Technischen Universität Bergakademie Freiberg, TUBA Freiberg, 26-27 (2011).

Sachs, S.; Schmeide, K.; Bernhard, G.
Interaction of humic acid with actinides: influence of heteroatomic functional groups other than carboxylic groups
Workshop Peat and Humic Substances. Current research in chemical, physical and biological characterization of peat. University of Applied Sciences Zittau/Görlitz, Proceedings, Heft 5, Zittau, 17-20 (2011).

Schmeide, K.; Joseph, C.; Sachs, S.; Steudtner, R.; Raditzky, B.; Günther, A.; Bernhard, G.
Joint project: Interaction and transport of actinides in natural clay rock with consideration of humic substances and clay organics – Characterization and quantification of the influence of clay organics on the interaction and diffusion of uranium and americium in the clay
Final Report, Helmholtz-Zentrum Dresden-Rossendorf, Dresden, Germany (2011).

Selenska-Pobell, S.; Reitz, T.; Geissler, A.; Herrmannsdörfer, T.; Merroun, M.
Fabrication of highly ordered magnetic bio-Au nanoclusters by using SlaA-layer ghosts of *Sulfolobus acidocaldarius* as a template
Nanotechnology 2011: Bio Sensors, Instruments, Medical, Environment and Energy, Taylor & Francis, Boca Raton, U.S.A., 189-192 (2011).

Vogel, M.; Günther, A.; Gube, M.; Raff, J.; Kothe, E.; Bernhard, G.
Interaction of *Chlorella vulgaris* and *Schizophyllum commune* with U(VI)
The New Uranium Mining Boom, Challenge and lessons learned (Merkel, B.; Schipek, M. eds.), Springer, Heidelberg, 185-192 (2011).

▶ LECTURES, ORAL PRESENTATIONS

Banerjee, D.; Weiss, S.; Zänker, H.; Scheinost, A.C.; Hennig, C.
Spectroscopic study of influence of silica on the stability of actinide(IV) colloids at near-neutral pH
Goldschmidt 2011, Earth, Life and Fire, August 14-19, 2011, Prague, Czech Republic. Mineralogical Magazine 75, 478 (2011).

Barkleit, A.
Wechselwirkungen von Actiniden mit Biomolekülen
2. Workshop zum Innovationsforum Geobiotechnologie, November 03-04, 2011, Dresden, Germany.

Barkleit, A.; Geipel, G.; Fahmy, K.; Tsushima, S.; Acker, M.; Taut, S.; Bernhard, G.
Am(III) and Eu(III) complexation with small organic molecules at elevated temperatures – studied by spectroscopy, calorimetry and density functional theory
Migration 2011 – 13th International Conference on the Chemistry and Migration Behaviour of Actinides and Fission Products in the Geosphere, September 18-23, 2011, Beijing, China.

Belin, R.C.; Martin, P.M.; Gavilan, E.; Reynaud, M.; Scheinost, A.C.
On the role of americium in the reduction process in plutonium-americium oxides
GLOBAL 2011 - Innovative Nuclear Energy Systems toward 2030 and beyond,December 11-16, 2011,Chiba, Japan.

Brendler, V.; Ekberg, C.; Ödegaard-Jensen, A.; Schikora, J.; Noseck, U.
Sensitivity and uncertainty analysis applied to radionuclide sorption onto single minerals and sediments
Migration 2011 – 13th International Conference on the Chemistry and Migration Behaviour of Actinides and Fission Products in the Geosphere, September 18-23, 2011, Beijing, China.

Eichler, S.; Madathil, S.; Fahmy, K.
Functional role of protonation and hydration at the lipid protein interface in membrane receptors
Annual Meeting of the German Biophysical Society, October 03-06, 2010, Ruhr-Universität-Bochum, Germany (2011).

Flügge, J.; Noseck, U.; Schneider, A.; Stockmann, M.
The impact of climate transitions on the radionuclide transport through a sedimentary aquifer
International Conference on Groundwater: Our Source of Security in an Uncertain Future, September 19-21, 2011, Pretoria, South Africa.

Foerstendorf, H.; Tsushima, S.; Brüning, S.; Li, B.
Exploring the mobility of actinyl ions in the biogeosphere: a spectroscopic and theoretical study of U(VI) complexes with organic phosphate groups
Goldschmidt 2011, Earth, Life and Fire, August 14-19, 2011, Prague, Czech Republic. Mineralogical Magazine 75, 856 (2011).

Frost, L.
The influence of microbes on radionuclide speciation concerning nuclear waste disposal
6. Graduate Students Seminar, October 05-07, 2011, Rabenberg, Germany.

Frost, L.; Osman, A.A.A.; Geipel, G.; Viehweger, K.; Moll, H.; Bernhard, G.
Interaction of U(VI) with some bioligands or the influence of different functional groups on complex formation
UMH VI – 6th International Conference Uranium Mining and Hydrogeology, September 18-22, 2011, Freiberg, Germany.

Geipel, G.
Laser-induced time-resolved luminescence measurements
Kick-Off Meeting Helmholtz Virtual Institute "Functional Nanomaterials for Multimodality Cancer Imaging", October 06-07, 2011, Dresden, Germany.

Geipel, G.
Uranium: from geosphere to biosphere
Metal Metabolism Seminar, King's College London, October 13, 2011, London, United Kingdom.

Geipel, G.; Günther, A.; Viehweger, A.; Bernhard, G.
Uranium – transfer from soil to plant cells
UMH VI – 6th International Conference Uranium Mining and Hydrogeology, September 18-22, 2011, Freiberg, Germany.

Geipel, G.; Viehweger, K.
Interactions of biomolecules with heavy metals
8th SUPRAPHONE Meeting 2011, September 07-10, 2011, Funchal, Spain.

Geipel, G.; Viehweger, K.; Bernhard, G.
Direct determination of uranium speciation in eukaryotic cells – challenges and limitations
10th Symposium on remediation in Jena, "Jenaer Sanierungkolloquium", October 04-06, 2011, Jena, Germany.

Günther, A.; Vogel, M.; Raff, J.; Kothe, E.; Bernhard, G.
Sorption of uranium(VI) by selected bacteria, algae and fungi and characterization of uranyl biomass species using different microscopic and spectroscopic methods
Migration 2011 – 13th International Conference on the Chemistry and Migration Behaviour of Actinides and Fission Products in the Geosphere, September 18-23, 2011, Beijing, China.

Günther, T.; Raff, J.; Pollmann, K.
A simple method to prepare microorganisms for AFM analysis
VAAM-Jahrestagung, April 03-06, 2011, Karlsruhe, Germany.

Hampel, U.
Reactor safety and radioecology research at the Helmholtz-Zentrum Dresden-Rossendorf
Helmholtz-Kurchatov Workshop, May 24, 2011, Moscow, Russia.

Hennig, C.
Combining real-space data analysis of HEXS and XAS to determine the structure of amorphous colloids
ADD2011 – Workshop on Analysis of Diffraction Data in Real Space, October 12-14, 2011, Grenoble, France.

Hennig, C.
Coordination chemistry of tetravalent actinides in presence of carboxylate ligands
Aoyama Gakuin University Tokyo, March 09, 2011, Tokyo, Japan.

Hennig, C.
Stability and structure of actinide(IV) colloids in aqueous solution
Tokyo Institute of Technology, March 08, 2011, Tokyo, Japan.

Hennig, C.; Takao, K.; Takao, S.; Meyer, M.; Jeanson, A.; Dahou, S.; Den Auwer, C.
The special case of Actinide(IV) complexation by the carboxylic function of small and large organic ligands
Goldschmidt 2011, Earth, Life and Fire, August 14-19, 2011, Prague, Czech Republic. Mineralogical Magazine 75, 1010 (2011).

Hennig, C.; Weiss, S.; Banerjee, D.; Zänker, H.
The influence of silica to stabilize actinide(IV) colloids at neutral pH
Actinide XAS 2011 – 6th Workshop on Speciation, Techniques, and Facilities for Radioactive Materials at Synchrotron Light Sources and Other Quantum Beam Sources, March 02-04, 2011, Harima Science Garden City, Hyogo, Japan.

Hennig, C.; Weiss, S.; Dreissig, I.; Banerjee, D.; Zänker, H.; Brendler, E.; Scheinost, A.C.; Bernhard, G.
Structure investigation of U(IV) and Th(IV) silica colloids at near-neutral pH by combining X-ray scattering and X-ray absorption spectroscopy
GDCh Wissenschaftsforum Chemie 2011, September 04-07, 2011, Bremen, Germany.

Hildebrand, H.
Untersuchung des Lebenszyklus von TiO_2- und Ag0-Nanopartikeln - NanoTRACK
1. Clustertreffen der BMBF-Fördermaßnahmen NanoCare und NanoNature, May 10-11, 2011, Frankfurt a. M., Germany.

Hildebrand, H.; Franke, K.
Radiolabelling of commercial Ag0 and TiO_2 nanoparticles with ^{110m}Ag and ^{44}Ti for life-cycle studies
7th annual CYCLEUR workshop on cyclotron research and radio-labelled nanoparticles, November28-29, 2011, Ispra, Italia.

Hildebrand, H.; Franke, K.
Radiolabelling of engineered nanomaterials as a tool for sensitive particle tracking
Goldschmidt 2011, Earth, Life and Fire, August 14-19, 2011, Prague, Czech Republic. Mineralogical Magazine 75, 1022 (2011).

Ikeda-Ohno, A.
Multiple spectroscopic and microscopic study on hydrolysis of tetravalent cerium: in-situ characterization of Ce(IV) hydrolytic species in an aqueous solution
Institute Pluridisciplinaire Hubert Curien, CNRS-Strasbourg, September 27, 2011, Strasbourg, France.

Ikeda-Ohno, A.
Synchrotron-based X-ray techniques for radioactive materials research: understanding the chemical behaviour of radionuclides in solution
CLS internal seminar, November 23, 2011, Canadian Light Source, Saskatoon, Canada.

Joseph, C.; Van Loon, L.R.; Jakob, A.; Schmeide, K.; Sachs, S.; Bernhard, G.
Effect of temperature and humic acid on the U(VI) diffusion in compacted Opalinus Clay
UMH VI – 6th International Conference Uranium Mining and Hydrogeology, September 18-22, 2011, Freiberg, Germany.

Kosmata, M.; Auerhammer, J.; Zier, M.; Schlaphof, F.; Schreiter, F.; von Borany, J.
Influence of proton elastic scattering on soft error generation of SRAMs
Conference on Radiation Effects on Components and Systems, September 19-23, 2011, Sevilla, Spain.

Krawczyk-Bärsch, E.; Lünsdorf, H.; Pedersen, K.; Lehtinen, A.; Arnold, T.
Retention of uranium in biofilms of a granitic nuclear waste repository research tunnel
Migration 2011 – 13th International Conference on the Chemistry and Migration Behaviour of Actinides and Fission Products in the Geosphere, September 18-23, 2011, Beijing, China.

Krawczyk-Bärsch, E.; Pedersen, K.; Lehtinen, A.; Arnold, T.
Uranium immobilization in biofilms from a granitic nuclear waste repository research tunnel – A microsensor and spectroscopic study
3rd Annual Workshop of ReCosy,March 21-24, 2011, Balaruc les Bains, France.

Lippmann-Pipke, J.; Kulenkampff, J.; Gründig, M.; Richter, M.
Matching 4D porous media fluid flow GeoPET data with COMSOL multiphysics simulation results
COMSOL Conference, October 26-28, 2011, Stuttgart, Germany.

Lippmann-Pipke; J.; Sherwood Lollar, B.; Niedermann, S.; Stroncik, N.A.; Naumann, R.; van Heerden, E.; Onstott, T.C.
Neon identifies two billion year old fluid component in Kaapvaal Craton
Goldschmidt 2011, Earth, Life and Fire, August 14-19, 2011, Prague, Czech Republic. Mineralogical Magazine 75, 1333 (2011).

Lippmann-Pipke, J.; Sherwood Lollar, B.; Niedermann, S.; Stroncik, N.A.; Naumann, R.; van Heerden, E.; Onstott, T.C.; Erzinger, J.; Zimmer, M.; Kujawa, C.; Boettcher, M.; Bester, A.; Moller, H.; Reches, Z.
Geogases in the Kaapvaal Craton – Origin and modes of transport
New Horizons for International Investigations into Carbon Cycing in the Deep Crustal Biosphere, January 18-23, 2011, Bloemfontein, South Africa.

Lippold, H.; Kulenkampff, J.; Gründig, M.; Lippmann-Pipke, J.
Radiotracer studies on the mobility of radionuclides in clay matrices containing organic matter: elementary processes and influence of heterogeneous structures
Abschlussworkshop zum Verbundvorhaben "Wechselwirkung und Transport von Actiniden im natürlichen Tongestein unter Berücksichtigung von Huminstoffen und Tonorganika", May 17-18, 2011, Karlsruhe, Germany.

Liu, J.; Lippold, H.; Wang, J.; Lippmann-Pipke, J.; Chen, Y.H.
Adsorption of thallium(I) onto geological materials: effect of pH and humic matter
Goldschmidt 2011, Earth, Life and Fire, August 14-19, 2011, Prague, Czech Republic. Mineralogical Magazine 75, 1341 (2011).

Martin, P.; Belin, R.; Robisson, A.C.; Dumas, J.C.; Scheinost, A.C.
Actinides chemistry in mixed oxide nuclear fuel
Actinide XAS 2011 – 6th Workshop on Speciation, Techniques, and Facilities for Radioactive Materials at Synchrotron Light Sources and Other Quantum Beam Sources, March 02-04, 2011, Harima Science Garden City, Hyogo, Japan.

Müller, K.
Spektroskopische Untersuchungen zum Verhalten von Neptunium und Uran in der Geosphäre
Jahresveranstaltung "Woman in Nuclear", November 24-25, 2011, Biblis, Germany

Müller, K.; Foerstendorf, H.; Rossberg, A.; Stolze, K.; Gückel, K.
Comparative study of the U(VI) complexation onto γ-Al_2O_3 by ATR FT-IR and EXAFS spectroscopy
Goldschmidt 2011, Earth, Life and Fire, August 14-19, 2011, Prague, Czech Republic. Mineralogical Magazine 75, 1513 (2011).

Paulik, S.; Mansel, A.; Schnorr, R.; Haupt, S.; Bernhard, G.; Kersting, B.
Wechselwirkung von wasserlöslichen Calixarenen mit divalenten Kationen (^{85}Sr, ^{56}Co)
GDCh Wissenschaftsforum Chemie 2011, September 04-07, 2011, Bremen, Germany.

Pietrzyk, U.; Zakhnini, A.; Axer, M.
EduGATE - Simple examples for educative purpose using the GATE simulation platform
NuklearMedizin 2011, April 13-16, 2011, Bregenz, Austria.

Planer-Friedrich, B.; Scheinost, A.C.
Thioantimonates in geothermal waters
Antimony 2011 – 2nd International Workshop on Antimony in the Environment, August 21-24, 2011, Jena, Germany.

Planer-Friedrich, B.; Suess, E.; Scheinost, A.C.; Wallschläger, D.
XAS versus IC-ICP-MS for arsenic-sulfur speciation analysis
ICOBTE 2011 – 11th International Conference on the Biogeochemistry of Trace Elements, July 03-07, 2011, Florence, Italy.

Pollmann, K.
Bakterien als Lieferanten für neue Recycling-Technologien: Rückgewinnung von Metallen aus Wässern mit neuen Biokompositmaterialien
1. Freiberger Ressourcen-Technologie Symposium, February 14-15, 2011, Freiberg, Germany.

Pollmann, K.
Die zunehmende Bedeutung von biotechnologischen Innovationen für angrenzende Branchen
6. Innovationsbörse Sachsen, March 30, 2011, Görlitz, Germany.

Pollmann, K.; Günther, T.; Weinert, U.; Marquard, A.; Kutschke, S.; Lehmann, F.; Raff, J.
Bioinspired nanocomposites based on self-assembling bacterial surface layer proteins
Euro BioMat 2011 – European Symposium on Biomaterials and Related Areas, April 13-14, 2011, Jena, Germany.

Pollmann, K.; Raff, J.; Kutschke, S.
Bio-basierte Konzepte zur Gewinnung von Metallen aus Mineralien
Workshop des Innovationsforums Geobiotechnologie, 10.-11.10.2011, Aue, Deutschland

Pollmann, K.; Raff, J.; Kutschke, S.
Biosorptive Kompositmaterialien für die Rückgewinnung von Wertstoffen: Neue Konzepte und Anwendungspotenziale; Biomining von Sekundärrohstoffen
Workshop 3 des Innovationsforums "Geobiotechnologie - mikrobiologische Verfahren in Bergbau und Umweltschutz", December 14-15, 2011, Hannover, Germany.

Prieur, D.; Martin, P.M.; Jankowiak, A.; Gavilan, E.; Scheinost, A.C.; Leorier, C.; Herlet, N.; Dehaudt, P.; Laval, J.P.; Blanchart, P.
XAS study of dense U1-YAmYO2-X (Y=0.10; 0.15; 0.20) compounds
Actinide XAS 2011 – 6th Workshop on Speciation, Techniques, and Facilities for Radioactive Materials at Synchrotron Light Sources and Other Quantum Beam Sources, March 02-04, 2011, Harima Science Garden City, Hyogo, Japan.

Raff, J.
Aus alt mach neu – Wie Bakterien beim Recycling von Handys & Co helfen können
Tag der Wissenschaften, July 06, 2011, Radebeul, Germany.

Raff, J.
S-Layer-basierte Materialien zur Detektion und Entfernung von Schad- und Wertstoffen
Biomatum-Seminar, May 17, 2011, Dresden, Germany.

Raff, J.; Pollmann, K.
Innovationspool Natur: Neue Biokompositmaterialien zur Rückgewinnung strategischer Metalle
Innovationsforum „Life Cycle und Recycling seltener Metalle mit strategischer Bedeutung“, March 01-02, 2011, Freiberg, Germany.

Sachs, S.; Schmeide, K.; Bernhard, G.
Interaction of humic acid with actinides: influence of heteroatomic functional groups other than carboxylic groups
Workshop Peat and Humic Substances. Current research in chemical, physical and biological characterization of peat, September 28-30, 2011, Zittau, Germany.

Sauerzapf, S.; Zakhnini, A.; Behe, M.; Weber, W.; Pietrzyk, U.; Mix, M.
Optimierung der Kleintierbildgebung mit nichtreinen Positronenstrahlern
Dreiländertagung der ÖGMP, DGMP und SGSMP, September 28- October 01, 2011, Vienna, Austria.

Scheinost, A.C.
Actinide redox reactions at the solid-water interface probed by XAFS
J-ACTINET Meeting, September 01-02, 2011, Tokyo, Japan.

Scheinost, A.C.
Probing redox reactions at the mineral/water interface by X-ray absorption spectroscopy: reduction of Se, Sn, Sb and Pu by Fe(II)-bearing minerals
LES Seminar, March 15, 2011, Villigen, Switzerland.

Scheinost, A.C.
The Rossendorf Beamline at ESRF: a multipurpose X-ray absorption spectroscopy and scattering beamline for environmental and materials sciences
SESAME User Meeting 2011, November 12, 2011, Amman, Jordan.

Scheinost, A.C.
X-ray absorption spectroscopy for environmental sciences: examples and technical challenges
SESAME User Meeting 2011, November 12, 2011, Amman, Jordan.

Scheinost, A.C.; Hennig, C.; Rossberg, A.; Banerjee, D.
ROBL: the first European actinide XAS beamline in its second decade of operation
Actinide XAS 2011 – 6th Workshop on Speciation, Techniques, and Facilities for Radioactive Materials at Synchrotron Light Sources and Other Quantum Beam Sources, March 02-04, 2011, Harima Science Garden City, Hyogo, Japan.

Scheinost, A.C.; Rossberg, A.
Advanced EXAFS analysis: examples from mineral/water interface redox reactions
J-ACTINET Computational Science School 2011, September 05-06, 2011, Tokyo, Japan.

Scheinost, A.C.; Schmeisser, N.; Denecke, M.; Banerjee, D.; Dardenne, K.; Hennig, C.; Rossberg, A.; Rothe, J.; Daehn, R.
AcXAS, a reference data base for XAS spectra of actinides and other radionuclides
ACTINET Plenary Meeting, February 01, 2011, Marcoule, France.

Schikora, J.
Realistic integration of sorption processes in long-term safety assessments
Doktorandenseminar – Kompetenzzentrum Ost für Kerntechnik December 08, 2011, Zittau, Germany.

Schindler, F.; Günther, A.; Freihorst, D.; Haferburg, G.; Raff, J.; Kothe, E.
Uranantwort von Bakterien und Pilzen
10. Internationales Symposium "Konditionierung radioaktiver Betriebs- und Stilllegungsabfälle", April 06-08, 2011, Dresden, Germany.

Schmeide, K.; Joseph, C.; Steudtner, R.
Temperature dependence of complexation, sorption and diffusion in the system uranium(VI)/clay organics/clay rock
Abschlussworkshop zum Verbundvorhaben "Wechselwirkung und Transport von Actiniden im natürlichen Tongestein unter Berücksichtigung von Huminstoffen und Tonorganika", May 17-18, 2011, Karlsruhe, Germany.

Selenska-Pobell, S.
Fabrication of magnetic bio-Au nanoclusters by using SlaA-layer ghosts of *Sulfolobus acidocaldarius* as a template
Nanotech Conference and Expo 2011, June 13-16, 2011, Boston, U.S.A.

Selenska-Pobell, S.; Reitz, T.; Geissler, A.; Merroun, M.; Herrmannsdörfer, T.
Bio-Au nanoparticles on archaeal and bacterial S-layers
Goldschmidt 2011, Earth, Life and Fire, August 14-19, 2011, Prague, Czech Republic. Mineralogical Magazine 75, 1834 (2011).

Steudtner, R.; Großmann, K.; Joseph, C.; Vogel, M.; Brendler, V.
Langlebige Radionuklide in Geo-/ Biosystemen
Zittauer Kraftwerkschemisches Kolloquium, September 22-23, 2011, Lückendorf, Germany.

Steudtner, R.
Vorstellung des Instituts für Radiochemie zum *Dies academicus*
Dies academicus 2011, June 08, 2011, Zittau, Germany.

Stockmann, M.; Brendler, V.; Schikora, J.; Noseck, U.; Flügge, J.
Realitätsnahe Einbindung von Sorptionsprozessen in Sicherheitsanalysen
Jahrestagung Kerntechnik, May 17-19, 2011, Berlin, Germany.

Tsushima, S.
Application of quantum chemical calculations to actinide solution chemistry: spectroscopy and photochemistry
Tokai Research and Development Center of the Japan Atomic Energy Agency (JAEA), March 09, 2011, Tokai, Japan.

Tsushima, S.
Aqueous coordination chemistry and photochemistry of uranium(VI)
Seminar at Katholieke Universiteit Leuven, January 14, 2011, Leuven, Belgium.

Tsushima, S.
Aqueous coordination chemistry of excited state uranyl(VI)
Actinide XAS 2011 – 6th Workshop on Speciation, Techniques, and Facilities for Radioactive Materials at Synchrotron Light Sources and Other Quantum Beam Sources, March 02-04, 2011, Harima Science Garden City, Hyogo, Japan.

Tsushima, S.
Exploring uranyl(VI) photochemistry by DFT calculations
Seminar talk at the Research Laboratory for Nuclear Reactors, Tokyo Institute of Technology, March 08, 2011, Tokyo, Japan.

Vogel, M.; Günther, A.; Gube, M.; Raff, J.; Kothe, E.; Bernhard, G.
Interaction of *Chlorella vulgaris* and *Schizophyllum* commune with U(VI)
UMH VI – 6th International Conference Uranium Mining and Hydrogeology, September 18-22, 2011, Freiberg, Germany.

Vogel, M.; Günther, A.; Raff, J.; Bernhard, G.
Uptake and binding of U(VI) by the green alga *Chlorella vulgaris*
10th Symposium on remediation in Jena, "Jenaer Sanierungkolloquium", October 04-06, 2011, Jena, Germany.

Weinert, U.; Günther, T.; Müller, N.; Pollmann, K.; Raff, J.
Entwicklung nanoskaliger funktionaler Schichten auf Basis von bakteriellen Hüllproteinen
7. Deutsches BioSensor Symposium, April 03-06, 2011, Heilbad Heiligenstadt, Germany.

Weinert, U.; Raff, J.; Günther, T.; Pollmann, K.
Fundamental and application oriented research on bacterial S-layers from uranium mining waste pile isolates
Visit of the working group of Prof. Betzel, DESY, January 26, 2011, Hamburg, Germany.

Zänker, H.; Weiss, S.; Hennig, C.; Dreissig, I.; Bernhard, G.
Uranium(IV)-silica colloids at near-neutral pH
41èmes Journées des Actinides, April 09-12, 2011, Stara Lesna, Slovakia

Zänker, H.; Weiss, S.; Hennig, C.; Dreissig, I.; Bernhard, G.
Die Bildung von Uran(IV)-Silica-Kolloiden im nahneutralen pH-Bereich
GDCh Wissenschaftsforum 2011 (Jahrestagung Nuklearchemie), September 04-07, 2011, Bremen, Germany.

Zirnstein, I.; Gagell, C.; Arnold, T.; Krawczyk-Bärsch, E.; Röske, I.
Biofilms growing in an underground uranium mine
10th Symposium on remediation in Jena, "Jenaer Sanierungkolloquium", October 04-06, 2011, Jena, Germany.

▶ POSTERS

Abu Sharkh, S.; Oertel, J.; Fahmy, K.
FTIR and calorimetric investigation of the effects of trehalose and multivalent cations on lipid structure
8th European Biophysics Congress, August 23-27, 2011, Budapest, Hungary.
European Biophysics Journal with Biophysics Letters 40, 72 (2011).

Barkleit, A.; Geipel, G.; Acker, M.; Taut, S.
Spectroscopic characterization of Eu(III) and Am(III) complexes with small organic molecules at elevated temperatures
HiTAC - High Temperature Aqueous Chemistry, November 09, 2011, Karlsruhe, Germany.

Baumann, N.
Uranium(VI) speciation in natural waters determined by TRLFS
The 12th Conference on Nuclear Science and Technology, July 01-02, 2011, Bangkok, Thailand.

Baumann, N.; Arnold, T.
Uranium(VI) speciation in natural occurring water samples at pH 3-4 determined by TRLFS
10th Symposium on remediation in Jena, "Jenaer Sanierungkolloquium", October 04-06, 2011, Jena, Germany (2011).

Dulnee, S.; Banerjee, D.; Rossberg, A.; Scheinost, A.C.
Sorption and interfacial redox of Sn(II) under anoxic conditions: Magnetite vs. anatase
Goldschmidt 2011, Earth, Life and Fire, August 14-19, 2011, Prague, Czech Republic. Mineralogical Magazine 75, 789 (2011).

Fischer, S.; Husar, R.
Investigation of actinides behaviour under specific environmental conditions
6. Graduate Students Seminar, October 05-07, 2011, Rabenberg, Germany.

Fischer, S.; Husar, R.
Investigation of actinides behaviour under specific environmental conditions
Doktorandenseminar – Kompetenzzentrum Ost für Kerntechnik December 08, 2011, Zittau, Germany.

Franke, K.; Gottschalch, U.; Hildebrand, H.
Radiolabelling of nanoparticles for life-cycle studies
3rd International Nuclear Chemistry Congress, September 18-23, 2011, Terrasini - Palermo, Italy.

Franke, K.; Hildebrand, H.; Mehnert, R.; Mai, E.; Freyer, A.; Bilz, E.; Isaacson, C.; Schirmer, K.; Ammann, A.; Sigg, L.
NanoTrack - Untersuchung des Lebenszyklus von Nanopartikeln anhand von [^{45}Ti]TiO_2 und [^{105}Ag]Ag0
WING.DE 2011, October 04-06, 2011, Berlin, Germany.

Franzen, C.; Jordan, N.; Müller, K.; Meusel, T.; Brendler, V.
Temperature impact on the sorption of selenate onto anatase
HiTAC - High Temperature Aqueous Chemistry, November 09, 2011, Karlsruhe, Germany.

Frost, L.; Moll, H.; Bachvarova, V.; Geißler, A.; Selenska-Pobell, S.; Bernhard, G.
The influence of microbes on the uranium speciation under aerobic and anaerobic conditions
Migration 2011 – 13th International Conference on the Chemistry and Migration Behaviour of Actinides and Fission Products in the Geosphere, September 18-23, 2011, Beijing, China.

Gaona, X.; Dähn, R.; Tits, J.; Scheinost, A.C.; Wieland, E.
Uptake of Np(IV) by C-S-H phases and cement paste: an EXAFS study
3rd Annual Workshop of ReCosy,March 21-24, 2011, Balaruc-les-Bains, France.

Groß, M.; Solioz, M.; Fahmy, K.
Spectroscopic investigation of the structure and function of the copper ATPase CopB of *Enterococcus hirae*
8th European Biophysics Congress, August 23-27, 2011, Budapest, Hungary. European Biophysics Journal with Biophysics Letters 40, 168 (2011).

Gückel, K.
Vibrational spectroscopy of actinyl complexes
6. Graduate Students Seminar, October 05-07, 2011, Rabenberg, Germany.

Gückel, K.; Foerstendorf, H.; Brendler, V.; Bernhard, G.
The impact of atmospheric carbonate on the sorption of actinyl(V/VI) ions onto gibbsite studied by in situ ATR FT IR spectroscopy
Migration 2011 – 13th International Conference on the Chemistry and Migration Behaviour of Actinides and Fission Products in the Geosphere, September 18-23, 2011, Beijing, China.

Heller, A.; Barkleit, A.; Bernhard, G.
Spektroskopische Untersuchung der Komplexbildung von Curium(III) und Europium(III) mit dem Bioliganden Citrat
GDCh Wissenschaftsforum Chemie 2011, September 04-07, 2011, Bremen, Germany.

Hildebrand, H.; Franke, K.
Investigation of the life cycle of nanoparticles by means of radiolabelling - NanoTRACK
1. Clustertreffen der BMBF-Fördermaßnahmen NanoCare und NanoNature, May 10-11, 2011, Frankfurt a. M., Germany.

Ikeda-Ohno, A.; Weiss, S.; Bernhard, G.; Hennig, C.
Characterization of Ce(IV) hydrolytic species in aqueous solution by X-ray absorption spectroscopy, high energy solution X-ray scattering, and dynamic light scattering
ADD2011 – Workshop on Analysis of Diffraction Data in Real Space, October 12-14, 2011, Grenoble, France.

Jordan, N.; Foerstendorf, H.; Scheinost, A. C.; Lützenkirchen, J.; Schild, D.; Weiss, S.; Heim, K.; Brendler, V.
Uptake of selenium(VI) and selenium(IV) onto anatase and rutile
Geological Disposal of Radioactive Waste: Underpinning Science and Technology, October 18-20, 2011, Loughborough, U.K.

Jordan, N.; Müller, K.; Franzen, C.; Foerstendorf, H.; Weiss, S.; Heim, K.; Brendler, V.
Temperature effect on selenium oxyanions retention onto anatase
Migration 2011 – 13th International Conference on the Chemistry and Migration Behaviour of Actinides and Fission Products in the Geosphere, September 18-23, 2011, Beijing, China.

Khesbak, H.; Savchuk, O.; Tsushima, S.; Fahmy, K.
Coupling of the hydration shell of B-DNA to conformational substates and peptide recognition studied by time-resolved FTIR spectroscopy
8th European Biophysics Congress, August 23-27, 2011, Budapest, Hungary.
European Biophysics Journal with Biophysics Letters 40, 45 (2011).

Kulenkampff, J.; Enzmann, F.; Gründig, M.; Wolf, M.; Lippold, H.; Lippmann-Pipke, J.
Direct observation of preferential transport pathways in salt rocks by means of GeoPET.
ABC-Salt (II) Workshop, November 07-08, 2011, Karlsruhe, Germany.

Lederer, F.; Günther, T.; Pollmann, K.
Heterologous expression of surface layer proteins
6. Graduate Students Seminar, October 05-07, 2011, Rabenberg, Germany.

Lederer, F.; Günther, T.; Raff, J.; Pollmann, K.
Recombinant S-layer production induces disordered cell division in *E. coli* filaments
VAAM-Jahrestagung, April 03-06, 2011, Karlsruhe, Germany.

Lederer, F.; Günther, T.; Raff, J.; Pollmann, K.
Recombinant S-layer production induces disordered cell division in *E. coli* filaments
FEMS 2011 – 4th Congress of European Microbiologists, June 26-30, 2011, Geneva, Switzerland.

Lindner, K.; Günther, A.; Bernhard, G.
Interaction of Uranium(VI) with Schiff Bases in organic solvents
6. Graduate Students Seminar, October 05-07, 2011, Rabenberg, Germany.

Lindner, K.; Günther, A.; Bernhard, G.
Spectroscopic investigation of the interaction between uranium(VI) and schiff bases
Doktorandenseminar – Kompetenzzentrum Ost für Kerntechnik December 08, 2011, Zittau, Germany.

Mansel, A.; Franke, K.; Fischer, S.; Steinbach, J.
Inbetriebnahme des HZDR-Zyklotrons in Leipzig: Herstellung und Reinigung von n.c.a. Radionukliden 56Co und 85Sr
GDCh Wissenschaftsforum Chemie 2011, September 04-07, 2011, Bremen, Germany.

Moll, H.; Bachvarova, V.; Frost, L.; Geissler, A.; Selenska-Pobell, S.; Bernhard, G.
Speciation of curium(III) bound by bacteria found in rocks considered for nuclear waste disposals
Migration 2011 – 13th International Conference on the Chemistry and Migration Behaviour of Actinides and Fission Products in the Geosphere, September 18-23, 2011, Beijing, China.

Moll, H.; Raff, J.; Li, B.; Bernhard, G.
Curium(III) complexation with surface-layer (S-layer) proteins from a uranium mining waste pile isolate
Migration 2011 – 13th International Conference on the Chemistry and Migration Behaviour of Actinides and Fission Products in the Geosphere, September 18-23, 2011, Beijing, China.

Müller, K.; Foerstendorf, H.; Rossberg, A.; Stolze, K.; Gückel, K.
Comparative study of the U(VI) complexation onto γ-Al_2O_3 by ATR FT-IR and EXAFS spectroscopy
Goldschmidt 2011, Earth, Life and Fire, August 14-19, 2011, Prague, Czech Republic.
Mineralogical Magazine 75, 1513 (2011).

Osman, A.A.A.; Geipel, G.
Study of formation and thermodynamic properties of aqueous U(VI) – Uric acid system by time-resolved laser-induced fluorescence spectroscopy (TRLFS)
6. Graduate Students Seminar, October 05-07, 2011, Rabenberg, Germany.

Paulik, S.; Mansel, A.
Control of the migration behaviour of radiotoxic heavy metals by means of calixarenes
6. Graduate Students Seminar, October 05-07, 2011, Rabenberg, Germany.

Pietrzyk, U.; Zakhnini, A.; Axer, M.
EduGATE - Simple examples for educative purpose using the GATE simulation platform
NuklearMedizin 2011, April 13-16, 2011, Bregenz, Austria.

Pollmann, K.
Aptamer modifizierte bakterielle Oberflächenstrukturen für die Entwicklung neuer Sensoren
BIONA Statusseminar, Industriekongress, March 16-17, 2011, Berlin, Germany.

Raff, J.; Weinert, U.; Günther, T.; Marquard, A.; Lehmann, F.; Kutschke, S.; Pollmann, K.
Bioinspred hybrid nanomaterials based on self-assembling proteins
DFG-NSF Research Conference, March 22-25, 2011, New York, U.S.A.

Richter, A.
THEREDA – The thermodynamic reference database for a nuclear waste disposal in Germany
Migration 2011 – 13th International Conference on the Chemistry and Migration Behaviour of Actinides and Fission Products in the Geosphere, September 18-23, 2011, Beijing, China.

Rossberg, A.; Lucks, C.; Tsushima, S.; Scheinost, A.C.
Structural characterization of thermodynamically predicted U(VI)-tartrate complexes: combing factor analysis with Landweber inversion method
Actinide XAS 2011 – 6th Workshop on Speciation, Techniques, and Facilities for Radioactive Materials at Synchrotron Light Sources and Other Quantum Beam Sources, March 02-04, 2011, Harima Science Garden City, Hyogo, Japan.

Sauerzapf, S.; Thomas, L.; Behe, M.; Weber, W.; Pietrzyk, U.; Zakhnini, A.; Mix, M.
Using Monte-Carlo Simulations to implement corrections for I-124 as a non-pure positron emitter in small animal and human PET imaging
IEEE Nuklear Science Symposium and Medical Imaging Conference, Ocotber 23-29, 2011, Valencia, Spain.

Sauerzapf, S.; Zakhnini, A.; Behe, M.; Thomas, L.; Axer, M.; Weber, W.; Pietrzyk, U.; Mix, M.
Optimierung des Energiefensters für I-124 anhand von Monte-Carlo Simulationen und PET-Messungen an Kleintier- und Human-Tomographen
NuklearMedizin 2011, April 13-16, 2011, Bregenz, Austria.

Sayed, A.; Elsayed, M.M.; Tucker, P.; Fahmy, K.
Structural and functional investigation of astaxanthin binding to the catalytic domain of matrix metalloprotease MMP-13
8th European Biophysics Congress, August 23-27, 2011, Budapest, Hungary.
European Biophysics Journal with Biophysics Letters 40, 58-59 (2011).

Scheinost, A.C.; Schmeisser, N.; Denecke, M.; Banerjee, D.; Dardenne, K.; Hennig, C.; Rossberg, A.; Rothe, J.; Daehn, R.
AcXAS, a reference data base for XAS spectra of actinides and other radionuclides
Actinide XAS 2011 – 6th Workshop on Speciation, Techniques, and Facilities for Radioactive Materials at Synchrotron Light Sources and Other Quantum Beam Sources, March 02-04, 2011, Harima Science Garden City, Hyogo, Japan.

Schindler, F.; Günther, A.; Freihorst, D.; Haferburg, G.; Raff, J.; Kothe, E.
Uranantwort von Bakterien und Pilzen
10. Internationales Symposium "Konditionierung radioaktiver Betriebs- und Stilllegungsabfälle", April 06-08, 2011, Dresden, Germany.

Schmeide, K.; Joseph, C.; Bernhard, G.
Sorption and diffusion of U(VI) in the system Opalinus Clay/pore water in the absence and presence of organic ligands
NEA ClayClub Workshop - Clays under Nano- to Microscopic Resolution, September 06-08, 2011, Karlsruhe, Germany.

Schmeide, K.; Joseph, C.; Steudtner, R.; Bernhard, G.
Influence of organic ligands and temperature on U(VI) sorption and diffusion in the system Opalinus Clay/Opalinus Clay pore water
Migration 2011 – 13th International Conference on the Chemistry and Migration Behaviour of Actinides and Fission Products in the Geosphere, September 18-23, 2011, Beijing, China.

Schmeide, K.; Steudtner, R.; Bernhard, G.
Formation of U(VI) lactate and citrate complexes and their sorption onto Opalinus Clay between 10 and 60°C
HiTAC - High Temperature Aqueous Chemistry, November 09, 2011, Karlsruhe, Germany.

Schott, J.; Acker, M.; Barkleit, A.; Brendler, V.; Taut, S.; Bernhard, G.
Temperature depending investigations to the sorption of Eu(III) on Opalinus Clay
HiTAC - High Temperature Aqueous Chemistry, November 09, 2011, Karlsruhe, Germany.

Schott, J.; Barkleit, A.; Acker, M.; Brendler, V.; Bernhard, G.
Complexation of An(III)/Ln(III) with borates
6. Graduate Students Seminar, October 05-07, 2011, Rabenberg, Germany.

Steinfeldt, N.; Sebek, M.; Günther, T.; Jähnisch, K.; Pollmann, K.; Raff, J.
S-layer supported Pt-nanoparticles as catalyst for the asymmetric hydrogenation
44. Jahrestreffen Deutscher Katalytiker mit Jahrestreffen Reaktionstechnik, March 16-18, 2011, Weimar, Germany.

Steudtner, R.; Müller, K.; Meusel, T.; Brendler, V.
Preliminary multi-method spectroscopic approach for the uranium(VI) hydrolysis at temperatures up to 60°C
HiTAC - High Temperature Aqueous Chemistry, November 09, 2011, Karlsruhe, Germany.

Steudtner, R.; Schmeide, K.; Bernhard, G.
Uranium(VI) complexation with lactate and citrate in dependence on temperature (7-65°C)
Goldschmidt 2011, Earth, Life and Fire, August 14-19, 2011, Prague, Czech Republic. Mineralogical Magazine 75, 1940 (2011).

Stockmann, M.; Brendler, V.; Schikora, J.; Noseck, U.; Flügge, J.
Development of a new methodology for realistic describing radionuclide retardation in safety assessment
Goldschmidt 2011, Earth, Life and Fire, August 14-19, 2011, Prague, Czech Republic. Mineralogical Magazine 75, 1947 (2011).

Suhr, M.; Günther, T.; Raff, J.; Pollmann, K.
Kinetic and structural studies on the adsorption of metals and actinides on cell surfaces by using multi-layer systems as a model of bacterial cell walls
6. Graduate Students Seminar, October 05-07, 2011, Rabenberg, Germany.

Weinert, U.; Müller, N.; Günther, T.; Pollmann, K.; Raff, J.
S-layer proteins as binding matrix for sensory layers
6. Graduate Students Seminar, October 05-07, 2011, Rabenberg, Germany.

Weinert, U.; Pollmann, K.; Nikolaus, N.; Strehlitz, B.; Raff, J.
Entwicklung hochspezifischer und sensitiver Biosensoren auf Basis von bakteriellen Hüllproteinen und Aptameren
10. Dresdner Sensor-Symposium, December 05-07, 2011, Dresden, Germany.

Wobus, A.; Zirnstein, I.; Meierhöfer, C.; Arnold, T.; Krawczyk-Bärsch, E.; Röske, I.
Microbial structure of biofilm communities in an uranium contaminated acid mine drainage environment
VAAM-Jahrestagung, April 03-06, 2011, Karlsruhe, Germany.

Wolf, M.; Kulenkampff, J.; Enzmann, F.; Gründig, M.; Richter, M.; Lippmann-Pipke, J.
Combined 3D high-resolution PET and CT measurements with lattice Boltzmann simulations of fluid flow in heterogeneous material
European Geosciences Union General Assembly 2011, April 03-08, 2011,Vienna, Austria.

Zakhnini, A.; Kulenkampff, J.; Sauerzapf, S.; Lippmann-Pipke, J.; Pietrzyk, U.
Monte Carlo simulations of a ClearPET: scatter and attenuation of gamma rays in various rock formations
IEEE Nuklear Science Symposium and Medical Imaging Conference, Ocotber 23-29, 2011, Valencia, Spain.

Zirnstein, I.; Gagell, C.; Arnold, T.; Krawczyk-Bärsch, E.; Röske, I.
Microbial life in uranium-contaminated milieus
6. Graduate Students Seminar, October 05-07, 2011, Rabenberg, Germany.

▶ PATENT

Pollmann, K.; Raff, J.; Lederer, F.
P0903 - Mikroröhren, umfassend Bestandteile der äußeren Membran von *E. coli* Zellen und rekombinant exprimierte S-Layer-Proteine, Verfahren zu ihrer Herstellung und Verwendung
DE102009032645B

▶ THESES

Fellmer, F.
Untersuchung der Wechselwirkungen zweiwertiger chemotoxischer Schwermetalle und deren Huminstoffspezies (Metallhumat-komplexe) mit Geomaterialien unter Verwendung von Radioisotopen
Martin LutherUniversity Halle-Wittenberg, Halle, Germany (2011).

Heller, A.
Spektroskopische Untersuchungen zur Komplexbildung von Cm(III) und Eu(III) mit organischen Modellliganden sowie ihrer chemischen Bindungsform in menschlichem Urin (*in vitro*)
Dresden University of Technology, Dresden, Germany (2011).
Available as: Wissenschaftlich-Technische Berichte, HZDR-006, Helmholtz-Zentrum Dresden-Rossendorf, Dresden (2011).

Khesbak, H.
Time-resolved hydration-perturbation-FTIR spectroscopy: A new method to identify water H-bond networks that couple hydration to DNA conformation
Dresden University of Technology, Dresden, Germany (2011).

Reitz, T.
U(VI) bioaccumulation by *Paenibacillus* sp. JG-TB8 and *Sulfolobus acidocaldarius*; Au(0) nanoclusters formation on the S-layer of *S. acidocaldarius*
TU Bergakademie Freiberg, Freiberg, Germany (2011).

Vogel, M.
Zur Aufnahme und Bindung von U(VI) durch die Grünalge *Chlorella vulgaris*
Dresden University of Technology, Dresden, Germany (2011).
Available as: Wissenschaftlich-Technische Berichte, HZDR-005, Helmholtz-Zentrum Dresden-Rossendorf, Dresden (2011).

Wolf, M.
Visualisierung und Quantifizierung der Fluiddynamik in Bohrkernen aus dem Salinar und Deckgebirge des Raumes Straßfurt mittels Positronen-Emissions-Tomographie
University of Leipzig, Leipzig, Germany (2011).

▶ MASTER, DIPLOMA, BACHELOR

Brüning, S.
Spectroscopic characterization of U(VI)-complexes with phosphorylated amino acids (P-Ser and P-Tyr)
University of Applied Sciences, Dresden, Germany (2011).

Funke, F.
Schwingungstechnisch entkoppelte kryogene Messzelle für konfokale Lasermikroskopie
University of Applied Sciences, Dresden, Germany (2011).

Groß, M.
Spektroskopische Untersuchungen zur Struktur und Funktion der Kupfer-ATPase CopB von *E. hirae*
Dresden University of Technology, Dresden, Germany (2011).

Husar, R.
Untersuchung der Wechselwirkung von Uran(VI) mit Modellpeptiden mit und ohne Phosphorylgruppe
Dresden University of Technology, Dresden, Germany (2011).

Müller, N.
Funktionalisierung von S-Layer Proteinen mit Fluoreszenzfarbstoffen und Aptameren
TU Bergakademie Freiberg, Freiberg, Germany (2011).

Münch, R.
Herstellung von Fusionsproteinen zur Untersuchung der Expression rekombinanter S-Layer-Proteine in *Escherichia coli* BL21(DE3)
TU Bergakademie Freiberg, Freiberg, Germany (2011).

Obeid, M.
Assessment of low-dose radiotoxicity in microorganisms using calorimetric metabolic monitoring
Dresden University of Technology, Dresden, Germany (2011).

Steiniger, C.
Herstellung und Charakterisierung S-Layer basierender katalytischer Microkapseln
University of Applied Sciences, Dresden, Germany (2011).

- SEMINARS (TALKS OF VISITORS)
- WORKSHOPS
- TEACHING ACTIVITIES

▶ SEMINARS

Prof. Dr. Wolfgang Maret
School of Biomedical & Health Sciences, Department of Nutrition and Dietetics, Nutritional Sciences Division, King's College London, United Kingdom
Zinc biochemistry: from the geosphere to the biosphere
January 28, 2011

Prof. Dr. Marc Solioz
Department Clinical Pharmacology, University Berne, Berne, Switzerland
Copper in bacteria, humans, and the hospital
March 03, 2011

Dr. Rubens M. Moreira
Centre for Development of Nuclear Technology, National Nuclear Energy Commission – CNE, Belo Horizonte/MG, Brazil
Tracer applications to environmental transport in Brazil – Surface and groundwater
March 09, 2011

Prof. Dr. Horst Geckeis
Institute for Nuclear Wate Disposal, Karlsruhe Institute of Technology, Karlsruhe, Germany
Nukleares Recycling – Option für die sichere Entsorgung hochradioaktiver Abfälle?
April 29, 2011

Dr. Sven Krüger
Department of Chemistry, Technische Universität München, Munich, Germany
Adsorption of actinyl ions on clay mineral surfaces: species and structures from quantum mechanical model calculations
July 22, 2011

Prof. Dr. Heino Nitsche
Department of Chemistry, University of California, Berkeley, U.S.A.
The periodic system in motion: new discoveries and chemistry of the heaviest elements
August 26, 2011

Dr. Tim E. Payne
Australian Nuclear Science and Technology Organization (ANSTO)
Contamination of the environment – The view from 'down under'
September 14, 2011

Dr. Eberhard Janneck
G.E.O.S. Ingenieurgesellschaft mbH, Freiberg, Germany
Von der Rohstofferkundung bis zur Wasserbehandlung – Dienstleistungen rund um den Bergbau
November 28, 2011

▶ WORKSHOPS (ORGANIZED BY THE IRC)

„Von der Entwicklung sensorischer Schichten bis hin zum fertigen Biosensor“

HZDR, Dresden, Germany, May 12, 2011.

Kothe, J.
Der Weg vom Assay zum Biosensor – Herausforderungen in der Entwicklung optischer Biosensoren

Raff, J.
Bakterielle S-Layer als Template für die Herstellung von Biosensoren und zur Funktionalisierung von Materialien

Nikolaus, N.
Aptamere als neue Rezeptoren für Biosensoren und Assays

1. Workshop des Verbundprojekts „Rückhaltung endlagerrelevanter Radionuklide im natürlichen Tongestein und in salinaren Systemen“

art'otel, Dresden, Germany, October 11-12, 2011.

Banik, N.
Neptunium/Plutonium interaction in the clay rock system – Latest results and focus on tetravalent Np complexation with organic matter (fulvic acid)

Eidner, S.
Sorption of lanthanide ions to mineral surfaces

Kautenburger, R.
Einfluss geochemischer Parameter auf die Mobilität von Europium und Uran in Opalinuston

Krüger, S.
Quantenmechanische Modellierungen zu Ionen und Komplexen von Actinoiden in niederen Oxidationsstufen

Skerencak, A.
Complexation of Cm(III) with organic and inorganic ligands at increased temperatures

Steudtner, R.
Spektroskopische Untersuchungen von U(VI) in salinaren Lösungen

Stöbener, N.
Ultraspurenanalyse von Np-237 mittels Resonanzionisations-Massenspektrometrie (RIMS)

Workshop of the Paul Scherrer Institute (PSI), Villigen, Switzerland, and the Institute of Radiochemistry (IRC)

PSI, Villigen, Switzerland, December 08-09, 2011.

Aimoz, L.
Structural an thermodynamic investigation of iodine uptake by layered double hydroxides

Churakov, S.
Zn absorption on edges of montmorillonite inferred from molecular simulations and EXAFS spectroscopy

Gimmi, T.
Up-scaling of molecular diffusion coefficients in clays

Jordan, N.
Sorption of selenium(VI) onto maghemite

Lippmann-Pipke, J.
Messung und Simulation anisotroper Diffusion in Opalinuston

Moll, H.
The speciation of curium(III) bound by the Mont Terri opalinus clay isolate *Sporomusa sp.* and to the Äspö strain *Pseudomonas fluorescens*

Schott, J.
The influence of temperature and clay organics on the retention behavior of Opalinus clay concerning radionuclides

Tits, J.
Actinide uptake by cementitious materials: effect of redox state

Zänker, H.
Actinide(IV) oxyhydroxide colloids *vs.* actinide-silica colloids: their relevance for environmental conditions

Status-Seminar 2011: „Long-lived radionuclides in the environment“

HZDR, Dresden, Germany, December 14-15, 2011.

Banerjee, D.
X-ray photoelectron spectroscopy investigation of Sn(II) reaction with magnetite and goethite

Dulnee, S.
Sorption and interfacial redox of Sn(II) under anoxic conditions: magnetite *vs.* anatase

Dumas, T.
X-ray study of chemical bonding in actinides (IV) and lanthanides (III) ferrocyanide

Franzen, C.
The importance of accurate pH measurements for sorption experiments at high ionic strength

Günther, A.
Komplexbildung von U(VI) mit ausgewählten Schiffschen Basen und 1,3 ß- Diketonen

Gückel, K.
Binary and ternary surface complexes of U(VI) on gibbsite studied by vibrational and EXAFS spectroscopy

Hennig, C.
Actual insights into the structure-stability relationship of thorium(IV)/silica colloids

Hildebrand, H.
Radiolabelling of engineered nanomaterials as a tool for sensitive particle tracking

Jordan, N.
Sorption mechanism of selenium(VI) onto maghemite: consequences on outer-sphere complexation classification

Krawczyk-Bärsch, E.
Immobilization of uranium in biofilms from granitic rock tunnel walls in Olkiluoto, Finland

Lippold, H.
Adsorption, Desorption und Austausch: Radiotracerstudien zur Reversibilität der Adsorption von Huminstoffen

Lucks, C.
Aqueous uranium(VI) complexes with acetic and succinic acid: combining multi-spectroscopic methods with factor analysis and quantum chemical calculations

Lütke, L.
Structural investigations of U(VI) with Mont Terri clay isolates and the Äspö-strain *Pseudomonas fluorescens* by XAS – First results

Mansel, A.
Steuerung des Migrationsverhaltens von Radionukliden mit Hilfe makrozyklischer, multifunktionaler Chelatliganden

Rossberg, A.
Speciation and structure of the uranium(VI) sorption complexes at the γ-Al_2O_3 - water interface

Sachs, S.
Study of the impact of Eu(III) on the viability of FaDu cells and the speciation of Eu(III) in cell culture medium

Scheinost, A.C.
XANES and EXAFS analysis of oxidation state and local structure of plutonium reacted with iron oxides under anoxic conditions

Zänker, H.
Actinide(IV)-silica colloids and their potential geochemical implications

Zakhnini, A.
Entwicklung effektiver γ-Streu- und Schwächungskorrekturverfahren für GeoPET-Aufnahmen mittels Monte-Carlo Simulationen

▶ TEACHING ACTIVITIES

Lectures

Bernhard, G.
Radiochemistry
Dresden University of Technology
Summer term 2011

Environmental chemistry
Dresden University of Technology
Summer term 2011

Brendler, V.
Radiochemie 2
University of Applied Sciences, Dresden
Summer term 2011

Fahmy, K.
Biophysics
Dresden-International-PhD-Programme (DIPP), Dresden University of Technology,
Winter term 2011/2012

DNA-Nanotechnology
Senioren-Akademie, Dresden University of Technology
WS 2011/12

Infrared spectroscopy
BIOTEC-Master-Course, Dresden University of Technology
Winter term 2011/2012

Lippold, H.
Radiochemistry and radiopharmacology – Part II: origin, properties and applications of ionising radiation
University of Leipzig
Summer term 2011

Radioanalytics
Lecture within the post-graduate course "Analytics and spectroscopy", University of Leipzig
Summer term 2011

Courses

- The laboratory course "Radiochemistry" was provided from August 9th to 12th and from 23rd to 26th, 2010, as a part of a module of the chemistry master degree program at the Dresden University of Technology.

  Advisers:

Dr. Auerhammer, J.	Heim, H.	Dr. Müller, K.
Dr. Barkleit, A.	Dr. Heller, A.	Schott, J.
Fischer, S.	Lederer, F.	Suhr, M.
Frost, L.	Lindner, K.	Weinert, U.
Gagell, C.	Lucks, C.	Zirnstein, I.
Gückel, K.		

- The IRC provided one experiment "Alpha spectrometric isotope dilution analysis of uranium" of the laboratory course "Instrumental Analysis" held by the Institute for Analytical Chemistry, Dresden University of Technology, during winter term

  Advisers:

Winter term 2010-11	*Winter term 2011-12*
Dr. Foerstendorf, H.	Fischer, S.
Gückel, K.	Dr. Foerstendorf, H.
Lucks, C.	Husar, R.
Müller, M.	Schott, J.
Weinert, U.	Suhr, M.
Weiß, S.	Weiß, S.

- Biophysics course of the Dresden-International-Graduate School
  December 04-08, 2011

  Advisers:

Dr. Fahmy, K.	Philip, J.
Groß, M.	Sayed, A.
Oertel, J.	

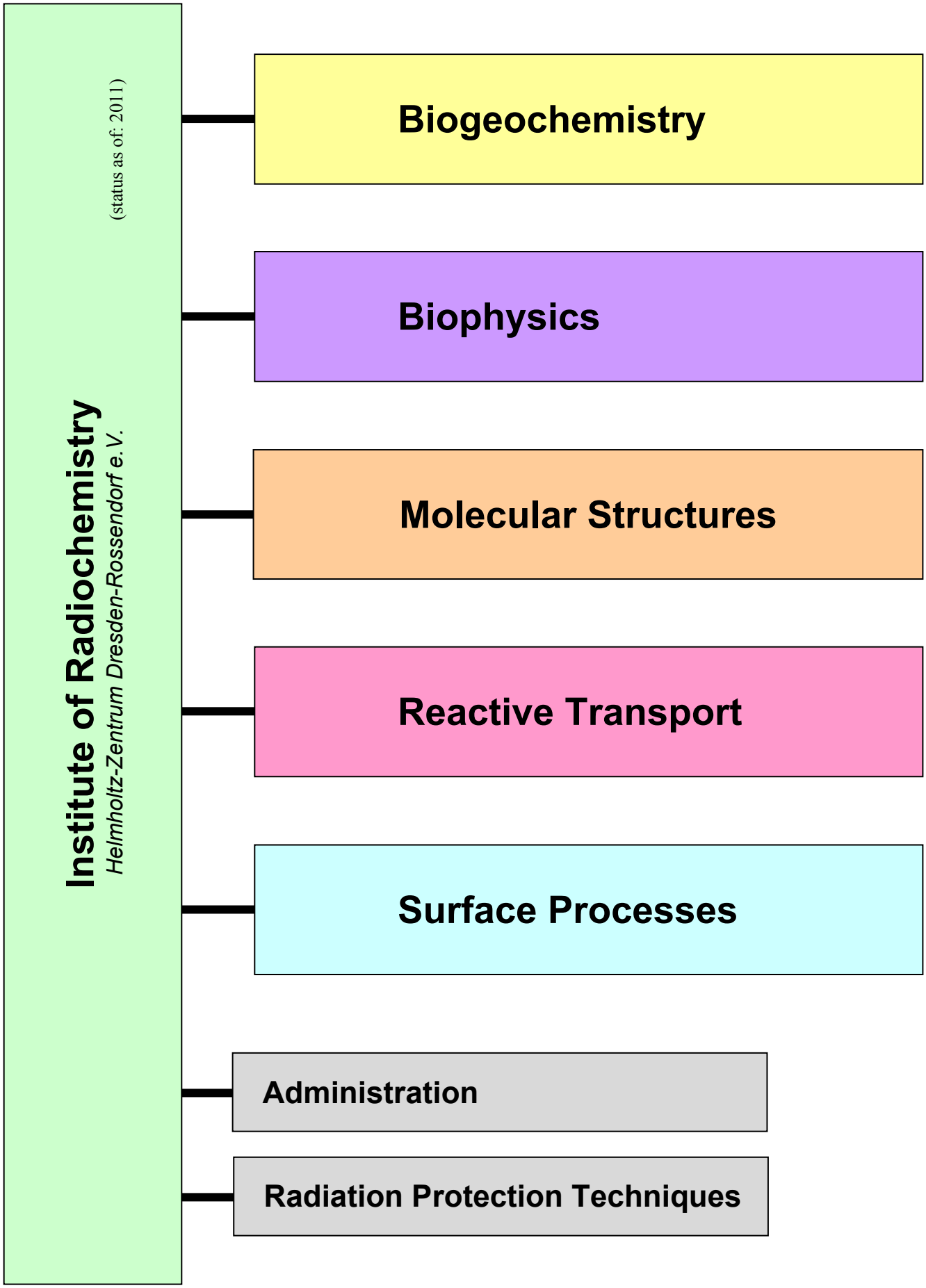
Institute of Radiochemistry
Helmholtz-Zentrum Dresden-Rossendorf e.V.
(status as of: 2011)
Biogeochemistry
Biophysics
Molecular Structures
Reactive Transport
Surface Processes
Administration
Radiation Protection Techniques

Prof. Dr. habil. G. Bernhard (Director)

ADMINISTRATION (status as of: 2011)
Gorzitze, Jana; Kirmes, Claudia; Kovács, Jenny; Mauersberger, Anke;
Glückert, Marion (ESRF); Gerstner, Katrin (FS Leipzig)

RADIATION PROTECTION TECHNIQUES
Heim, Heidemarie; Falkenberg, Dirk; Henke, Steffen; Hiller, Bernd; Rumpel, Annette

D I V I S I O N S

BIOGEO-CHEMISTRY

Dr. Geipel, Gerhard

Dr. Arnold, Thuro
Bachvarova, Velina
Dr. Baumann, Nils
Dudek, Monika
Flemming, Katrin
Förtsch, Gerd
Gagell, Corinna
Dr. Geißler, Andrea
Grambole, Genia
Dr. Günther, Alix
Gürtler, Sylvia
Dr. Heller, Anne
Heller, Sylvia
Dr. Krawczyk-Bärsch, Evelyn
Lindner, Katja
Lütke, Laura
Dr. Moll, Henry
Müller, Manuela
Dr. Raff, Johannes
Dr. Sachs, Susanne
Seibt, Jana
Dr. Selenska-Pobell, Sonja
Steinberg, Janine
Thiedt, Jana
Dr. Viehweger, Katrin
Dr. Vogel, Manja
Zirnstein, Isabel

External Ph. D. students
Brockmann, Sina
Eslami, Neda
Ilyashuk, Alina
Müller, Melanie
Osman, Ahmed. A. A.

BIOPHYSICS

Dr. habil. Fahmy, Karim

Abu Shark, Sawsan E.
Attia, Enas M. H.
Eichler, Stefanie
Fischermeier, Elisabeth
Kummer, Ulrike
Dr. Oertel, Jana
Philipp, Jenny
Sayed, Ahmed
Dr. Tsushima, Satoru

Junior Research Group
Dr. Pollmann, Katrin
Bobeth, Caroline
Günther, Tobias
Hauptmann, Tobias
Dr. Kutschke, Sabine
Lederer, Franziska
Lehmann, Falk
Marquard, André
Suhr, Matthias
Weinert, Ulrike

EXIST – Fellowship for business start up / ForMaT Project Mangement Jülich
NANOLAB/Kryofluor.
Dr. Großmann, Kay
Sobirai, Dirk
Trepte, Paul

MOLECULAR STRUCTURES

Dr. habil. Scheinost, Andreas C.

Dr. Banerjee, Dipanjan
Dulnee, Siriwan
Exner, Jörg
Fengler, Matthias
Dr. Hennig, Christoph
Kirsch, Regina
Lucks, Christian
Dr. Rossberg, André

REACTIVE TRANSPORT

Dr. Lippmann-Pipke, Johanna

Bütow, Claudia
Fellmer, Friederike
Dr. Franke, Karsten
Gruhne, Stefan
Gründig, Marion
Dr. Hildebrand, Heike
Dr. Kulenkampff, Johannes
Korn, Nico
Dr. Lippold, Holger
Dr. Mansel, Alexander
Paulilk, Sebastian
Schößler, Claudia
Schymura, Stefan
Willnow, Nicole
Wolf, Martin
Zakhnini, Abdelhamid

SURFACE PROCESSES

Dr. Brendler, Vinzenz

Dr. Auerhammer, Jutta
Dr. Barkleit, Astrid
Dr. Bok, Frank
Eckardt, Carola
Fischer, Sarah
Dr. Foerstendorf, Harald
Franzen, Carola
Fritsch, Katharina
Gückel, Katharina
Gürtler, Sylvia
Heim, Karsten
Heine, Katja
Husar, Richard
Dr. Ikeda-Ohno, Atsushi
Dr. Jordan, Norbert
Joseph, Claudia
Kretzschmar, Jerome
Li, Bo
Müller, Christa
Dr. Müller, Katharina
Neubert, Heidrun
Dr. Richter, Anke
Ritter, Aline
Schaefer, Ursula
Dr. Schmeide, Katja
Schott, Juliane
Dr. Steudtner, Robin
Dr. Stockmann, Madlen
Weiß, Stephan
Dr. Zänker, Harald

GUEST SCIENTISTS

Dr. Lopéz Fernandéz, Margarita	*Department of Microbiology, Universidad de Granada, Spain*
Dr. Radeva, Galina	*Institute of Molecular Biology, Bulgarian Academy of Sciences, Sofia, Bulgaria*
Sabau, Andrea	*Laboratoire de Radiochimie Sciences Analytiques et Environnement, Université Nice Sophia Antipolis, France*

MASTER/DIPLOMA/BACHELOR

Brüning, Sebastian	Meusel, Tilmann	Obeid, Muhammad	Steiniger, Claudia
Funke, Franziska	Müller, Nico	Sauerbier, Marcel	Wimmer, Christin
Groß, Magdalena	Münch, Robert	Schikora, Johannes	Zachmann, Tilo

GRADUATE ASSISTANTS, STUDENT ASSISTANTS, TRAINEES

Bittner, Lars	Kissauer, Frances	Pfützner, Birke	Zegke, Markus
Gröschel, Annett	Küchler, Stefanie	Probst, Anline	
Hastel-Kadule, Max-Lou	Lippmann, Christian	Pufe, Johanna	

ACKNOWLEDGEMENTS

With the beginning of 2012, the Institute of Radiochemistry (IRC) was merged into the newly founded Institute of Resource Ecology at the Helmholtz-Zentrum Dresden-Rossendorf e.V. (HZDR). The HZDR is financed in a major part by the ***Federal Republic of Germany*** and in a minor part by the ***Free State of Saxony***.

The Commission of the European Communities (EU) supported the following projects:

- ACTINET Integrated Infrastructure Initiative (ACTINET-I3)
  Contract No.: 232631
- CROCK
  Crystalline Rock Retention Processes
  Contract No.: FP7-269658
- HEXANE
  Heavy Elements X-ray Absorption Spectroscopies Network
  Contract No.: 230807
- Mont Terri BN-experiment
  Microbiology investigation of the Mont Terri BN-experiment, phase 16
  Contract No.: 32.0450.BN1_0L_PH16
- Redox phenomena controlling systems (RECOSY)
  Contract No.: 212287
- UMBRELLA
  Using microbes for the regulation of heavy metal mobility at ecosystem and landscape scale: An integrative approach for soil remediation by geobiological processes
  Contract No.: 226870

The following projects were supported by the ***Bundesministerium für Wirtschaft und Technologie (BMWi)*** and by the ***Bundesministerium für Bildung und Forschung (BMBF)***:

- Aptamer modifizierte bakterielle Oberflächenstrukturen für die Entwicklung neuer Sensoren (AptaSens)
  Contract-No.: 01RB0805A
- Beiträge zur Modellierung des Actinidentransports in potentiellen Wirtsgesteinsformationen
  Contract No.: BMWi 02E10176
- Mikrobielle Diversität im Tongestein (Opalinus-Ton) und Wechselwirkung dominanter Mikroorganismen mit Actiniden
  Contract No.: BMWi 02E10618
- NanoAqua ZIM – Kooperationsprojekt: Entwicklung von neuen Nano-Biokomposit-Materialien und Verfahren zur photokatalytischen Wasseraufbereitung
  Contract No: BMWi KF2306401
- NANOPHARM – Neue photokatalytisch aktive Verbundmaterialien zur Eliminierung von pharmazeutischen Reststoffen
  Contract-No.: 03X0094G
- NanoTrack – Untersuchung des Lebenszyklus von Nanopartikeln anhand von [^{45}Ti]TiO_2 und [^{105}Ag]Ag0
  Contract-No.: 03X0078A
- Verbundprojekt: Actinidenmigration im natürlichen Tongestein – Charakterisierung und Quantifizierung des Einflusses von Tonorganika auf die Wechselwirkung von U und Am im Ton
  Contract No.: BMWi 02E10156
- Verbundprojekt Partitioning II: Multifunktionelle Komplexbildner mit N, O, S-Donorfunktionen für d- und f-Elemente
  Contract No.: BMBF-FZK 02NUK014B
- Verbundprojekt: Realitätsnahe Einbindung von Sorptionsprozessen in Transportprogramme für die Langzeitsicherheitsanalyse (ESTRAL)-TV2
  Contract No.: BMWi 02E10528
- Verbundprojekt: Rückhaltung endlagerrelevanter Radionuklide im natürlichen Tongestein und in salinaren Systemen – Geochemisches Verhalten und Transport von Radionukliden (Np, U, Pu und weitere RN) in salinaren Systemen in Gegenwart endlagerrelevanter Organika
  Contract No.: BMWi 02E10971
- Verbundprojekt Strahlung und Umwelt II: Radionuklide in der Umwelt, ihr Transport in die Nahrungsketten zum und im Menschen, Teilprojekt F
  Contract No.: BMBF-FZK 02NUK015F
- Verbundprojekt: Verhalten langlebiger Spalt- und Aktivierungsprodukte im Nahfeld eines Endlagers und Möglichkeiten ihrer Rückhaltung (VESPA)
  Contract No.: FZK-BMWi 02E10790

Five projects were supported by the ***Deutsche Forschungsgemeinschaft (DFG)***:

- Imaging and image simulation of organic target compound migration between different biogeochemical interfaces of a soil horizon using position emission tomography and the lattice Boltzmann equation approach (BIG)
  Contract No.: LI 872/5-1
- Sorptions- und Redoxreaktionen von SN II und Sn IV an der Magnetite/Wasser-Grenzfläche in An- und Abwesenheit organischer Liganden (Zinn-Redox)
  Contract No.: SCHE 509/3-1
- Sorptionsprozesse von Np(V) an Alumosilikaten. Schwingungsspektroskopische Untersuchungen
  Contract No.: FO 619/1-2

- Strukturbestimmung von ternären aquatischen U(VI)-Sorptionskomplexen mittels neuester entwickelter kombinierter EXAFS-Auswertemethoden (ITFA, MCTFA) (STAUME II)
  Contract No.: RO 2254/3-2
- Transport von CNP in Geomatrizes
  Contract No.: FR 1643/3-1

The ***Bundesamt für Strahlenschutz (BfS)*** supported one project:

- Vervollständigung einer Thermodynamischen Standarddatenbasis (THEREDA-SZ II)
  Contract-No.: WS 2051 - 8732-9

The ***BMBF and MOST*** supported one project:

- Joint German-Israeli Water Technology Research Program
  Contract-No.: 02WA1223

The ***BAF*** supported one project:

- Selektion uranbindender DNA-Moleküle
  Durchführung molekularbiologischer Arbeiten als Teilschritt zur Selektion uranbindender DNA-Moleküle
  Contract-No.: 6142303143

One project was supported by ***Andra***:

- Pollutant Trapping
  Ion transfer from surface to crystal: Mechanisms of pollutant trapping
  Contract-No.: RCOT ASEV 110027

Alfatih A. Osman and Alina Ilyashuk were granted by the ***Deutscher Akademischer Austauschdienst DAAD***.

INDEX OF AUTHORS